



SCHOOL OF MECHANICAL,
INDUSTRIAL & AERONAUTICAL
ENGINEERING



Design Report

Electrically Enhanced Personal Transportation

MECN4005 - Design Project

Edward Rycroft

Student Number: 1478715

Supervisor: Mr. T. Smit

A project report submitted to the Faculty of Engineering and the Built Environment, University of the Witwatersrand, Johannesburg, in partial fulfilment of the requirements for the degree of Bachelor of Science in Engineering (Mechanical).

Johannesburg, August 2019

EXECUTIVE SUMMARY

The assigned low-level task was to design a vehicle or device for the personal transportation of a single user with capabilities for electric, manual, or combined propulsion on asphalt, pavement, cement, gravel, or flat soil. Briefly, it was desired for a mass lower than 19kg, support for users up to 100kg, 50km electric range, and speeds of 25km/hr on a level grade and 15km/hr on slopes with gradients up to 3% with maintained performance in the presence of winds up to 10km/hr. For an initial idea, preliminary concepts were generated for the Cycle, Skateboard, Scooter, Wheelchair, and Roller Skates, where the Cycle was found to be the most promising due to its high level of accommodation for each mode of propulsion. The design development was then undertaken for the electric propulsion, manual propulsion, wheel arrangement, and frame structure through analytical calculations and finite element analyses. The electric propulsion was found to be satisfactory with a Heinzmann DirectPower PRA 180-25 brushless DC hub motor producing 250W of continuous rated power, as limited by legal regulations; and 835.2W.hr battery pack using 80 Panasonic NCR18650PF cells each rated at 2.90A.hr for a range of 50km depending on the terrain. Comparing chain, belt, and shaft drives for manual propulsion, it was decided that a chain drive with an ISO 606 081-100 roller chain would provide versatility, where a gear ratio of 1:2.15 was used between the 43-teeth driving sprocket and 20-teeth driven sprocket while receiving a pedalling input using 170mm cranks constructed from aluminum 6061-T6. For the wheel arrangement, it was concluded that two wheels would offer the best compromise between operating skill and performance with decreased drag, weight, and rolling resistances. Specifically, Challenge Gravel Grinder TLR pneumatic tyres were chosen to be fitted to the designed wheels consisting of rims with a diameter of 622mm and profile classification of 19C and 36 stainless steel spokes of 2.6mm diameter connecting the rims to the hubs on each wheel, where the front hub was designed with a 9mm steel AISI 4140 axle and SKF 609-2RSH bearings. To accommodate male and female users between the 5th and 95th percentiles, the aluminium 6061-T6 frame and front fork were sized according to a conventional medium to large diamond structure for a seat tube angle of 73° , top tube length of 585mm, and wheelbase of 1095mm. The construction of the headset, stem, and handlebars was proposed with a width of 640mm for a steering torque up to 6.4N.m. An ABS enclosure with a volume of 22.0L is also to be fitted within the frame for the controller and battery pack. Overall, the design can be seen as fairly successful, where the independent electric propulsion and manual propulsion are able to reach sustained speeds of at least 25km/hr on a level grade within 4.809s and 15km/hr on a slope with a gradient up to 3% within 1.631s while experiencing an incoming wind at 10km/hr; and the combined propulsion is able to achieve sustained speeds of at least 30km/hr on slopes up to 3% gradient and 20km/hr on slopes up to 6% gradient with wind speeds over 10km/hr. The total mass of the designed components is 17.02kg, which allows for the controller, braking system, and miscellaneous accessories to have a mass up to 1.98kg. Finally, for further development, it is recommended that the controller and braking system be designed.

LIST OF CONTENTS

Individual Declaration	i
Executive Summary	ii
List of Contents	iii
List of Figures	vi
List of Tables	viii
List of Symbols	ix
1 Introduction	1
1.1 Background	1
1.2 Motivation	2
1.3 Task Statement As Given	3
1.4 Literature Review	3
1.4.1 Expected Operating Conditions	4
1.4.2 User Ergonomics	4
1.4.3 Bicycles	5
1.4.4 Skateboards	8
1.4.5 Scooters	10
1.4.6 Wheelchairs	11
1.4.7 Roller Skates	12
1.4.8 Wheel Considerations	13
1.4.9 Suspension Systems	16
1.4.10 Electric Propulsion	17
1.4.11 Material Properties	20
1.4.12 Standards And Regulations	21
1.4.13 Vehicle Dynamics	22
1.5 Task Statement As Understood	23
2 Preliminary Concepts	24
2.1 Criteria	24

2.2	Concept Generation	25
2.2.1	Cycle Concept	25
2.2.2	Skateboard Concept	25
2.2.3	Scooter Concept	27
2.2.4	Wheelchair Concept	27
2.2.5	Roller Skates Concept	27
2.3	Concept Evaluation	28
3	Product Requirement Specification	32
3.1	Electric Propulsion	32
3.2	Manual Propulsion	33
3.3	Structural Components	34
4	Design Development	35
4.1	Electric Propulsion	36
4.1.1	Motor	36
4.1.2	Battery Pack	41
4.1.3	Controller Considerations	44
4.2	Wheel Arrangement	46
4.2.1	Initial Considerations	46
4.2.2	Tyres	47
4.2.3	Rims And Spokes	49
4.2.4	Front Hub	55
4.3	Manual Propulsion	61
4.3.1	Gearing	61
4.3.2	Power Transmission	64
4.3.3	Cranks	70
4.4	Frame Structure	72
4.4.1	General Factors	72
4.4.2	Ergonomic Sizing	76

4.4.3	Strength And Stiffness	77
4.4.4	Enclosure	81
4.5	Braking System	83
4.5.1	Maximum Performance	83
4.5.2	Mechanism Type	84
4.6	Other Accessories	85
5	Design Specification	86
5.1	Final Description	86
5.2	Performance Evaluation	88
5.3	Manufacturing	90
5.4	Cost Analysis	101
6	Conclusions	101
7	Recommendations	102
	References	113
A	Ethics Clearance	114
B	Additional Engineering Drawings	114
C	Component Data Sheets	114
D	Miscellaneous Comments	114

LIST OF FIGURES

1	Standing dimensions of a male and female for 97.5th, 50th, and 2.5th percentiles	5
2	Primary components of a traditional bicycle, shown on a Cube Stereo 140 HPC	7
3	Cube Cross Hybrid Pro 400 as an example of an electric bicycle	8
4	Tern Vektron D8 as an example of a folding electric bicycle	8
5	Primary components of a traditional skateboard, shown on a Yocaher Graphic	9
6	Second generation Boosted Plus as an example of an electric skateboard	10
7	Primary components of a traditional scooter, shown on a Vokul Trii S2 Pro Scooter	11
8	Xiaomi Mi Scooter as an example of an electric scooter	11
9	Primary components of a traditional wheelchair, shown on a Karman LT-980	12
10	Primary components of traditional roller skates, shown on quad and inline skates	13
11	Thundrblade inline skates as an example of an electric roller skates	13
12	Comparison between a tyre with an inner tube and a tubeless tyre	14
13	Average variation in strain within a spoke and maximum allowable peak strain	15
14	Variation in rolling resistance with inflation pressure for pneumatic tyres	16
15	Suspension systems on a bicycle, scooter, and skateboard	17
16	Comparison between the construction of brushed and brushless DC motors	18
17	Motor power at different speeds for various user masses, gradients, and wind speeds	19
18	Fatigue characteristics for the relevant materials based on general classification	21
19	Simplified free-body diagram of a bicycle with drag, weight, and rolling resistance.	23
20	Schematic of the Cycle concept, with the side and front views	26
21	Schematic of the Skateboard concept, with the side and bottom views	26
22	Schematic of the Scooter concept, with the side and front views	27
23	Schematic of the Wheelchair concept, with the side and front views	28
24	Schematic of the Roller Skates concept, with the side, front, and bottom views	28
25	Schematics of the possible arrangements of the motor	36
26	Comparison between peak rated power for various cases during acceleration	40
27	Example and dimensions of the Heinzmann DirectPower PRA 180-25	41
28	Basic layout and dimensions of the battery pack	44
29	Timing diagram for the voltage strokes and power stage utilising six transistors	45

30	Views of most practical wheel arrangements with two, three, and four wheels	47
31	Example of the Challenge Gravel Grinder TLR for inspection of the tread	48
32	Outline the of straight-side, hooked-beam, and crotchet-type rim profiles	49
33	Schematic of the components of a spoke to connect the hub and rim of a wheel	50
34	Approximation of the fluctuating tensile load experienced within a spoke	51
35	Arrangement to test rim strength and free-body diagram during operation	53
36	Deformation and stress experienced in the rim for the suitable thicknesses	55
37	Construction of the front hub with a sectioned view	56
38	Free-body diagram of the loads experienced by the axle in the front hub	56
39	Axial force, shear force, and bending moment diagrams for the front axle	57
40	Lacing for a flange on the front wheel	59
41	Boundary conditions, deformation, stress experienced in the hub shell	60
42	Schematics of the possible power transmission methods for manual propulsion	65
43	Standard construction and components of a roller chain	67
44	Ratings chart used to select the most appropriate roller chain	69
45	Example of the Shimano Octalink V2 BB-ES300 bottom bracket	70
46	Deformation experienced in the crankset for the test cases	71
47	Set up and results of the Shape Generation tool used in Autodesk Inventor 2019.	73
48	Outline of a diamond frame with dimensions for the 5th and 95th percentile users.	73
49	Arrangement and components of the headset.	75
50	Loading of the first test, loading of the second test, and loading of the third test	78
51	Exploded view of the model used for the first and second tests.	78
52	Deformation and stress experienced in the final frame iteration for the first test	79
53	Deformation and stress experienced in the final frame iteration for the second test	79
54	Deformation and stress experienced in the final frame iteration for the third test	80
55	Proposed cross-sections for the members of the frame.	80
56	Compartments and dimensions of the enclosure within the frame quadrilateral.	82
57	Mass distribution and forces during braking.	83
58	Renderings of the primary components and final showcase.	87
59	Flow diagram of the parallel manual and electric power	88

LIST OF TABLES

1	Trends in South Africa for the average trip characteristics for various purposes	1
2	Trends in the United States for the average trip characteristics for various purposes	2
3	Approximate frontal area of the parts of a user for a bicycle	5
4	Experimental results for operation in a typical city setting	19
5	Expected properties for the relevant materials based on general classification	20
6	Summary of the electric bicycle regulations in various regions	22
7	Assessment of the preliminary criteria importance based on a weighting matrix	29
8	Evaluation of the preliminary concepts based on scoring with weighted criteria	31
9	Weighting matrix and evaluation for the arrangement of the motor	37
10	Collection of operating cases for a motor with a continuous rated power of 250W	39
11	Comparison between the typical characteristics of different types of batteries	42
12	Comparison between various candidate lithium-ion cells	43
13	Comparison between various candidate hybrid tyres	48
14	Dimensional parameters of the crotchet-type rim profile	50
15	Designation and parameters for common and standard straight spokes	52
16	Simulation results to determine the required rim thickness with aluminium	54
17	Simulation results to determine the required rim thickness with steel	54
18	Comparison between various candidate bearings for the axle in the front hub	59
19	Collection of operating cases for various gear ratios with manual propulsion	63
20	Collection of operating cases for various gear ratios with combined propulsion	63
21	Weighting matrix and evaluation for the transmission of manual power	66
22	Comparison of the suitable gear ratios	68
23	Dimensions for the members of medium and large frames for common bicycles	76
24	Dimensions for the final members of the frame.	81
25	Masses of the components for the designed sub-systems.	90
26	Parts list including the item number, part name, and required quantity.	92
27	Capital costs analysis as an order of magnitude or ratio estimate	101

LIST OF SYMBOLS

The general symbols used, with a description and relevant units, are as follows:

A	frontal area, cross-sectional area	m^2
A_t	tensile stress area	m^2
a	acceleration	m/s^2
a_{rel}	reliability modifying factor	-
a_{skf}	SKF modifying factor	-
α	angular acceleration	rad/s^2
C	basic dynamic load rating; or centre distance	N; or m
C_0	basic static load rating	N
C_d	drag coefficient	-
C_r	rolling coefficient	-
d	diameter	m
d_c	crankset diameter, driving sprocket diameter	m
d_w	wheel diameter, driven sprocket diameter	m
δ	deformation	m
E	elastic modulus	Pa
E_b	battery energy	J
E_c	cell energy	J
E_d	drag resistance energy	J
E_{in}	input energy	J
E_k	kinetic energy	J
E_m	motor energy	J
E_r	rolling resistance energy	J
E_{out}	output energy	J
E_w	weight resistance energy	J
ε	normal strain	-
η	efficiency	-
η_c	contamination factor	-
F	force	N
F_1	arbitrary reaction force	N
F_2	arbitrary reaction force	N
F_a	axial force	N
F_d	drag resistance force	N
F_f	friction driving force, friction braking force	N
F_i	arbitrary force component	N
F_{max}	maximum force	N

F_{min}	minimum force	N
F_p	pre-load axial force	N
F_r	rolling resistance force	N
F_t	pre-tension force	N
F_{ut}	ultimate tensile force	N
F_w	weight resistance force	N
F_x	x force component	N
f_1	application factor	-
f_2	driven teeth factor	-
G	gear ratio	-
g	gravitational acceleration	9.81m/s ²
γ	steering angle	rad, °
h	cross-sectional height	m
I	mass moment of inertia; or area moment of inertia	kg.m ² ; or m ⁴
I_c	cell current	A
K	condition factor	-
K_f	fatigue stress concentration factor	-
K_s	static stress concentration factor	-
k_a	surface condition factor	-
k_b	size factor	-
k_c	load factor	-
k_d	temperature factor	-
k_e	reliability factor	-
k_f	miscellaneous-effects factor	-
κ	viscosity ratio	-
L_{bas}	basic life cycles	10 ⁶ cycles
$L_{bas,hr}$	basic life time	hr
L_{skf}	SKF modified life cycles	10 ⁶ cycles
$L_{skf,hr}$	SKF modified life time	hr
l	length, chain length	m
l_t	fork trail length	m
M	bending moment	N.m
M_o	arbitrary moment component	N.m
m	mass	kg
m_{eff}	effective mass	kg
m_u	user mass	kg
m_d	design mass	kg
m_f	front wheel mass	kg
m_i	arbitrary mass component	kg

m_r	rear wheel mass	kg
$\%m_f$	fraction of mass on front wheels	%
$\%m_r$	fraction of mass on rear wheels	%
μ	static friction coefficient	-
N_1	arbitrary reaction force	N
N_2	arbitrary reaction force	N
N_f	normal force at front wheels	N
N_l	number of chain links	-
N_p	number of parallel cells	-
N_r	normal force at rear wheels	N
N_s	number of series cells	-
n	design factor, safety factor	-
ω	angular velocity	rad/s, rev/min
ω_c	crankset angular velocity	rad/s, rev/min
ω_w	wheel angular velocity	rad/s, rev/min
P	power; or applied dynamic load	W; or N
P_0	applied static load	N
P_b	battery power	W
P_c	cell power, crankset power	W
P_d	drag resistance power, design power	W
P_i	arbitrary power component	W
P_k	kinetic power	W
P_m	motor power	W
P_r	rolling resistance power	W
P_u	fatigue load limit	N
P_w	weight resistance power, wheel power	W
p	life exponent factor; or pitch	-; or m, tpi
ϕ	caster angle	rad, °
r	radius	m
r_c	crankset radius	m
r_t	turning radius	m
r_w	wheel radius	m
ρ	density	kg/m ³
S_e	endurance strength	-
S_{ut}	ultimate tensile strength	Pa
S_y	yield strength	Pa
σ_a	axial normal stress, alternating stress	Pa
σ_{eq}	equivalent combined stress, von Mises stress	Pa
σ_b	bending normal stress	Pa

σ_m	midrange stress	Pa
σ_{max}	maximum stress	Pa
T	torque	N.m
T_c	crankset torque	N.m
T_p	pre-load torque	N.m
T_o	arbitrary torque component	N.m
T_w	wheel torque	N.m
t	time	s, min, hr
τ_b	transverse shear stress	Pa
θ	gradient angle	rad, °
V	shear force	N
V_c	cell voltage	V
v	velocity	m/s
v_w	wind velocity	
w	cross-sectional width, wheelbase	m
X	arbitrary placeholder variable	-
x	distance	-
x_d	design mass x distance	m
x_f	front wheel mass x distance	m
x_g	centre of mass x distance	m
x'_g	relative centre of mass x distance	m
x_i	arbitrary x distance	m
x_r	rear wheel mass x distance	m
Y	arbitrary placeholder variable	-
y_d	design mass y distance	m
y_g	centre of mass y distance	m
y'_g	relative centre of mass y distance	m
y_i	arbitrary y distance	m
y_r	rear wheel mass y distance	m
y_u	user mass y distance	m
Z	arbitrary placeholder variable	-
Z_c	number of crankset teeth, number of driving teeth	-
Z_w	number of wheel teeth, number of driven teeth	-

Throughout the report, the relevant description and units are displayed with the symbols presented in equations. If there is a discrepancy or confusion between the displayed information and this listed information, the displayed information should be assumed to precede over this listed information.

1 INTRODUCTION

It is first necessary to investigate and assess the state of personal transportation. This is done to infer if there are issues with current modes of personal transportation and if a beneficial opportunity exists and can be motivated which could improve and offer an alternative solution to personal transportation.

1.1 BACKGROUND

A personal transportation vehicle or device refers to a design that assists an individual adult user with various trips during daily travel. These commutes allow the individual to travel for various activities that primarily include attending educational institutions, going to work, fulfilling errands and shopping, or participating in social and recreational activities, which clearly shows that personal transportation is essential for mobility to take part in modern society [1, 2, 3].

For each of these activities, the percentage distribution can be estimated in an attempt to model the transportation trends. To provide a global comparison, this is shown in Table 1 and Table 2 for South Africa and the United States based on the respective National Household Transport Surveys (it should be acknowledged that the data was collected from a sample and there will be an inherent sampling error when evaluating the population based on this data). Although there is a lack of exact data for the trip distance in South Africa, it can reasonably be assumed that the results in the United States provides a general approximation with an unobtrusive deviation due to the fair similarities in activity distribution, daily trip rate, and trip time. With this assumption, the average trip distance is 14.8km with 2.80 to 3.19 daily trips to produce a total average daily commuting distance between 41.4km and 47.2km, considering private cars, motorcycles, bicycles, and walking [1, 2, 4, 5].

Table 1: Trends in South Africa for the average trip characteristics for various purposes [1, 2].

	Work	Shopping Errands	School	Social Recreation	Total / Average
Relative Distribution	23.7%	24.1%	28.4%	23.7%	100%
Personal Transport Use	63.5%	46.4%	78.4%	67.7%	64.6%
Trip Distance [km]	-	-	-	-	< 20
Daily Trip Rate [Trips/Day]	-	-	-	-	2.80
Average Trip Time [min]	38.0	22.9	29.8	17.9	27.3

The monthly cost of transportation in South Africa is averaged at R371 for trains, R472 for buses, R515 for minibus-taxis, R1140 for private cars [1]. Because of these high costs and other factors including overcrowding and overloading, a lack and poor condition of facilities, and a lack of security and safety, 48% of minibus-taxi passengers, 42% of train passengers, and 33% of bus passengers were dissatisfied with the overall quality of the services, where only 8.7% of users feel that there are no transportation problems [1, 2]. In relation, the factors influencing the choice of personal transportation

Table 2: Trends in the United States for the average trip characteristics for various purposes [4, 5].

	Work	Shopping Errands	School	Social Recreation	Total / Average
Total Activity Distribution	18.4%	26.2%	6.60%	27.2%	78.4%
Personal Transport Use	88.2%	88.5%	70.5%	77.1%	83.0%
Relative Distribution	23.5%	33.4%	8.40%	34.7%	100%
Trip Distance [km]	18.5	11.4	10.3	16.7	14.8
Daily Trip Rate [Trips/Day]	0.59	1.30	0.37	0.93	3.19
Average Trip Time [min]	-	-	-	-	27.08

mode are weighted at 32.6% for travel time, 26.1% for the cost of travel, 9.2% for flexibility, 8.7% for safety from accidents, 5.9% for comfort, 4.9% for reliability, and 12.6% for other factors [1].

1.2 MOTIVATION

Because personal transportation is largely accomplished through private cars with internal combustion engines, there are frequently adverse effects. These effects include unsustainable environment damage due to local and regional air pollution with emission of pollutants with approximately 3.57g/km of hydrocarbons, 3.15g/km of carbon monoxide, 1.82g/km of carbon dioxide, and 2.29g/km of nitrogen oxides (approximate contribution of 20% to climate change); expensive costs to initially purchase the vehicle and a continuous high operating cost to use the vehicle; and misspent time delayed in traffic [3, 6, 7, 8]. These ideas can also be applied to public services, where there is still environment damage, a steep cost to use the services, and a lack of accessibility [6]. Also, affordable modes of personal transportation that mitigate these effects are evidently either not widely and economically available or not dominantly adopted when available and, so, there is an opportunity for more attractable modes of personal transportation that do not require specialised skills or disregard safety.

Specifically in South Africa, approximately 75.9% of the population travel at least one trip on a typical day but there is a lack of access to satisfactory public services, where 76% of households do not have access to train services and 38% of households do not have access to bus services due to no availability or a need to travel excessive distances for access [1, 2]. There is also a lack of access to private cars and motorcycles, where only 39.8% of households are able to afford access and only 26.9% of adults have licences, and travel is often performed through manual modes by walking or cycling which can be time-consuming and extremely fatiguing over extended distances [1, 2].

So, there is an apparent need for a mode of personal transportation that consumes less energy, produces fewer harmful emissions, and is less expensive to initially purchase and operate, while offering more flexibility and convenience than public services [9]. This personal transportation can be achieved through manual propulsion modes, but the user may become fatigued after long periods of exertion. If the personal transportation were to have electrical enhancements, there would be support

for the user while still avoiding the typical negative effects of personal transportation - assuming an electricity supply is available, as is usually the case, and generated through environmentally clean methods. Thus, there is an opportunity for an alternative to current personal transportation modes which can be realised through the development of a vehicle or device with manual and electric modes of propulsion. This would ultimately aid in ensuring sustainable, equitable, and uncongested mobility.

There are also other opportunities for manual personal transportation with electrical enhancements besides travel on roads over short distances. These include navigation on university or school campuses; aid for the elderly or disabled when it is necessary to walk due to restricted car permission and admittance; possibilities for improved social well-being, health (physical, mental, and psychological), and economic benefits; and recreational activities for enjoyment [7, 9, 10]. It is not explicitly necessary for the personal transportation to fulfil each of these specialised cases, but it would be an additional benefit for increased usage and potential to create a sustainable transportation system.

However, it should be recognised that there is partial competition in this domain, with regards to personal transportation where contemporary innovations and improved technologies are being explored to promote alternatives to private cars. Considering this, it is still evident that the economic market is far from saturation or capture by a single product or design, and there is still a prominent demand for an alternative form of personal transportation meeting the requirements of the user in terms of performance, cost, safety, comfort, and accessibility [9, 10].

1.3 TASK STATEMENT AS GIVEN

The task is to design a traditionally human-powered transportation vehicle or device for personal transportation and implement an electrical system to enhance the design and substantially reduce or eliminate the need for significant and exhausting human physical effort, such that the methods of manual propulsion and electric propulsion can be used independently or in combination.

1.4 LITERATURE REVIEW

To create the optimal design, it is crucial to source information to develop each aspect of the design. This will involve describing and defining the conditions in which the design will operate, along with the ergonomics of the average user. Also, existing concepts, prototypes, components, and designs should be reviewed and benchmarked to aid in the generation and evaluation of preliminary concepts based on expected performance achievements, and the identification of and solutions to common design issues and misconceptions. The compliance standards and regulations need to be investigated as well, such that the design is created to be safe and legal. Finally, general vehicle dynamics are presented to supplement the progression of the design development.

1.4.1 EXPECTED OPERATING CONDITIONS

The expected environmental conditions are a maximum temperature of 40°C and minimum temperature of -10°C, with a relative humidity between 30% and 90%. It is also expected for fair levels of precipitation periodically during the year which may create wet conditions. These expectations represent universal conditions where values within the ranges are commonly experienced throughout South Africa and the rest of the world where it would be viable to use personal transportation without excessive protection from the environment - excluding regions with snow and extreme heat.

The terrain on which the vehicle or device will operate includes asphalt, pavement, cement, gravel, or flat soil where there may be minor obstacles. From observations, these obstacles will be repetitive cracks, debris, bumps, or steps up to about 10mm high or deep and 35mm wide. However, there may occasionally be larger obstacles, such as noticeable defects and potholes over 40mm high or deep and 400mm wide [11], where the user would need to detect these obstacles and navigate to avoid them. The experienced vibrational frequencies are between 5.5Hz and 50Hz, with higher displacements at lower frequencies and lower displacements at higher frequencies [12]. The terrain may also have unclean and wet conditions where dirt, dust, and splash resistance would be required.

The expected slope conditions can be classified where common slopes include modest slopes up to gradients of 3% and significant slopes up to gradients of 6% [12, 13]. A severe slope can be seen as a slope with a gradient of 12%, but this is usually avoided during commuting because it is very difficult to climb [12]. It is also common for high wind speeds to vary between 10km/hr and 20km/hr, while exceeding 20km/hr is rare for normal conditions but should be anticipated intermittently.

1.4.2 USER ERGONOMICS

To ensure ease of use and user comfort, it is necessary to consider the dimensions of the average male and female at various ages, such that they are able to operate the personal transportation optimally. These dimensions for various positions and body shapes are suitably described in “The Measure of Man and Woman: Human Factors in Design” by Tilley and Dreyfuss [14], which can be used as an ideal reference when considering the arrangement of the user in various positions while operating the vehicle or device. A sample of the standing dimensions of a male and female is seen in Figure 1. The approximate frontal area of the parts of a user are also shown in Table 3 for reference. Moreover, the mass of a male ranges between 66kg and 98kg, while the mass of a female ranges between 54kg and 85kg, for the 10th and 90th percentiles respectively [15].

It is also important to know the mass an average male and female can lift, so the maximum mass of the vehicle or device can be quantified based on an individual lifting the vehicle or device with no external aid. Firstly, lifting is defined as “the act of manually grasping and raising an object of definable size” [17]. With this, it is estimated by Matheson et al. [17] that a male can lift at least 33kg while a female can lift at least 19kg for the 50th percentile individual between 15 years and 50 years.

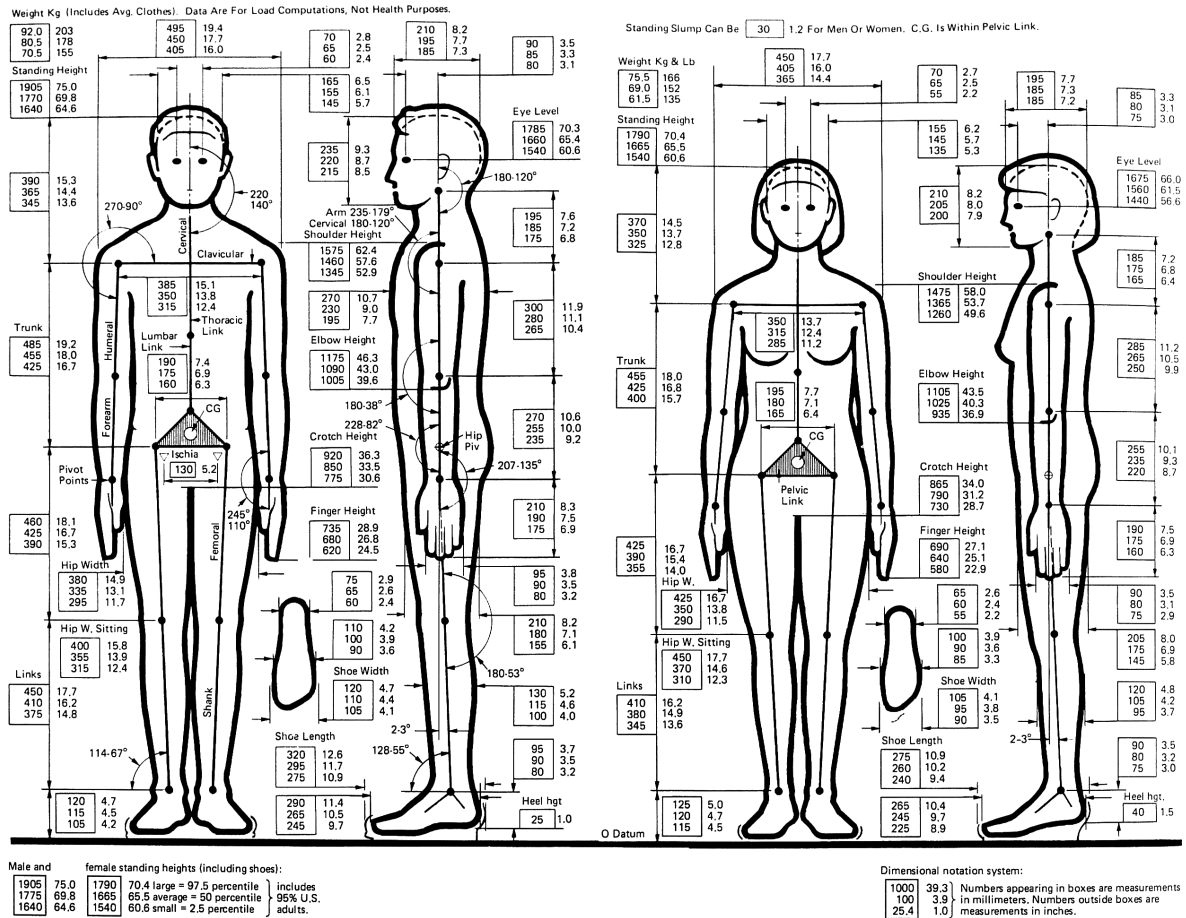


Figure 1: Standing dimensions of a male and female for 97.5th, 50th, and 2.5th percentiles [14, 16].

Table 3: Approximate frontal area of the parts of a user for a bicycle [13].

	Head	Torso	Arms	Upper Legs	Lower Legs	Feet	Hands	Total
Area [m ²]	0.036	0.127	0.090	0.094	0.053	0.025	0.023	0.448
Percentage	8.0%	28.2%	20.0%	20.8%	11.8%	5.5%	5.8%	100%

1.4.3 BICYCLES

A traditional bicycle basically relies on manual propulsion through pedalling with a steel, aluminium, titanium, or carbon fibre frame mounted between two wheels and handlebars for steering. It has been found to be one of the most efficient means of self-propelled transportation at 84W to 172W for speeds between 9.66km/hr and 30.6km/hr respectively, but the continuously sustainable power can be up to 260W for males and 210W for females [18, 19, 20]. From experimentation, the sustained power output from a healthy non-athletic male for a given period of time is empirically related by Equation 1, which results in an average power of 240W for 45 minutes of sustained effort [13]. The primary components of a traditional bicycle are labelled in Figure 2.

$$P = 85 + \frac{400}{t^{0.25}} \quad (1)$$

Where P , power, W; and t , time, min (only valid for the experiment range of $0.2\text{min} < t < 60$).

The components of a wheel include the hub, spokes, rim, and tyre, where the spokes connect the rim to the hub consisting of a hub shell, axle, and bearings, and the tyre is then be mounted onto the rim. According to the International Organization of Standardization (ISO) in ISO 5775, the standard and common wheel sizes include bead seat diameters of 507mm, 559mm, 584mm, and 622mm [21, 22]. Generally compared to smaller wheels, larger wheels will allow for better traction due to a larger contact surface with the ground, but have a larger mass and are less manoeuvrable due to a greater mass moment of inertia. Conventionally, a front wheel hub uses 100mm wide fork spacing and a rear wheel hub uses 130mm or 135mm wide fork spacing for clearance to mount components [23].

A suspension system helps the user control the bicycle on rough terrain, where full suspension refers to both front and rear suspension, while hardtail suspension refers to only front suspension. Typically, full suspension is used for harsh off-road trails with many obstacles, while hardtail suspension is used for slightly smoother off-road trails - if the bicycle will only be riding on smooth roads or paths, it may not be necessary for front or rear suspension. A full suspension will tend to offer more comfort but a higher mass with more components, compared to a hardtail suspension.

The purpose of the brakes is to reduce the speed of the bicycle or prevent the bicycle from moving once it is stationary. The most common types of brakes are rim brakes and disc brakes which are controlled by a lever on the handlebars and operate by dissipating kinetic energy as thermal energy through friction. Rim brakes consist of one or two rubber pads which are moved to contact the rim of the wheel and create increasing friction based on the force applied to the rubber pads. The advantages of rim brakes are that they are inexpensive, lightweight, and effective, but they may perform poorly if the rim is not correctly aligned or if the friction coefficient and efficiency is decreased due to wet conditions. Disc brakes operate in a similar manner to rim brakes, except the rubber pads apply friction to a steel disc with a diameter of 160mm, 185mm, or 203mm mounted to the hub [12, 24]. The benefits of disc brakes are that they have a higher mechanical advantage and do not operate on the rim which tends to offer more predictable behaviour. Uncommon types of brakes include plunger or spoon, hub, drum, coaster, and band brakes [12, 24]. It should be highlighted that these types of brakes are not exclusively used on bicycles and can be used on other vehicles or devices.

The crankset encompasses two cranks arranged at 180° on either side of the bicycle with pedals at the ends, and a collection of driving sprockets which are chosen with a front derailleur where the number of sprockets can vary from one to three gears. The cadence or pedalling speed is preferably 60rev/min to 110rev/min but 50rev/min is tolerable, and the effective pedalling force from the user can usually be above 200N on a standard crank between 165mm and 180mm with 170mm being the most common [12, 25]. For the power transmission from the pedals to the rear wheel, a roller chain is used to connect the driving sprocket to a cogset mounted to the rear wheel hub [25]. The cogset is

usually a cluster of driven sprockets mounted with threads (freewheel hub with thread-on freewheel sprockets) or splines (freehub with splines and a cassette of sprockets), where a rear derailleur is used to shift between the sprockets and the number of sprockets can vary from six to twelve gear ratios or be substituted for a single gear ratio [25, 26, 27]. The mounting mechanism also has an overrunning clutch so it is possible to coast with the wheel freely rotating without rotating the pedals.

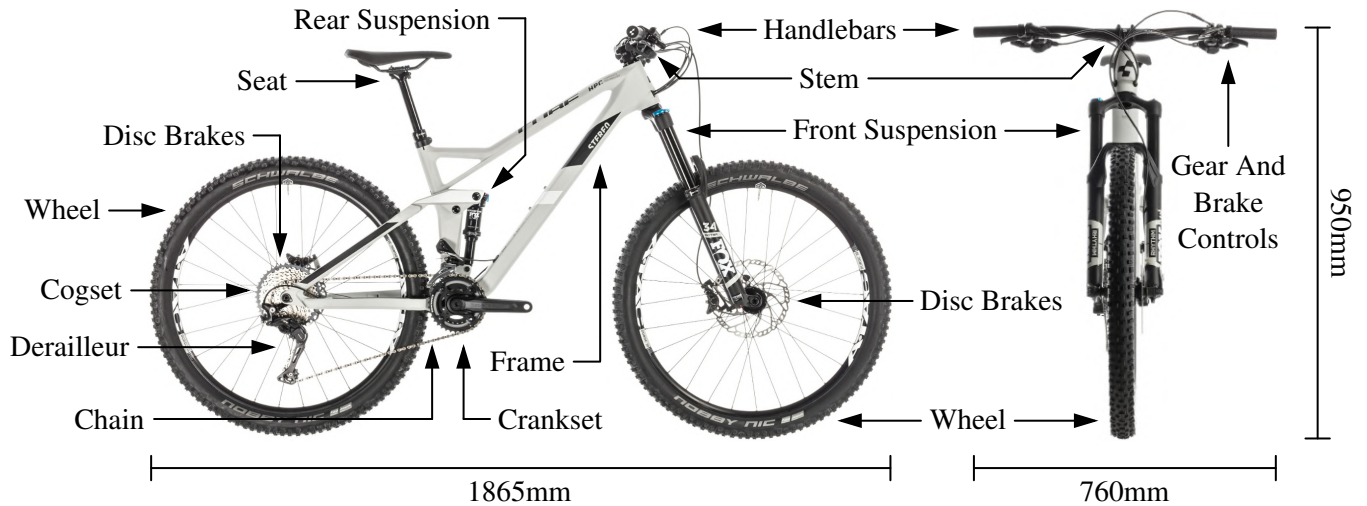


Figure 2: Primary components of a traditional bicycle, shown on a Cube Stereo 140 HPC [28]. Some components are optional depending on the purpose for commuting, racing on road, or going off-road.

With electrical enhancements, pedal-assisted electric bicycles or e-bikes combine propulsion from manual pedalling with assistance from an electrical system. Typically, the additional components include a pedal movement or force detector, motor, battery, and controller, where the motor is located in one of the wheel hubs or in the frame affecting the crankshaft [9]. As with most vehicles or devices offering electrical assistance to manual propulsion, this decreases the energy expenditure of the user and allows for the user to travel a further distance, where travel distances tend to be almost twice as far as traditional bicycle trips; or it allows for the user to travel the same distance in a short amount of time, where average travel speeds are found to be at least 10% to 15% greater than traditional bicycle speeds [9, 10]. Essentially, the primary advantage of electric bicycles includes the auxiliary power, while the disadvantages include the additional mass, charging, and higher purchase cost.

An example of an electric bicycle is the Cube Cross Hybrid Pro 400. This hardtail, commuting bicycle is seen in Figure 3 and features the common components of a traditional bicycle, along with a lithium-ion motor, battery, controller, and transmission, which results in a total mass of 22.86kg. It is able to achieve a range between 32km and 97km depending on the terrain and maximum speed of 32km/hr - limited as per US regulations [29, 30]. The motor is the Bosch Performance Line CX with a 250W continuous rated output, 600W peak rated output, and maximum torque of 75N.m [29, 30]. The capacity of the battery is 396W.hr with a recharging time of about 3.5hr [29, 30]. The price of the Cube Cross Hybrid Pro 400 is US\$2600 (R37700, as of US\$1 = R14.50) [29].

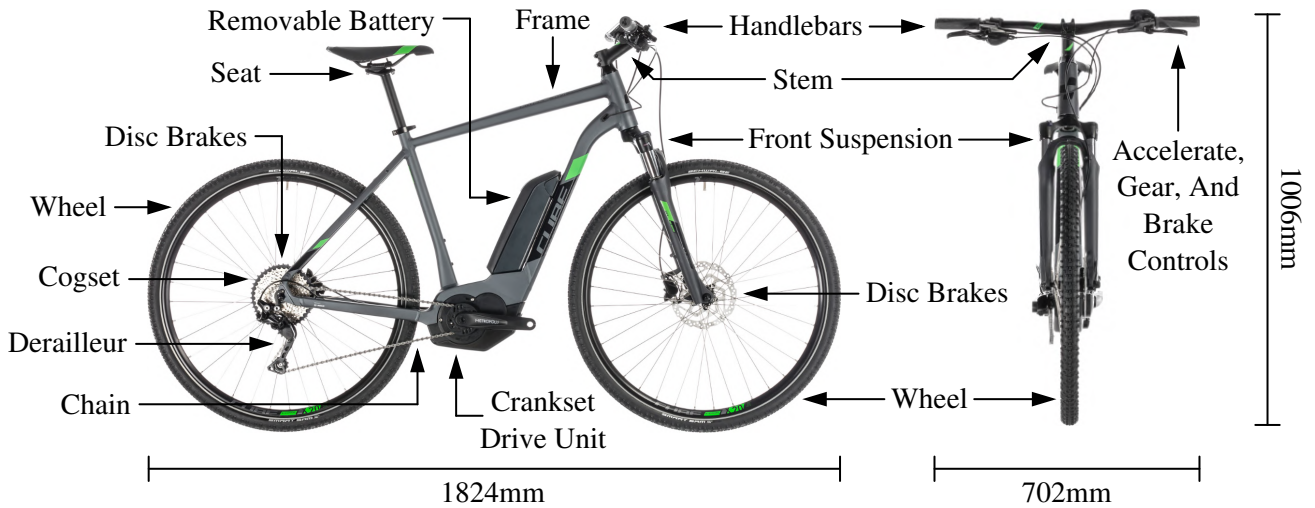


Figure 3: Cube Cross Hybrid Pro 400 as an example of an electric bicycle [30].

For a typical electric bicycle, it is estimated that the energy consumption rate is 20W.hr/km, compared to 210W.hr/km/person for public transport and 660W.hr/km/person for private cars; time to charge the battery is 2hr to 8hr; minimum range is 35km to 50km with a speed up to at least 20km/hr with only electric propulsion; and operating cost is estimated at US\$0.007/km, compared to US\$0.62/km for private cars (R0.10/km and R8.99/km respectively, as of US\$1 = R14.50) [8, 9, 31].

Folding bicycles are also available, such as the Tern Vektron D8 in Figure 4, where the advantages are limited to the bicycle folding to become more compact and easier to take on public services [32]. For personal transportation as a direct trip, these bicycles offer no advantages and may only hinder performance since they usually have smaller wheels at 428mm and heavy structures at 22.5kg [32].

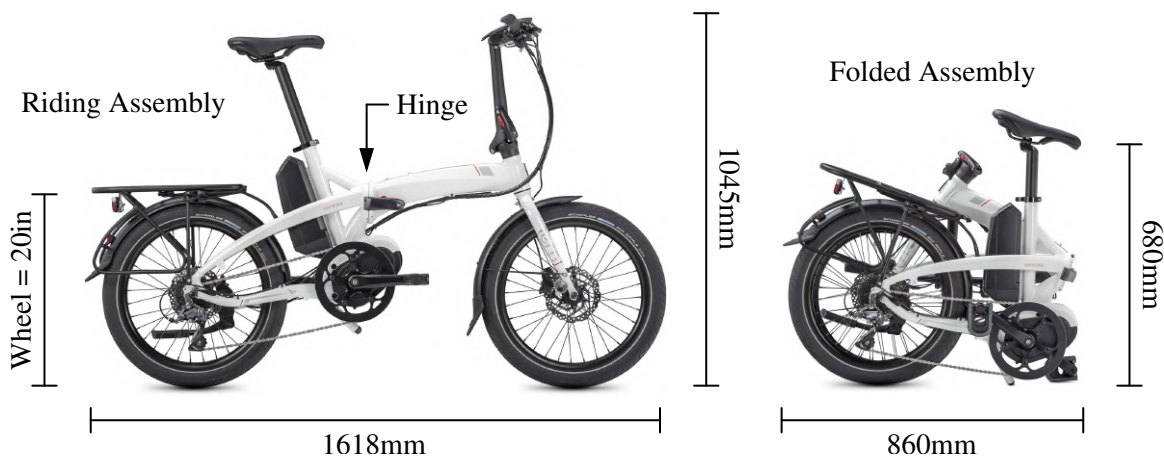


Figure 4: Tern Vektron D8 as an example of a folding electric bicycle [32].

1.4.4 SKATEBOARDS

A traditional skateboard, as seen in Figure 5 with the primary components, utilises manual propulsion through pushing against the ground with one foot while balancing on the deck of the skateboard with the other foot - braking is performed by dragging the pushing foot along the ground to create

resistance. The dimensions of the deck can vary but are generally classified based on length with less than 560mm for penny boards, 710mm to 840mm for standard boards, 840mm to 910mm for cruisers, and greater than 910mm for longboards (typically, longboards are better suited for long distance travel) with wheelbases from 330mm and widths from 190mm, while the decks are usually constructed from maple wood, bamboo, baltic birch plywood, plastic, resin, or carbon fibre with a concave, convex, or flat profile [33, 34]. The trucks mount to the deck to connect the wheels and are commonly constructed from steel or aluminium with a polyurethane bushing used to adjust the turning ability of the skateboard [33, 34]. The diameter of the wheels are constructed from polyurethane and vary from 48mm to 85mm, where larger wheels roll faster and offer comfort over obstacles while smaller wheels allow for a lower centre of gravity and better control [33, 34].

Although traditional skateboarding prefers smooth surfaces, adaptations are applied for more extreme terrain in mountain boarding or all-terrain boarding. These boards have larger trucks with built-in suspension systems, brakes on the wheels operated by a hand-held lever, and bindings to help secure the user to the board. The expense of these additions is a much heavier structure.

For longboards, the performance can vary where a trip distance is usually up to 6.44km and the speeds range from 13.3km/hr to 18.4km/hr with an average of 16.2km/hr [19, 35]. There is also an estimated energy expenditure of 114W to 140W, which is comparable to walking at 7km/hr with an expenditure of 93W and more efficient than running at 15km/hr with an expenditure of 256W [18, 19].

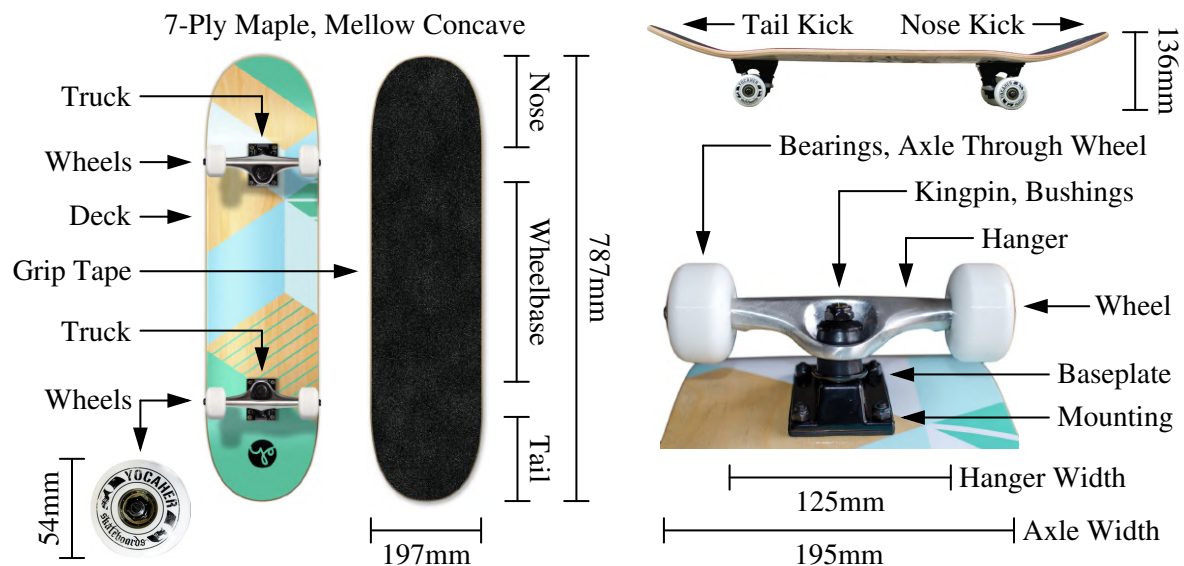


Figure 5: Primary components of a traditional skateboard, shown on a Yocaher Graphic [36].

An example of an electric skateboard is the second generation Boosted Plus, as seen in Figure 6. This longboard offers a range of 22.5km with a maximum speed of 35.4km/hr with only electric propulsion and is able to effectively climb gradients up to 25% [37]. The overall mass is 7.71kg and the construction features 190mm machined trucks, 85mm polyurethane wheels, a polymer sidewall around the edges, and a composite deck consisting of a poplar core, high-density foam, triaxial fibreglass, and a protective covering [37, 38]. The time to charge the battery is about 1.75hr [37].

The Boosted Plus uses a belt-drive transmission system between brushless direct current (DC) motors and the rear wheels, which allows for increased torque and acceleration [37]. Alternate electric propulsion could use hub or in-wheel motors, which allows for quiet operation, high durability, and significantly less resistance if manually pushing, but has a much higher cost for equivalent performance. Regardless of the motor arrangement, the electric propulsion system can also be used to provide regenerative braking, where the acceleration and braking are controlled by a wireless Bluetooth remote [37]. The price of the Boosted Plus is US\$1400 (R20300, as of US\$1 = R14.50) [37].

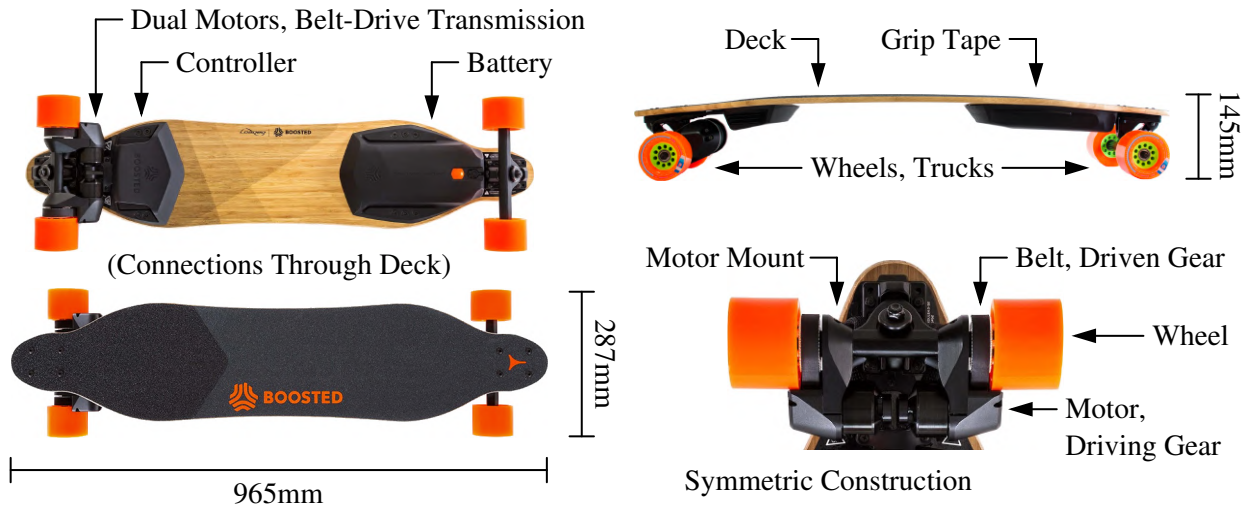


Figure 6: Second generation Boosted Plus as an example of an electric skateboard [37, 39].

1.4.5 SCOOTERS

Traditional scooters are similar to traditional skateboards in that they have manual propulsion through pushing against the ground with one foot, but they provide steering by turning the front wheel. The main components of a traditional scooter include the handlebars, frame bar, clamp, deck, brake, and wheels, which are labelled in Figure 7. The handlebars are attached to the frame bar which is connected to the deck via the clamp. It is possible to have a frame bar with a fixed height or adjustable height, where it may also be possible for the frame bar to fold towards the deck.

With regards to materials, the frame bar and deck may be constructed from steel or aluminium where the height must be sufficient for the user to comfortably turn the front wheel with a width of 457.2mm to 558.8mm and the length between 482.6mm and 558.8mm must be long enough for the user to comfortably balance and operate the brake [40, 41]. Like skateboards, the wheels are usually constructed from polyurethane with diameters ranging from at least 100mm to 125mm, where there is conventionally a front and rear wheel but the number of wheels can be increased if the shape of the deck is modified [40, 41, 42]. Finally, braking can be performed with disc brakes or by standing on a brake pad to contact the rear wheel so the rotation of the wheel is slowed through friction.

As seen in Figure 8, a recent electric scooter is the Xiaomi Mi Scooter which can be folded and has 217mm pneumatic rubber tyres at 3bar to 4bar, an aluminium frame, and a mass of 12.2kg to

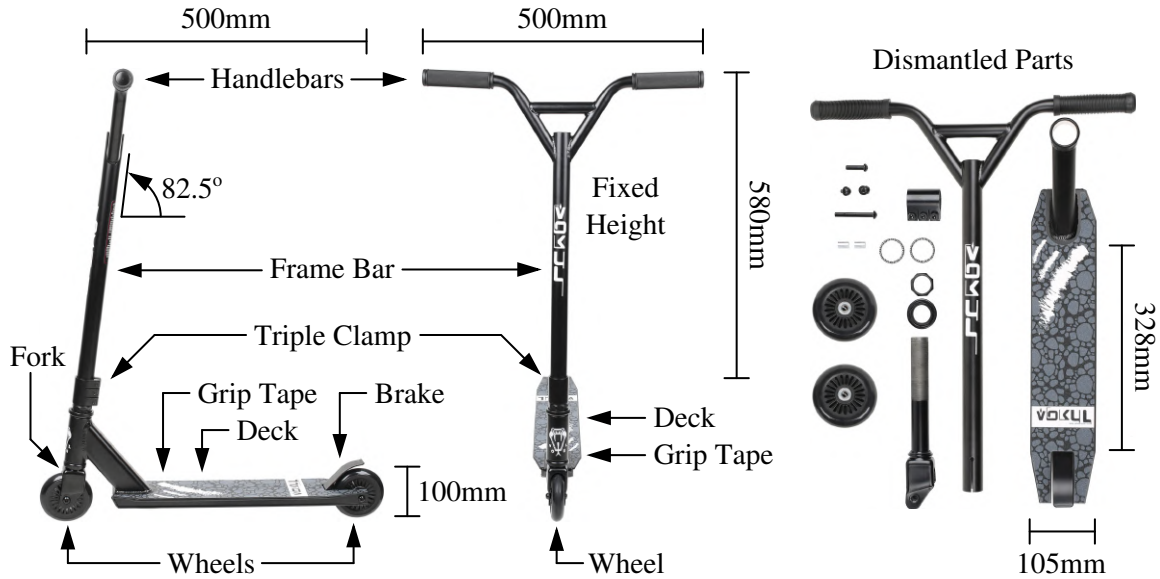


Figure 7: Primary components of a traditional scooter, shown on a Vokul Trii S2 Pro Scooter [40].

support users up to 100kg [43]. The scooter has a range of 30km with a maximum speed of 25km/hr and torque of 16N.m from the brushless DC hub motor in the front wheel [43]. With only electric propulsion, the scooter can climb gradients up to 14% and there is an average power consumption of 11W.hr/km with a charging time around 5hr [43]. For braking, the scooter features regenerative braking and a disc brake on the rear wheel [43]. The price is US\$500 (R7250, as of US\$1 = R14.50).

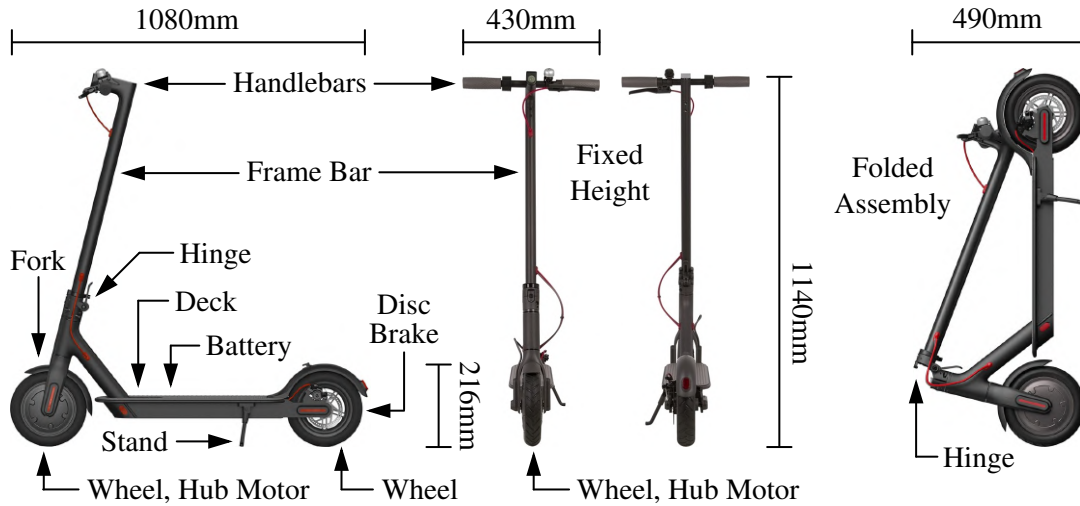


Figure 8: Xiaomi Mi Scooter as an example of an electric scooter [43].

1.4.6 WHEELCHAIRS

A traditional wheelchair is conventionally used to aid disabled or elderly individuals and is basically a chair with wheels, where the user sits between the wheels and uses their arms to manually rotate the wheels with an energy expenditure up to 219.8W at only 3km/hr [44] (wheelchairs can also be propelled by an attendant pushing on handles while walking or running, but this is not suitable for individual personal transportation and will not be considered). So, a traditional wheelchair consists

of a seat supported by a frame and two main wheels which may be cambered, while two caster wheels ensure balance and easy manoeuvrability. The main wheels are similar to bicycle wheels with solid or pneumatic rubber tyres, diameters ranging from 508mm to 610mm, and handrims attached to the rims to easily rotate the wheel. To brake while moving, the user will usually hold their palms against the handrims, but there are also friction brakes located on the main wheels to keep the wheelchair stationary once it is at rest. These components are shown on a lightweight and foldable wheelchair in Figure 9, with an x-brace frame and optional footplates to support the feet of the user.

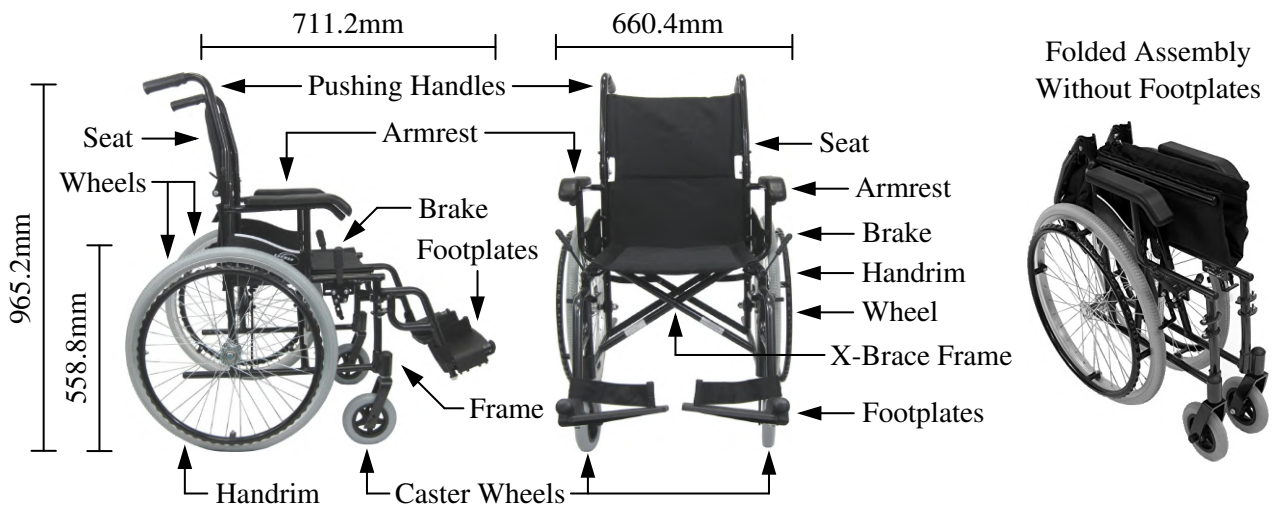


Figure 9: Primary components of a traditional wheelchair, shown on a Karman LT-980 [45].

Like the mentioned personal transportation vehicles and devices, electric wheelchairs are available with the addition of a motor, battery, controller, and transmission, but they often do not have manual propulsion. A typical electric wheelchair without manual propulsion, such as the Forcemech Navigator, can achieve a range of 25.7km, maximum speed of 8.05km/hr, and gradients up to 21.3% with a brushless DC motor, while the frame is constructed from aluminium with polyurethane wheels [46]. The price of a Forcemech Navigator is US\$3000 (R43500, as of US\$1 = R14.50) [46].

1.4.7 ROLLER SKATES

Traditional roller skates can be defined as shoes or bindings that fit onto shoes which enable the user to roll on wheels, and have conventionally been used for recreation or sport and not focussed on personal transportation. The most common types of roller skates are quad roller skates, with four wheels in a rectangular arrangement, and inline skates or blades, with two to five wheels arranged in a line, but there can be variations in the number and position of the wheels. Although inline skates are generally faster than quad roller skates, average speeds between 12.9km/hr and 17.7km/hr are commonly achievable by both types with an energy expenditure between 100W and 184W [18].

A comparison between quad roller skates and inline skates is seen in Figure 10, where the primary components are actually shared. The boot consists of a shell to secure and protect the feet of the user and there may either be a soft inner liner into which the user inserts their feet or straps to secure

the shoes of the user [47, 48]. The frame can be constructed from high-grade polyurethane, steel, aluminium, or carbon fibre; houses the wheels and toe stop or heel brake; and fastens to the boot with the mounts spaced at 165mm, 167mm (Universal Frame System (UFS)), or 195mm [47, 48, 49]. The wheels then range from diameters of 47mm to 150mm depending on the use and are usually constructed from polyurethane for high durability and low rolling resistance [47, 48, 50].



Figure 10: Primary components of traditional roller skates, shown for comparison on Epic Skates Super Nitro quad roller skates (left) and K2 F.I.T. 84 Boa inline skates (right) [51, 52].

There are no prevailing or successful electric roller skates which maintain simple manual propulsion. However, there is potential for the development of electric roller skates, as seen with the Thundrblade prototype in Figure 11, which are two-wheel inline skates and appear to use a friction drive where a roller attached to the motor directly rotates against the rear wheel [53]. It is also expected for the Thundrblade to have a range of 11.3km with swappable batteries, maximum speed of 40km/hr, mass of 2.27kg, ability to climb gradients up to 20%, regenerative braking, and 2hr charging time [53]. It should be noted that the Thundrblade was listed on Indiegogo at a decreased price of US\$850 (R12325, as of US\$1 = R14.50), but did not receive sufficient funding for a successful campaign [53].

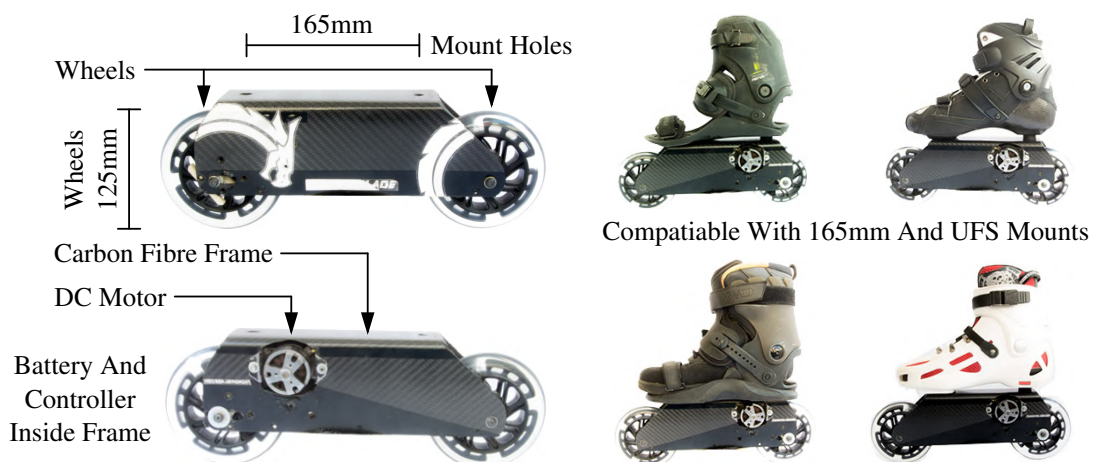


Figure 11: Thundrblade inline skates as an example of an electric roller skates [53].

1.4.8 WHEEL CONSIDERATIONS

With regards to bicycles, scooters, wheelchairs, and possibly skateboards, it is possible to use wheels with pneumatic rubber tyres which allow for the forces from minor obstacles to be absorbed through

elastic deformation such that the transmitted force to the suspension system and user is decreased. These pneumatic tyres may have an inner tube or be tubeless, where an inner tube is a sealed elastic rubber in the form of a torus which is inserted within the tyre between the clincher rim and inflated to fill the tyre via a protruding valve; while tubeless tyres utilise the bead of the tyre with the aid of a sealant to form an airtight seal against the clincher rim when the tyre is inflated. The construction of a tyre with an inner tube and a tubeless tyre are shown in Figure 12. The specific structure of the tyre consists of an outside tread manufactured from rubber to contact the ground and provide resistance to punctures; sidewall manufactured from rubber to provide a thin layer of protection for the sides of the casing; casing or carcass manufactured from nylon, cotton, or silk to provide a foundation and deform while rolling; and beads manufactured from steel wire or Kevlar to provide mounting to the rim [54, 12]. Alternatively, solid rubber tyres can be used which can handle higher loads and require less maintenance with no risk of punctures but they offer less comfort with decreased absorption of forces from minor obstacles and an increased mass and rolling resistance.

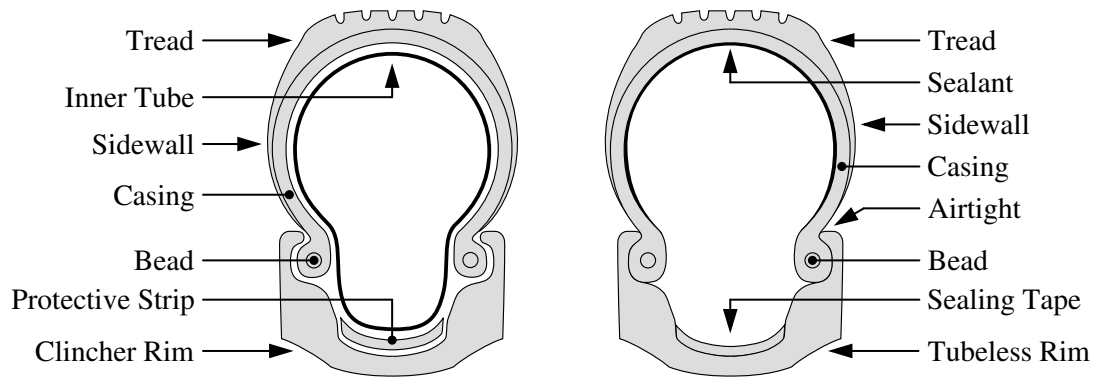


Figure 12: Comparison between a tyre with an inner tube (left) and a tubeless tyre (right).

For a wheel with spokes connecting the rim to the hub, the wheel will operate as a pre-tensioned structure, where the tensile stresses are reduced when the wheel is subjected to compressive loads [55]. This arrangement is used because it is not possible for the spokes to directly support the applied compressive load without buckling and, so, it is necessary for a pre-tensile load to already exist such that the spokes are able to support the applied compressive load by reducing the overall tensile load up to the point at which they become slack, which sets the load limit for the wheel since the other components will not fail before this point [55]. An experiment with strain gauges attached to the spokes of different bicycle wheels was performed by Gavin [56] and the results when a radial load was applied under normal operating conditions revealed the strain variation experienced in a spoke as the wheel rolls, which is seen in Figure 13, and showed that the spoke strains are mostly insensitive to the spoke pattern, although the spoke pattern does affect the stiffness of the wheel.

Considering solid polyurethane wheels which are commonly used on skateboards, scooters, and roller skates, the wheels can offer a lightweight and durable option with a range of possible properties. The main influence on the characteristics and performance of the wheel is the hardness, which is measured with a Shore durometer based on the ASTM D2240 scales - specifically the type A scale. For wheels,

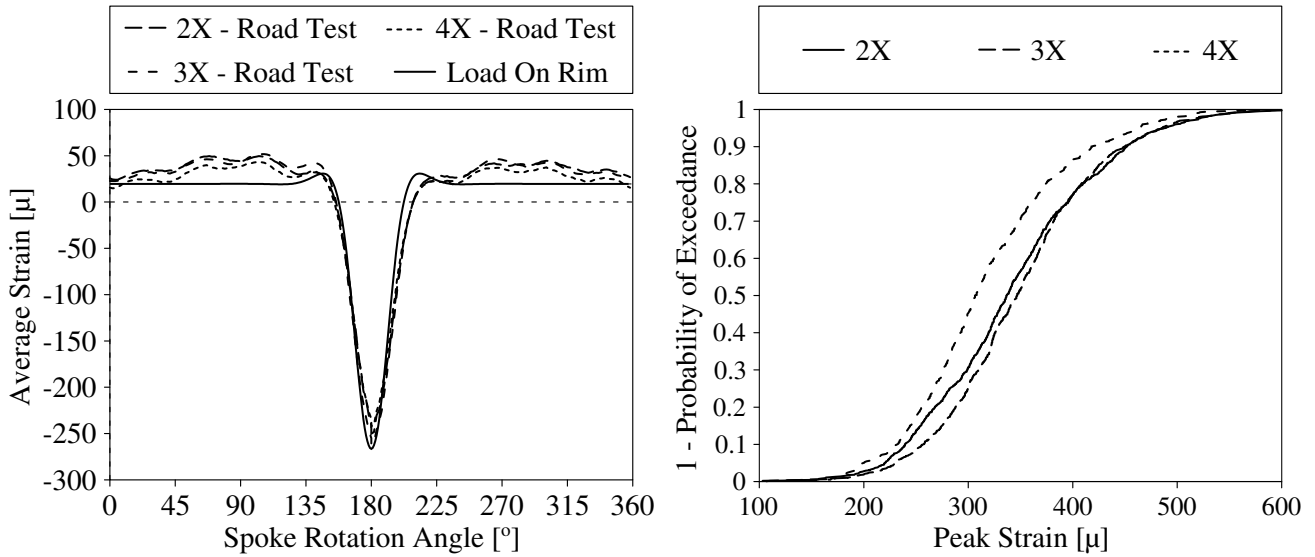


Figure 13: Average variation in strain within a spoke (left) and cumulative probability distribution for the allowable peak strain (right) for a bicycle and user with a combined mass of 95kg using wheels with 36 spokes of 1.83mm diameter with an elastic modulus of 206GPa on a rim with a diameter of 622mm [56]. The average variation results are presented relative to the pre-tensioned condition, where a positive value indicates a pre-strain gain and a negative value indicates a pre-strain loss [56].

the Shore durometer hardness typically ranges from 78A to 100A, where a hard wheel performs better at high speeds while a soft wheel will be smoother over minor obstacles [57].

Rolling resistance is the resistance to the steady motion of a wheel caused by power absorption in the surfaces of the wheel and ground, which is related to the imperfect elastic deformation of these surfaces due to the load being carried [12]. Essentially, a stiff wheel will typically have a lower rolling resistance than a flexible wheel, and hard ground will typically have a lower rolling resistance than soft ground. The effect of the rolling resistance can be quantified through a rolling coefficient which can range from 0.002 for high quality racing to 0.008 for inexpensive utility pneumatic tyres depending on inflation pressure, wheel diameter, and tyre construction or from 0.047 to 0.060 for solid polyurethane wheels depending on hardness and wheel diameter [12, 13]. The variation of rolling resistance with inflation pressure for miscellaneous pneumatic bicycle tyres is seen in Figure 14.

Comparing larger wheels to smaller wheels, the following general findings are noteworthy:

- As mentioned, a larger wheel allows for better traction due to a larger contact surface with the ground and a lower tyre energy loss compared to smaller wheels [12].
- A larger wheel can roll over minor obstacles and provide user comfort better than a smaller wheel, which may even abruptly stop if the obstacle is large enough [12].
- The bearing wear is reduced in a larger wheel compared to a smaller one, because a larger wheel allows the bearings to rotate slower - this also enables them to contribute less friction [12].
- A larger wheel reduces the degree of sinking in softer ground compared to smaller wheels [12].

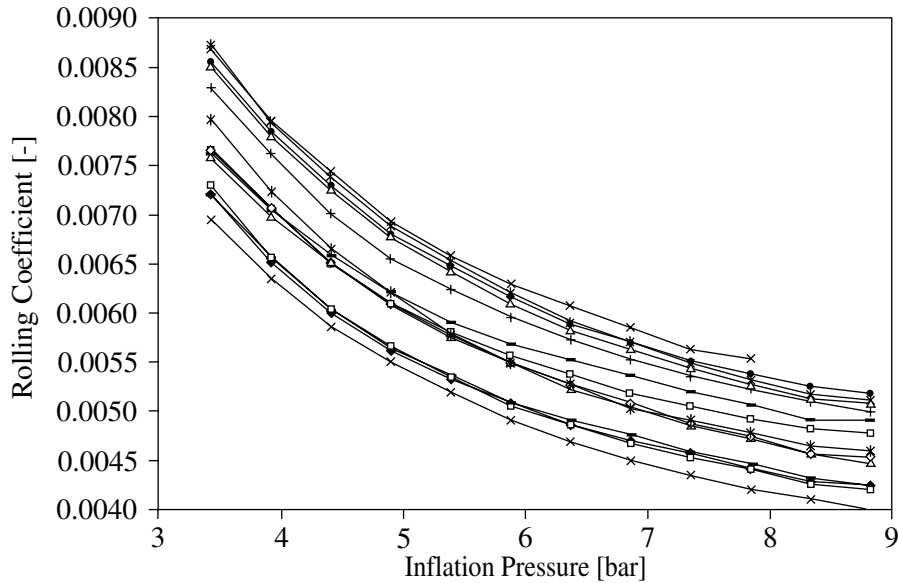


Figure 14: Variation in rolling resistance with inflation pressure for pneumatic bicycle tyres [12, 58].

- A larger wheel has a greater mass, which makes the wheel more stable but less manoeuvrable due to a greater mass moment of inertia, and drag contribution than smaller wheels [12].
- The frame is supported at a higher height with larger wheels for increased clearance.

1.4.9 SUSPENSION SYSTEMS

The suspension minimises the force transmitted when minor obstacles are encountered to provide greater comfort and improved traction by keeping the wheels in contact with the ground, especially for smaller wheels. The factors contributing towards the total suspension are the user adaptability, suitable tyres, and optional independent suspension system [12, 24]. Essentially, the user is able to control their upper-body motion and stiffness to absorb significant impacts as comfortably as possible; the tyres can partially absorb small irregularities without transferring forces to the frame and user; and a suspension system utilises sprung and damped elements to react to and reduce the impulses from shocks [12, 24]. Overall, the user adaptability has the greatest suspension capacity [12].

It is necessary to distinguish whether a suspension system is required and, if so, the type of suspension system for operation on asphalt, pavement, cement, gravel, or flat soil. Examples of typical suspension systems implemented on various vehicles and devices are seen in Figure 15. These suspension systems consist of a pivot or telescopic arrangement, where a helical compression spring isolates the parts of the system so the transferred shocks are reduced and a dashpot dissipates energy by critically or over damping the system to prevent oscillations [24]. This damping basically converts the kinetic energy of the spring into heat and can be achieved through viscous friction by forcing oil through small orifices or using inherent material properties with elastic deformation [24].

For vigorous off-road conditions with major obstacles, a suspension system is definitely recommended to improve comfort but also reduce the forces exerted on the frame. For normal road conditions

with minor obstacles, a suspension system is unnecessary as the shocks will be inconsequential. However, particularly for pavement, gravel, and flat soil, there are arguments for whether or not suspension should be implemented. While being used on rough off-road conditions, hybrid, gravel, touring, and cyclo-cross bicycles typically do not have suspension systems due to their large wheels over 507mm, as with the Trek Checkpoint AL 4 or BMC Crossmachine CX01, because omitting the suspension system greatly reduces mass, maintains reliable braking, and improves performance while lowering cost. Due to the small wheels around 216mm, skateboards for mountain boarding often require suspension in some form integrated into the trucks which increases cost. Scooters and wheelchairs rarely feature suspension because they are generally only aimed at use on smooth surfaces.

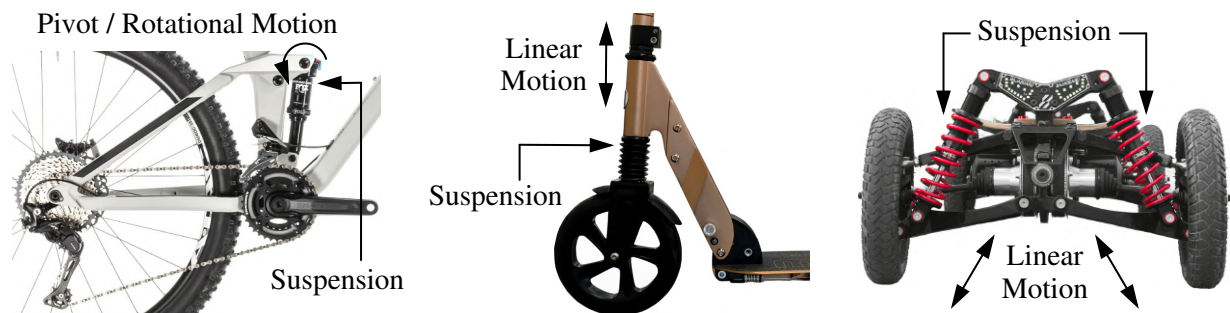


Figure 15: Suspension on a bicycle (left), scooter (middle), and skateboard (right) [28, 59, 60].

So, a fine-tuned suspension system will offer greater comfort and reduce the forces exerted on the frame, but there will be a significantly greater mass, decreased performance, higher cost, and more complex design. Thus, for operation on asphalt, pavement, cement, gravel, or flat soil, it is concluded that a vehicle or device with small wheels less than approximately 428mm in diameter will most likely require a suspension system for optimal comfort, while a vehicle or device with larger pneumatic wheels should offer adequate comfort without a suspension system - if the vehicle or device has solid wheels, then a suspension system is also advisable as the wheel will provide little relief.

1.4.10 ELECTRIC PROPULSION

Considering the methods of electric propulsion, brushed and brushless DC motors are easily capable of achieving the desired performance, while synchronous, induction, and other types of motors are uncommon, because they often require additional components to accommodate alternating current (AC) without explicit advantages [31]. The physical difference between brushed and brushless DC motors, shown with the basic constructions in Figure 16, is the location of the coils, magnets, and delivering of current, where a brushed DC motor consists of permanent magnets creating a magnetic field as the stator to cause the rotation of excited coils as the rotor, while a brushless DC motor utilises the sequential excitation of coil pairs as the stator to create a rotating magnetic field to rotate a permanent magnet as the rotor. A brushed DC motor offers simple control, but it may have a low efficiency around 75% to 80%, large size, and wear of the brushes leading to lower efficiency, arcing, and dust residue [13, 31]. Conversely, a brushless DC motor usually has a higher efficiency around

85% to 90%, better heat dissipation, lower rotor inertia, and less wear, but it is more complex to control with rotary encoders or Hall effect sensors to determine the rotor position [13, 31].

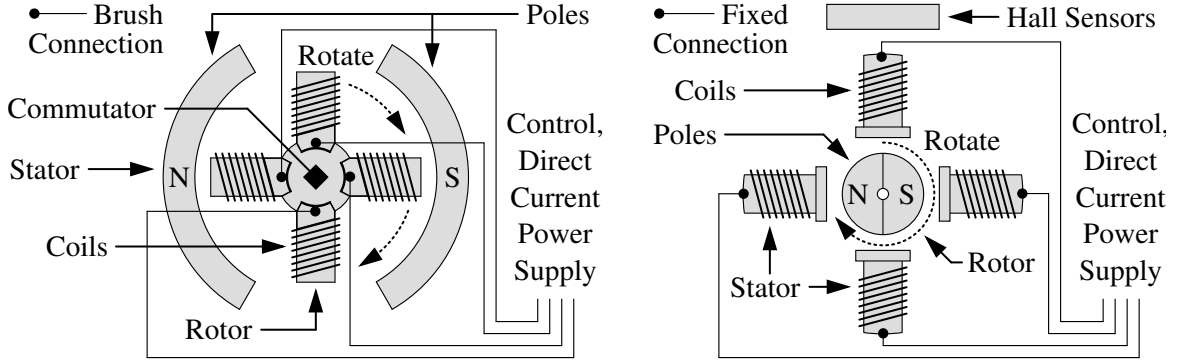


Figure 16: Comparison between the construction of brushed (left) and brushless (right) DC motors.

These motors are usually implemented as hub motors or mid-drive systems, where the performance may vary with different advantages and disadvantages. For reference and to compare performance for a continuous rated power of 250W, an electric bicycle hub motor can typically generate a maximum torque of 35N.m to 111N.m depending on whether the motor is gearless or geared with a mass from 3.5kg to 5.1kg and nominal angular speeds up to 210rev/min, as based on the Heinzmann Direct-Power, CargoPower, and Classic series [61]; while electric bicycle mid-drive systems can typically generate a maximum torque of 40N.m to 63N.m (without the implementation of gear ratios) with a mass from 2.9kg to 4.0kg and nominal angular speeds between 90rev/min and 120rev/min, as based on the Bosch Active and Performance series [62]. These values will vary for other vehicles or devices but the general comparison will remain fairly similar. Notably, regenerative braking can be implemented for a gearless hub motor to increase efficiency and increase braking potential, but it cannot be used for a mid-drive system since the wheel can only be rotated forward by the crankset.

The power requirement of electric propulsion, which is also applicable to manual propulsion, is given by the power needed to accelerate while overcoming drag resistance from the air, weight resistance from the slope, and rolling resistance from the ground [12, 13, 31]. The components of drag, weight, and rolling resistance are given in Equation 2 to Equation 4 respectively. The nature of these components show that, on flat ground at low speeds less than 10km/hr, rolling resistance consumes the most power ($P_w = 0$ and $P_r > P_d$); on flat ground at high speeds greater than 10km/hr, drag resistance consumes the most power ($P_w = 0$ and $P_d > P_r$); and on slopes with uphill gradients, weight resistance consumes the most power ($P_w > P_r$ and $P_w > P_d$) [12, 31]. There may also be power losses due to bumps and vibrations, but these losses are minimal compared to the other losses [12].

$$F_d = \frac{1}{2} \rho C_d (v + v_w)^2 A \rightarrow P_d = F_d v = \frac{1}{2} \rho C_d (v + v_w)^2 A v \quad (2)$$

$$F_w = mg \sin(\theta) \rightarrow P_w = F_w v = mg \sin(\theta) v \quad (3)$$

$$F_r = C_r mg \cos(\theta) \rightarrow P_r = F_r v = C_r mg \cos(\theta) v \quad (4)$$

Where F_d , drag resistance force, N; ρ , density, kg/m^3 ; C_d , drag coefficient; v , velocity, m/s; v_w , wind velocity, m/s; A , frontal area, m^2 ; P_d , drag resistance power, W; F_w , weight resistance force, N; m , mass, kg; g , gravitational acceleration, 9.81m/s^2 ; θ , gradient angle, rad; P_w , weight resistance power, W; F_r , rolling resistance force, N; C_r , rolling coefficient; and P_r , rolling resistance power, W.

As experimentally found by Muetze and Tan [31] from a brushed DC hub motor in an electric bicycle, the typical power requirements are seen in Figure 17 with variations of user mass, climbing gradient, and wind speed. The results from operating in a city setting were also gathered, as shown in Table 4.

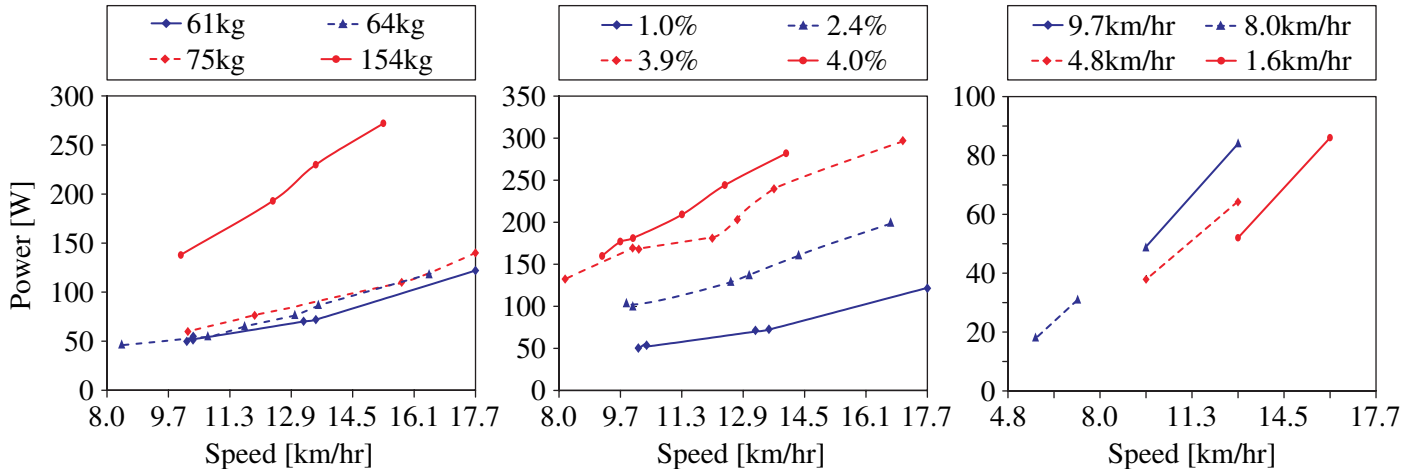


Figure 17: Experimental variations in motor power usage at different speeds for various user masses (left), climbing gradients (middle), and average incoming wind speeds (right) on a 20kg electric bicycle [31]. For the climbing gradient and wind speed results, the mass of the user was 61kg [31].

Table 4: Experimental results for operation in a typical city setting [31].

	User 1	User 2	User 3	User 4
User Mass [kg]	50	75	85	95
Average Power [W]	35.6	133.9	66.3	179.0
Maximum Power [W]	204.0	389.1	368.6	857.0
Average Torque [N.m]	4.7	8.2	5.9	9.9
Maximum Torque [N.m]	27.9	40.8	26.4	50.2
Average Velocity [km/hr]	8.7	20.4	12.2	20.9
Maximum Velocity [km/hr]	14.8	33.6	29.4	39.0
Operational Time [min]	18	16	22	25
Energy Expenditure [W.hr]	11.9	35.7	24.3	77.6

Considering the energy storage, it is only reasonable to consider a battery converting chemical energy into electrical energy with an anode, cathode, and electrolyte, because other energy storage or on-board energy generation methods (such as supercapacitors, engine generators, fuel cells, photovoltaic

panels, or mechanical means with potential energy) will not offer reliable performance with the necessary amount of energy, are not as readily available and flexible, have higher costs to purchase and/or operate, and may have significant obstructions on other system components due to large dimensions and/or mass [63]. For the type of the battery, lead-acid and nickel-cadmium batteries have steep performance degradation over time and serious hazardous and environmental issues if mishandled. As a result, it is preferable for nickel-metal hydride or lithium-ion batteries to be used for better performance, longer life, less environmental risk, and improved quality, although the purchase cost may be higher [8, 9]. The capacity of a battery is described by the conversion of electrical energy to rotational kinetic energy at the motor and can be related to range and speed through the conservation of energy.

1.4.11 MATERIAL PROPERTIES

From the review of existing vehicles and devices, the relevant materials appear to be aluminium, steel, and polyurethane. Additionally, due to their unique and useful properties, other common materials are also considered including titanium, stainless steel, and various plastics. The properties for the general classification of these materials are shown in Table 5 with fatigue characteristics in Figure 18.

Table 5: Expected properties for the relevant materials based on general classification [64].

	Density [kg/m ³]	Elastic Modulus [GPa]	Yield Strength [MPa]	Ultimate Strength [MPa]	Fracture Toughness [MPa.√m]
Aluminium Alloys	2500-2900	68-82	30.0-500	58.0-550	22-35
High Carbon Steel	7800-7900	200-215	400-1155	550-1640	27-92
Medium Carbon Steel	7800-7900	200-216	305-900	410-1200	12-92
Low Carbon Steel	7800-7900	200-215	250-395	345-580	41-82
Stainless Steel	7600-8100	189-210	170-1000	480-2240	62-280
Titanium Alloys	4400-4800	90-120	250-1245	300-1625	14-120
Natural Rubber Elastomers	920-930	0.002-0.003	20.0-30.0	22.0-32.0	0.15-0.25
Butyl Rubber Elastomers	900-920	0.001-0.002	2.0-3.0	5.0-10	0.07-0.1
ABS Thermoplastics	1010-1210	1.10-2.90	18.5-51.0	27.6-55.2	1.19-4.30
PVC Thermoplastics	1300-1580	2.14-4.14	35.4-52.1	40.7-65.1	1.46-5.12
Polyurethane Elastomers	1020-1250	0.002-0.003	25.0-51.0	25.0-51.0	0.2-0.4
Polyurethane Thermoplastics	1120-1240	1.31-2.07	40.0-53.8	31.0-62.0	1.84-4.97
Phenolic Thermosets	1240-1320	2.76-4.83	27.6-49.7	34.5-62.1	0.79-1.21

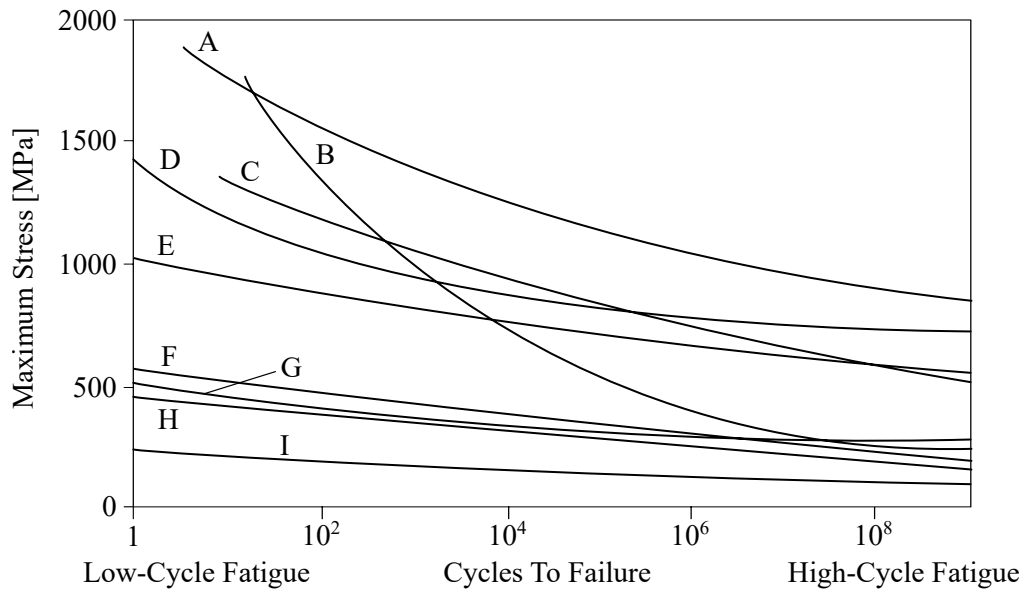


Figure 18: Fatigue characteristics for the relevant materials [12]. A = Kevlar and epoxy, B = S-glass and epoxy, C = graphite and epoxy, D = steel AISI 4130, E = titanium IMI 318, F = aluminium 7075-T6, G = medium-carbon steel, H = aluminium 2024-T6, and I = magnesium.

1.4.12 COMPLIANCE STANDARDS AND REGULATIONS

Unfortunately, there appears to be no direct regulations with regards to electric skateboards, scooters, wheelchairs, and roller skates for personal transportation and operation without the need for an official license and registration in South Africa. The only regulations present are applicable to electric bicycles. However, with new designs entering the market, it can reasonably be assumed that similar regulations will also be applied to electric skateboards, scooters, wheelchairs, and roller skates.

In South Africa, the South African Bureau of Standards (SABS) defines an electric bicycle in SANS 311:2007, where it is stated that “cycles equipped with an auxiliary electric motor that have a maximum continuous rated power of 250W, of which the output is progressively reduced and finally cut off as the vehicle reaches a speed of 25km/hr or sooner” are not classified in any vehicle category and can be regarded with the same regulations as traditional bicycles [65].

For comparison, the relevant regulations in other regions are summarised in Table 6. This summary is based on the overall regulations with maximum power and speed, while there may be other details requiring further investigation. If the conditions are satisfied, the vehicle is regarded as a traditional bicycle; but if the conditions are not satisfied, the vehicle will be regarded as a form of motorcycle.

For traditional bicycles in South Africa, the regulations in the National Traffic Act 93 of 1996 state that the bicycle must have a mass less than 40kg, is not allowed on highways, and must be equipped with at least one brake located on the rear wheel, while the user must wear an acceptable protective helmet for safety [70, 71]. The projections from the bicycle are limited to less than 600mm from the front wheel axle, less than 900mm from the rear wheel axle, and less than 450mm on either side of

Table 6: Summary of the electric bicycle regulations in various regions [8, 9, 13, 66, 67, 68, 69].

	Legislation	Maximum Power [W]	Maximum Speed [km/hr]
European Union	EU Regulation 168/2013	250	25
United States	Consumer Product Safety Commission	750	32
Canada	Motor Vehicle Safety Regulations	500	32
Australia	Australian Vehicle Standards	200	-
New Zealand	NZ Transport Agency Vehicle Classes	300	-
India	Automotive Research Association of India	250	30
China	National Standard: GB 17761-2018 Safety Technical Specification For Electric Bike	400	25

the wheels [70, 71]. It is also recommended but optional for the bicycle to feature a front white light with an intensity such that a diffused beam angled downwards strikes the ground at a distance greater than 3m and less than 30m, while a rear red light should also be fitted with a diffused beam parallel to the ground - alternatively, the bicycle may feature front white and rear red retro-reflectors [70, 71].

1.4.13 VEHICLE DYNAMICS

As mentioned, the main forms of resistance to propulsion include drag, weight, and rolling. The vehicle and user will experience drag resistance primarily in the form of bluff-body pressure drag because there is relative motion and accelerating into the incoming air, and skin-friction drag because of viscous forces from the air layered against the vehicle and user - however, the bluff-body pressure drag will be significantly greater than the skin-friction drag and the skin-friction drag can be reasonably neglected [12]. The effects of weight resistance become apparent on slopes with modest to significant gradients and occur because the weight of the vehicle and user has a component parallel to the slope. Reiterating, rolling resistance is present due to energy lost in elastic deformation of the wheels and possible deformation of the ground if it is relatively soft. The simplified free-body diagram in Figure 19 illustrates these forces using a bicycle, although this could be easily adapted for an arbitrary frame carrying the user and supported by wheels in contact with the ground.

With regards to acceleration at lower speeds, it is difficult to predict the acceleration during manual propulsion due to the highly variable input forces from different users - conversely, the steady-state input forces are similar at higher speeds and can be accurately calculated. For electric propulsion, it is usually easier to predict the acceleration characteristics since the motor will have consistent operation.

For a more accurate representation, there has been extensive research into the dynamics and stability of two-wheeled vehicles and devices with the development of complex equations of motion that describe the motion, especially during steering. This is often compared to being more difficult to control than the dynamics of an aircraft since the mass distribution on an aircraft is fairly constant, but the

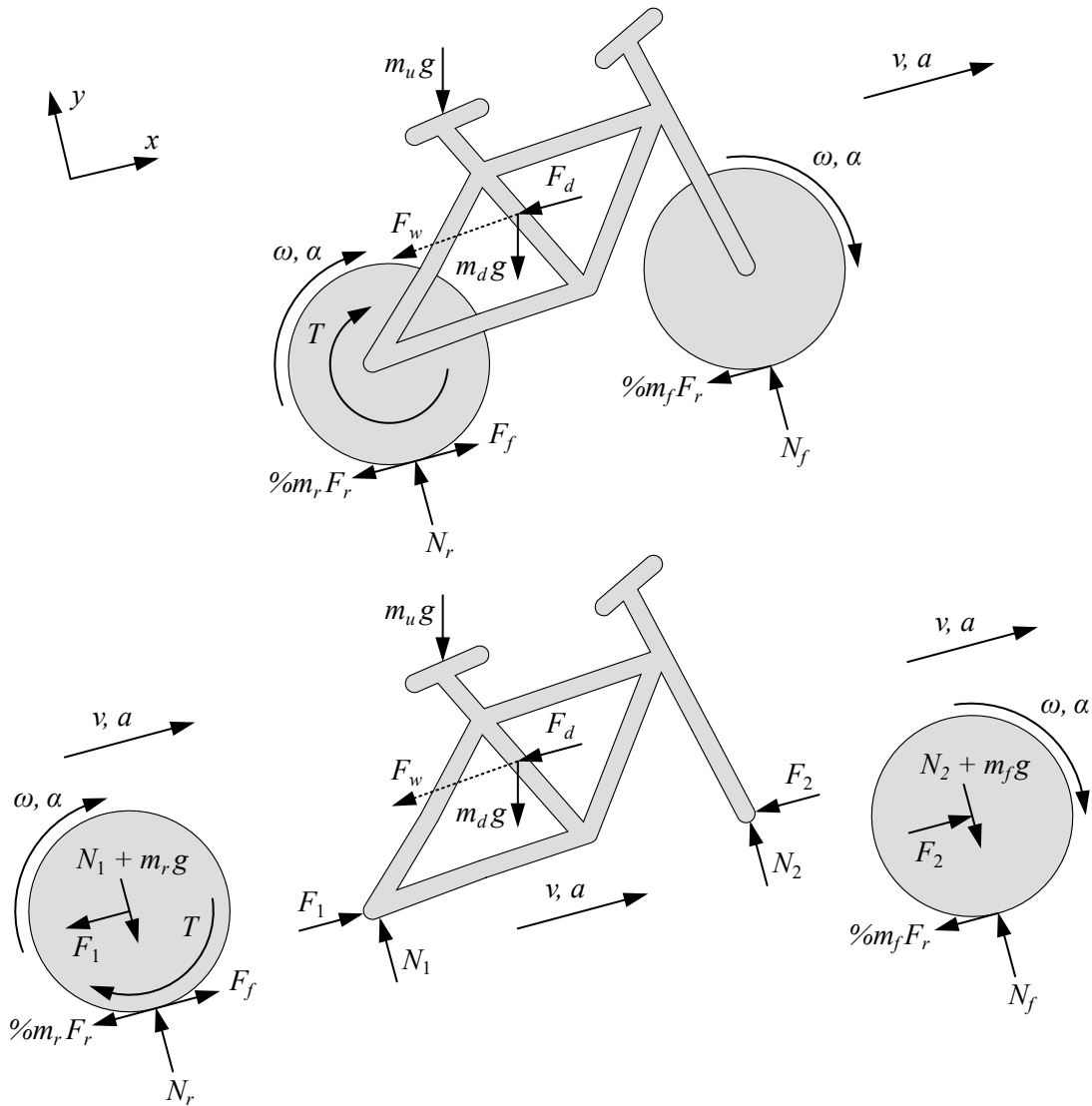


Figure 19: Simplified free-body diagram of a bicycle with drag, weight, and rolling resistance.

mass distribution on a two-wheeled vehicle is dominated by the mass of the user who is constantly shifting their centre of mass [12, 72]. From these formulations, it is presented that the balancing of a two-wheeled vehicle or device is accomplished through marginally changing the steering angle - locked steering denying wheel reorientation would be unbalanced almost as if the vehicle or device were at rest [12, 72]. With regards to design, as acknowledged by Wilson [72] for bicycles, “unfortunately the equations purporting to describe bicycle motion and self-stability are difficult and have not been validated experimentally, so design guidance remains highly empirical”. Although the final design may not resemble a two-wheeled vehicle or device, this does reveal that the design methods may be related to rules of thumb, observations, and gatherings from previous trials and errors.

1.5 TASK STATEMENT AS UNDERSTOOD

It is necessary to design a personal transportation vehicle or device for commuting that is able to support adult users up to 100kg and operate on asphalt, pavement, cement, gravel, or flat soil. The

total mass of the design should be less than 19kg, such that it can be lifted by the average user between 15 years and 50 years. The design must allow for fully independent electric propulsion, fully independent manual propulsion, or a combination of manual propulsion with electric propulsion, but the primary mode of operation is expected to be electric propulsion with assistance from manual propulsion when necessary in high speed winds and on slopes with excessive gradients. Since the purpose of the design is for commuting, the design should be optimised for frequent stopping and starting with typical speeds up to 25km/hr, although speeds higher may be possible.

So, with regards to only electric propulsion, the design must be able to achieve a range of at least 50km to exceed the daily commuting distance of a typical user and speed of 25km/hr within 5s on a level grade and 15km/hr within 5s on slopes with gradients up to 3% while experiencing wind up to 10km/hr. For only manual propulsion, the design should be able to achieve equivalent speeds to the electric propulsion and must be efficient with minimal effort so as to minimise fatigue. The combined propulsion should obtain speeds up to 30km/hr on a level grade and be able to climb slopes with gradients of 6% at speeds of 20km/hr with wind up to 10km/hr. Finally, the design should comply with the relevant regulations and standards to be considered legal and roadworthy.

2 PRELIMINARY CONCEPTS

Before the sub-system of the design are considered with the respective requirements and constraints, the overall preliminary concepts for the design are considered to refine and judge the most effective way in which to pursue the design development. This involves defining the ideas for preliminary concepts and evaluating these ideas through a conceptual evaluation with criteria based on the common notions and aims of existing designs and the requisite task. Once the most promising preliminary concept is found, the relevant product requirement specifications are defined in Section 3 for each sub-system of the design and the design will be further developed in Section 4.

2.1 CRITERIA

The following criteria will be used to evaluate and compare the preliminary concepts:

1. The design must efficiently convert the input work for manual propulsion.
2. The design must be capable of a high maximum speed with each type of propulsion.
3. The design must have a large range without the user experiencing fatigue.
4. The design must be able to brake as fast as possible.
5. The design must have responsive steering when manoeuvring.
6. The design must be as lightweight as possible.
7. The design must be easily maintainable by the user.
8. The skill level to operate the design must be sufficiently low for an average user.
9. The user must be as comfortable as possible while operating the design.
10. The design must be cost effective and affordable.

2.2 CONCEPT GENERATION

There is a limited number of combinations of common sub-systems for the preliminary concepts, where the variable sub-systems include the manual propulsion, steering, braking, and user position. The other sub-system, which can be adapted to fit the design, include the wheel positions to ensure the user is stable with the respective user position and steering; suspension system, if it is possible with the layout of the design; frame to link the necessary components; and electric propulsion integrated as effectively as possible (battery, controller, motor, and transmission).

The combinations of these sub-systems if presented with the Cycle, Skateboard, Scooter, Wheelchair, and Roller Skates concepts. These concepts are basically based on the ideas of manual propulsion through directly rotating a wheel or pushing with a foot against the ground; steering through angling a wheel relative to the other wheels to change the arc of the wheels, shifting the weight of the user to change the arc of the wheels, or rotating a wheel to change the relative velocity between the wheels; braking through mechanical brakes, dragging with a foot along the ground to create resistance, or directly slowing the rotation of a wheel (along with electrical means); and positioning the user as sitting or standing. In the following concept explanations, the generalised descriptions provide the overall ideas of the concepts, while the figures present a possible implementation of the concepts.

Also, it should be noted that other possible combinations of the sub-systems are not considered as they are rationally proven to be unconventional layouts where the average user cannot efficiently and comfortably provide manual propulsion with accurate steering (a high degree of skill is required). In other words, these combinations are significantly inferior compared to the mentioned combinations. For example, steering by shifting the weight of the user with manual propulsion through directly rotating a wheel (in the form of a unicycle) can be challenging to learn and operate efficiently.

2.2.1 CYCLE CONCEPT

The Cycle concept has a frame between more than one wheel, as illustrated in Figure 20 with two wheels. Manual propulsion is provided by rotating one or more of the wheels with pedals, while steering is managed by angling one or more of the wheels relative to the other wheels to change the arc of the wheels. For optimal comfort, the user is most likely to be seated with their hands on a handlebar performing the steering and their feet performing pedalling, where it may also be possible for the user to stand on the pedals. For safety, braking will rationally be performed by mechanical brakes with controls on the handlebar for convenient access. As decided, suspension will be unnecessary.

2.2.2 SKATEBOARD CONCEPT

The Skateboard concept, as seen in Figure 21, features enlarged wheels offering support and a deck or platform on which the user stands. Manual propulsion is achieved by balancing on the deck with one foot and pushing against the ground with the other foot, which also allows for braking when the user drags the pushing foot along the ground. Steering is possible through the user shifting their

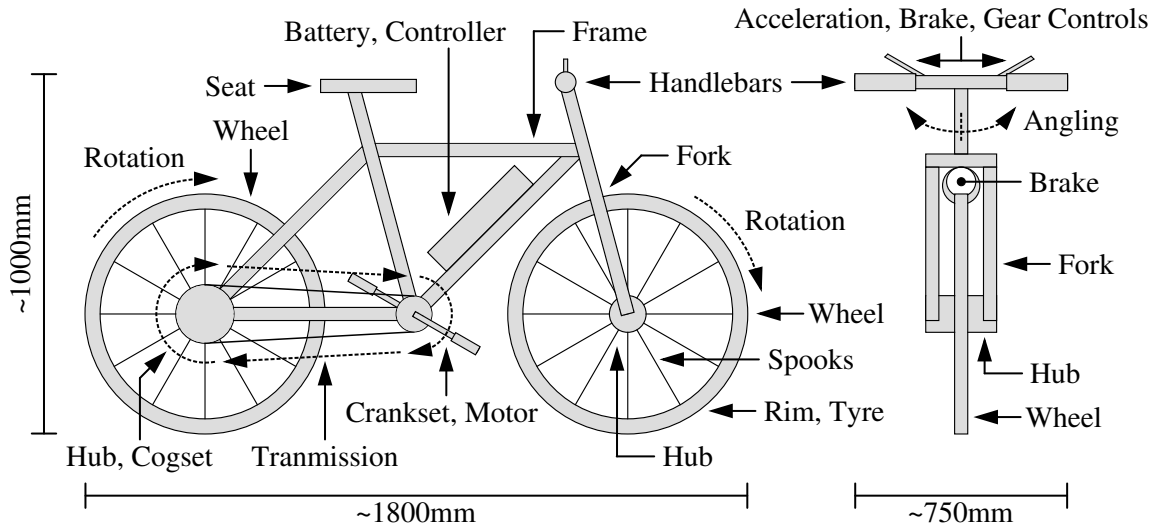
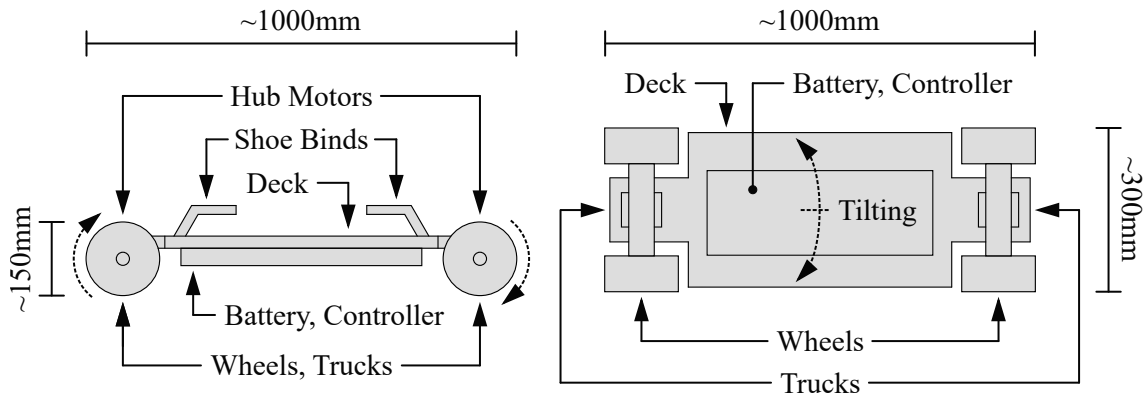


Figure 20: Schematic of the Cycle concept, with the side view (left) and front view (right).

weight between the sides of the deck such that the wheels on the inside of the turn move together and the wheels on the outside of the turn move apart, due to a pivot and the bushings in the trucks. By increasing the height of the deck, a basic suspension system may also be introduced within the trucks. It is also possible to include binds, which the user can use to secure themselves to the deck and help steer by easily lifting the board (although, this may make manual propulsion more difficult).



(Electric propulsion control provided from the user via a hand-held remote).

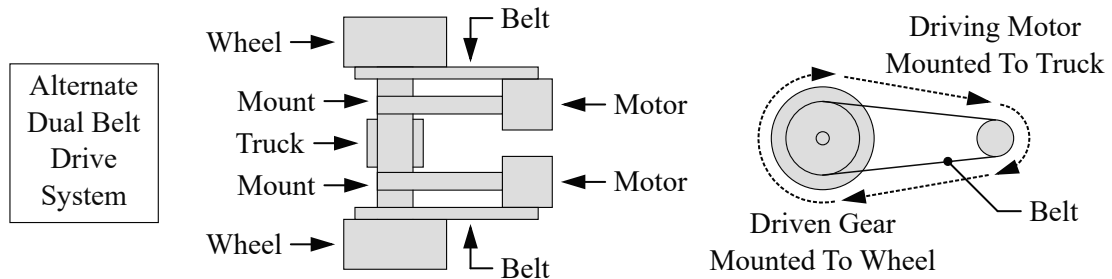


Figure 21: Schematic of the Skateboard concept, with the side view (top left) and bottom view (top right) and an illustration of an alternate electric propulsion system (bottom).

2.2.3 SCOOTER CONCEPT

The Scooter concept also has front and rear wheels and utilises a deck or platform on which the user stands with manual propulsion achieved through pushing against the ground with one foot. However, steering is applied by angling the front wheels relative to the rear wheel to change the arc of the wheels. Braking can be implemented with a brake pad on a pivot above the rear wheel that is lowered to contact the wheel, dragging a foot along the ground, or mechanical brakes integrated into the wheels. It may also be possible to integrate suspension into the front fork, while using larger wheels to reduce the effects of obstacles. An conception of the Scooter is seen in Figure 22.

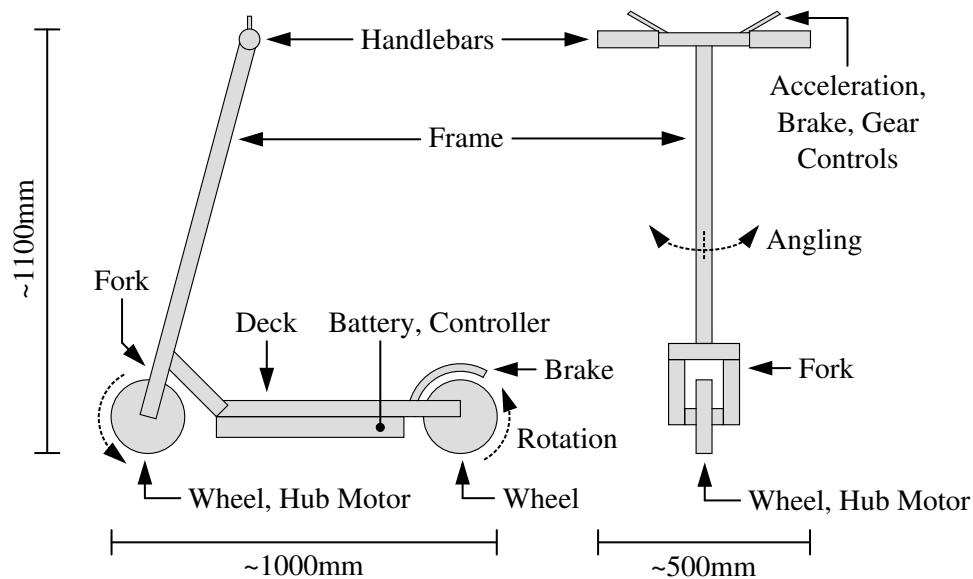


Figure 22: Schematic of the Scooter concept, with the side view (left) and front view (right).

2.2.4 WHEELCHAIR CONCEPT

For the Wheelchair concept in Figure 23, the user is seated between more than one wheel and executes manual propulsion by directly rotating one or more of the wheels. The user is then able to steer by controlling the rate of rotation of the wheels in an attempt to change the relative rate of rotation between the wheels; and brake by decreasing the rate of rotation of the wheels or using mechanical brakes attached at the wheels. There will also be enough space for a suspension system linking the wheels to the frame, if deemed necessary. (It is emphasised that the Wheelchair is not necessarily for disabled individuals, but it is proposed as a means of personal transportation like the other concepts).

2.2.5 ROLLER SKATES CONCEPT

As seen in Figure 24, the Roller Skates concept offers a unique alternative, where wheels are fastened to each foot of the user with a frame and straps, so the user does not have to change their shoes when using the Roller Skates. The user is then able to stand and perform manual propulsion, braking, and steering by manoeuvring the wheels through conventional roller skating techniques of lifting, pushing, and angling the wheels. Unfortunately, it is unlikely for it to be possible to incorporate suspension

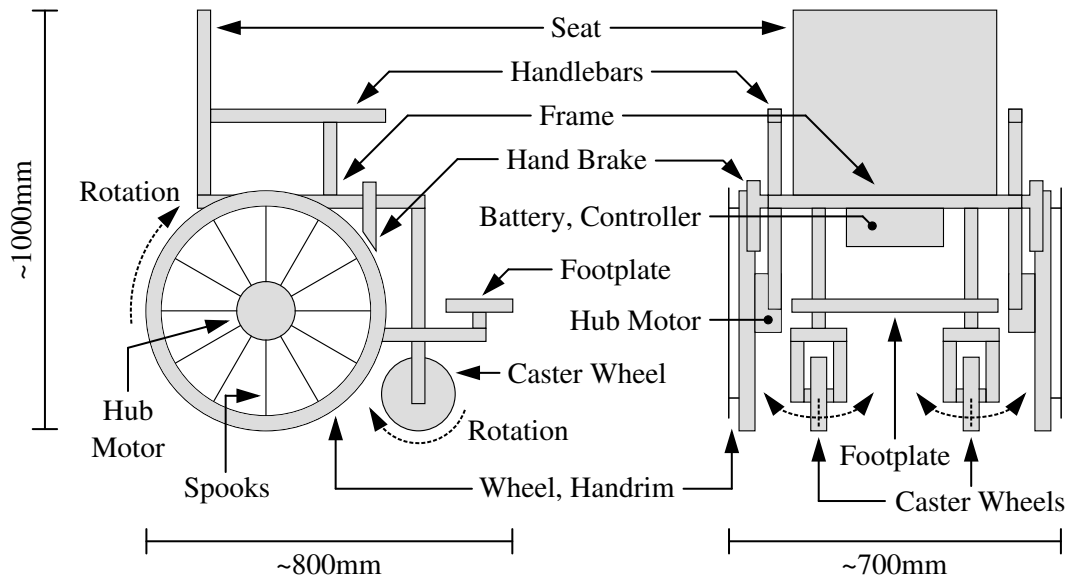


Figure 23: Schematic of the Wheelchair concept, with the side view (left) and front view (right).

due to the lack of space and need for the Roller Skates to be light so that they can be manoeuvred, but this may not be an issue since the Roller Skates can easily evade obstacles.

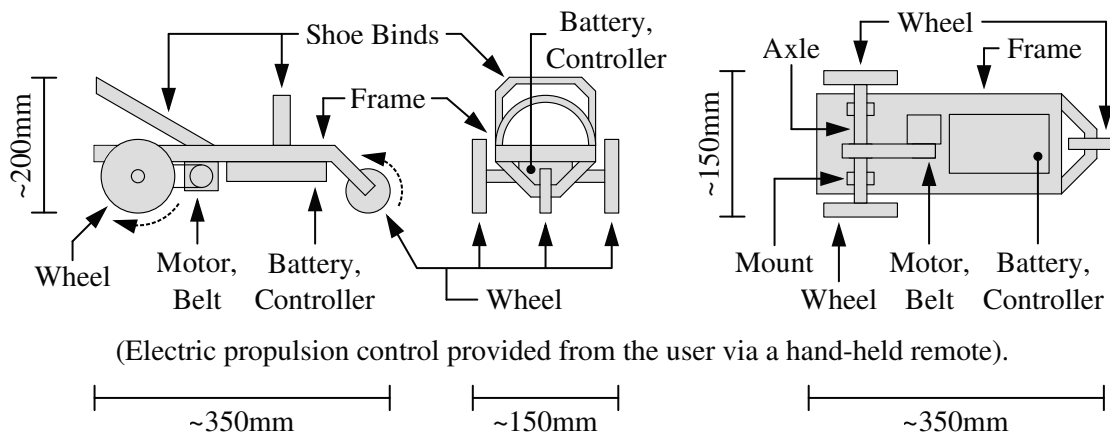


Figure 24: Schematic of the Roller Skates concept, with the side view (left), front view (middle), and bottom view (right). (A single Roller Skate is shown, but it is necessary for a pair of Roller Skates).

2.3 CONCEPT EVALUATION

Because the importance of each criterion is not equal relative to the purpose of the design, it is necessary to use a weighting matrix to determine the order of importance or weight of the criteria, where each criterion is individually compared against the other criteria to find the more important criterion in the comparison. With the weighted criteria, it is possible to evaluate which concept to pursue into further development by scoring each preliminary concept with the criteria points.

The resulting weighting matrix is shown in Table 7. The upper-tier ratings include the range, braking, speed, and steering qualities of the concepts. The range, with regards to the manual range before the user becomes exhausted and the available electric range, is rated as the most important criterion,

because this is a primary concern of personal transportation and directly associated with aspects of user fatigue, trip time (assuming the user is able to travel at a higher average speed with a combination of manual and electric propulsion), safety, alterations to a planned trip, availability for unplanned trips, possible use cases for longer trips, and overall wider adoption. The criterion rated second is the available braking potential, because this is directly associated with the safety of the user where it is critical to be able to brake quickly and carefully to avoid accidents and injury. The next operational function considered is the maximum speed with each type of propulsion, which is rated third since it is essential in improving convenience by decreasing trip time. The steering ability when manoeuvring is rated fourth, because this will allow for flexibility when navigating on ragged terrain to avoid large obstacles and safety when performing sharp turns at higher speeds.

The middle-tier ratings include the operating skill level, efficiency with manual propulsion, and weight of the concepts. A sufficiently low operating skill level is rated fifth, since this is crucial for ease of use and successful adoption, but not directly related to the purpose of personal transportation and offers no performance advantages. The efficiency in converting the input work to manual propulsion is rated sixth, because this will allow for the user to input a minimum amount of effort to achieve equivalent performance, which will result in less fatigue. Subsequently, the need for the design to be lightweight is rated seventh, because a lower mass will slightly improve performance (this is a slight improvement since the user is expect to already be significantly heavier than the design) but it will definitely have an influence on the ease of lifting and storing the design when it is not in use.

The lower-tier ratings include the maintainability, user comfort, and cost of the concepts. The ease of maintenance is rated eighth, as this is preferable so that it is simple to repair the design with readily available parts after wear has occurred from continuous use. The comfort of the user is

Table 7: Assessment of the preliminary criteria importance based on a weighting matrix. For the individual comparisons, it should be noted that if $X > Y$ and $Y > Z$, then $X > Z$ automatically.

Label	Criteria	Weighting Matrix Comparing Importance										Weight	Percent
A	1. Manually Efficient	A	B	C	D	E	A	A	H	A	A	5	9.1%
B	2. High Maximum Speed		B	C	D	B	B	B	B	B	B	8	14.5%
C	3. Large Range			C	C	C	C	C	C	C	C	10	18.2%
D	4. Brake As Fast As Possible				D	D	D	D	D	D	D	9	16.4%
E	5. Responsive Steering					E	E	E	E	E	E	7	12.7%
F	6. Lightweight						F	F	H	F	F	4	7.3%
G	7. Easily Maintainable							G	H	G	G	3	5.5%
H	8. Low Operating Skill Level								H	H	H	6	10.9%
I	9. User Comfort									I	I	2	3.6%
J	10. Cost Effective										J	1	1.8%

rated ninth, but it still carries importance since it is related to the operating smoothness and quality, which are important for user satisfaction and adoption. Finally, the need to be cost effective and affordable is rated tenth, because it is preferable to have good performance at a higher cost such that user satisfaction is maximised, although it may be at the expense of increased adoption.

Subsequently, the final concept scoring is shown in Table 8, with the following scoring levels:

- 0 = Does Not Comply
- 1 = Deficient
- 2 = Below Average
- 3 = Acceptable
- 4 = Good
- 5 = Perfect

Also, since each concept has electrical components allowing for electric propulsion and regenerative braking, the performance of these components in the evaluation is based on the availability of space for the components, effect on manual propulsion and other user operations, and expected values from existing designs. Specifically, the electric propulsion is limited by regulations and the achievable speed with electric propulsion may be similar for each concept. So, the concern of the criteria for achieving a high maximum speed is primarily associated with the ability of manual propulsion to generate a high maximum speed, although obvious deterrents are still considered.

The lowest performing concept is the Roller Skates, which only scored 53% of the total score. This was primarily because of the expectations for a low electric range, due to a lack of available space; inferior braking ability, which requires a significant stopping distance to safely slow down from higher speeds; and moderately high skill level to operate, which may be unfamiliar to the majority of users. Furthermore, although the Roller Skates are expected to be lightweight and cost effective, its advantages are not viewed as important criteria relative to the main purposes of personal transportation.

Although having advantages and disadvantages in different areas, the Wheelchair and Skateboard achieved similar scores of 62% and 64% respectively. The Wheelchair was found to be unsatisfactory because it had a lack of manual range, since the arms of the user provide propulsion which can quickly cause fatigue; and poor manual efficiency, due to a high energy exertion to steer and brake. Essentially, the Wheelchair was seen to be focussed on user comfort when inactive and it did not have the optimal manual propulsion for able-bodied individuals. The Skateboard presents challenges because it requires a moderately high skill level to operate safely, and it also proved to be unsatisfactory in braking, because it is necessary to reduce speed in a slower manner and over a significant stopping distance such that the rider can remain stable on the deck and does not become uncontrollably unbalanced - notably, it did show promising advantages of responsive steering when lifting the board with the binds to quickly change direction and maintainability owing to the minimal amount of parts and traditional skateboard parts often being common and accessible.

Table 8: Evaluation of the preliminary concepts based on scoring with weighted criteria. (For the concept name contractions: Skate = Skateboard, Wheel = Wheelchair, and Roller = Roller Skates).

Criteria	Total Weight	Max. Weighted Score	Cycle		Skate		Scooter		Wheel		Roller	
			Score / 5	Weighted Score	Score / 5	Weighted Score	Score / 5	Weighted Score	Score / 5	Weighted Score	Score / 5	Weighted Score
1. Manually Efficient	5	25	5	25	3	15	3	15	1	5	4	20
2. High Maximum Speed	8	40	5	40	3	24	3	24	2	16	3	24
3. Large Range	10	50	5	50	3	30	3	30	4	40	1	10
4. Brake As Fast As Possible	9	45	4	36	2	18	5	45	3	27	2	18
5. Responsive Steering	7	35	4	28	5	35	4	28	3	21	3	21
6. Lightweight	4	20	1	4	4	16	3	12	3	12	5	20
7. Easily Maintainable	3	15	4	12	5	15	3	9	4	12	3	9
8. Low Operating Skill Level	6	30	3	18	2	12	5	30	4	24	2	12
9. User Comfort	2	10	4	8	3	6	4	8	5	10	3	6
10. Cost Effective	1	5	1	1	4	4	4	4	3	3	5	5
Total Score		275		222		175		205		170		145

The second best concept was the Scooter with a score of 75%. The Scooter showed superior braking, due to the available options while using the handlebars for stability, which include a brake pad on a pivot above the rear wheel (although, this may wear the rear wheel), dragging with a foot along the ground, mechanical brakes, and the possibility of easily stepping off in dire situations; and the observation that the use of a traditional scooter often comes naturally and requires minimal practice to become sufficiently capable. It also did not suffer any excessively negative disadvantages, but it did fail to excel with regards to electric range, because of a limit to the available space without the need for expansion to create space for additional capacity, which may then be cumbersome and decrease user comfort; manual range, due to the lack of mechanical advantage for manual propulsion which may cause fatigue on steep uphill gradients; maximum speed, since only one leg of the user is being used for manual propulsion while pushing; and a fair manual efficiency, assuming that there is a similar efficiency to that of a skateboard due to the similar method of manual propulsion through pushing (although, a small amount of energy may be retained since it is easier to balance on the deck due to support from the handlebars, but this was viewed as negligible).

Finally, the Cycle obtained the highest score at 81%, because of its substantial advantages in accomplishing a large range without user fatigue, due to the possibility of implementing a transmission system with various gear ratios for the manual propulsion; easily achieving a high maximum speed,

since both legs of the user are expected to provide manual propulsion; and extraordinary efficiency with a minimal loss of input work, due to the user being seated with a handlebar offering support while comfortably performing manual propulsion. Unfortunately, the Cycle concept did have minor disadvantages for expected weight and cost, which should be examined and minimised without impairing the more important criteria. This indicates that the Cycle is the most promising preliminary concept to pursue into further development and analysis.

3 PRODUCT REQUIREMENT SPECIFICATION

Since the Cycle was found to be the best preliminary concept, it is necessary to define the requirements, constraints, and criteria for the relevant sub-systems. The requirements and constraints will be used to judge whether the final design is successful, and the criteria will be used to guide the choices for and distinguished between the possible solutions to the sub-systems. The grouped sub-systems include the electric propulsion, manual propulsion, and structural components relative to the frame structure, wheel arrangement, steering, and user positioning. Unfortunately, the primary braking system will not be thoroughly designed as will be mentioned in Section 4.5.

3.1 ELECTRIC PROPULSION

The electric propulsion must fulfil with the following requirements:

- The design must allow for electric propulsion compounded with manual propulsion, such that it is possible to perform fully independent manual propulsion, fully independent electric propulsion, or a combination of manual propulsion and electric propulsion simultaneously.
- The performance must be measured relative to the average user with a mass of 76kg.
- The electric propulsion must be able to achieve a speed of 25km/hr on a level grade.
- The electric propulsion must be able to achieve 25km/hr in less than 5s when accelerating from rest on a level grade (average acceleration greater than 1.389m/s^2 over 5s).
- The electric propulsion must be able to climb slopes with gradients of 3% at speeds of 15km/hr.
- The electric propulsion must be able to achieve 15km/hr in less than 5s when accelerating from rest on slopes with gradients up to 3% (average acceleration greater than 0.8333m/s^2 over 5s).
- The electric propulsion must fully operate and still achieve the desired performance with a speed no less than 15km/hr under directly incoming wind resistance with speeds up to 10km/hr.
- The battery pack must use nickel-metal hydride or lithium-ion cells for environmental concerns.
- The battery pack must allow for a range over 50km with independent electric propulsion.
- The battery pack must have a life of at least 80% after 400 cycles.
- The battery pack must have a charging time less than 8hr from fully uncharged to reach full capacity while accounting for an efficiency loss of at least 20%.

The electric propulsion must comply with the following constraints:

- The electric propulsion must not affect the manual propulsion technique of the user.
- The electric propulsion must be limited to speeds less than or equal to 25km/hr.
- The electric propulsion must have a continuous rated power less than or equal to 250W.
- The battery pack must satisfy a design factor of 1.2 to ensure the desired capacity.
- The battery pack must be charged with an AC voltage input of 230V at 50Hz.
- The battery pack must be fully tamper-proof, such that the batteries are sealed in an enclosure.
- The battery pack must also have an enclosure that is flame retardant.
- The components must be electrically insulated with no exposed circuitry.
- The components must be able to operate between a temperature range from -10°C to 40°C.
- The components must have projections less than 450mm on either side of the wheels.
- The components must be dirt, dust, and splash resistance.

The following criteria will be used for the optimal development of the electric propulsion:

1. The design must be as efficient as possible.
2. The design must maximise performance.
3. The design must be as lightweight as possible.
4. The design must be flexibility integrated with the other sub-systems.
5. The design must allow for a stable mass distribution.
6. The design must be easy to maintain, repair, or replace.
7. The design must be simple to control.
8. The design must minimise additional drag.
9. The design must be cost effective.

3.2 MANUAL PROPULSION

The manual propulsion must fulfil with the following requirements:

- The performance must be measured relative to the average user with a mass of 76kg.
- The manual propulsion will be operated by a single user for personal transportation purposes.
- The manual propulsion must be able to achieve a speed of 25km/hr on a level grade.
- The manual propulsion must be able to climb slopes with gradients of 3% at speeds of 15km/hr.
- The manual propulsion must be able to still achieve the desired performance with a speed no less than 15km/hr under directly incoming wind resistance with speeds up to 10km/hr.
- The combined propulsion must be able to achieve a speed of 30km/hr on a level grade.
- The combined propulsion must be able to climb slopes with gradients of 6% at speeds of 20km/hr.

- The combined propulsion must fully operate and still achieve the desired performance with a speed no less than 20km/hr under directly incoming wind resistance with speeds up to 10km/hr.

The manual propulsion must comply with the following constraints:

- The manual propulsion must not hinder the performance of the electric propulsion.
- The manual propulsion must demand a continuously sustained power no greater than 240W.
- The manual propulsion must demand a continuously sustained input force no greater than 200N.
- The manual propulsion must have a sustained cadence between 50rev/min to 110rev/min.
- The manual propulsion must have parts satisfying a design factor of 1.2 to ensure safe operation.
- The manual propulsion must have dimensions accommodating the average male and female users, with considerations for the 5th percentile and 95th percentile male and female.
- The manual propulsion must have a ground clearance of at least 100mm at the lowest point.
- The manual propulsion must follow common standards so that parts are repairable or replaceable.
- The components must have projections less than 450mm on either side of the wheels.
- The components must be dirt, dust, and splash resistance.

The following criteria will be used for the optimal development of the manual propulsion:

1. The design must transmit the input power efficiently.
2. The design must be as lightweight as possible.
3. The design must be durable with a long life.
4. The design must be flexibility integrated with the other sub-systems.
5. The design must be easy to maintain, repair, and replace.
6. The design must withstand shocks while operating.
7. The design must low likeliness of operating issues.
8. The design must be cost effective.

3.3 STRUCTURAL COMPONENTS

The structural components must fulfil with the following requirements:

- The design must seamlessly incorporate the manual and electric propulsion, without the need for modifications to individually access one of the methods or combine both of the methods.
- The total mass, including the other sub-systems of the design, must be less than 19kg, such that it can be lifted by an average male or female user between 10 years and 50 years.
- The frame and wheels must support user masses up to at least 100kg.
- The wheels must be able to operate on asphalt, pavement, cement, gravel, or flat soil.
- The steering mechanism must have a steering angle up to 60° on either side of the inline plane.

- The steering mechanism must have a steering torque of at least 5.3N.m.
- The steering mechanism must be capable of a turning radius of below 2.5m at a steering angle below 30° so that it is possible to turn around on a road about 5m wide.

The structural components must comply with the following constraints:

- The design must have a safety factor greater than 1.2 when analysed under extreme operating conditions with known loads, unless otherwise declared by a relevant standard.
- The frame must have deformations less than 1mm when statically analysed based on ideal operating conditions, to guard against uncertainties and large dynamic amplifications from shocks due to impacts from minor obstacles during actual operating conditions.
- The frame must have a safety factor greater than 10 when statically analysed based on ideal operating conditions, to guard against uncertainties and large dynamic amplifications from shocks due to impacts from minor obstacles during actual operating conditions.
- The frame must have a ground clearance of at least 100mm at the lowest point.
- The frame must have dimensions accommodating the average male and female users, with considerations for the 10th percentile and 90th percentile male and female.
- The steering mechanism must operate with an input force from 10N from each arm of the user.
- The design must have projections limited to less than 600mm from the front wheel axle, less than 900mm from the rear wheel axle, and less than 450mm on either side of the wheels.
- The design must follow common standards so that parts are repairable or replaceable.

The following criteria will be used for the optimal development of the structural components:

1. The design must be as lightweight as possible.
2. The design must be stable once mounted by the user.
3. The design must be simple to manufacture.
4. The design must allow for comfortable user ergonomics.
5. The design must minimise additional drag.
6. The design must have strong joints with minimum loss of strength.
7. The design must resist corrosion.
8. The design must be cost effective.

4 DESIGN DEVELOPMENT

To develop the design further, an iterative design process is pursued, where various possible solutions are considered and selected based on which will obtain the most successful results. Because it will require integration with the manual propulsion and structural components, the electric propulsion is considered first, so that the overlapping aspects can be accounted for in the development of the other

sub-systems - in other words, it is expected for the other sub-systems to be highly dependent on the electric propulsion, but the electric propulsion is much less dependent on these other sub-systems.

Next, the wheel arrangement will be considered to begin to define the structure of the design with the number, size, and type of wheels. With this information, the factors of the manual propulsion can be investigated with regards to the power input and transmission mechanisms. The frame and steering will be considered to accommodate the user positioning and finalise the construction and links between the sub-systems. Finally, a remark on the braking system will be mentioned.

4.1 ELECTRIC PROPULSION

The components for electric propulsion include the motor, battery pack, and controller, which need to be reviewed and specified. Specifically with the motor and battery pack, it is important for the components not to be over-specified or over-sized, as this may create adverse effects such as increased mass and produce difficult manual propulsion, while offering improved electric propulsion that is redundant due to the performance constraints or lack of applicability to personal transportation.

4.1.1 MOTOR

As illustrated in Figure 25, the possibilities for the arrangement of the motor include the Hub Drive, Mid-Drive, or Friction Drive. The Hub Drive uses a motor integrated as the hub of a front or rear wheel, which will allow for simple mounting identical to a typical wheel and low maintenance due to an enclosed direct drive, but it can have an increased mass and shift the centre of gravity [31]. The Mid-Drive uses a motor integrated into the crankset, where it is possible to utilise gear ratios through a power transmission for finer performance control, but it may require extra maintenance due to the increased number of parts relying on the power transmission [31]. The Friction Drive uses a motor attached to the frame with a roller in direct contact with a front or rear wheel, where the roller uses friction to rotate the wheel and provides a lightweight and compact solution, but it will apply additional wear to the tyre and can be significantly less efficient due to losses through slipping.

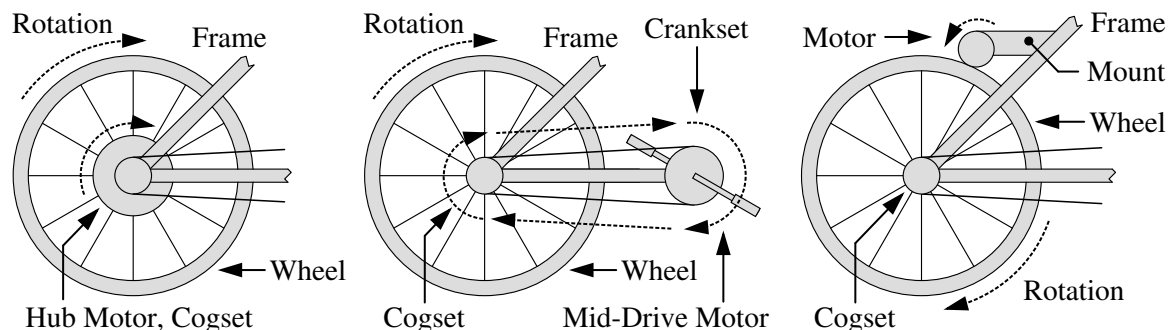


Figure 25: Schematics of the available arrangements of the motor, with possibilities for the Hub Drive (left), Mid-Drive (middle), and Friction Drive (right) each shown on a rear wheel.

With the reference to the expectations presented in Section 1.4.10, it is possible to weight the criteria and decide on the best motor arrangement by performing a conceptual evaluation in Table 9. In the criteria weighting, the performance, efficiency, and mass were seen to be the most essential, because they are central to achieving and maximising the requirements; flexible integration and simple control are also seen as significant criterion as these will be related to the compliance with other sub-systems which should be maximised to remove uncertainties and improve reliability; a contrast in mass distribution and drag effects is expected to be present but minimal, so these criteria are rated low to remove bias arising from only a minor difference; and the cost and ease of maintenance were less of a priority, because they do not directly benefit performance and are focussed on convenience.

As a result, the Hub Drive achieved the highest score of 80%, because it stands out with its potential for a direct drive and regenerative braking to increase efficiency, ability to be integrated without limiting the customisation of the other sub-systems, straightforward control with predictable behaviour, and capacity to be directly optimised for a consistent performance range. Although the Mid-Drive offers excellent maximisation of performance, efficiency with a typical operating range, and low-central mass distribution due to the integration with the power transmission, it scored 73% because it is unable to compete with regards to flexible integration, since it will fix the characteristics of the crankset and require the frame to have the necessary mounting points and shape without the possibility for customisation; control difficulty, where the user must still choose the correct gear ratio for best performance (this can be seen as a converse result of the maximisation of performance); maintenance, where there will be additional strain on the power transmission and there will be a limited

Table 9: Weighting matrix and evaluation of the possibilities for the arrangement of the motor.

Label	Criteria	Weighting Matrix									Total Weight	Percent Weight	Max. Weighted Score	Hub		Mid		Friction	
														Score / 5	Weighted Score	Score / 5	Weighted Score	Score / 5	Weighted Score
A	1. Efficient	A	B	A	A	A	A	A	A	A	8	17.8%	40	5	40	5	40	1	8
B	2. Max. Performance		B	B	B	B	B	B	B	B	9	20.0%	45	4	36	5	45	3	27
C	3. Lightweight			C	C	C	C	C	C	C	7	15.6%	35	2	14	3	21	5	35
D	4. Flexible Integration				D	D	D	D	D	D	6	13.3%	30	5	30	1	6	5	30
E	5. Mass Distribution					E	E	G	E	E	4	8.9%	20	2	8	5	20	3	12
F	6. Easy Maintenance						F	G	F	F	3	6.7%	15	4	12	2	6	3	9
G	7. Simple Control								G	G	5	11.1%	25	5	25	3	15	2	10
H	8. Minimise Drag									H	2	4.4%	10	5	10	5	10	3	6
I	9. Cost Effective										1	2.2%	5	4	4	2	2	3	3
	Total Score												225		179		165		140

collection of compatible replacement parts; and cost, which is expected to be the highest since the available motors are specialised. Unfortunately, the Friction Drive performed poorly in most aspects, due to the mediocre performance, low efficiency, and lack of predictable behaviour for control which is likely to arise from slipping at higher speeds and in wet conditions - it obtained a score of 62%.

To select a specific motor and with considerations for the wheel arrangement, the type of motor as a brushed or brushless DC motor is explored. As mentioned in Section 1.4.10 when considering equivalent performance, brushless DC motors are more reliable, durable, and efficient with low noise and electromagnetic interference due to the lack of a commutator and brushes; while brushed DC motors only provide the benefits of simpler control and a lower purchase cost, but they will experience more wear and require maintenance or replacement due to the friction of the brushes. Also, with recent improvements in hub motors, brushless DC hub motors have become readily available because of their solid performance and quality. Thus, it is recommended to source a brushless DC hub motor.

The maximum continuous rated power of the motor is considered to justify whether the requirements for independent electric propulsion can be fulfilled while adhering to the constraints. To find the required continuous rated power when the design is no longer accelerating, independent electric propulsion is considered on a level grade at 25km/hr with no incoming wind, on a level grade at 15km/hr with a 20km/hr incoming wind, and on a slope of 3% gradient at 15km/hr with no incoming wind. Through the conservation of energy, the resulting relationship for the consumption of power is summarised in Equation 5. Since the specific design parameters required to perform this estimation are not yet known, conservative assumptions are made with a constant air density of 1.2kg/m³, frontal area of 0.55m², drag coefficient of 1.2, and rolling coefficient of 0.008 with a total mass of 95kg from the maximum design mass of 19kg and average user mass of 76kg [12, 13]. These parameters will be checked against more specific values once the values can be more accurately estimated. It is also assumed that sufficient power is supplied to reach these steady-states of constant speed.

$$\sum_{i=1}^n F_i = 0 \rightarrow \sum_{i=1}^n P_i = 0 \rightarrow P_m = P_d + P_w + P_r \quad (5)$$

Where F_i , arbitrary force component, N; P_i , arbitrary power component, W; P_m , motor power, W; P_d , drag resistance power, W; P_w , weight resistance power, W; and P_r , rolling resistance power, W.

The results are a predicted continuous rated power of 184.4W on a level grade at 25km/hr with no incoming wind, 187.0W on a level grade at 15km/hr with a 20km/hr incoming wind, and 176.1W on a slope of 3% gradient at 15km/hr with no incoming wind. Since the allowable continuous rated power limit of the motor is 250W, there is still potential for improvement with regards to the possible speed, incoming wind, and slope under the mentioned cases. These additional cases are shown in Table 10 with the required power maximised to 250W, where the continuous torques to maintain 25km/hr varies from 9.126N.m to 11.19N.m for the common wheel sizes between 507mm (261.6rev/min) and 622mm (213.2rev/min). This indicates that the use of a motor with a continuous rated power of

250W will offer useful performance improvements, such as climbing steeper slopes up to 9% with higher incoming wind speeds, and should not be considered to be over-specified.

Table 10: Collection of maximum operating cases for a motor with a continuous rated power of 250W for a sustained period of time. The cases are based on different operating speeds (limited to a maximum of 25km/hr), wind speeds, slope gradients, and optimised to seek a total power of 250W.

Speed		Wind		Slope		Drag		Weight		Rolling		Total [W]
[km/hr]	[m/s]	[km/hr]	[m/s]	Grad.	[°]	[W]	Frac.	[W]	Frac.	[W]	Frac.	
25	6.94	5.6	2	0%	0	198.2	79%	0	0%	51.78	21%	250
15	4.17	27	7.35	0%	0	218.9	88%	0	0%	31.07	12%	250
10	2.78	42	11.7	0%	0	229.3	92%	0	0%	20.71	8%	250
25	6.94	0.1	0.03	1%	0.57	133.5	53%	64.72	26%	51.77	21%	250
15	4.17	23	6.28	1%	0.57	180.1	72%	38.83	15%	31.06	12%	250
10	2.78	39	10.8	1%	0.57	203.4	81%	25.89	10%	20.71	8%	250
22	6.11	0	0	2%	1.15	90.5	36%	113.9	45%	45.57	18%	250
15	4.17	18	5.09	2%	1.15	141.3	57%	77.65	31%	31.06	12%	250
10	2.78	36	9.93	2%	1.15	177.5	71%	51.76	21%	20.71	8%	250
19	5.35	0	0	3%	1.72	60.6	24%	149.5	60%	39.87	16%	250
15	4.17	13	3.72	3%	1.72	102.5	41%	116.4	47%	31.05	12%	250
10	2.78	32	8.96	3%	1.72	151.7	61%	77.63	31%	20.70	8%	250
13	3.65	0	0	6%	3.43	19.2	7.7%	203.6	81%	27.15	11%	250
10	2.78	20	5.44	6%	3.43	74.3	30%	155.0	62%	20.67	8%	250
10	2.78	0	0	9%	4.89	8.5	3.4%	220.9	88%	20.63	8%	250

Subsequently, the acceleration before reaching steady-state can be considered with Equation 6 and simplified in Equation 7 which can be solved using numerical integration. This utilises an effective mass to account for the translational kinetic energy of the design and user as well as the rotational kinetic energy of each wheel, as described by Equation 8. To generate an approximation, the rotation of the wheels can contribute up to 30% of the design mass to the effective mass, which results in an estimate added mass of 5.7kg when considering the maximum design mass of 19kg [12, 13].

With this, the necessary peak rated power when accelerating from rest can be predict, which is seen in Figure 26 with 250W, 400W, and 600W values for various cases. Evidently, 250W is not acceptable and results in a time of 17.31s to accelerate up to 25km/hr on a level grade with no incoming wind, but 600W allows for a time of 4.809s to reach 25km/hr. With an increased slope up to 3% and incoming wind up to 10km/hr, it is also seen that 600W allows for acceleration up to 15km/hr in 1.631s. Thus, the selected motor should have a peak rated power around 600W to achieve satisfactory performance, although a greater value will allow for better performance on slopes and with incoming wind.

$$\sum_{i=1}^n F_i = m \frac{dv}{dt} \rightarrow \sum_{i=1}^n P_i = m_{eff} v \frac{dv}{dt} \rightarrow P_m - P_d - P_w - P_r = m_{eff} v \frac{dv}{dt} \quad (6)$$

$$\therefore \int_{v_1}^{v_2} \frac{m_{eff} v}{P_m - \frac{1}{2} \rho C_d (v + v_w)^2 A v - mg \sin(\theta) v - C_r mg \cos(\theta) v} dv = \int_{t_1}^{t_2} dt \quad (7)$$

$$E_k = \sum_{i=1}^n \frac{1}{2} m v^2 + \sum_{i=1}^n \frac{1}{2} I \omega^2 \approx \frac{1}{2} m_{eff} v^2 \rightarrow P_k = \sum_{i=1}^n m v \frac{dv}{dt} + \sum_{i=1}^n I \omega \frac{d\omega}{dt} \approx m_{eff} v \frac{dv}{dt} \quad (8)$$

Where F_i , arbitrary force component, N; m , mass, kg; v , velocity, m/s; t , time, s; P_i , arbitrary power component, W; m_{eff} , effective mass, kg; P_m , motor power, W; P_d , drag resistance power, W; P_w , weight resistance power, W; P_r , rolling resistance power, W; ρ , density, kg/m³; C_d , drag coefficient; v_w , wind velocity, m/s; A , frontal area, m²; g , gravitational acceleration, 9.81m/s²; θ , gradient angle, rad; C_r , rolling coefficient; E_k , kinetic energy, J; I , mass moment of inertia, kg.m²; ω , angular velocity, rad/s; and P_k , kinetic power, W.

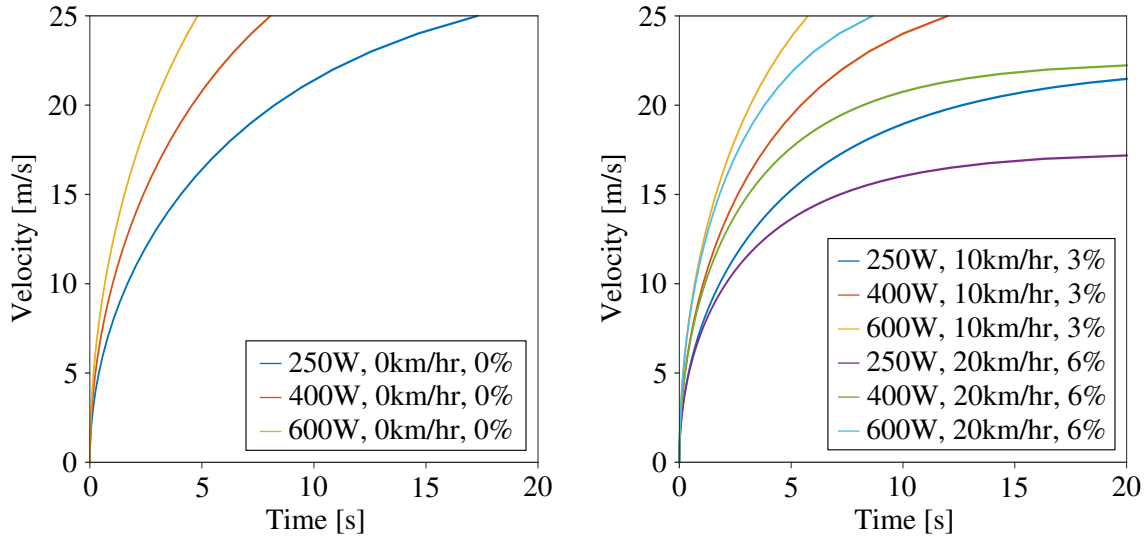


Figure 26: Comparison between peak rated power of 250W, 400W, and 600W for various cases with the time to accelerate from rest up to a maximum speed of 25km/hr. (Since numerical integration was used to find the time to reach the corresponding speeds, there may be slight absolute errors, although this is expected to be negligible since it is only required for an approximation).

A suitable brushless DC hub motor is the Heinzmann DirectPower PRA 180-25. Notably, the motor is gearless, has Hall effect sensors to provide feedback with three-phase control, and operates at a voltage of 36V with a nominal continuous rated power of 250W and maximum peak rated power over 950W [61, 73]. The motor also features a mass of 4.7kg, nominal angular speed of 210rev/min, nominal continuous torque of 11.4N.m, maximum peak torque of 30N.m for 10min or 40N.m for 4min or 60N.m for an impulse, compatibility with rims from 428mm to 622mm, IP54 rating for dirt, dust, and splash protection, and support for regenerative braking [61, 73]. Compared to similar motors such as the Heinzmann CargoPower RN 111, which offers higher performance, and the SR SunTour R250 HP or Heinzmann Classic RN 120, which are geared and offer lower performance, this motor provides favourable performance with regards to torque and angular speed characteristics with

a high dynamic response, and greater performance is unnecessary while lower performance may be inadequate. For further validation, the motor is capable of providing the performance for operating in a city setting, found by Muetze and Tan [31] and presented in Section 1.4.10. The motor is seen in Figure 27 and additional technical information can be found on the data sheet in Appendix C.

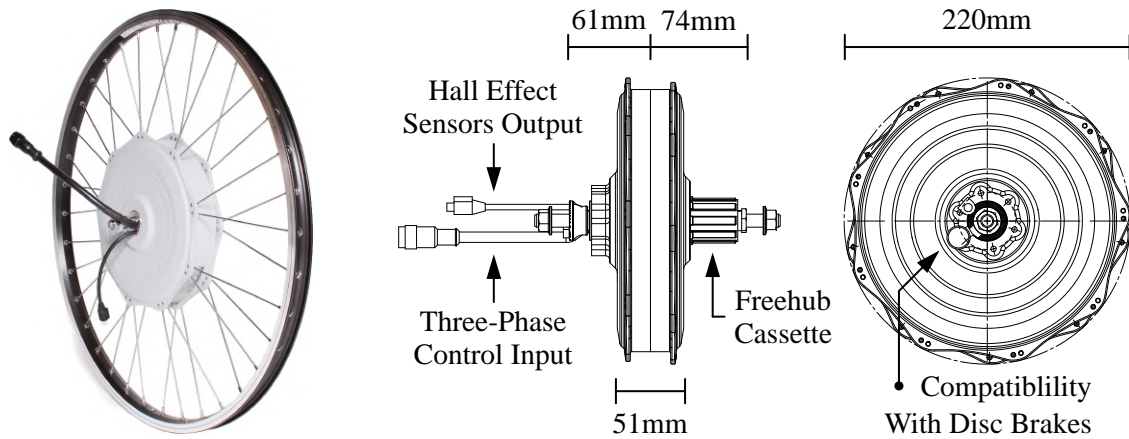


Figure 27: Example and dimensions of the rear wheel Heinzmann DirectPower PRA 180-25 [73].

The placement of the hub motor in a front or rear wheel also needs to be decided. The hub motor has variations for both options, where the rear wheel option is 0.2kg heavier with a Shimano Hyperglide freehub for mounting up to eleven sprockets on a cassette. However, placing the hub motor in a rear wheel will allow for significant performance improvements since it offers better traction when climbing steep gradients and is more suited for poor terrain conditions with minor obstacles [31], whereas placing the hub motor in a front wheel will only allow for a better mass distribution. Fortunately, when placing the hub motor in a rear wheel, the poor mass distribution towards the rear can be overcome by placing the controller components and battery pack as far forward as possible. Thus, placing the hub motor in a rear wheel is clearly the preferable and most beneficial choice.

4.1.2 BATTERY PACK

To compare nickel-metal hydride and lithium-ion battery, the expected characteristics are listed in Table 11. Based on these characteristics, it would be most practical to use a lithium-ion battery pack, because they offer a higher energy density, so they have a lower mass; tend to have a longer life cycle, so they will be more reliable; and are more common, so they tend to be less expensive [74]. Additionally, lithium-ion polymer batteries are available, which use a polymer instead of a liquid as the electrolyte and tend to have an energy density between 10% and 15% greater than normal lithium-ion batteries but also have a higher cost and less customisability [74]. There have been recent advancements in improving the charging ability of lithium-ion batteries, where it is possible to use higher currents to significantly reduce the charging times. However, there is a very slight risk of a lithium-ion battery erupting and possibly igniting due to thermal runaway if exposed to high temperatures above 70°C, but this is highly unlikely with a proper configuration and enclosure.

Table 11: Comparison between the typical characteristics of nickel-metal hydride, lithium-ion, or lithium polymer batteries batteries, with the typical characteristics of nickel-cadmium batteries for supplement [13, 63]. (For the energy to cost ratio, a conversion of US\$1 = R14.50 was used).

	Nickel-Cadmium (NiCd)	Nickel-Metal Hydride (NiMH)	Lithium-Ion (Li-Ion)
Power / Mass [W/kg]	150	250-1000	1800
Energy / Mass [W.hr/kg]	40-60	60-120	100-265
Energy / Volume [W.hr/L]	50-150	140-300	250-693
Energy / Cost [W.hr/US\$]	-	1.37	2.8-5
Energy / Cost [W.hr/R]	-	0.0945	0.193-0.345
Charge, Discharge Efficiency	70%-90%	66%-92%	80%-90%
Self-Discharge Rate [/month]	10%	14%-71%*	0.35%-2.5%
Time Durability [months]	-	-	24-36
Cycle Durability [cycles]	2000	180-2000	400-1200
Nominal Cell Voltage [V]	1.2	1.2	3.6/3.7/3.8/3.85

* The self-discharge rate of nickel-metal hydride batteries is highly temperature dependent.

Under ideal conditions, the conservation of energy states that the electrical energy from the battery will be converted into rotational kinetic energy of the motor which will then be used to provide propulsion as translational kinetic energy and overcome drag, weight, and rolling resistance. This is described in Equation 9. So, to obtain an estimate for the capacity of the battery pack, it is assumed that the motor will be operating at the maximum continuous rated power of 250W to provide an average speed of 18km/hr to account for stopping and acceleration over the required range of 50km.

This assumption is fairly valid since the motor may likely operate at a lower continuous rated power on flat and downhill terrain, and it will occasionally operate at a higher peak rated power to accelerate from rest and, thus, an average operating power of 250W is plausible and realistic. Furthermore, the gathered results by Muetze and Tan [31] from operating in a city setting, showed a maximum average operating power of 179W from the heaviest user who had the highest average speed of 20.9km/hr. These results also showed that the average average speed of the fastest three users was 18km/hr [31].

$$\sum_{i=1}^n E_{in} = \sum_{i=1}^n E_{out} \rightarrow E_b = E_m = E_k + E_d + E_w + E_r \rightarrow E_b = n \frac{P_m}{v} x \quad (9)$$

Where E_{in} , input energy, J; E_{out} , output energy, J; E_b , battery energy, J; E_m , motor energy, J; E_k , kinetic energy, J; E_d , drag resistance energy, J; E_w , weight resistance energy, J; E_r , rolling resistance energy, J; n , design factor; P_m , motor power, W; v , velocity, m/s; and x , distance, m.

Thus, it is required for the battery to have a capacity of approximately 2500kJ or 694.4W.hr to ensure the range of 50km at an average speed of 18km/hr. However, since this is an initial approximation, a design factor of 1.2 is implemented which can be seen to account for inefficiencies in the motor and

battery up to 20%, such that it is required for the battery to have a capacity of 3000kJ or 833.3W.hr. Accordingly, this allows for the significant elimination of the need for manual propulsion.

Considering reputable manufacturers, the required capacity is available with two Bosch PowerPack 400 or Heinzmann Downtube Battery, which were specifically designed for electric bicycles and offers individual capacities of 400W.hr and 515W.hr respectively with masses of 2.6kg and 3.5kg respectively [62, 75]. However, the battery pack is fairly simple and does not require a complex design and, so, there is a possibility of developing a custom battery pack to fulfil the requirements.

Since it is essential for the battery pack to be reliable and safe, Panasonic and Samsung lithium-ion cells are considered with possible configurations shown in Table 12 using Equation 10 to determine the required number of cells and total capacity. This indicates that the best performance of 835.2W.hr and 3.84kg with a prominent cycle life would be achievable from Panasonic NCR18650PF cells with 10 sets of cells in series and 8 parallel cells in each set, which utilises the design factor to allow for discharge safety and compensation for manufacturing variations between the cells (if these cells are not acceptable for unanticipated reasons, the Samsung INR18650-29E cells can be adapted since the dimensions are common) [76]. The data sheet of the Panasonic NCR18650PF cells is included in Appendix C and shows acceptable discharge between temperatures of -20°C and 60°C [76].

$$E_c = P_c t = V_c I_c t \rightarrow E_b = P_b t = (N_p V_c)(N_s I_c t) \quad (10)$$

Where E_c , cell energy, J; P_c , cell power, W; t , time, s; V_c , cell voltage, V; I_c , cell current, A; E_b , battery energy, J; P_b , battery power, W; N_p , number of parallel cells; and N_s , number of series cells.

Table 12: Comparison between various candidate lithium-ion cells, where each cell has a nominal voltage of 3.6V to produce a total output voltage of 36V. [77, 78, 76, 79, 80, 81, 82].

	Nominal Capacity [A.hr]	Maximum Mass [g]	Parallel Cells [cells]	Series Cells [cells]	Total Cells [cells]	Total Capacity [A.hr]	Total Capacity [W.hr]	Total Mass [kg]	Expected Cycle Life
Pan. UR18650RX	2.05	47.5	12	10	120	24.6	886	5.70	>1.70Ah after 400cycles
Pan. UR18650AA	2.25	43.1	11	10	110	24.8	891	4.74	>1.75Ah after 400cycles
Pan. NCR18650PF	2.90	48.0	8	10	80	23.2	835	3.84	>2.30Ah after 500cycles
Sam. ICR18650-22F	2.20	44.5	11	10	110	24.2	871	4.90	>1.51Ah after 300cycles
Sam. ICR18650-25R	2.50	45.0	10	10	100	25.0	900	4.50	>1.50Ah after 250cycles
Sam. ICR18650-26J	2.60	45.0	9	10	90	23.4	842	4.05	>1.79Ah after 300cycles
Sam. INR18650-29E	2.85	48.0	8	10	80	22.8	820	3.84	>1.87Ah after 500cycles

It is also necessary to implement a battery management system to monitor the voltage, state of charge, depth of discharge, state of power, and temperature to ensure safety by keeping the cells at an equilibrium voltage and instituting over-charge, over-discharge, and short circuit protection. The mounting and enclosure of the battery pack will be considered in Section 4.4 with the frame design, but the cell arrangement and basic dimensions of the battery pack are seen in Figure 28 and occupy a maximum area of approximately 0.02738m^2 with an extruded height 65.3mm .

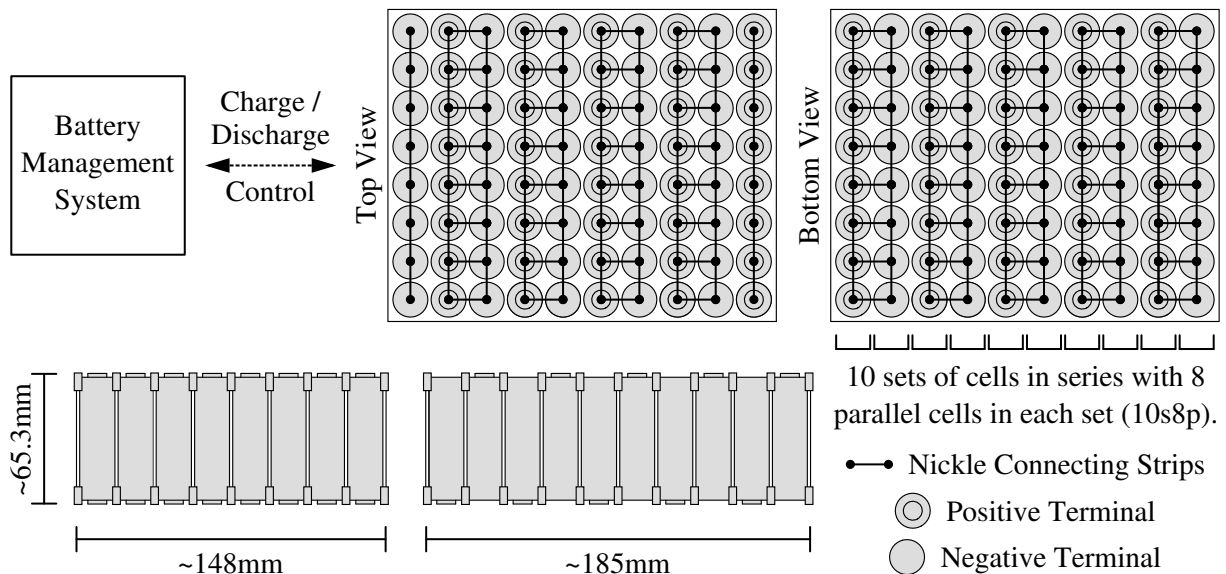


Figure 28: Basic layout and dimensions of the battery pack using Panasonic NCR18650PF cells.

Finally, a single cell uses standard charging specifications and needs a minimum current of 1.375A and voltage of 4.20V [76]. From the ratio of the total capacity to the charging current, the maximum charging time is approximately 16.9hr to charge the cell to full capacity assuming no efficiency loss, which is unacceptable. Instead, to have a charging time of 8hr , a charging current of 2.90A is required when assuming no efficiency loss or 3.48A is required when assuming a 20% efficiency loss. The Bosch Standard and Fast chargers can be used as benchmarks using the maximum charging currents of 4A and 6A respectively - each of these chargers is compatible with an AC voltage input of 220V to 240V and frequency of 50Hz to 60Hz [62]. With these charging currents and a realistic efficiency loss of 20% , the charging times will be 6.96hr and 4.64hr respectively which are appropriate.

4.1.3 CONTROLLER CONSIDERATIONS

Since the hub motor is brushless and utilises the sequential excitation of pole pairs to create a rotating magnetic field, the controller will need to output rectangular or trapezoidal voltage strokes to the desired poles relative to the rotor position, as measured by the Hall effect sensors [13, 74]. The speed of the motor will then be controlled based on the magnitude of these voltage strokes set through pulse width modulation by varying the duty cycle. As an example, this is illustrated in the timing diagram in Figure 29, where the voltage strokes are applied to two out of the three phases at any moment, such that the stator flux and rotor flux are near perpendicular to generate maximum torque [13, 74].

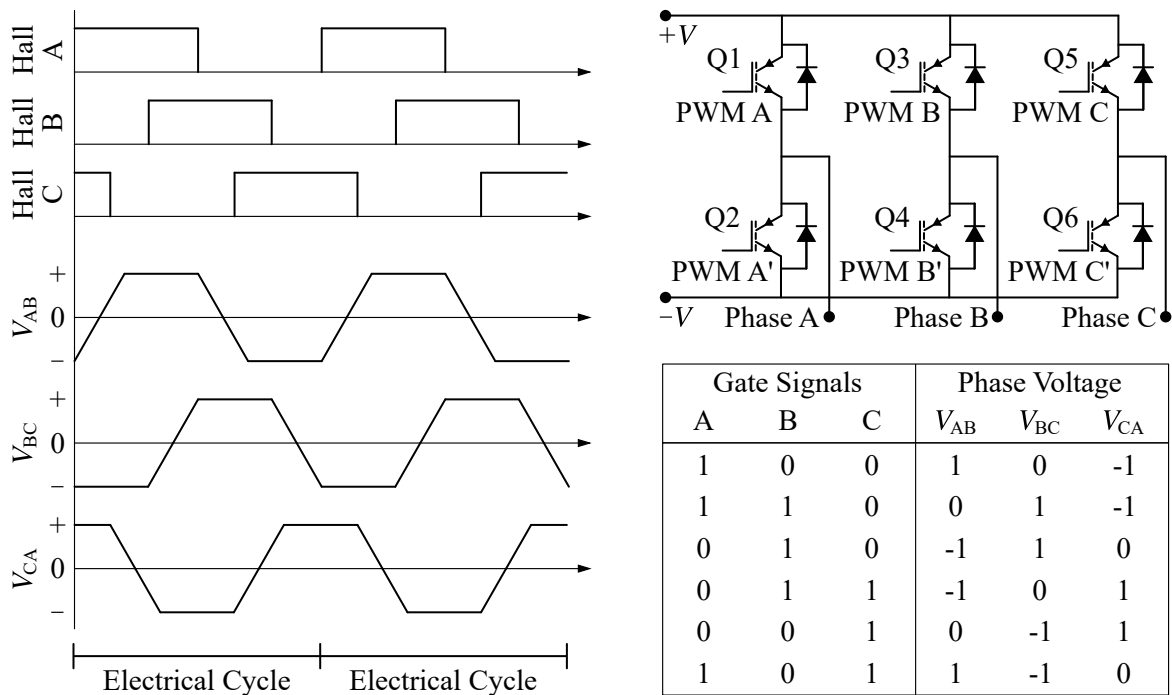


Figure 29: Timing diagram for the distribution of voltage strokes (left) and motor driving circuit with a power stage utilising six transistors to control the phase voltages (right).

The voltage stroke distribution can be performed with a regular power stage utilising six transistors, as shown in Figure 29 [13, 74]. It is essential for the timing of the voltage strokes to be accurate otherwise an offset will decrease efficiency [74]. This can be achieved using a generic electronic speed controller with motor drivers, where an overview of the control system features the user providing an input for the desired speed supplied as a current signal from the throttle and the battery pack supplying power which the controller then distributes to the hub motor proportionally based on the input.

The control system will not be developed further, as the primary components have been broadly outlined and it is only required to establish the specific electronic details. The following recommendations should be implemented with the final development:

- The simplest method of control is using the controller as a basic switch to supply power to the motor, however this is not desirable as it can offer erratic control. Instead, there should be a control console mounted with options for different operating modes which limit the maximum continuous rated power delivered by the motor, such as Economic with a limit of 40W, Tour with a limit of 100W, Performance with a limit of 170W, and Sport with no limit to the 250W. Additional limits may also be applied to the maximum peak rated power in each of these modes.
- There should be speed control to limit the maximum speed attained while using electric propulsion to 25km/hr (on public roads). However, there could be an additional operating mode as Turbo that utilises the full power of the motor and does not limit the maximum speed, which the user may use in private facilities and where legal regulations do not apply.

- For more fluent assistance with manual propulsion, a torque or cadence sensor mounted on the bottom bracket or cranks could be investigated which will measure the pedalling input from the user and provide feedback to the controller for smoother acceleration and steady speed control.
- Regenerative braking should also be integrated to increase the braking performance, range, and overall efficiency. The recharging efficiency for the conversion of kinetic energy to electrical energy ranges from 40% to 60% and can extend the range of the design by up to 15% depending on the terrain and level of regenerative braking employed [13]. This is most useful with downhill slopes greater than 3% and can be especially utilised to limit the speed if a high speed is not desired [13]. Further information is presented in Section 4.5.
- A user interface equipped to the handlebar showing the operating time, current speed, distance travelled, remaining battery pack capacity, and warning when the battery capacity is below 20%. More advanced features may be included, such as a trip log or navigation, but this might be more convenient and inexpensive to facilitate by permitting the user to mount a smartphone.
- A security mechanism to deter theft by detecting the absence or presence of the owner and reacting appropriately by electrically locking or unlocking the motor assembly.

4.2 WHEEL ARRANGEMENT

The wheel arrangement will be decided based on practicality for the best operation. The components of the wheel will need to be defined with regards to the rim and connections between the rim and hubs which must be capable of delivering the desired performance. Also, since the rear wheel will use the hub motor, the front hub will require special attention to ensure it can survive the applied loads.

4.2.1 INITIAL CONSIDERATIONS

The number of wheels is considered first, where it is most practical to have two, three, or four wheels because the use of more wheels will not offer any benefits. Ordinarily, increasing the number of wheels improves the stability of the design, where less skill is required to balance. But, it is also necessary to consider the effects on performance from increasing the number of wheels, where greater overall dimensions are expected as the number of wheels increases, as compared in Figure 30. This indicates that an arrangement with two wheels will likely have the most responsive steering with the ability to lean, least drag due to the significantly smallest frontal area, and least mass due to less structural members needed for the frame, which is very consequential because a decreased frontal area and mass will proportionally experience a decreased drag resistance and weight resistance. Thus, since it is reasonably simple and safe to stably operate with two wheels after traditional practice, it is decided to continue the design development with two wheels to maximise performance.

Pneumatic tyres will also be considered since they are vastly more common and have better performance compared to solid tyres (it may still be possible to fit a solid tyre if desired by the user, as long as the rims follow the corresponding standards). Moreover, because it is a conventional and lightweight

design, the overall wheel will be formed using a tyre mounted on a rim which is connected to a central hub through stretched spokes - there are commonly 20 to 48 spokes [55].

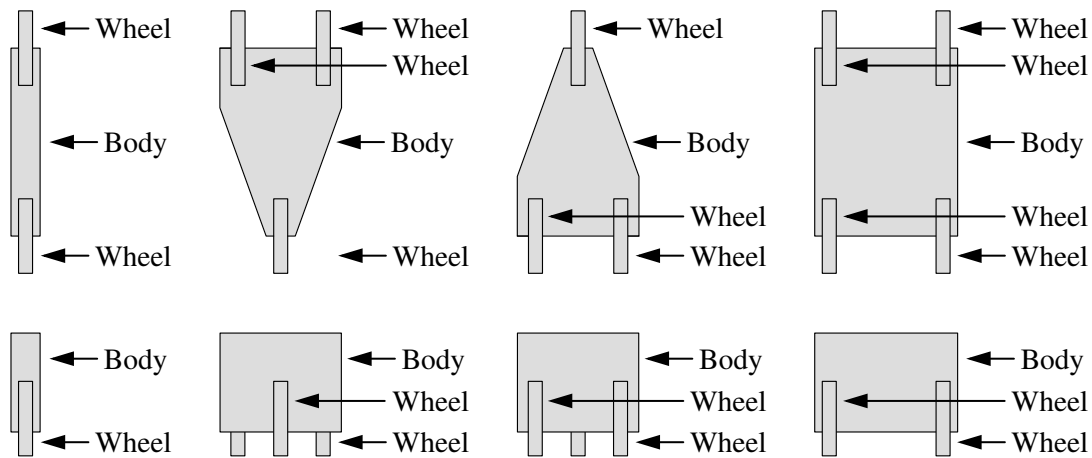


Figure 30: Approximate top view (top) and front view (bottom) of the most practical wheel arrangements with two wheels (left), three wheels (left-middle and right-middle), and four wheels (right).

4.2.2 TYRES

Conventionally, road tyres are usually slick with a smooth outer tread and only suited to travelling on smooth surfaces, otherwise the tyre may begin to slip due to a lack of traction. At the other extreme, off-road tyres are knobby with bumps on the outer tread and suited for fully off-road conditions due to increased traction. However, off-road tyres can be up to 180% heavier than road tyres which substantially increases rolling resistance and decreases performance. So, it is recommended to use a hybrid or cross tyre which performs well on smooth surfaces (like asphalt, pavement, and cement) and is also able to operate decently on rough surfaces (like gravel and flat soil), although it may not be suited for fully off-road conditions with major obstacles and soft sand or deep mud.

The available tyres generally include ISO sizes of 584mm and 622mm (also known as 650B or 27.5in and 700C or 28in) with widths ranging from 28mm to 57mm [83]. Since there are significant benefits to a larger wheel, a 622mm tyre is favoured with a width no greater than about 42mm to decrease the mass of the wheel for better acceleration and allow for an even compromise with manoeuvrability. As previously demonstrated, this diameter also produces an angular speed and torque very near the nominal angular speed and torque of the hub motor at 25km/hr. To choose a tyre, the various characteristics of different tyres relative to their performance and cost need to be compared.

The Gran Fondo Cycling Magazine [83] conducted an experiment to find an optimal all-round tyre, where hybrid tyres with tubes and hybrid tubeless tyres were considered with nine different tyres fitting the desired criteria of 622mm and a minimal width less than or equal to 42mm. In the experiment, the rolling resistance was compared by mounting the tyres on the same rim with the same pressure and testing them at 20km/hr on a controlled Schwalbe test bench; the puncture resistance was compared by penetrating the central tread and sidewall with objects of different sizes and measuring the

required puncture force and depth; and a practical test was performed by using each wheel on asphalt, gravel, and flat soil to consider traction, handling, and comfort, although the results may be slightly subjective based on the preferences of the user [83]. The findings are summarised in Table 13.

Table 13: Comparison between various candidate hybrid tyres with relative ratings for mass, rolling resistance, and puncture resistance [83]. To find the combined rating, an average puncture rating was used and each rating was weighted equally. (For the cost, a conversion of €1 = R16.80 was used).

	Size Design	Mass [g]	Mass Rating	Roll Rating	Puncture Ratings		Combined	Cost [€]	Cost [R]
					1.5mm	5mm			
Challenge Gravel Grinder TLR	38-622	365	100%	89.3%	78.5%	65.9%	87.2%	45.90	771.12
Compass Barlow Pass Extralight TC	38-622	381	95.6%	100%	67.8%	53.0%	85.3%	84.00	1411.20
Donnelly X'Plor MSO TLR	40-622	569	44.1%	83.7%	100%	67.8%	70.6%	64.99	1091.83
MAXXIS Rambler Silk Shield TR	40-622	426	83.3%	87.0%	60.7%	97.4%	83.1%	59.50	999.60
MAXXIS Ravager Silk Shield TR	40-622	523	56.7%	71.5%	61.9%	100%	69.7%	59.50	999.60
Panaracer GravelKing SK TLC	43-622	487	66.6%	90.7%	60.7%	64.0%	73.2%	42.90	720.72
Schwalbe G-One Bite Evo TLE	40-622	472	70.7%	93.2%	71.4%	64.1%	77.2%	59.90	1006.32
Schwalbe G-One All-Round Evo	40-622	440	79.5%	85.9%	89.3%	84.1%	84.0%	59.90	1006.32
WTB Resolute TCS Light	42-622	457	74.8%	95.7%	42.8%	86.9%	78.5%	45.50	764.40
WTB Riddler TCS Light	37-622	431	81.9%	83.5%	71.4%	73.8%	79.3%	45.50	764.40

It was concluded that a tubeless tyre can have an average decreased rolling resistance of 10%; widths between 37mm and 40mm provide the best compromise between handling, traction, and comfort on smooth and rough surfaces; and shallow tread patterns are preferable as long as the correct pressure is used [83]. With these conclusions and the results, it is clear that the Challenge Gravel Grinder TLR offers the optimal all-round performance, since it has a very light mass of 365g, low rolling resistance, adequate puncture resistance, and low cost. The tyre is also tubeless ready (and compatible with using an inner tube if desired) and features subtle bumps along the central tread for smooth rolling and aggressive bumps along the side tread to aid with handling, as seen in Figure 31.



Figure 31: Example of the Challenge Gravel Grinder TLR 38-622 for inspection of the tread [84, 85].

These tyres should be inflated with a pressure of 2.75bar to 5.2bar, which is in accordance with the ISO 5775-1 recommendations for a pressure above 2bar such that the deflection of the tyre while rolling does not exceed 30% of the section height [84, 22]. It is recommended for a higher pressure to reduce the rolling resistance by 4% to 8%, however a lower pressure will offer more comfortable with an increased ability to absorb shocks from minor obstacles [12]. Ultimately, the specific choice of inflation pressure will be unique to each user based on personal preference.

4.2.3 RIMS AND SPOKES

The rims are essentially a bent extrusion of a smooth profile to form a circle. On the inside face of the rim, there are periodic holes to mount nipples for the spokes and an enlarged hole for the valve. Considering the ISO 5775 designations [86], the designations of clincher rims include straight-side, hooked-beam, and crotchet-type profiles, where a straight-side profile is more traditional and relies on the resistance to stretching of the bead to keep the tyre on the rim, while the hook-beam and crotchet-type profiles are preferable and interlock with the bead to keep the tyre on the rim [55]. These profiles are illustrated in Figure 32, where it is evident that the hook-beam and crotchet-type profiles are very similar and the choice of profile is fairly arbitrary. However, the crotchet-type profile is more common and there is an availability of more rim widths [86] and, so, the crotchet-type profile is selected and shown with more detail in Table 14. It is also observed that the crotchet-type profile inherently has straight outside edges which will better accommodate the possibility of rim brakes.

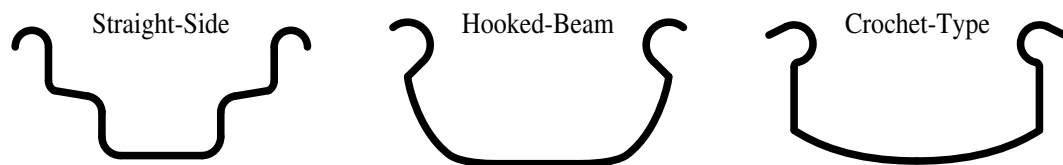


Figure 32: Outlines of the upper edges for mounting the tyre on straight-side, hooked-beam, and crotchet-type rim profiles defined in ISO 5775-2 (dimensional parameters are not shown) [86].

To decide on the rim width of the profile, the recommended crotchet-type designations in ISO 5775-1 for the Challenge Gravel Grinder TLR with a width of 38mm are 17C, 19C, 21C, or 23C [22]. It is recognised that a smaller rim width will have a lower mass, but it is also necessary to consider the available compatibility range for other tyre widths so that there is potential for customisation if the user would like to replace the tyres without changing the rims. Thus, the 19C designation is preferred as it is expected to have the second lowest mass depending on the thickness for sufficient strength and will allow for compatibility with the greatest range of tyre widths from 28mm to 62mm, since the 17C designation is only compatible with a range of tyre widths from 25mm to 52mm [22].

Now, the spokes need to be designed before progressing with the rim development to account for sufficient clearance of the nipples and the size of the mounting holes within the rim. The anatomy of a spoke is seen in Figure 33. For the rear wheel, the Heinzmann DirectPower PRA 180-25 features 18 mounting points for the spokes on each side of the hub, so it is required for the rear rim to have

Table 14: Dimensional parameters of the crotchet-type rim profile defined in ISO 5775-2 [86].

Nominal Rim Width Code	$A \pm 0.5$ [mm]	$B \pm 0.3$ [mm]	$G \pm 0.5$ [mm]	H , min. [mm]	R_2 [mm]
	13C	13	1.5	5.5	2.2
15C	15				
17C	17				
19C	19				
21C	21				
23C	23				
25C	25	6.5		3.5	1.1 ± 0.25
27C	27				
29C	29				

36 holes spaced evenly at 10° for the nipples [73]. For consistency and to allow for the rims to be identical, 36 holes will also be used for the front rim [55].

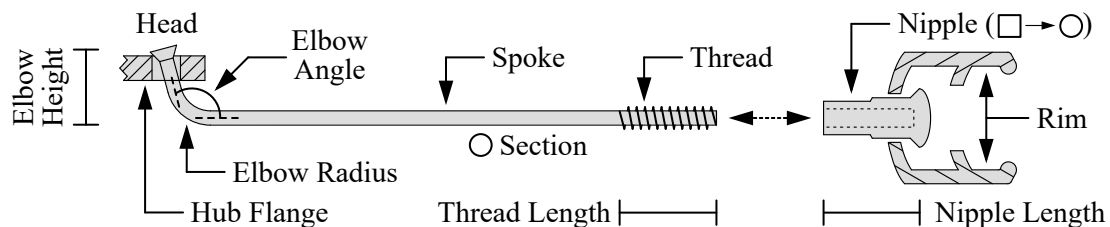


Figure 33: Schematic of the components of a spoke to connect the hub and rim of a wheel.

The spokes are the most common components of the wheel to fail, where failure usually occurs through low-cycle fatigue due to a spoke being unloaded from its pre-tension and then reloaded as the wheel rolls - this is almost exclusively from radial loads arising from the weight of the design and user [12, 55, 56]. When one spoke fails, there is an unbalance of forces on the rim which results in irregular deformations of the rim, the sudden failure of more spokes, and the eventual buckling of the wheel [55,

56]. The point of failure is usually at the elbow or near the thread, because these are the thinnest points and there are stress concentrations [55, 56]. So, based on the experimental results presented in Section 1.4.8 for normal operating conditions, it is seen that there is a maximum strain of 51.8μ in tension and minimum strain of 266.5μ in compression relative to the pre-tensioned condition. However, it is also shown that a peak minimum strain of 600μ is possible with a 0% probability of being exceeded which should be considered instead for a conservative estimate. The experienced force can then be determined with Equation 11 by assuming axial and linear elastic behaviour. Thus, the maximum change in force is 28.07N in tension and minimum change in force is 325.1N in compression (under normal operating conditions, the minimum change in force is 144.4N which is somewhat similar to the force of 116.3N found with the experimental load of 930N and common assumption that the load-affected zone spans evenly across four spokes on each wheel [55]).

$$\sigma_a = \frac{F_a}{A} = E\varepsilon \rightarrow \Delta\sigma_a = \frac{\Delta F_a}{A} = E\Delta\varepsilon \rightarrow \Delta F_a = EA\Delta\varepsilon \quad (11)$$

Where σ_a , axial normal stress, Pa; F_a , axial force, N; A , cross-sectional area, m^2 ; E , elastic modulus, Pa; and ε , normal strain.

It is also assumed that the spokes are tensioned to approximately 1180N, as is common for high quality wheels [55] and, as a result, there will be a fluctuating tensile load between a maximum and minimum of 1208N and 855N respectively, as simplified in Figure 34. With the information in Table 15 and a fatigue stress concentration factor of 2.0 [87, 88], the fatigue safety can be predicted with the Modified Goodman failure criterion using Equation 12 to Equation 15 [87, 89].

$$\sigma_{max} = K_f \frac{F_{max}}{A} = K_f \frac{F_t + \Delta F_{max}}{A} \quad \text{and} \quad \sigma_{min} = K_f \frac{F_{min}}{A} = K_f \frac{F_t - \Delta F_{min}}{A} \quad (12)$$

$$\sigma_m = \frac{\sigma_{max} + \sigma_{min}}{2} \quad \text{and} \quad \sigma_a = \left| \frac{\sigma_{max} - \sigma_{min}}{2} \right| \quad (13)$$

$$S_{ut} = \frac{F_{ut}}{A} \quad \text{and} \quad S_e = 0.5k_a k_b k_c k_d k_e k_f S_{ut} \quad \text{for steel} \quad (14)$$

$$\frac{\sigma_a}{S_e} + \frac{\sigma_m}{S_{ut}} = \frac{1}{n_f} \quad (15)$$

Where σ_{max} , maximum stress, Pa; K_f , fatigue stress concentration factor; F_{max} , maximum force, N; A , cross-sectional area, m^2 ; F_t , pre-tension force, N; σ_{min} , minimum stress, Pa; F_{min} , minimum force, N; σ_m , midrange stress, Pa; σ_a , alternating stress, Pa; S_{ut} , ultimate tensile strength, Pa; F_{ut} ,

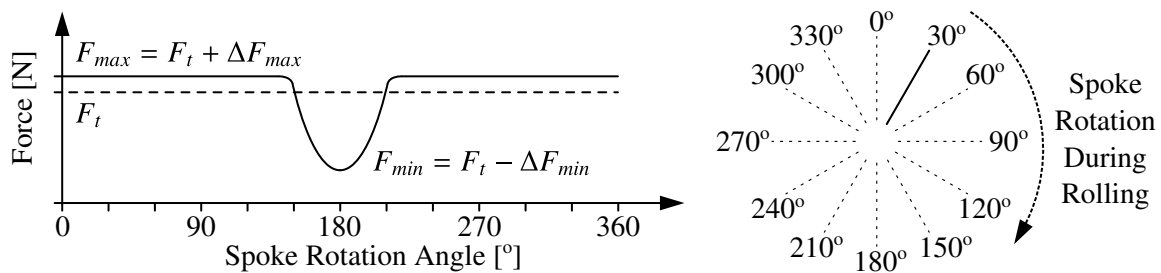


Figure 34: Approximation of the fluctuating tensile load experienced within a spoke, where the tension is decreased when a compressive load is introduced as the spoke rotates to the bottom side.

ultimate tensile force, N; S_e , endurance strength, Pa; k_a , surface condition factor; k_b , size factor; k_c , load factor; k_d , temperature factor; k_e , reliability factor; and k_f , miscellaneous-effects factor. (The endurance strength modifying factors $k_a, k_b, k_c, k_d, k_e, k_f$ are found from Budynas and Nisbett [87]).

Table 15: Designation and parameters for common and standard straight spokes [55, 90, 91]. Stainless steel is considered, while the endurance limit modifying factors resulted in $k_a k_b k_c k_d k_e k_f = 0.542$.

Spoke Diameter [mm]	Gauge Designation	Elbow Angle [°]	Elbow Height [mm]	Elbow Radius [mm]	Thread Length [mm]	Nipple Diameter [mm]	Nipple Length [mm]	Rim Hole Diameter [mm]	Force Ultimate Tensile [N]	Stress Maximum [MPa]	Stress Minimum [MPa]	Stress Midrange [MPa]	Stress Alternating [MPa]	Stress Ultimate Tensile [MPa]	Stress Endurance [MPa]	Fatigue Safety Factor
1.8	15	95	6	1.8	9	4.0	12	4.4	2000	949	672	811	139	786	210	0.59
2.0	14								2400	769	544	657	112	764	205	0.71
2.3	13		7	1.9		4.3	13	4.7	3000	585	412	497	85.0	722	197	0.89
2.6	12	100	7.5	2.1	10	4.6		5.0	3600	455	322	389	66.5	678	188	1.08

Thus, through iterations to minimise the spoke diameter, it is found that stainless steel spokes with a diameter of 2.6mm are satisfactory with a fatigue safety factor of 1.08 [55]. Stainless steel is used because it will prevent corrosion and offer the best performance compared to other materials like aluminium, which has poor fatigue resistance, and titanium, which has problems with galling in the threads [55]. The corresponding standard nipple has an overall length of 13mm, diameter of 4.6mm, 10mm threads, and 0.454mm or 56tpi pitch, and should be manufactured from brass for smooth turning by acting like a bearing, suitable strength to avoid stripping, and reasonable mass of around 1g [55, 90, 91]. For the nipple holes in the rim, the diameter needs to be 5mm and the clearance needs to be 4mm. Also, since it is seen that the Challenge Gravel Grinder TLR tyre uses a Presta valve, there must be a valve hole with a diameter of 6.3mm located equally between two nipple holes to minimise interference (commonly available adapters can be used for conversion to Schrader or Woods valves).

With these dimensions, it is possible to construct the outline of the rim. To complete the profile, it is necessary to determine the necessary thickness such that the rim is strong enough to withstand the applied loads and safe for operation without buckling. Since the rim will experience significant compressive loads while rolling, this can be done using the proposed test in the Japanese Industrial Standard (JIS) D 9421, which is based on ISO 5775 but includes additional information with regards to rim strength. The test states that, when a static load of 500N (for 19mm to 25mm rim widths or 300N for 13mm to 17mm rims widths) is applied to the rim without a hub or spokes while it is positioned between two rigid supports, the permanent deformation measured must be less than or

equal to 1mm [92], which implies that yielding will have occurred. This arrangement is shown in Figure 35 along with the free-body diagram of the wheel during operation for comparison. During operation, the resulting contact force with the ground can be assumed to be vertical, but the resulting contact pressure with the ground will generally not be uniformly distributed over the contact area and the leading part will experience a greater pressure than the trailing part due to the forward rolling of the wheel which offsets the force and is the cause of rolling resistance [12].

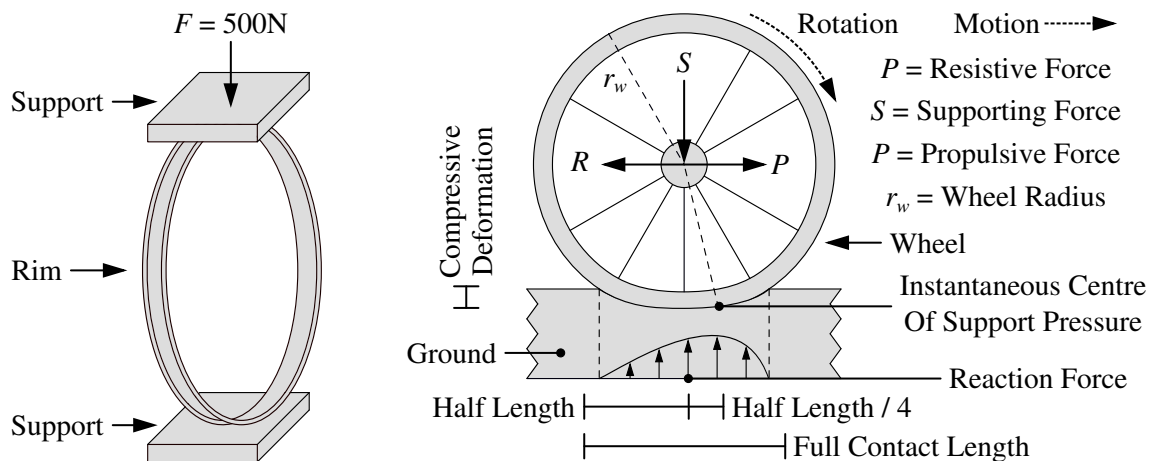


Figure 35: Arrangement to test rim strength without support from the hub, spokes, or tyre (left) and free-body diagram showing the actual loads and exaggerated deformations during operation (right).

Unfortunately, a physical test with a prototype cannot be performed, but it is possible to create a finite element analysis to provide a prediction of the results. To obtain a conservative result and account for possible modelling and discretization errors in the simulation, the test will have the same arrangement but the deciding criterion for safety is modified and based on no yielding occurring, such that the maximum stress must be equal to or less than the yield strength with no permanent deformation.

So, various thicknesses are compared for aluminium 6061-T6, since it has a good combination of strength to mass properties and corrosion resistance with a density of 2700kg/m^3 , elastic modulus of 68.9GPa , and yield strength of 276MPa [93, 94]; and medium carbon steel AISI 1035, since it has a high yield strength of 370MPa with a density of 7850kg/m^3 and elastic modulus of 196GPa [95, 94]. In the simulations, the contacts between the supports and rim were set as no separation to allow for an accurate and linear analysis; the mesh settings were consistent with an initial mesh having quadratic order elements, medium relevance, fast transition, and maximum element size of 6mm ; and convergence was applied to offer automatic refinement until the difference in maximum stress between consecutive iterations was less than 2% . The overall results are shown in Table 16 and Table 17 for aluminium and steel respectively, with an instance of the most suitable choices for aluminium and steel in Figure 36 - it is recognised that these results will be substantially lower with support from the spokes and hub to form a more rigid structure.

From the results, it is clear that aluminium with a 2.3mm thickness will provide safe performance and the lowest weight of approximately 0.879kg . A higher grade of steel could be considered, but the

Table 16: Simulation results from the finite element analyses performed in ANSYS Mechanical 18.2 using aluminium 6061-T6 to determine the required thickness of the rims with a 19C designation.

Thickness: 2.0mm		Thickness: 2.2mm		Thickness: 2.3mm	
Approximate Mass: 0.757kg		Approximate Mass: 0.838kg		Approximate Mass: 0.879kg	
Converged	Deformation: 10.35mm	Converged	Deformation: 9.031mm	Converged	Deformation: 8.359mm
	Max. Stress: 325.0MPa		Max. Stress: 289.9MPa		Max. Stress: 268.1MPa
	Min. Safety Factor: 0.751		Min. Safety Factor: 0.952		Min. Safety Factor: 1.029

Table 17: Simulation results from the finite element analyses performed in ANSYS Mechanical 18.2 using steel AISI 1035 to determine the required thickness of the rims with a 19C designation.

Thickness: 1.6mm		Thickness: 1.8mm		Thickness: 2.0mm	
Approximate Mass: 1.741kg		Approximate Mass: 1.969kg		Approximate Mass: 2.200kg	
Converged	Deformation: 4.938mm	Converged	Deformation: 4.232mm	Converged	Deformation: 3.635mm
	Max. Stress: 422.8MPa		Max. Stress: 368.8MPa		Max. Stress: 325.4MPa
	Min. Safety Factor: 0.875		Min. Safety Factor: 1.003		Min. Safety Factor: 1.137

extra strength is unlikely to significantly decrease the mass lower than the aluminium results and the walls will become so thin that the rim will not actually be able to support the forces from the spokes [55]. An additional advantage of aluminium is that, if rim brakes are to be used, aluminium and steel have a similar dynamic sliding friction coefficient of 0.28 and 0.32 against the brake pad under dry conditions, but this coefficient drops by only 14.3% for aluminium under wet conditions to 0.24 while it noticeably drops by 46.9% for steel under wet conditions to 0.17 - this is because aluminium has a

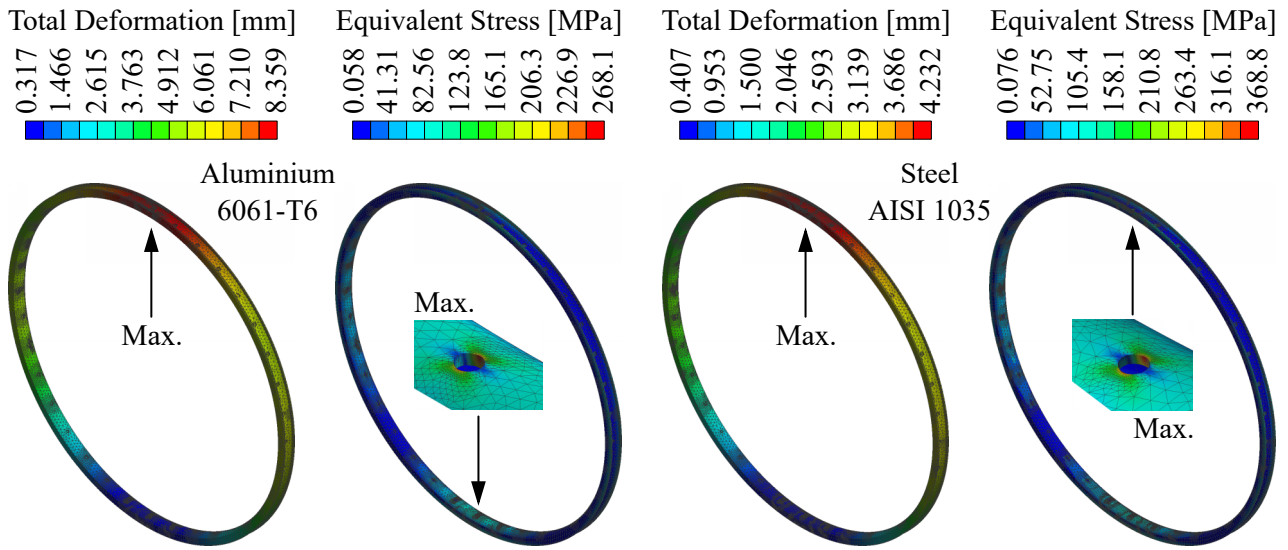


Figure 36: Deformation and stress experienced in the 19C designated rim for the 2.3mm aluminium 6061-T6 (left) and 1.8mm steel AISI 1035 (right), as simulated with ANSYS Mechanical 18.2.

greater micro-roughness which is able to better penetrate residual water film, while steel is smoother and the residual water film is not clearly disrupted but remains more intact [55].

Finally, since it was also possible to use a 17C designation with the chosen tyre, the different in mass should be compared to see if there is a major reduction. So, with the adjusted profile and same thickness of 2.3mm, a 17C designation would result in a decreased mass of 0.836kg, but it would not be suitable to carry the load due to a resulting maximum stress of 291.12MPa when applying the previous finite element analysis - it would actually be required for a greater thickness. Thus, the compromise of the 19C designation for a greater compatibility with tyre widths is justified.

4.2.4 FRONT HUB

The desired construction of the front hub, seen in Figure 37, is fairly simple to produce a lightweight and robust structure where a non-rotating axle provides support, the bearings allow for the hub shell to freely rotate, and the lock nuts secure the components and prevent loosening under vibrations. To begin to specify the design for the hub, the axle is first considered which is fixed to the forkends with axle nuts and must allow for the standard 100mm spacing between the inside surfaces of the forkends.

For the axle, it is expected for the maximum force to be applied during braking, because maximum braking will cause a moment up to the point just before the rear wheel lifts off the ground, where the front axle will be supporting the total mass of the design and user. Additionally, the maximum deceleration from braking is usually greater in magnitude than maximum acceleration while pedalling. Thus, assuming maximum braking with a high deceleration of 6.5m/s^2 while drag and rolling resistance are neglected, there will be radial forces of 773.5N from braking and 1167N from the maximum 119kg mass of the design and user exerted on the front axle to create a resultant force of 1400N,

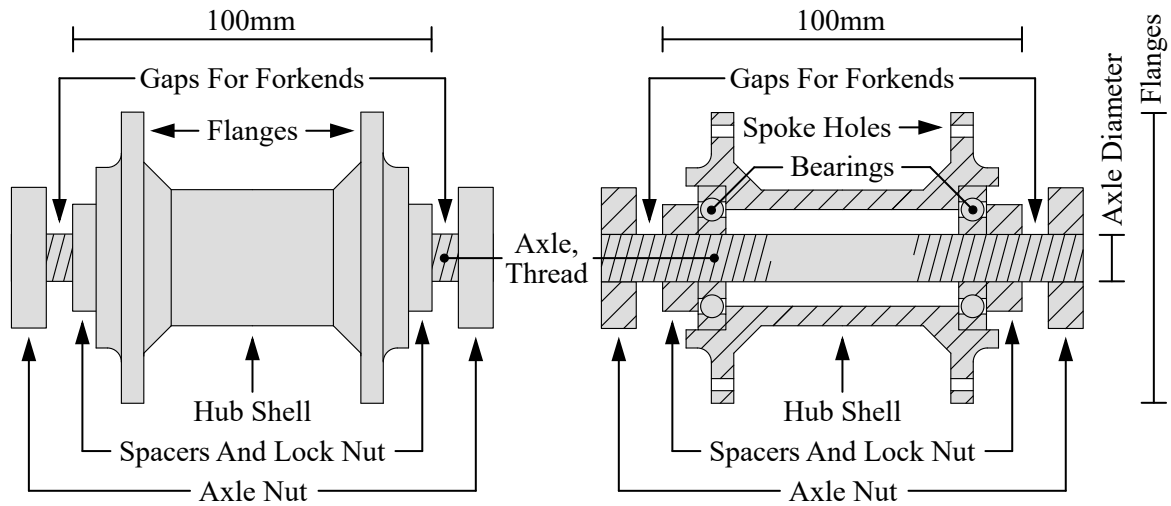


Figure 37: Construction of the front hub (left) with a sectioned view (left).

which is comparable to the maximum experimental value of 1550N found by De Lorenzo and Hull [96] for vigorous off-road conditions with heavy impacts after periods of being airborne. The free-body diagram of the axle seen in Figure 38 with general dimensions, where the bearings provide reaction forces of equal magnitude at 700N due to symmetry.

It is also necessary to account for the axial stresses from the elongation on either side of the axle up to the lock nuts due to the pre-load tightening of the axle nuts, where this pre-load is the only axial force acting on the axle. The torque when installing the axle nut should be above 25N.m but not above 45N.m otherwise the front fork may be damaged and, so, the pre-load force can be estimated using Equation 16 for a reusable connection and with a non-plated bolt condition factor of 0.3 [87, 89, 97].

$$F_p = \frac{T_p}{Kd} \quad (16)$$

Where F_p , pre-load axial force, N; T_p , pre-load torque, N.m; K , condition factor; and d , diameter, m.

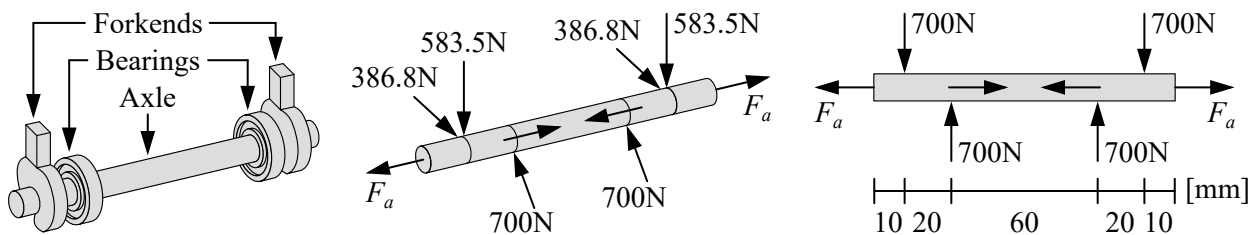


Figure 38: Free-body diagram of the loads experienced by the axle in the front hub. For the dimensions, it is assumed that the spacing between the forkends and bearings in 20mm.

From these forces, the axial force, shear force, and bending moment diagrams can be created in Figure 39. This indicates that equal maximum stresses will occur just to the left of 30mm and just to the right of 90mm. It is now possible to iterate with various axle diameters until safety is achieved using Equation 17, Equation 18, and Equation 19 for the axial, shear, and bending stresses respectively. In these iterations, the maximum pre-load torque of 45N.m is adopted, the adjusted tensile stress area is

used for the axial stress, a conservative static stress concentration factor of 3.0 will be applied for the shear and bending stresses to account for the threads [87, 88], and a high grade steel AISI 4140 with a yield strength of 1110MPa and ultimate tensile strength of 1185MPa will be considered [87, 98].

$$\sigma_a = \frac{F_p}{A_t} \quad (17)$$

$$\tau_b = \frac{4V}{3A} = \frac{16V}{3\pi d^2} \quad (18)$$

$$\sigma_b = \frac{Md}{2I} = \frac{32M}{\pi d^3} \quad (19)$$

$$\sigma_{eq} = \sqrt{(\sigma_a + K_s \sigma_b)^2 + 3(K_s \tau_b)^2} \quad (20)$$

$$S_e = (0.566 \times -9.68 S_{ut} \times 10^{-11}) S_{ut} \quad (21)$$

Where σ_a , axial normal stress, Pa; F_p , pre-load axial force, N; A_t , tensile stress area, m²; d , diameter, m; τ_b , transverse shear stress, Pa; V , shear force, N; A , cross-sectional area, m²; σ_b , bending normal stress, Pa; M , bending moment, N.m; I , area moment of inertia, m⁴; σ_{eq} , equivalent combined stress, Pa; K_s , stress concentration factor; S_e , endurance strength, Pa; and S_{ut} , ultimate tensile strength, Pa.

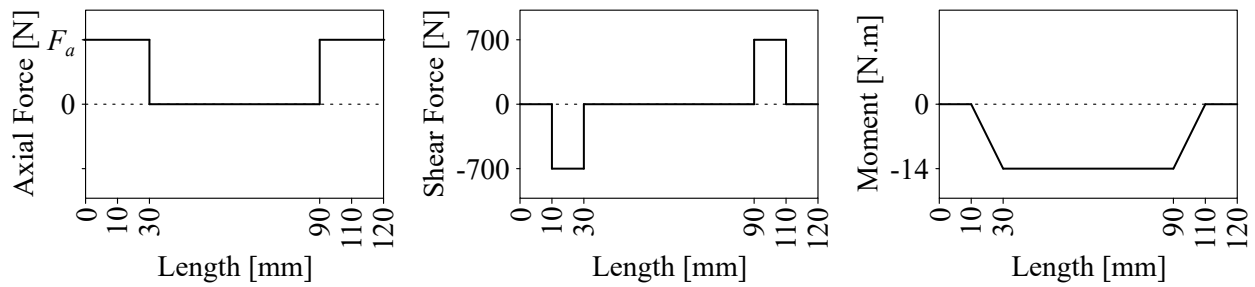


Figure 39: Axial force, shear force, and bending moment diagrams for the front axle.

With a 9mm diameter, it is found at the maximum location that there will be an axial stress of 352.4MPa from a pre-load force of 16670N, shear stress of 14.67MPa without the stress concentration factor applied, and bending stress of 195.6MPa without the stress concentration factor applied. The equivalent combined stress from Equation 20 produces a total stress of 922.6MPa, which has a corresponding safety factor of 1.21. This diameter is actually fairly regular for the front axle in the front hub of a bicycle which uses a standard thread of M9x1mm [99].

The fatigue performance of the axle can also be examined with Equation 13, where the minimum stress from only the pre-load stress, the maximum stress is the combined stress with a fatigue stress concentration factor of 2.0 used instead of the previous static stress concentration factor, and the endurance strength can be estimated using Equation 21 (this equation has been slightly manipulated where the fatigue stress concentration factor present in the original has been removed and used when finding the equivalent combined stress instead) [89]. This results in a midrange stress of 548.9MPa, alternating stress of 196.475MPa, and endurance strength of 534.8MPa, which shows using the Modified Goodman failure criterion in Equation 15 that there is a fatigue safety factor of 1.20. Thus, this diameter should be suitable, even when shocks from minor obstacles are encountered, because it is

safe for the extreme case of maximum braking and the presence of the spacers between the forkends and bearings will actually make the axle more rigid and help to reduce the substantial bending stresses.

Subsequently, the bearings can be chosen, where single row deep groove ball bearings are considered since there will be primary radial loading but there may be minimal axial loads during turning - the axial pre-load force from the axle is completely supported through the compression of the lock nuts and does not affect the bearings. Also, it is useful for the bearings to be sealed with shields or contact seals to prevent contamination and increase the effectiveness of the bearing without maintenance. The static safety of the bearings is given by Equation 22, and the dynamic life is given by Equation 23. To determine a suitable bearing, the combined radial load on each bearing is taken as 700N and, using the SKF Bearing Catalogue [100], it is expected for slight contamination with a factor of 0.4 and rated viscosity of approximately 205mm²/s or ISO VF 68 lubrication between the operating temperatures. Thus, considering the relevant bearings in Table 18 with bore diameters of 9mm, it is found that the most suitable bearing is the 609-2RSH with contact seals, because it is safe from static failure with a safety factor of 2.37 and is predicted to have a life of at least 6115hr when operating at an average of 18km/hr or 2202 days when commuting 50km each day (the average speed has no effect on the number of days for the same commuting distance per day). After this point, it will be required for maintenance or replacement of the bearings which is understandable. The data sheet for the SKF 609-2RSH bearings is included in Appendix C, but the dimensions follow ISO 15:1998 so the bearing may be replaced by an identical bearing from another manufacturer if necessary [100].

$$n = \frac{C_0}{P_0} \quad (22)$$

$$L_{bas} = \left(\frac{C}{P}\right)^p \rightarrow L_{bas,hr} = \frac{10^6}{60\omega} L_{bas} \rightarrow L_{skf} = a_{rel}a_{skf} \left(\frac{C}{P}\right)^p \rightarrow L_{skf,hr} = \frac{10^6}{60\omega} L_{skf} \quad (23)$$

Where n , static safety factor; C_0 , basic static load rating, N; P_0 , applied static load, N; L_{bas} , basic life cycles, 10⁶ cycles; C , basic dynamic load rating, N; P , applied dynamic load, N; p , life exponent factor, 3 for ball bearings or 3.33 for roller bearings; $L_{bas,hr}$, basic life time, hr; ω , angular velocity, rev/min; L_{skf} , SKF modified life cycles, 10⁶ cycles; a_{rel} , reliability modifying factor; a_{skf} , SKF modifying factor; and $L_{skf,hr}$, SKF modified life time, hr. (a_{rel} and a_{skf} are from the SKF Bearing Catalogue [100] with the fatigue load limit, P_u [N], contamination factor, η_c , and viscosity ratio, κ).

The mounting of the spokes to the hub can also be decided, although this can be changed by rebuilding the wheel if the user desires. The options for mounting are based on the lacing and number of times the spokes cross which sets the angle at which the spokes protrude from the hub. The most common mounting options are lacing as radial or zero-cross (0X, with no crossings), one-cross (1X, with one crossing), two-cross (2X, with two crossings), three-cross (3X, with three crossings), and four-cross (4X, with four crossings), where the flange exit or tangential angle increases as the number of crossings increases [55]. A higher crossing allows for the torque from the wheel to be braced axial through the spokes to the hub (or vice versa) and a stronger build where the applied torque when accelerating or braking affects each consecutive spoke equally but in an opposite direction such

Table 18: Comparison between various candidate bearings for the axle in the front hub. The constant values include $d = 9\text{mm}$, $P_0 = 700\text{N}$, $P = 700\text{N}$, $\eta_c = 0.4$ for slight contamination, $\kappa = 2.17$, and $a_{rel} = 0.21$ for 99% reliability, and an average speed of 18km/hr producing an angular velocity of 137.6rev/min used to estimate the life in terms of time and distance.

Bearing Classification	Outer Diameter [mm]	Width [mm]	Basic Static Rating [N]	Basic Dynamic Rating [N]	Fatigue Load Limit [N]	Static Safety Factor	Basic Life [10^6 cycles]	Basic Life Time [hrs]	Basic Life Distance [km]	SKF Modifying Factor	SKF Life [10^6 cycles]	SKF Life Time [hrs]	SKF Life Distance [km]	SKF 50km Trips Amount
618	17	4	640	1430	27	0.91	8.53	1033	18590	0.64	1.15	138.8	2498	49.9
619	20	6	865	2080	36	1.24	26.2	3178	57200	0.81	4.46	540.6	9730	195
609	24	7	1660	3900	71	2.37	173	20950	377100	1.39	50.5	6115	110100	2202
629	26	8	1960	4750	83	2.80	313	37850	381200	1.68	110	13350	240300	4807

that the average tension and compression experienced in the hub does not change; while a lower crossing offers a less sturdy structure but a marginally lower mass since the spokes can be shorter [55]. However, a radial lacing is ineffective when using disc brakes, because disc brakes require the transfer of torque from the disc to the hub and then through the wheel and, since it offers less benefits and to allow for the possibility of disc brakes, the radial lacing is discarded. So, with a preference for strength but a concession for mass, a three-cross lacing will be adopted, as seen in Figure 40.

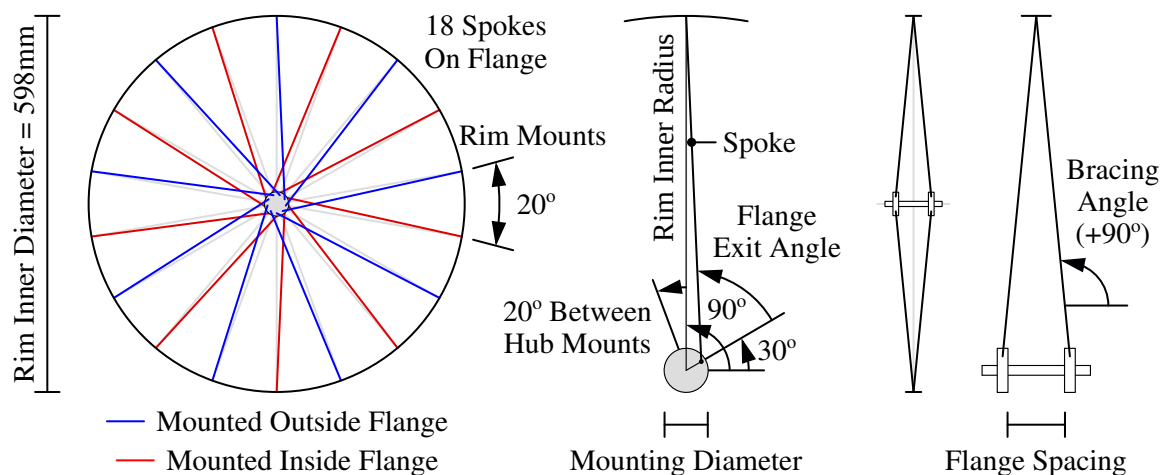


Figure 40: Lacing for a flange on the front wheel - only half the mounting holes on the rim are shown, where the other half for the other flange will be identical but offset by 10° . It should be highlighted that this does not apply to the rear wheel, where the bracing from the spokes will actually be slightly offset from the centreline to accommodate for the freehub.

With a flange diameter of 70mm to produce a moderate stiffness, the mounting holes will be placed at a pitch circle diameter of 60mm. The spokes will have a total length of about 295.6mm with approximate flange exit angles of 65.2° and bracing angles of 8° . Since the spokes have an elbow height of 7.5mm to the centreline of the 2.6mm diameter, the flange should be no more than 6.2mm thick. It is also estimated for a head clearance of 3mm to avoid interference between and overlapping of the spoke heads at the hub. For one-cross lacing on the hub motor with an exit angles of 30.8° and the mounting pitch circle diameter of 208mm, it is required for a spoke length of about 197.1mm on the left and 195.5mm on the right, and bracing angles of 9.3° on the left and 5.6° on the right (it is uncertain if a one-cross lacing is used, but this is assumed based on the mounting hole positions). Overall, a front spoke will have a mass of 13g, while a rear spoke will have a mass of 8g.

Finally, the hub shell needs to be specified and should be constructed from aluminium 6061-T6 for a low mass and to be softer than the spokes such that it allows the flange to conform and elastically deform until there is full contact between spoke and flange [55]. The applied forces will be exerted on the flanges from the tension in the spokes with reaction forces at the bearings. So, the flanges will be positioned directly above the bearings at 80mm apart to minimise bending developed within the hub shell. The shape of the hub shell can be based on the placement of the bearings and mounting holes for the spokes to allow for a finite element analysis to be performed to evaluate the strength of the hub shell. However, most of the dimensions are set and optimisations cannot be substantially performed to decrease mass, but minor details are used to remove material beneath the mounting holes.

In the simulation, a radial lacing from the spokes is considered since this creates the weakest hub shell, where a tensile magnitude of 1208N is applied to each mounting hole in the relevant direction. The initial mesh settings are quadratic order elements, fine relevance, slow transition, and maximum element size of 3mm, but convergence was also applied for a difference less than 2% for the maximum

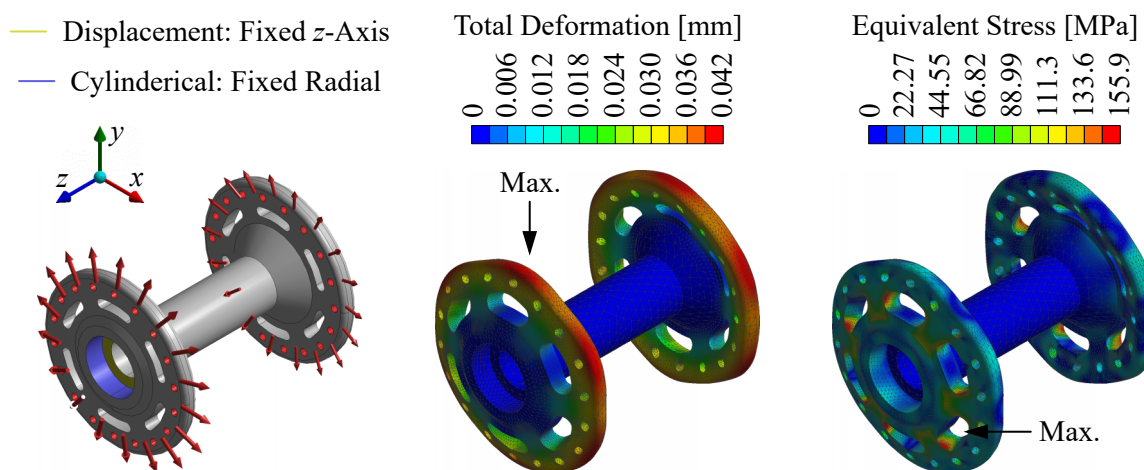


Figure 41: Arrangement of the boundary conditions with the applied loads and supports, and deformation (exaggerated) and stress experienced in the hub shell for aluminium 6061-T6 with a radial tensile force of 1208N applied from the spokes, as simulated in ANSYS Mechanical 18.2.

stress. The arrangement of the boundary conditions are seen in Figure 41 with the final results, which predict a maximum stress of 155.9MPa and safety factor of 1.77 at the rounded corners of the details.

Overall, with a total front hub mass of approximately 0.286kg for the hub shell, axle, bearings, and spacers, the front wheel is estimated to have a mass of 2.036kg including the hub, spokes, rim, and deflated tyre. On the rear wheel, the estimated mass is 6.294kg including the rear hub motor, spokes, rim, and deflated tyre. If the total mass of the design is around 19kg, the 8.330kg combined mass of the front and rear wheels will be 43.84% of this mass which is 2.63kg higher than the assumed 30% or 5.7kg for the electric propulsion, but this is still acceptable given that the difference is only 2.768% of the total 95kg mass and the motor has a maximum rated output well over the investigated 600W. Finally, if disc brakes are chosen for the braking system, slight modification will need to be applied to a side of the front hub shell for the standard mounting and transfer of torque.

4.3 MANUAL PROPULSION

The manual propulsion converts the input energy from the user into rotational kinetic energy of the rear wheel and translational kinetic energy of the design and user, which is achieved through gearing and power transmission. The primary aim of the manual propulsion is to supplement and offer assistance to the electric propulsion when additional power is needed and, for this purpose, the manual propulsion must be designed to offer increased torque for assistance on excessive slopes with gradients above 3%. Fully independent manual propulsion will be minimally used at lower speeds up to 20km/hr, with low wind speeds around 10km/hr, and on slopes up to moderate gradients of 3%.

4.3.1 GEARING

It is necessary to determine whether it is required for multiple gears or if it would be acceptable to have a single-gear power transmission. The possibility of using a single-gear power transmission is considered based on typical steady-state cases when only manual propulsion will be used, with the results shown in Table 19. Assuming a perfect efficiency, the relationships to derive the results are described by Equation 24 to Equation 27 and seen in the free-body diagram of the rear wheel in Figure 19. As with the electric propulsion, it was conservatively assumed that there is a frontal area of 0.55m², drag coefficient of 1.2, rolling coefficient of 0.008, and maximum design mass of 19kg with an average user mass of 76kg for a total mass of 95kg - the total mass was assumed to be distributed with approximately 60% on the rear wheel and 40% on the front wheel [12]. For a realistic model, this investigation was also based on a limiting maximum continuous power of 240W, effective pedalling force up to 200N assuming a standard crank length of 170mm to produce a maximum continuous torque of 34N.m, cadence range of 50rev/min to 110rev/min, and the use of the chosen 622mm rims and Challenge Gravel Grinder TLR tyre with a height of approximately 36mm when inflated.

$$P = T\omega \rightarrow P_w = \eta P_c \quad (24)$$

$$G = \frac{Z_w}{Z_c} = \frac{d_w}{d_c} = \frac{T_w}{T_c} = \frac{\omega_c}{\omega_w} \quad (25)$$

$$\sum_{i=1}^n T_o = 0 \rightarrow T_w - F_f r_w + \%m_r F_r = 0 \quad (26)$$

$$\sum_{i=1}^n F_i = 0 \rightarrow F_f - F_d - F_w - F_r = 0 \quad (27)$$

Where P , power, W; T , torque, N.m; ω , angular velocity, rad/s; P_w , wheel power, W; P_c , crankset power, W; η , efficiency; G , gear ratio; Z_w , number of wheel teeth; Z_c , number of crankset teeth; d_w , wheel diameter, m; d_c , crankset diameter, m; T_w , wheel torque, N.m; T_c , crankset torque, N.m; ω_c , crankset angular velocity, rad/s; ω_w , wheel angular velocity, rad/s; T_o , arbitrary torque component, N.m; F_f , friction driving force, N; r_w , wheel radius, m; $\%m_r$, fraction of mass on rear wheel, kg; F_r , rolling resistance force, N; F_i , arbitrary force component, N; F_d , drag resistance force, N; and F_w , weight resistance force, N.

Through iterating with various gear ratios, the most suitable gear ratios were found to be between 1:1.74 and 1:2.18 to achieve decent performance above 20km/hr with varying wind speeds up to 15km/hr and slopes up to gradients of 3%. Typical values for single-speed power transmissions range between 2.0 to 3.0, but it should be emphasised that these calculations maximise torque within the acceptable cadence such that the manual propulsion can act as a supplement to the electric propulsion while still acceptably achieving the requirements during commuting at lower speeds and on moderate slopes. Conversely, typical single-speed power transmissions are optimised for only manual propulsion where the wheels are smaller at 559mm and it is necessary to achieve high speeds up to 40km/hr on mostly flat and downhill terrain while maintaining a smaller cadence range around 90rev/min [12].

Before declaring a verdict, the primary combination of electric propulsion and manual propulsion also needs to be considered. This is shown in Table 20, where a continuous rated power of 250W is considered from the motor. It is evident that a gear ratio of 1:1.74 is not capable of a speed of 30km/hr due to a very high cadence of 131.8rev/min, where the limit of this high cadence is reached with a gear ratio of 1:2.09. So, with a slight division between the need for an increased torque versus an increased cadence, gear ratios between 1:2.09 and 1:2.18 are the most acceptable with speeds of at least 30km/hr on slopes up to 3% gradient and speeds of at least 20km/hr on slopes up to 7% gradient, depending on the wind speeds. Furthermore, with a peak performance with increased pedalling force for short periods, even steeper slopes could be climbed at greater wind speeds. From this, it seems as though a single-speed power transmission optimised for the operating conditions may be suitable.

However, there are still additional advantages of a single-speed power transmission which include a narrowly increased efficiency regarding a chain drive with a typical range between 96% and 99% due to a constant chain tension, straight chainline from the front and rear sprockets, and lack of friction in the rear derailleur; while multiple gears tend to have an efficiency between 86% and 98% depending on the derailleur and chosen gear [12]. From the increased simplicity by removing the front and rear derailleurs, gears, and shifting components, there is also a decreased mass with up to 0.4kg for

Table 19: Collection of expected operating cases for various gear ratios with continuous manual propulsion over a sustained period. The cases are based on different operating speeds, wind speeds, and slope gradients. The optimal gear ratios found from iterations are presented satisfying the desired criteria.

Speed		Wind		Slope		Drag [N]	Weight [N]	Rolling [N]	Friction [N]	Torque [N.m]	Ratio 1:2.18		Ratio 1:2.09		Ratio 1:1.74		Power [W]
[km/hr]	[m/s]	[km/hr]	[m/s]	Grad.	[°]						[N.m]	[r/min]	[N.m]	[r/min]	[N.m]	[r/min]	
25	6.94	191	5	0	0	27.5	0	7.46	35.0	10.6	23.1	87.7	22.1	91.4	18.4	110	211.7
20	5.56	153	15	0	0	37.4	0	7.46	44.9	14.0	30.6	70.1	29.3	73.2	24.4	87.9	224.5
25	6.94	191	0	1%	0.57	19.1	9.32	7.46	35.9	10.9	23.8	87.7	22.8	91.4	19.0	110	218.0
20	5.56	153	10	1%	0.57	27.5	9.32	7.46	44.3	13.8	30.1	70.1	28.9	73.2	24.0	87.9	221.1
20	5.56	153	5	2%	1.15	19.1	18.6	7.45	45.2	14.1	30.8	70.1	29.5	73.2	24.6	87.9	226.2
15	4.17	115	10	2%	1.15	19.1	18.6	7.45	45.2	14.1	30.8	52.6	29.5	54.9	24.6	65.9	169.6
20	5.56	153	0	3%	1.72	12.2	27.9	7.45	47.6	15.0	32.6	70.1	31.3	73.2	26.1	87.9	239.7
15	4.17	115	5	3%	1.72	12.2	27.9	7.45	47.6	15.0	32.6	52.6	31.3	54.9	26.1	65.9	179.8

Table 20: Collection of expected operating cases for various gear ratios with continuous combined propulsion over a sustained period. The cases are based on different operating speeds, wind speeds, and slope gradients. The optimal gear ratios found from iterations are presented satisfying the desired criteria.

Speed		Wind		Slope		Drag [N]	Weight [N]	Rolling [N]	Friction [N]	Torque [N.m]	Ratio 1:2.18		Ratio 1:2.09		Ratio 1:1.74		Power [W]
[km/hr]	[m/s]	[km/hr]	[m/s]	Grad.	[°]						[N.m]	[r/min]	[N.m]	[r/min]	[N.m]	[r/min]	
30	8.33	229	5	0	0	37.4	0	7.46	44.9	3.61	7.88	105	7.55	110	6.29	132*	86.77
30	8.33	229	0	3%	1.72	27.5	27.9	7.45	62.9	9.86	21.5	105	20.6	110	17.2	132*	236.9
20	5.56	153	10	6%	3.43	27.5	55.8	7.44	90.8	14.3	31.2	70.1	29.9	73.2	24.9	87.9	229.4
15	4.17	115	20	6%	3.43	37.4	55.8	7.44	101	12.6	27.4	52.6	26.3	54.9	21.9	65.9	150.9
20	5.56	153	5	7%	4.00	19.1	65.1	7.44	91.6	14.6	31.9	70.1	30.6	73.2	25.4	87.9	234.2
15	4.17	115	15	7%	4.00	27.5	65.1	7.44	100	12.3	26.9	52.6	25.8	54.9	21.5	65.9	148.1
15	4.17	115	15	8%	4.57	27.5	74.3	7.43	109	15.5	33.9	52.6	32.5	54.9	27.0	65.9	186.6
15	4.17	115	0	10%	5.71	6.9	92.7	7.42	107	14.8	32.2	52.6	30.9	54.9	25.7	65.9	177.4

* The value violates the maximum power of 240W, maximum torque of 34N, maximum cadence of 110rev/min, or minimum cadence of 50rev/min.

slightly improved performance (this will marginally aid with shifting the centre of gravity forward to correct the mass distribution), higher cost effectiveness, and greater reliability and resilience with less maintenance and lower likelihood of operating issues like derailing and skipping [12]. As is obvious, the main advantage of multiple gears is the versatility offered from different gear ratios which provide relief so the user can maintain a constant cadence, but this is mostly applicable when manual propulsion is the primary form of propulsion and needs to be compatible with a wide range of operating conditions. Thus, it is decided that a single-speed power transmission will be developed, because it can be optimised for the operating condition and, within these operating conditions, it will allow for better performance due to an increased efficiency and decreased mass.

4.3.2 POWER TRANSMISSION

Firstly, it is established that the manual propulsion will utilise rear wheel drive rather than front wheel drive, because it has been decided that the hub motor will provide the best performance at the rear wheel. Also, trying to use front wheel drive will require an extremely complex steering mechanism, if it is even possible. Subsequently, compared to other atypical forms of manual power input (such as oscillating motions, linear sliders, hand pedalling, or step pedalling), it will be vastly more efficient and effective to use circular pedalling with the legs of the user [12], which is the conventional method involving continuously rotating each foot.

The method of transmitting the power from pedalling to the rear wheel needs to be evaluated. Because of the need for separation between the driving gear and driven gear, the possible concepts include the Chain Drive, Belt Drive, and Shaft Drive, which are seen in Figure 42. The Chain Drive uses front sprocket attached to the cranks and a rear sprocket attached to the rear wheel to form the desired gear ratio with a roller chain to transmit power between the sprockets. The Belt Drive uses front pulley attached to the cranks and a rear pulley attached to the rear wheel to form the desired gear ratio with a timing or toothed belt to transmit power between the pulleys. The Shaft Drive uses a front bevel gear attached to the cranks and a rear bevel gear attached to the rear wheel to form the desired gear ratio with a shaft with bevel gears at the end to transmit power between the gears - alternatively, the desired gear ratio could be divided into stages with the shaft gears.

Table 21 compares and evaluates the best concept. For the scoring, the need for a low likelihood of operating issues and durable life are rated first and second respectively because they are related to robustness, but the immediate nature of operating issues under slightly contaminated and wet conditions are viewed as more important than the long-term nature of durability. The third rated criterion is the ability to withstand shocks, because it is essential for endurance when minor obstacles are encountered, otherwise the performance will become inconsistent and unreliable. The fourth rated criterion is the ease of maintenance, repairability, and replacement, because this will provide convenience but, more importantly, it will allow the user to customise the gear ratio if the chosen value is not suitable for their needs. The flexibility to be integrated with the other sub-systems is rated fifth, because this could affect the reliability and performance of the other sub-systems with far reaching repercussions

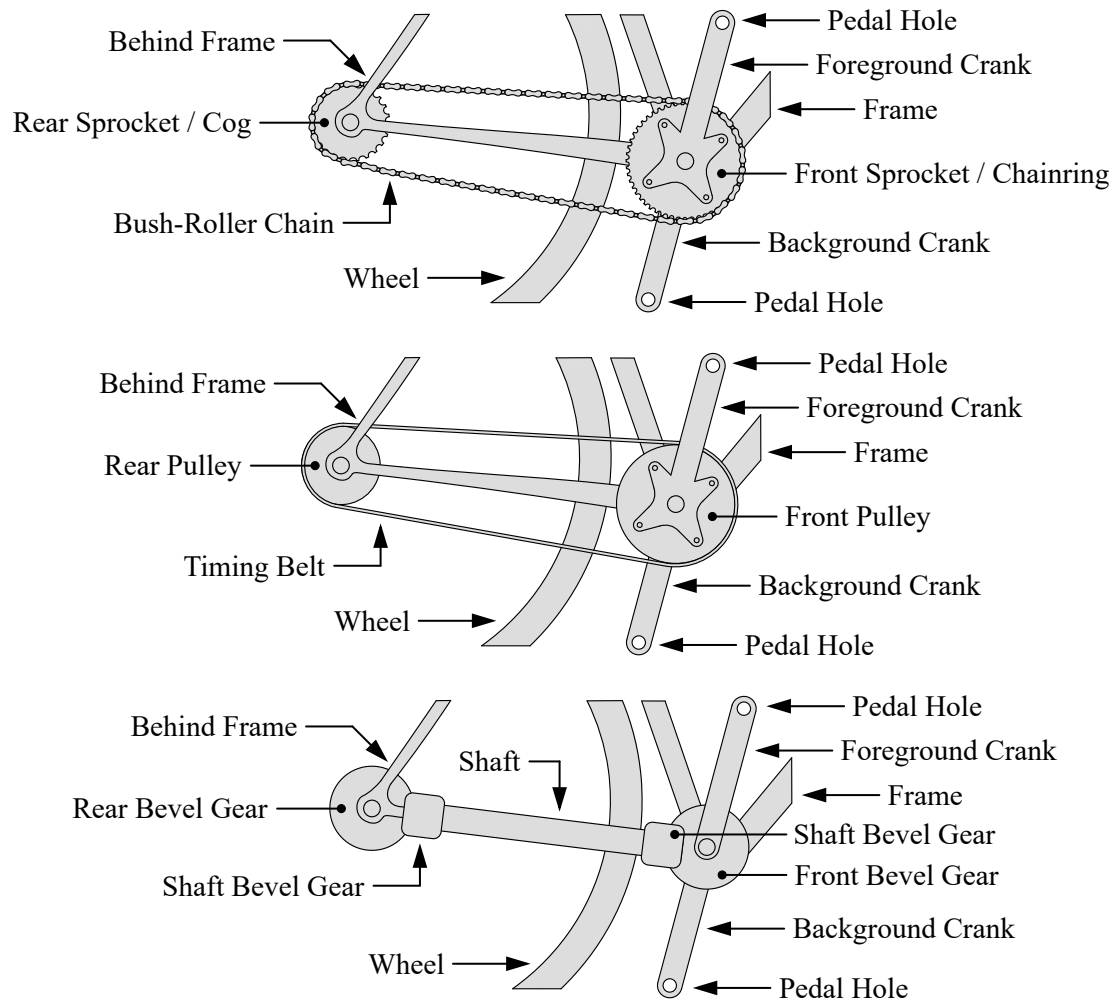


Figure 42: Schematics of the possible power transmission methods for manual propulsion, with possibilities for the Chain Drive (top), Belt Drive (centre), and Shaft Drive (bottom).

along the lines of an increased mass and instability to accommodate the integration. The need to be lightweight is rated sixth, because the mass of the components is expected to be extremely low compared to the total mass of the design and user, where a decreased mass will only have a minimal overall performance improvement. The efficiency, although important to the design, is allocated a low weighting at seventh, because it is difficult to accurately judge efficiency based on the wide expected ranges without an actual design, but it is still useful to generally acknowledge the dissimilarities. Finally, the cost effectiveness is rated eighth, since it is not viewed as decisive to the design purpose.

Although it excelled with low operating issues, high durability, and high efficiency, the Shaft Drive obtained a score of 66%, because it showed difficult integration with the frame, where it would be integrated into the members of the rear forkend for best compatibility; allows for inferior shock absorption since it is rigid and needs very tight tolerances to ensure precise clearance and positioning of the gears; and failed to convey a low mass with the gears being reasonably heavier than sprockets or pulleys [12, 94]. In the highest weighted criteria, the Chain Drive has a slight probability of derailing or twisting, but this is made almost negligible with a correct chainline and tensioning; very

Table 21: Weighting matrix and evaluation of the possibilities for the transmission of manual power.

Label	Criteria	Weighting Matrix							Total Weight	Percent Weight	Max. Weighted Score	Chain		Belt		Shaft		
		A	B	C	D	E	F	G				Score / 5	Weighted Score	Score / 5	Weighted Score	Score / 5	Weighted Score	
A	1. Efficient	A	B	C	D	E	F	G	A	2	5.6%	10	4	8	3	6	5	10
B	2. Lightweight		B	C	D	E	F	G	B	3	8.3%	15	3	9	5	15	2	6
C	3. Durable Life			C	C	C	C	G	C	7	19.4%	35	3	21	4	28	5	35
D	4. Flexible Integration				D	E	F	G	D	4	11.1%	20	5	20	2	8	1	4
E	5. Easy Maintenance					E	F	G	F	5	13.9%	25	4	20	3	15	2	10
F	6. Withstand Shocks						F	G	F	6	16.7%	30	4	24	5	30	2	12
G	7. Low Operating Issues							G	G	8	22.2%	40	4	32	3	24	5	40
H	8. Cost Effective								H	1	2.8%	5	5	5	4	4	2	2
	Total Score											180		139		130		119

good durability, but it may be prone to rust if exposed to wet conditions without protection; decent ability to withstand shocks since it is flexible [94]; and easily maintained through periodic lubrication which may be bothersome but fairly simple, or repaired through replacement and customisation with commonly available chain and sprocket variations, since there is optimal integration without affecting the other sub-systems where the chain can be disassembled or assembled and the sprockets follow standard mounting on a freehub. Overall, the Chain Drive obtained a score of 78%. The Belt Drive obtained a score of 72%, because it excelled with a very low mass and enhanced ability to withstand shocks [94], but it suffers since there is a risk of cutting or tearing if it contacts sharp or abrasive surfaces, and there is very limited availability of parts for replacement and customisation. Generally, the Chain Drive and Belt Drive exhibited similar characteristics, but the major distinction is the poor ability of the Belt Drive to be flexibly integrated with the frame, because it must be either incorporated as the frame is being built, but then it cannot be replaced which is very deterring; or it requires for a split in the frame, usually near the rear forkends, which will result in a weaker frame prone to distortion or a frame with an increased mass. Therefore, according to the evaluation, the Chain Drive will offer the most versatile power transmission.

The common chains used for bicycles have a standard construction, seen in Figure 43, and follow ISO 606 for short-pitch precision roller chains as a simplex chain, where a pitch of 12.7mm is normal and the minimum internal width between the inner plates generally varies at 2.3mm, 3.3mm, 4.0mm, or 4.8mm [101]. The length of the chain and actual centre distance are dependent on the pitch of the chain, diameters of the sprockets, number of links, and contemplated centre distance between the sprockets, as given by Equation 28 and Equation 29 respectively [94].

$$N_l \approx \frac{\pi(d_c + d_w)}{2p} + \frac{2C}{p} + \frac{(d_c - d_w)^2}{4Cp} = \frac{Z_c + Z_w}{2} + \frac{2C}{p} + \frac{(Z_c - Z_w)^2}{4\pi^2 C} \rightarrow l = N_l p \quad (28)$$

$$C = \frac{p}{8} \left(2N_l - Z_c - Z_w + \sqrt{(2N_l - Z_c - Z_w)^2 - \left(\frac{\pi}{3.88} (Z_c - Z_w)^2 \right)} \right) \quad (29)$$

Where N_l , number of chain links (round up to the nearest integer - preferably even); d_c , driving sprocket diameter, mm; d_w , driven sprocket diameter, mm; C , centre distance, mm; p , pitch, mm; Z_c , number of driving teeth; Z_w , number of driven teeth; and l , chain length, mm.

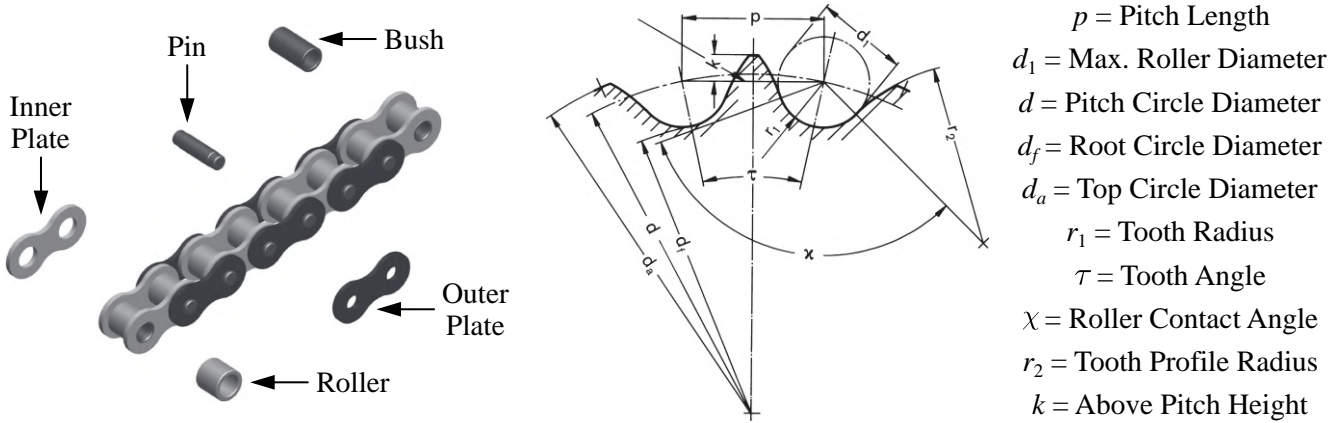


Figure 43: Standard construction and components of a roller chain [102].

A gear ratio between 1:2.09 and 1:2.18 is required, but it would be preferable for a compromise of a lower cadence and increased torque in a greater gear ratio with a standard crank length of 170mm. As is required, this will allow for decent performance when frequently stopping and starting and on flat and uphill terrain with speeds up to 30km/hr, but coasting may need to be used on downhill terrains at higher speeds which is acceptable since these speeds are already excessive. So, the number of teeth on and diameter of each sprocket needs to be determined relative to the desired gear ratio.

As a starting point, there will be variations in components of velocity and oscillations in acceleration of the chain created by the polygonal effect and, so, the number of teeth on the driven sprocket should be greater than 19 teeth to minimise these variations negligibly below 2% [94, 103, 102]. It is also preferable for an even number of pitches in the chain, a driving sprocket with an odd number of teeth, and a driven sprocket with an even number of teeth because this will ensure a uniform wear distribution over both the chain and sprocket teeth [94, 102]. The shocks experienced will be greater for a greater angular speed of the driven sprocket and, so, the diameter of the driven sprocket should be maximised [94]. With regards to efficiency generally, the efficiency of the power transmission decreases as the size of the rear sprocket decreases, the torque transferred or chain tension decreases, and the type of lubrication or lack of lubrication has a negligible effect on efficiency [12]. However, it is still necessary to minimise the size of the sprockets to decrease mass and allow for suitable usability, clearance above the ground, and avoidance of interference with other sub-systems.

The possible gear ratios with driving sprockets with teeth from 37 to 50 and driven sprockets with teeth from 17 to 23 are shown in Table 22. This indicates that the most suitable gear ratio matching

the criteria is 1:2.15 with 43 teeth on the driving sprocket and 20 teeth on the driven sprocket. There should also be a fair range of customisation for the driven sprocket if the user desires.

Table 22: Comparison of the suitable gear ratios presented as a ratio under unity (1:X).

Driver Driven	37	38	39	40	41	42	43	44	45	46	47	48	49	50
17	2.18	2.24	2.29	2.35	2.41	2.47	2.53	2.59	2.65	2.71	2.76	2.82	2.88	2.94
18	2.06	2.11	2.17	2.22	2.28	2.33	2.39	2.44	2.50	2.56	2.61	2.67	2.72	2.78
19	1.95	2.00	2.05	2.11	2.16	2.21	2.26	2.32	2.37	2.42	2.47	2.53	2.58	2.63
20	1.85	1.90	1.95	2.00	2.05	2.10	2.15	2.20	2.25	2.30	2.35	2.40	2.45	2.50
21	1.76	1.81	1.86	1.90	1.95	2.00	2.05	2.10	2.14	2.19	2.24	2.29	2.33	2.38
22	1.68	1.73	1.77	1.82	1.86	1.91	1.95	2.00	2.05	2.09	2.14	2.18	2.23	2.27
23	1.61	1.65	1.70	1.74	1.78	1.83	1.87	1.91	1.96	2.00	2.04	2.09	2.13	2.17

To check that a pitch of 12.7mm is acceptable, the design power can be determined based on factors for the dynamic overloads during application and effects of the number of teeth of the driven sprocket. The application factor takes into account the characteristics of the operating conditions with regards to lubrication, contamination, and shocks during operation. This is shown in Equation 30. These modifying factors are determined with reference to the Renold Chain Designer Guide [103] to ensure a minimum life expectancy with proper installation and lubrication of 15000hr. For evaluation, it is reasoned that there will be slight shocks as there will be frequent stopping and starting of pedalling, but there will be more significant shocks at the driven sprocket due to the wheel encountering minor obstacles - a factor of 1.4 was chosen. There will be 20 teeth on the driven gear which results in a factor of 0.95. This results in an overall design factor of 1.33.

$$P_d = f_1 f_2 P \quad (30)$$

Where P_d , design power, W; f_1 , application factor; f_2 , driven teeth factor; and P , power, W.

Considering continuous operation with the maximum torque of 34N.m and a peak cadence of 110rev/min, the generated power is 391.7W - although it is unlikely the user will be able to produce this power level. Also, the maximum torque at a cadence of 50rev/min generates 178.0W of power. Applying the overall design factor, the design powers are 520.9W and 231.4W respectively. From the ratings chart in Figure 44, this shows that a 12.7mm chain is the best choice of chain with manual lubrication.

The required sizing of the chain is satisfied with the ISO 606 081-100 roller chain corresponding to a pitch of 12.7mm and minimum internal width of 3.30mm. This also sets the corresponding dimensions of the sprockets where the pitch circle diameters is equal to the product between the pitch and a factor for the number of teeth on the sprocket, where the factors are 13.70 for the driving 43-teeth sprocket and 6.392 for the driven 20-teeth sprocket which produce pitch circle diameters of 174.0mm and 81.18mm respectively [103, 102]. The remaining dimensions of the sprockets were

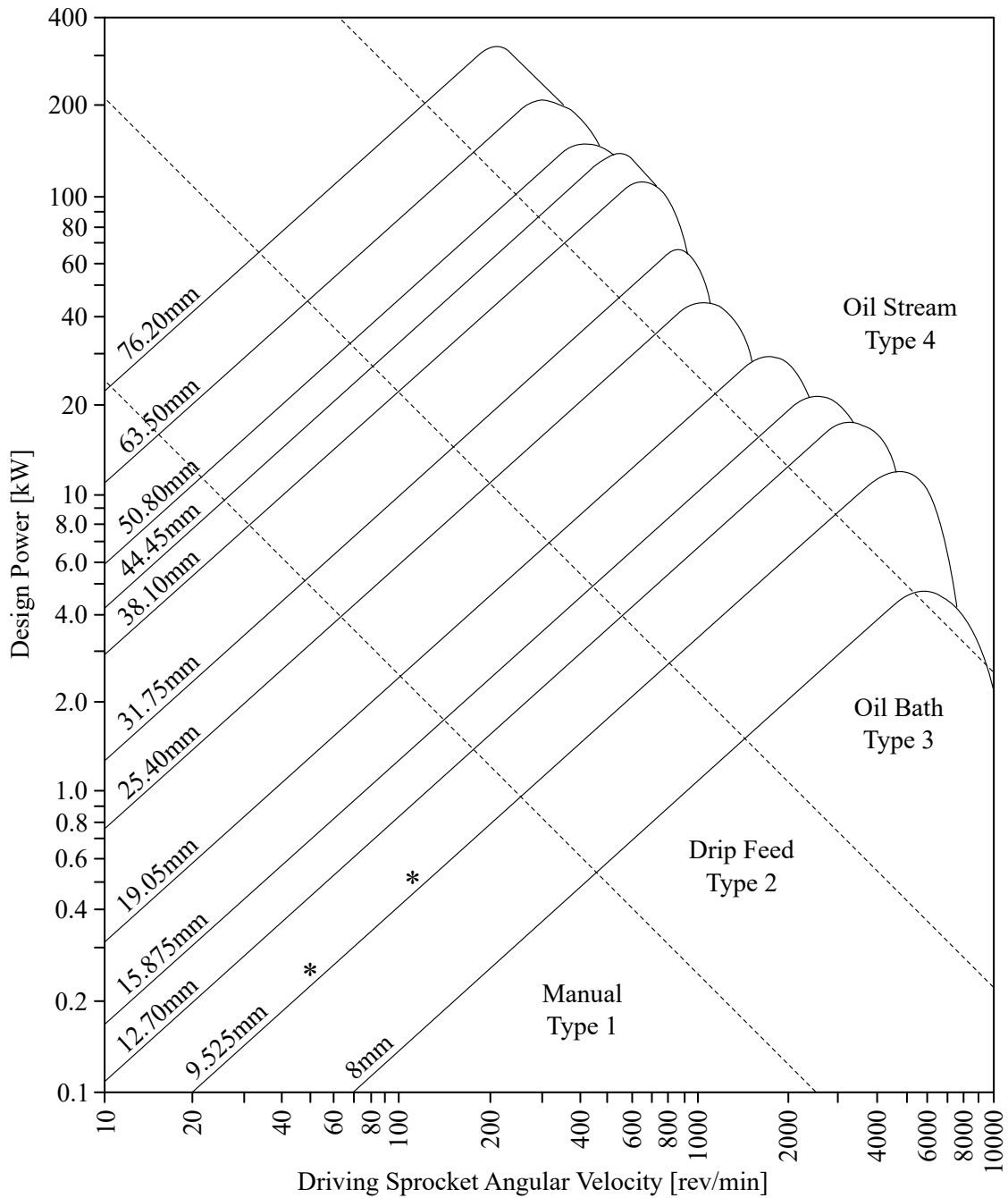


Figure 44: Ratings chart used to select the most appropriate roller chain to ensure a successful design based on the required design power and driving sprocket angular velocity [103].

automatically calculated by Autodesk Inventor Professional 2019 for accuracy. The centre distance of the sprockets will be finalised with the frame in Section 4.4, but the actual centre distance should be between 30 and 50 times greater than the pitch - in other words, between 381mm and 635mm [94, 103]. Although it is not necessary since the rating chart guarantees that the chain will be acceptable, the reliability can easily be further checked with the Roller Chain Design Accelerator in Autodesk Inventor Professional 2019 which predicts a design power of 571W, tangential velocity of 1.049m/s,

effective tension of 373.5N, static safety factor of 20.45 (recommended to be greater than 7), and dynamic safety factor of 13.64 (recommended to be greater than 5).

Finally, due to the nature of the relative motion between the chain elements, the chain will experience wear, which will result in increasing gaps between the pairs of elements creating a larger pitch and an increased overall chain length [94]. Consequently, this increase in pitch will cause the chain to wind around the sprockets at a greater diameter than the design diameter which will lead to accelerated wear and, so, the life limit of the chain should be considered once the elongation percentages exceeds 2% [94, 103, 102]. The user will be required to perform this maintenance by measuring the elongation with commonly available tools and replacing the chain when it is no longer acceptable. For slower elongation and minimised wear and rust, periodic lubrication must also be manually applied by the user using a mineral oil with a SAE 30 or BS 4231/100 rating [103, 102].

4.3.3 CRANKS

In the crankset, the sprocket will be mounted to a crank on one side of the design while there will be another crank on the other side of the design. The mounting of the sprocket can use a four bolt arrangement with a thread of 5mm diameter by 0.8mm pitch and common bolt centre diameter of 64mm, which should allow compatibility with other sprockets [104]. Both of the cranks will be mounted to a bottom bracket within the frame. A suitable bottom bracket is the Shimano Octalink V2 BB-ES300, which has a shell width of 68mm within the frame and basically consists of a hollow spindle and central sealed cartridge unit screwed into the frame using standard threads of 34.8mm diameter and 1.058mm pitch or 1.370in by 24tpi and two mounting shafts with eight splines of 9mm length and 2.8mm width on either side for the cranks where a crank bolt screws into the shafts following the cranks to secure them on the splines, as seen in Figure 45 [105, 106, 107]. A universal pedal hole of 14.28mm in diameter with a thread of 1.27mm pitch or 0.5625in by 20tpi (there must be normal thread on the sprocket pedal and reverse thread on the other pedal to counteract precession unscrewing the pedals) is also required at the end of each crank [108]. Based on observations, it is also reasoned that a clearance of 9mm between the crank and sprocket will be sufficient for the chain. As previously mentioned, a crank length of 170mm is desired.



Figure 45: Example of the Shimano Octalink V2 BB-ES300 bottom bracket [105].

In ISO 4210-8 [109], a safety test is submitted to evaluate the crank strength where a force of 1300N is applied to each crank at 45° separately in each direction. During actual use, the maximum loads are expected to be applied when the maximum user of 100kg is in a standing position is distributed across both cranks being either horizontal or vertical which would only apply a single component of about 490.5N to each crank. So, the proposed test can be seen as conservative since a vertical and horizontal component are applied at the same time with magnitudes of 920N. The resulting displacements and stress for this test can be evaluated with a finite element analysis. To produce the lowest mass and determine if it is suitable, aluminium 6061-T6 is considered for each component. For the contacts on the right crank, a no separation contact was applied for the interactions between the crank, sprocket, and bolts. For the mesh, quadratic order elements were used with a fine relevance and slow transition. The overall maximum element size was set at 2mm, but body sizing was applied near the bottom bracket connection through a 30mm sphere of influence to allow a finer resolution with element sizes

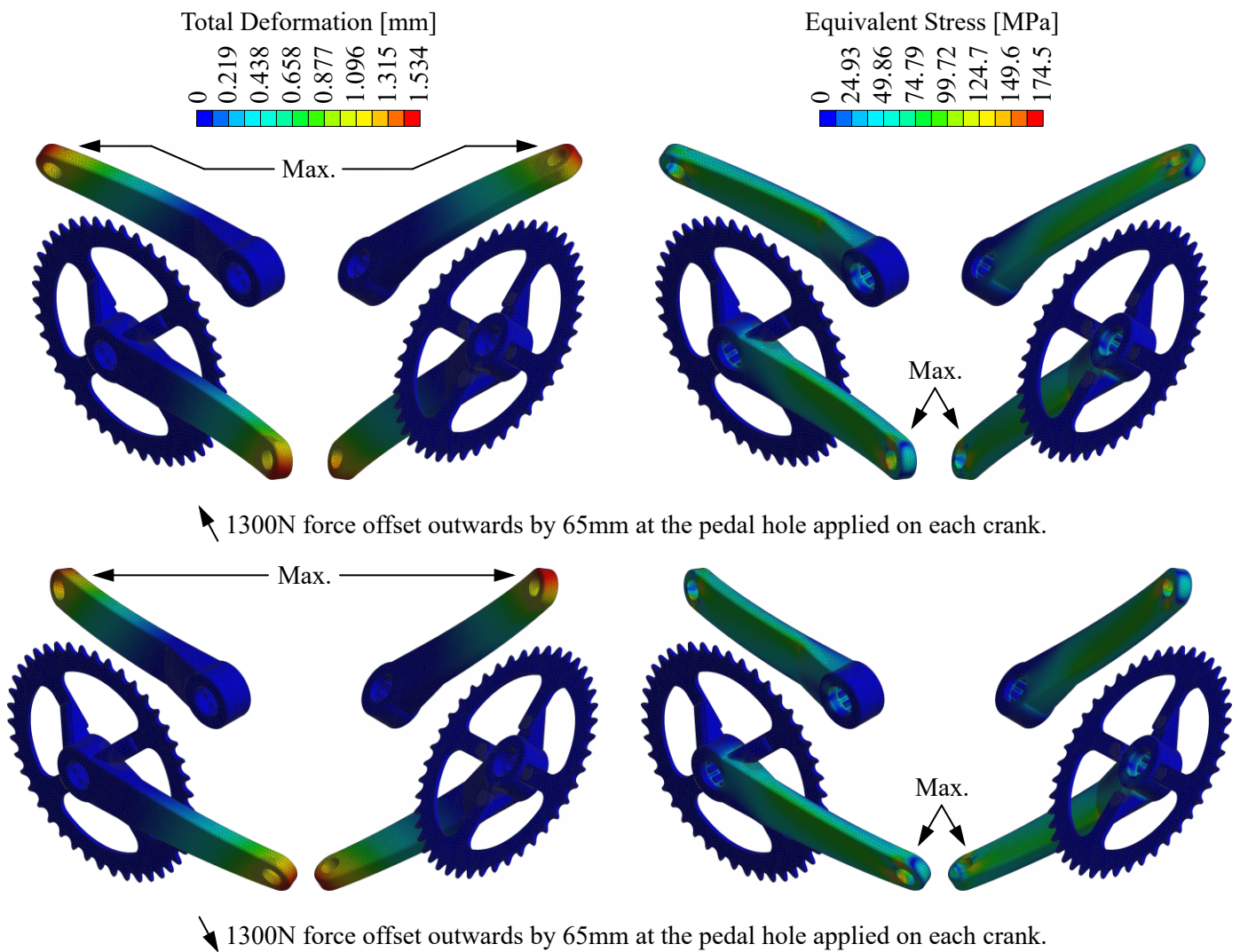


Figure 46: Deformation (exaggerated) and stress experienced in the crankset for the test cases using ANSYS Mechanical 18.2. Convergence within 2% was achieved with a first maximum stress of 173.4MPa and second maximum stress of 174.5MPa for a change of 0.6%.

up to only 1mm for the spline and members connecting the cranks and sprocket. For the supports, a combination of cylindrical and displacement boundary conditions were used to accurately model the spline and crank bolt. The forces are simulated using remote forces at the required offset of 65mm outwards from the pedal holes to account for the overhang of the pedals.

After several iterations of reinforcing areas of high stress and removing material from areas of low stress up to the point where the deformation became disproportionate, the final results for the force applied in each direction are seen in Figure 46. As it is expected since it is assumed that the material is linearly elastic with identical properties in tension and compression, the displacements and stresses are the same in each case, but the manner in which deformation occurs has an opposite appearance. The maximum deformation was found to be 1.534mm, which is rather high; and the maximum stress was found to be 174.5MPa with a safety factor of 1.6, which is acceptable. To evaluate the displacement during normal operation, a force of 490N was applied at the same offsets but parallel to each crank and the maximum displacement was 0.6217mm which will not be noticeable (with a maximum stress of only 64.09MPa). The combined mass of the cranks is estimated at 0.555kg and it is expected for the rear sprocket, chain, and bottom brake to have a mass of no more than 0.4kg.

4.4 FRAME STRUCTURE

The primary factors to consider for the frame are the mass, strength, and stiffness. The mass should always be minimised as much as possible to provide the best performance for propulsion. The strength needs to be satisfactory so that the frame is able to operate on the desired terrain with minor obstacles. The stiffness partially affects the feel of the frame with the most effect coming from the handlebar, where a stiffer frame with a responsive feel is preferable but an extremely stiff frame should be avoided as this will produce greater discomfort over minor obstacles [12]. Furthermore, it is also realised that the stability of the design will generally decrease as the size of the frame is increased, centre of mass is moved to the rear, and centre of mass is moved higher [72].

4.4.1 GENERAL FACTORS

To initially decide on the position of the members of the frame, the Shape Generation tool in Autodesk Inventor Professional 2019 was used to reduce mass while maximising strength for a given load case. The results were limited and not directly developed further as they are only intended to be a conceptual guide - shown in Figure 47. As is modernly conventional, a diamond frame will be adapted which utilises two triangular structures bracing the rear wheel and a front quadrilateral structure (although a small head tube almost forms a triangular structure) connecting the front fork, where the primary stresses are experienced directly in tension or compression but there may still be bending stresses in the front fork or torsional stresses in the entire frame as the user pedals. The outline of the diamond frame is seen in Figure 48, with the outline of a user representing the range of dimensions from the 5th to 95th percentile individuals. For consolation, the Shape Generation results vaguely resembled a diamond frame with the quadrilateral structure divided into two triangles for better triangulation.

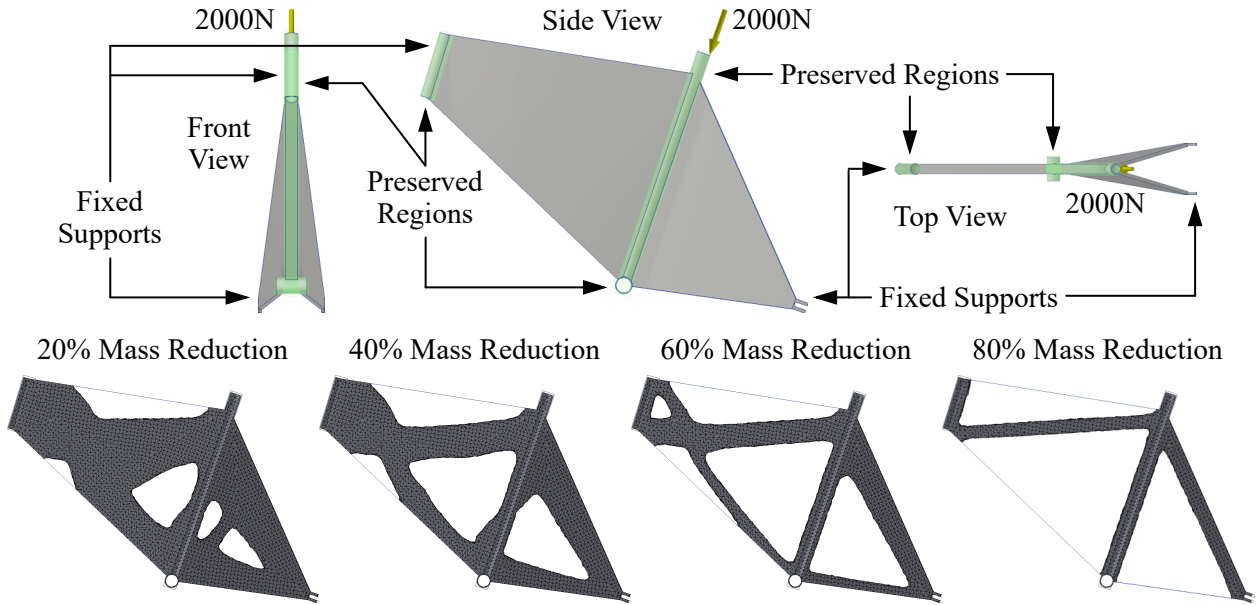


Figure 47: Set up and results of the Shape Generation tool used in Autodesk Inventor 2019.

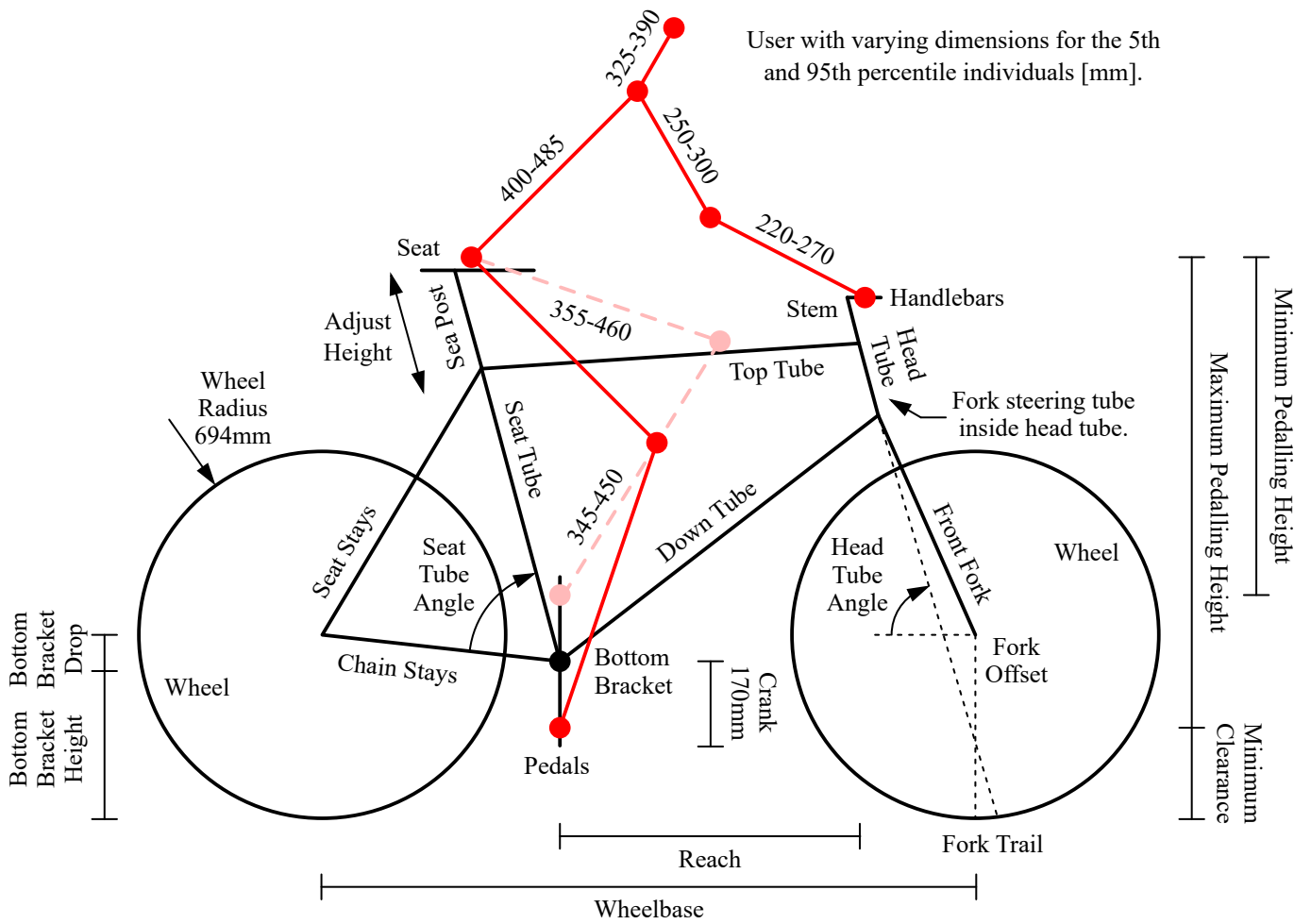


Figure 48: Outline of a diamond frame with dimensions for the 5th and 95th percentile users.

The diamond frame can be arranged with a step-over top tube, where the top tube is horizontal, or step-through top tube, where the top tube is lowered at the connection to the seat tube or even absent. The step-over layout offers greater strength for a lower mass due to better load distribution without the need for additional reinforcing, but the step-through layout is much easier to mount and dismount for smaller or older users - there is speculation about step-over frames being aimed at males and step-through frames being aimed at females, but this is misleading and based on past traditions when females commonly wore dresses or skirts while riding. For convenience but favouring performance, the target will be for a combination of these types tending towards a step-over top tube, where the top tube is slightly inclined so the design is easy to mount but still aligned enough to resist the loads.

Each of the tubes need to be as strong and light as possible, with little concern for the area occupied as long as it is not excessive. So, thin-walled cross-sections will be the most suited to withstand tension, compression, bending, torsion, or a combination of stresses. The chain stays and seat stays need to avoid and leave clearance for the rear wheel, so the best strength while remaining as compact as possible can be achieved from a solid cross-section. It is desired for the top tube and down tube to feature flat surfaces to allow for the aesthetic and flush integration of the enclosure for the controller components and battery pack. The seat tube and head tube must each have circular cross-sections to accommodate the adjustable seat post and fork headset respectively, which need internal diameters of 27.2mm (ranges from 22mm to 35mm, but this is the most common) and 30.2mm respectively for compatibility with standard parts [110, 111]. For the cross-sections seat stays and chain stays, it is reasoned that, when supporting the vertical weight of the user, the seat stay will experience mostly axial loads due to its near vertical angle, so a circular cross-section should suffice; while the chain stay may experience bending and axial loads due to its near horizontal angle, so the cross-section can be elongated to form an ellipse for additional support. The best performing cross-section will have to be determined through iterating with different shapes and various thicknesses.

The possible failure modes of the members can occur through plastic yielding from an excessive stress or buckling from excessive bending and collapse. The materials usually used to construct frames to avoid failure include steel, aluminium, titanium, and carbon fibre. For the best performing frame, carbon fibre should be used because it has an exceptionally low strength-to-mass ratio, but titanium also performs well since it has a strength similar to that of steel but nearly half the density [12, 112]. However, titanium and carbon fibre will realise a material cost that is as much as triple the cost of an aluminium or steel frame. So, as with the cranks for the manual propulsion, aluminium will be considered first for a compromise with a low mass at an acceptable cost with inherent corrosion resistance and, if it is found inadequate, steel will then be considered as the most appropriate option.

A further factor is the chain for the manual propulsion which will require tensioning for optimal performance. This can either be achieved through the addition of a spring-loaded jockey or idler sprocket mounted to the frame, or using horizontal and backwards facing forkends instead of traditional dropouts such that the wheel can be installed at a corresponding distance to enable the correct tension in

the chain. The use of these customised forkends is definitely simpler and will increase the reliability if installed correctly since there are no additional moving parts.

The headset attaches the front fork to the handlebar through the head tube and is seen in detail in Figure 49 with a threaded arrangement using a standard fork steering tube outer diameter of 25.4mm and pitch of 1.058mm or 1in by 24tpi and stem outer diameter of 22.2mm [111]. With the use of angular contact bearings in a cup and cone arrangement, this creates a rotatable interface and allows the front wheel to be steered with the fork steering tube freely rotating within the head tube. A single-piece stem with a pinch clamp can then be used to firmly grip and hold the handlebar in place. This stem will use a wedge to fasten within the steering tube, where the bolt can be tightened to pull the wedge up the chamfer of the stem to secure the stem and prevent relative motion of the steering tube. For user familiarity and predictable steering, the handlebar will have a straight horizontal shape with a standard outer diameter of 25.4mm at the stem clamp and a slight inwards taper towards the ends.

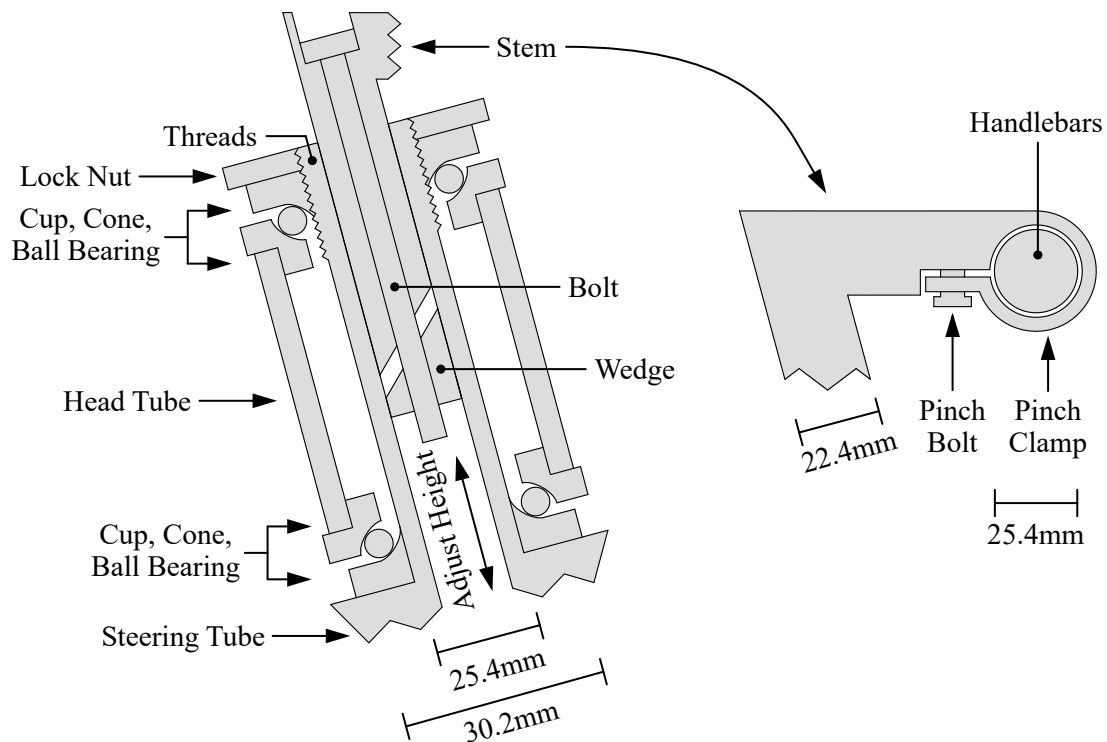


Figure 49: Arrangement and components of the headset.

Finally, it is likely for the enclosure to be constructed from a lightweight polymer material and be mounted within the quadrilateral structure of the frame. However, as shown in Table 5, a polymer generally has a yield strength from 18.5MPa to 53.8MPa, which is significantly less than the 276MPa of aluminium 6061-T6 or 370MPa of a lower grade steel. Thus, although the enclosure must not carry any of the applied loads, the deformations of the quadrilateral structure must be limited through an increased stiffness since the enclosure will deform with the frame and may fracture if the deformations are unrestrained. When evaluating the thickness of the top tube and down tube, the chosen thickness

must also be suitable to allow for strong connection points to fasten the enclosure - likely with two bolts through the bottom of the top tube and two bolts through the top of the down tube.

4.4.2 ERGONOMIC SIZING

Considering the effects of the user positioning on performance, it is necessary to minimise drag resistance to maximise performance, since drag resistance contributes greatly to overall resistance at high speeds. The lowest drag resistance can be achieved by using a position where the user is leaning forward at an extreme angle such that the centre of their back is the highest part of their body with their knees almost against their chest and their arms brought as close inwards as possible [12]. However, this is only suitable for track or time trial racing where it is necessary for the best performance without much concern for comfort [12]. For sustained periods of commuting by the average user, this will not be tolerable and may even cause injuries due to strain from incorrect technique. Instead, a more recreational position is suggested for better comfort, where the user adopts a more upright posture.

The conventional frame sizes range from small to extra large primarily based on seat tube lengths from 430mm to 660mm respectively. The 5th to 95th percentile standing height of a male ranges from 1640mm to 1905mm, while the 5th to 95th percentile standing height of a female ranges from 1540mm to 1790mm. Using the frame sizing chart included in Appendix C, it is seen that a seat tube length of 540mm to 550mm will be comfortable for users with heights from 1590mm to 1840mm, where this seat tube length is typical of medium to large sized frames. This size should not affect comfort while using electric propulsion, however pedalling may not be perfectly comfortable for

Table 23: Dimensions for the members of medium and large frames for gravel, touring, commuting, and electric bicycles [113, 114, 115, 116, 117]. A = Trek FX Sport 5, B = Trek Verve+ 2, C = Cube Editor, D = BMC Alpenchallenge AMP City One, and E = Momsen 700 GP300.

	Medium					Large				
	A	B	C	D	E	A	B	C	D	E
Seat Tube Length [mm]	457	500	480	480	520	508	550	520	538	540
Seat Tube Angle [°]	74	70.5	73	73.5	73.2	73.5	70	73	73.5	73
Head Tube Length [mm]	160	160	150	157	150	185	160	170	193	165
Head Tube Angle [°]	71	68.5	71	72	71.25	71.5	68.5	72	72	71.25
Top Tube Length [mm]	570	601	570	583	560	590	607	586	608	575
Bottom Bracket Drop [mm]	65	62	50	70	82.5	65	62	50	70	50
Chain Stays Length [mm]	438	502	430	435	450	438	502	430	435	450
Fork Offset [mm]	50	45	-	45	-	45	45	-	45	-
Fork Trail [mm]	70	95	-	65	-	67	95	-	65	-
Wheelbase [mm]	1067	1148	1048	1083	1049	1072	1148	1055	1085	1069
Reach Distance [mm]	403	383	400	405	380	409	383	409	425	388

the outlying individuals at the extreme percentiles, but it is the best compromise that should still be reasonably acceptable by adjusting the seat post and stem to vary the pedalling height and required reach. For an idea of the expected dimensions and to see how the dimensions vary as the frame size increases, the dimensions for the members of medium and large frames are listed in Table 23 based on relatable Trek, Cube, BMC, and Momen gravel, touring, commuting, and electric bicycles.

For the width of the handlebar, it is necessary for the user to be able to achieve the required leverage and control for steering while still remaining compact so as to avoid colliding with protruding obstructions. The shoulder width of the 5th and 95th percentile individuals ranges from 365mm to 495mm respectively and, so, a handlebar width of around 640mm will offer acceptable leverage of 6.4N.m if the user applies a force of only 10N at each end, as compared to the maximum required steering torque of 5.3N.m [118, 119]. This width should also have sufficient area to mount and easily access the electrical propulsion and braking controls. For comparison, racing road bicycles usually have a width of 340mm to 500mm while off-road bicycles can have widths up to 780mm.

4.4.3 STRENGTH AND STIFFNESS

Unfortunately, most documented test methods to determine if the frame has an acceptable strength and stiffness involve practical tests with a model frame undergoing certain empirical dynamic requirements, as described in ISO 4210-6 [12, 120]. This follows the logic that, if past successful frames passed tests which were found to be competent, then new frames must be able to pass these test as well [12]. To be able to investigate and compare frame integrity for various iterations without performing practical tests, three static cases are developed for finite element analysis which consider the basis of the proposed dynamic tests and expected operating conditions.

In the first and second cases, the maximum mass of the user at 100kg or approximately 1000N will be considered with inclusion of the frame weight due to gravity at 9.81m/s^2 , enclosure weight estimated up to 200N acting on the down tube, possible deceleration up to 6.5m/s^2 producing a force of about 700N, and maximum approximate drag of 50N. The first test is for a typical situation where the user is seated with minimal weight supported by the handlebar or cranks, but an additional force of 200N is applied at the bottom bracket to account for inefficient pedalling technique; and the frame is constrained with displacement supports restricting motion at the front and rear fork ends. The second test will have the same constraints as in the first test, but it will consider when the user is completely standing on the pedals with a pushing force of 100N on the ends of the handlebar. The third test only examines the front fork to investigate strength and deflection where a horizontal force of 1000N is applied at the front forkend with a cylindrical support at the steering tube and a compression only support at the surface that would contact the headset, requiring a non-linear analysis. These tests are graphically shown in Figure 50. For clarity, the frame can be viewed as being secured to a rig with the proposed constraints while the suggested forces are applied.

Essentially, the first and second tests represent normal operating conditions and, so, the safety factor should remain above 10 due to a high level of uncertainty with regards to dynamic amplifications occurring during operation and when obstacles are impacted. The third test can be seen as a maximum situation, possibly occurring during a severe collision, because the horizontal force will produce an extreme bending stress instead of a lesser combination of axial and bending stresses from a more aligned force - a typical safety factor around 1.8 will be satisfactory. With these safety factors, the static analyses may not accurately indicate durability but they do provide a useful target.

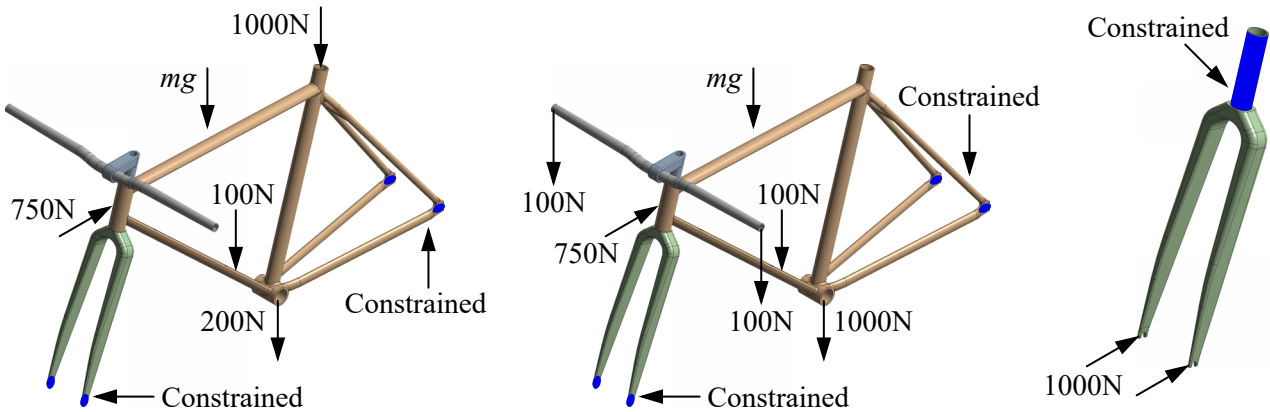


Figure 50: Loading of the first test (left), loading of the second test (middle), and loading of the third test (right). (The model shown was an iteration using semi-circular tubes for the top tube and bottom tube which were found to lack stiffness, while the front fork was found to fail).

The exploded view of the model used for the first and second tests is seen in Figure 51, where bonded contacts are used between the handlebar, stem, and front fork, and no separation contacts are used between each of the bearing spacers and the front fork and frame respectively. The bearing spacers were also set to have a rigid stiffness behaviour, such that they are only included to provide the correct positioning of the other components. The third test simply used the front fork. For the meshes, initial settings were chosen with quadratic order elements, fine relevance, slow transition, and a maximum

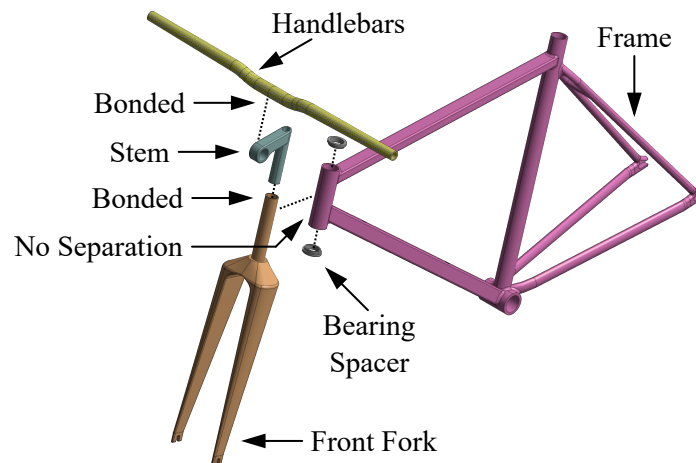


Figure 51: Exploded view of the model used for the first and second tests.

element size of 8mm with automatic refinement through convergence for a 2% change in magnitude. The results for the best performing iteration with different cross-sections and thicknesses for the members are shown in Figure 52, Figure 53, Figure 54 for each test respectively.

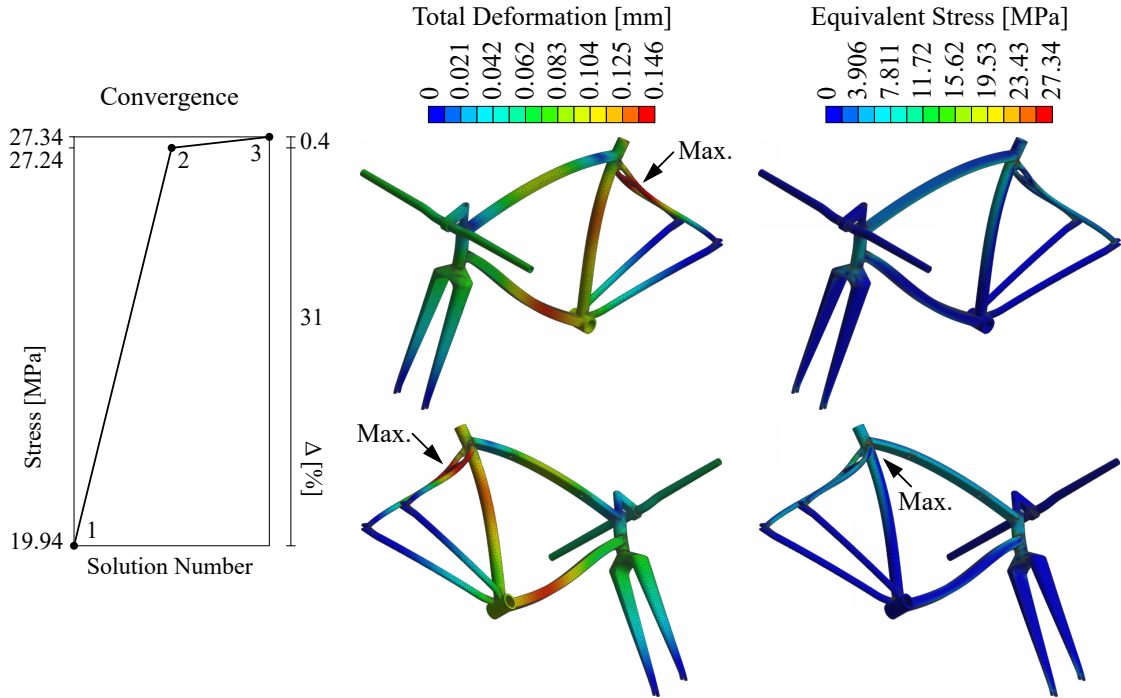


Figure 52: Deformation (exaggerated) and stress experienced in the final frame iteration with aluminium 6061-T6 for the first test, as simulated in ANSYS Mechanical 18.2.

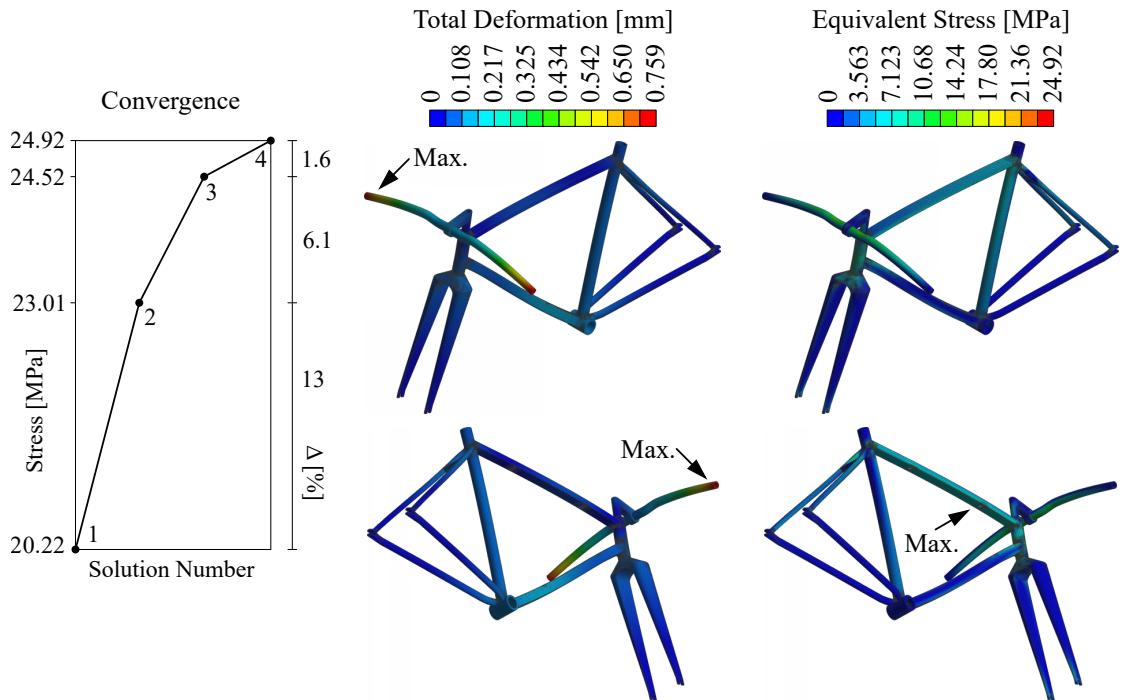


Figure 53: Deformation (exaggerated) and stress experienced in the final frame iteration with aluminium 6061-T6 for the second test, as simulated in ANSYS Mechanical 18.2.

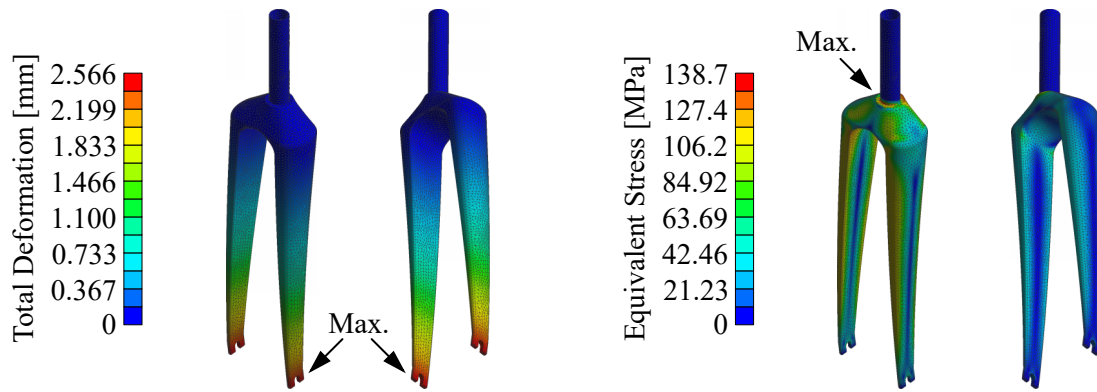


Figure 54: Deformation (exaggerated) and stress experienced in the final fork iteration with aluminium 6061-T6 for the third test, as simulated in ANSYS Mechanical 18.2.

From iterations with different cross-sections, it is generally gathered that the strength is primarily related to the thicknesses of the members and the stiffness is primarily related to the diameters of the members, while the mass increases as both the thicknesses and diameters increase as is expected. The final cross-sectional shapes and thicknesses for the members of the frame are seen in Figure 55 with the final dimension in Table 24. These members allow mass to be minimised while the frame only experiences maximum stresses of 27.34MPa in the first test and 24.92MPa in the second test, which leads to safety factors of 10.1 and 11.0 respectively with the 276MPa yield stress of aluminium 6061-T6. For the third test, a maximum stress of 138.7MPa was experienced. These results are satisfactory given the mentioned uncertainty, but it is still advisable for further optimisation of the frame. The mass of the frame is 2.365kg, mass of the fork is 0.654kg, and combined mass of the headset, stem, and handlebars is approximately 0.507kg with aluminium 6061-T6 which is acceptable.

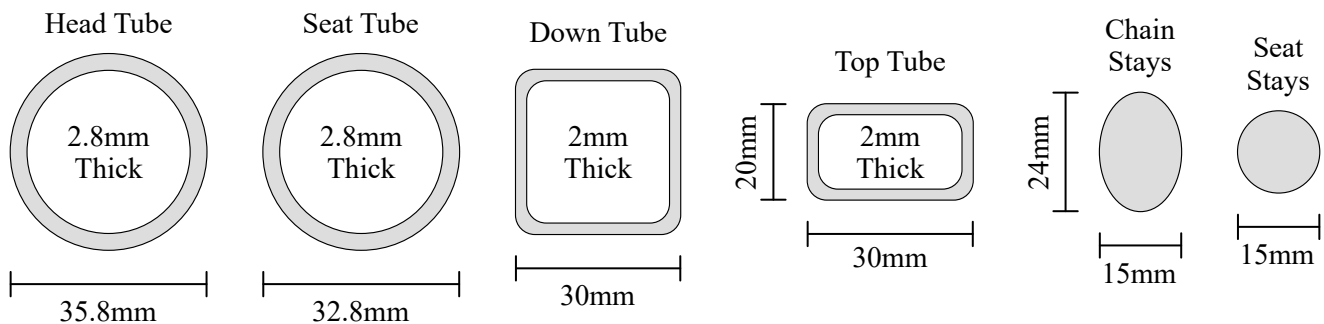


Figure 55: Proposed cross-sections for the members of the frame.

The frame forms a rigid statically indeterminate body which unfortunately cannot be easily solved analytically without making various assumptions. Because of the rigid connections, the frame cannot be analysed as a truss with pinned members only experiencing axial stresses in tension and compression. However, if it was assumed that each member only support an axial load equal to the maximum applied force of 1000N, then the stress experienced is 3.789MPa for the seat tube, 5.435MPa for the top tube, 4.464MPa for the down tube, 3.445MPa for the head tube, 3.537MPa for a chain stay, and 5.659MPa for a seat stay. These results are similar with regards to the order of magnitude to the

Table 24: Dimensions for the final members of the frame.

Seat Tube Length [mm]	Seat Tube Angle [°]	Head Tube Length [mm]	Head Tube Angle [°]	Top Tube Length [mm]	Down Tube Length [mm]	Bottom Bracket Drop [mm]	Chain Stays Length [mm]	Seat Stays Length [mm]	Front Fork Length [mm]	Fork Offset [mm]	Fork Trail [mm]	Wheelbase [mm]	Reach Distance [mm]
495	73	130	73	585	640	45	510	445	390	50	105	1095	420

stresses found in the central body of the members in the finite element analysis, where larger stresses would be generated from stress concentrations at the joints and when the geometry rapidly changes.

For the chain power transmission, the adjustable mounting at the rear forkends allows for a lenient centre distance from 442.8mm to 465.4mm between the front sprocket at the bottom bracket and rear sprocket at the rear forkends. Using the minimum centre distance, Equation 28 results in a chain length of 102 links, rounded up to the nearest even integer. Thus, with Equation 29, the actual centre distance needs to be 445.3mm which is within the acceptable range.

Since the wheelbase is 1.095m, an approximate turning radius of 2.185m is calculated for a steering angle of only 30°, found using Equation 31 which is approximately valid for an upright turning without leaning. Through manipulation with the models of the designs, it is also found that a steering angle greater than 90° can be achieved without the front wheel contacting the frame, although the extreme angles may not actually be useful or operable. With the 170mm cranks, the ground clearance is found to be at least 120mm to the bottom surface of the crankset when in the lowest position.

$$r_t = \frac{w}{\gamma \cos(\phi)} = \frac{w}{\gamma \cos(\arctan(l_t/r_w))} \quad (31)$$

Where r_t , turning radius, m; w , wheelbase, m; γ , steering angle, rad; ϕ , caster angle, rad; l_t , fork trail length, m; and r_w , wheel radius, m.

4.4.4 ENCLOSURE

The best location for the enclosure is within the quadrilateral structure of the frame. As desired, this will allow for the controller components and battery pack to be mounted as far forward as possible to counteract the effects of the hub motor on the mass distribution. Additionally, this will avoid interference with the crankset and pedalling. Considering the common polymers in Table 5, ABS thermoplastic will provide the lightest mass with a density around 1060kg/m³, a decent yield strength around 34.75MPa, electrical insulation, and flame retardants if treated.

The dimensions seen in Figure 56 produce a compartment for the controller components and battery pack with a sufficient area of 0.03147m^2 to accommodate the controller components and required area of at least 0.02738m^2 for the battery cells, which can actually be reduced with more efficient stacking. The corresponding mass is minimised to 0.368kg , using an internal width of 70mm to account for the cabling and 65.3mm battery cells and a thickness of 3mm for the surrounding walls enclosing the compartment. An adhesive and waterproof sealant or gasket can be used to seal the enclosure once installed to establish dirt, dust, and splash resistance and a basic level of tamper-proofing.

The mass of the design including the electrical propulsion, manual propulsion, wheels, and frame components is estimated to be 16.65kg . With the enclosure mass, this allows for a mass of 1.98kg for the controller components, braking system, and other accessories mentioned in Section 4.6, which may be constraining but can be achieved with optimisations to minimise mass. For a lower enclosure mass of 0.314kg , a 2mm wall could be used but the trade-off of a weaker structure is not acceptable.

To differentiate the design from currently existing designs, it is suggested to possibly use a larger enclosure and incorporate a storage compartment for the user, because the design will primarily be used for commuting and the user may need to store belongings - this could even include a 5V output USB port for charging auxiliary devices. An example of this is seen in Figure 56 with the same area for the controller components and battery pack, but an extra storage compartment with an area of 0.00932m^2 . However, this addition increases the mass significantly to 0.505kg with a 3mm wall which will only be acceptable if the mass can be drastically decreased for another component.

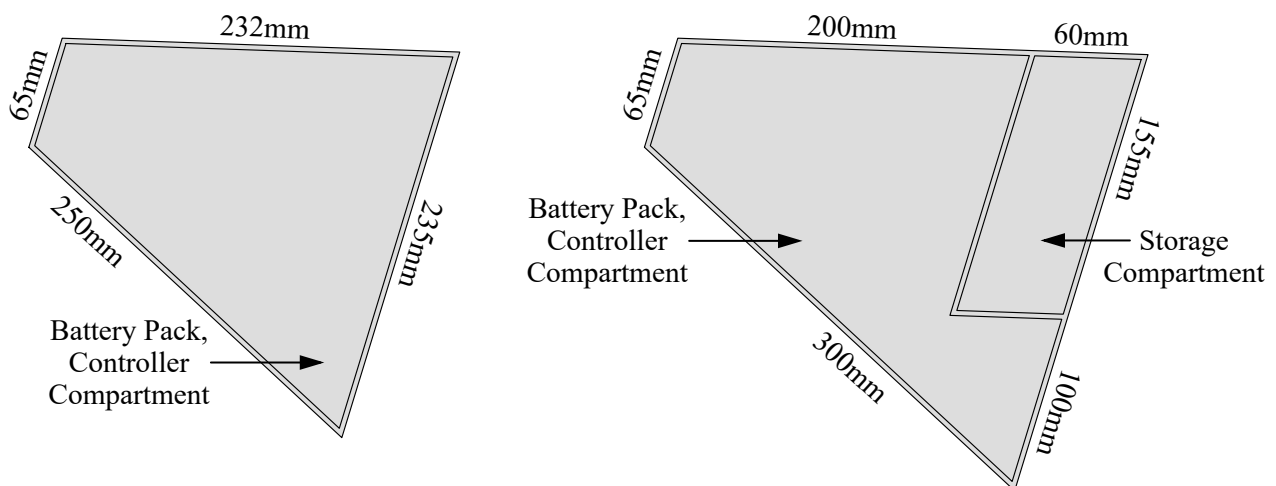


Figure 56: Compartments and dimensions of the enclosure within the frame quadrilateral.

With the enclosure slightly protruding from the sides of the frame, the design frontal area can be accurately found as 0.096m^2 and, so, the total frontal area is approximately 0.544m^2 with 0.448m^2 from the user. This is basically equal to the assumed area of 0.55m^2 in the analyses of the electric propulsion and manual propulsion and verifies the accuracy of the drag resistance calculations, although a high drag coefficient was still used which justifies the claim that the results are conservative.

4.5 BRAKING SYSTEM

Unfortunately, due to a lack of time, the braking system cannot adequately be developed. The current state of the design features auxiliary braking through regenerative braking from the hub motor, but this is not sufficient for emergency situations when it is required to immediate brake. However, the maximum braking performance can be analysed where slipping does not occur and both wheels remain in contact with the ground. It is also possible to discuss the various braking mechanisms.

4.5.1 MAXIMUM PERFORMANCE

For a conservative estimate and to simplify the analytical model, the effects of drag and rolling resistance are neglected such that only the braking system reduces speed. The expected mass distribution during braking is seen in Figure 57, where the rear normal force will be zero during maximum braking due to a moment about point O . In this arrangement, it is also assumed that the centre of mass of the user is located at a height of 1.192m and with a distribution such that there is 60% of their mass on the rear wheel and 40% of their mass on the front wheel. This allows for the coordinates of the centre of mass to be calculated with Equation 32 and Equation 33. Thus, the maximum braking deceleration is given by Equation 34 and found to be 5.684m/s^2 with a frictional braking force of 55.76N .

$$x_g = \frac{\sum m_i x_i}{\sum m_i} = \frac{m_r x_r + m_d x_d + \%m_r m_u x_r + \%m_f m_u x_f + m_f x_f}{m_r + m_d + m_u + m_f} \quad (32)$$

$$y_g = \frac{\sum m_i y_i}{\sum m_i} = \frac{m_r y_r + m_d y_d + m_u y_u + m_f y_f}{m_r + m_d + m_u + m_f} \quad (33)$$

$$\sum F_x = F_f = \mu mg = ma \quad \text{and} \quad \sum M_o = mgx'_g - F_f y'_g = 0 \rightarrow a = \frac{x'_g}{y'_g} g \quad (34)$$

Where x_g , centre of mass x distance, m; m_i , arbitrary mass component, kg; x_i , arbitrary x distance, m; m_r , rear wheel mass, kg; x_r , rear wheel mass x distance, m; m_d , design mass, kg; x_d , design mass x

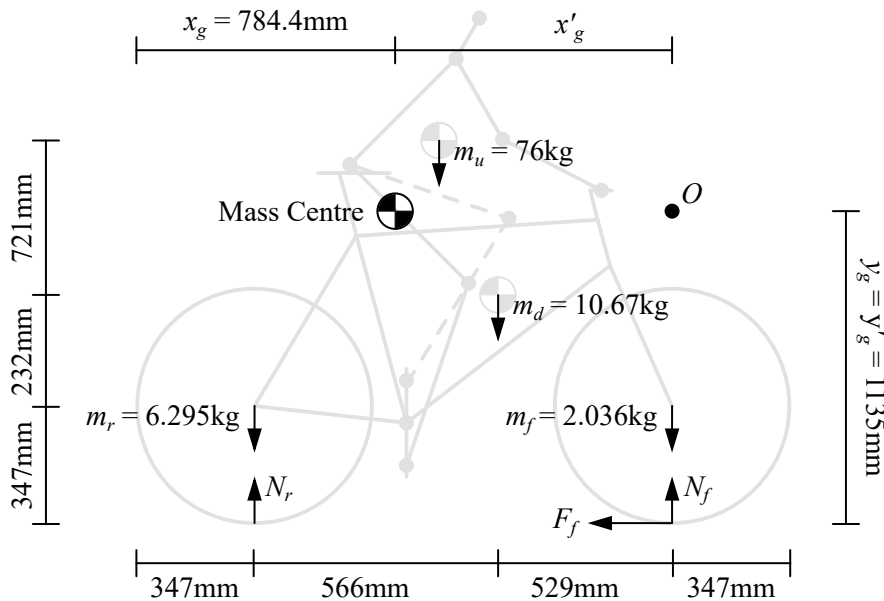


Figure 57: Mass distribution and forces during braking.

distance, m; $\%m_r$, fraction of mass on rear wheel; m_u , user mass, kg; $\%m_f$, fraction of mass on front wheel; m_f , front wheel mass, kg; x_f , front wheel mass x distance, m; y_g , centre of mass y distance, m; y_i , arbitrary y distance, m; y_r , rear wheel mass y distance, m; y_d , design mass y distance, m; y_u , user mass y distance, m; y_f , front wheel mass y distance, m; F_x , x force component, N; F_f , friction braking force, N; μ , static friction coefficient; m , mass, kg; g , gravitational acceleration, 9.81m/s^2 ; a , acceleration, m/s^2 ; M_o , arbitrary moment component, N.m; x'_g , relative centre of mass x distance, m; and y'_g , relative centre of mass y distance, m.

For pneumatic rubber tyres, the static friction coefficient between the tyre and ground can range from 0.9 for asphalt to 0.6 for gravel [12]. Using the minimum static friction coefficient, this shows that the maximum driving or braking force before slipping occurs is 559.2N and, so, the wheel will be able to freely roll without slipping during braking. Because the braking deceleration is greater than the propulsion acceleration, it is also confirmed that the wheels will not slip during propulsion.

4.5.2 MECHANISM TYPES

Firstly, regenerative braking from the motor is an energy recovery mechanism which acts by reducing the speed of the design through the conversion of some kinetic energy into electrical energy, instead of dissipating the kinetic energy as heat through friction like mechanical brakes. This is performed by running the motor in reverse as a generator, such that the produced electrical energy can be supplied to charge the battery pack. The process of implementing regenerative braking is controlled by the battery management system and controller. The advantage of regenerative braking is an increased braking performance while also increasing range and decreasing wear on the primary braking system. However, the performance relies upon the correct motor, battery pack, and controller operation, and it can be temporarily inactivated when the battery pack is fully charged or the controller temperature becomes elevated so it should not be solely relied upon [74].

As mentioned in Section 1.4.3, the most common types of mechanical braking systems are rim brakes and disc brakes. The operation of rim brakes involves rubber pads being pressed against the side surfaces of the rim, where the advantages include an intrinsically light and simple construction, low input force for a high braking force due to operation at a large radius on the wheel, lack of forces applied to the hub and spokes to transfer the braking torque, and ability to easily change a wheel without affecting the braking system [12]. The operation of disc brakes involves rubber pads being pressed against the side surfaces of a steel disc mounted to the hub of the wheel, where the advantages include unchanged performance under wet conditions due to isolation from the environment, less frequent adjustment since the positioning is fixed (although, under unlikely conditions, this may be a disadvantage if a heavy shock or impact causes a misalignment), and accommodation for a slightly skew rim while maintaining even braking as the wheel rotates [12]. With the correct design and installation, similar braking performance is achievable by either rim or disc brakes.

Both these types of brakes use an activation method employing a flexible Bowden cable in which an inner wire in tension is located within an outer tube in compression. The inner wire can then be pulled by the user with a lever on the handlebar, which will cause the inner wire to move relative to the fixed outer tube. This is the most inexpensive activation, but it is also possible for hydraulic activation using disc brakes which involves a more complicated installation. A brake switch should also be fitted to the activation mechanism to provide feedback to the controller to stop electric propulsion accordingly.

The other mentioned types of brakes include plunger or spoon, hub, drum, coaster, and band brakes. It may also be possible to implement a drag brake, where a flap could be deployed to increase the frontal area and drag resistance; or pedal brake, where the ability to coast is removed such that the wheel rotation is fixed to the manual propulsion and the user is able to directly control the wheel rotation with the pedals. However, these methods should not be considered as they have many disadvantages in the form of additional wear, inconsistent performance varying with speed, slow response times, large mass additions, significantly degraded performance under wet conditions, and high operating skill levels, without offering any compelling advantages over rim or disc brakes. Thus, only rim brakes and disc brakes should be directly compared and, to distinguish the best mechanism relevant to the design for personal transportation, a formal conceptual evaluation should be performed.

If the braking system is to be designed, the following criteria are recommended for the optimal development of the braking system once the requirements and constraints have been defined:

1. The design must have a large immediate effect.
2. The design must have a large sustained effect.
3. The design must operate consistently under wet and dry conditions.
4. The design must be as lightweight as possible.
5. The design must be durable with a long life.
6. The design must be easy to maintain, repair, and replace.
7. The design must have a short deployment or activation time.
8. The design must minimise additional drag when not braking.

4.6 OTHER ACCESSORIES

Some other accessories will need to be added to complete the final design. This includes the seating arrangement, pedals on the cranks, input method to the control system, handle grips, and other minor features. These accessories will not be developed, but they were be briefly mentioned.

The seat post will simply be a tube with the standard outer diameter of 27.2mm, but a thickness needs to be chosen for sufficient strength and the mounting mechanism to the seat needs to be added. A suitable seat needs to be either purchased or developed with standard mounting for compatibility with standard seat posts and consideration for the comfort of the user. If comfort is to be maximised, it

may also be possible to investigate using a suspension seat post, which can be very effective without increasing the mass unreasonably but will require a more complex design with a higher cost [24].

It is recommended that the chosen pedals are plain pedals so they can be used with almost any shoe. It is possible to use toe-clippable or clipless pedals with a fixed connection to allow for more efficient pedalling where the foot of the user is attached to the pedal so it is possible to push down and pull up, but these require special cleated shoes and increased skill level to avoid falling [108].

For the input method to the control system of the hub motor, it is necessary to either use a push button, thumb, twist, or trigger throttle mounted on the handlebar. The push button may be inferior due to the lack of sensitive input, but each of the remaining methods will be fairly similar and the final choice should be primarily based on cost. With the throttle, rubber handle grips should be placed at the ends of the handlebar for comfort and grip with a standard internal diameter of 22.2mm, outer diameter around 30mm, and width of about 130mm [111]. There is also a possibility of using vertical grips at the ends of the handlebar to provide an additional hand position.

Finally, as recommended for all cycles in South Africa through the National Road Traffic Act 93 of 1996, the design should feature a front white light with an intensity such that a diffused beam angled downwards strikes the ground at a distance between 3m and 30m; and the design should feature a rear red light with an intensity such that a diffused beam is visible for 30m rearwards. Alternatively, front white and rear red retro-reflectors could be used as a more inexpensive but less effective option.

5 DESIGN SPECIFICATION

A final description of the sub-systems is presented where the final design and layout is summarised. An evaluation of the calculated performance specification is also necessary to verify the satisfaction of the requirements and constraints for each sub-system. The manufacturing processes for the parts are then characterised and, finally, the engineering drawings are submitted.

5.1 FINAL DESCRIPTION

In short, the final design features electrical propulsion through a Heinzmann DirectPower PRA 180-25 brushless DC hub motor with a continuous rated power of 250W, and manual propulsion through a pedal crankset with 170mm cranks and chain driven power transmission utilising a single-speed gear ratio of 1:2.15. The hub motor is used in the rear wheel with an axle diameter of 10mm, while the front hub features a 9mm steel AISI 4140 axle, single row deep groove ball bearings bearings to support the loads with accommodation for slight misalignment, and an aluminium 6061-T6 hub shell. Each of the wheels has an ISO 622mm classification with a 19C crotchet-type rim made from aluminium 6061-T6, 36 stainless steel spokes with diameters of 2.6mm, and Challenge Gravel Grinder TLR tyres for outstanding performance on asphalt, pavement, cement, gravel, and flat soil. The frame is also made from aluminium 6061-T6 to provide a solid structure and light mass.

The length of the frame or wheelbase is 1095mm, where the wheels of 347mm radius including the tyre protrude from the front and rear axles. The width of the design is set by the handlebar which is 640mm wide and centred at the frame for protrusion of 320mm on either side. The overall height of the design will be dependent on the height of the seat chosen by the user, but can be estimated to be within the range from 890mm for a shorter user to 960mm for a taller user. To provide a clearer layout of the final design, renderings showing the components are seen in Figure 58 with a final showcase.

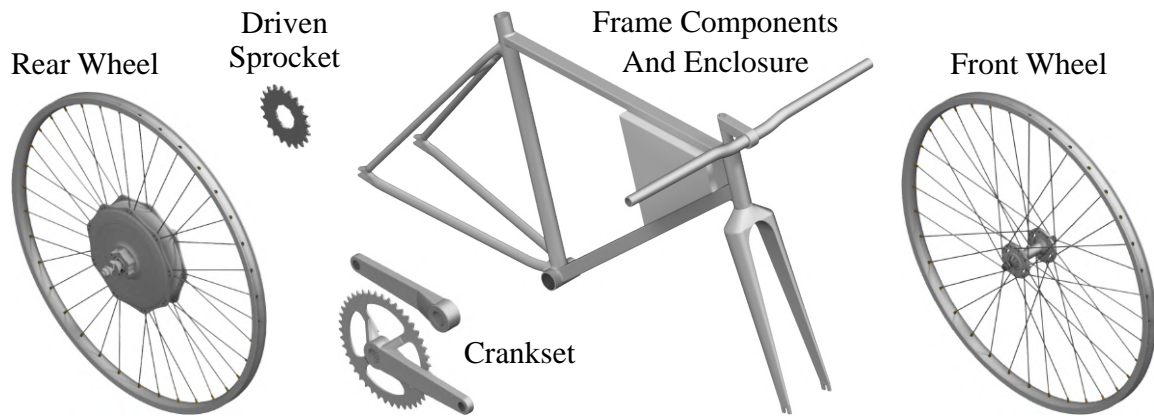


Figure 58: Renderings of the primary components (top) and final showcase of the design in the expected operating environment with some other accessories for completeness (bottom).

A summary of the power flow is also included in Figure 59, which shows the interactions of the sub-systems, where the manual propulsion and electric propulsion act in parallel to allow for the option of either fully independent manual propulsion, fully independent electric propulsion, or a combination of manual propulsion and electric propulsion simultaneously.

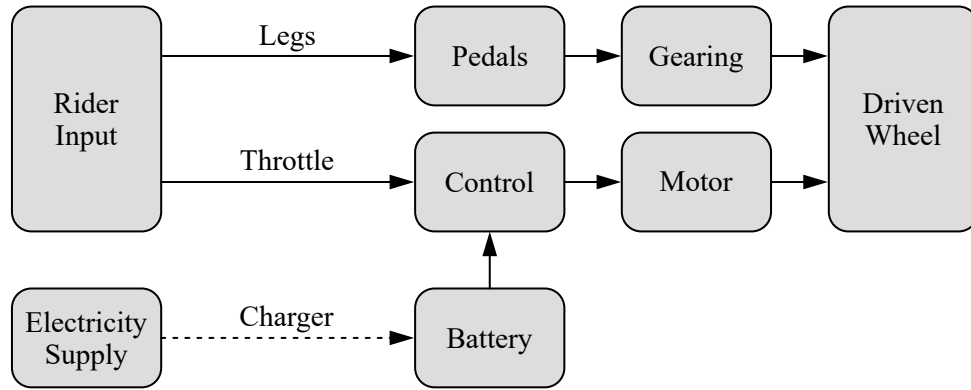


Figure 59: Flow diagram of the parallel manual and electric power.

5.2 PERFORMANCE EVALUATION

Beginning with the electrical propulsion, it was required to achieve a speed of 25km/hr on a level grade within 5s when accelerating from rest and 15km/hr on a slope with a gradient up to 3% within 5s when accelerating from rest. With a continuous rated power output of 184.4W and 176.1W, the design can sustain these required speeds and, with a peak rated power output of 600W, the acceleration estimations show that the design is capable of achieving these speeds with times of approximately 4.809s and 1.631s respectively - although the hub motor can actually output up to 950W for even better performance. With wind speeds of 10km/hr, the design can maintain a speed of at least 15km/hr with a continuous rated power of less than 250W for slopes with gradients up to 3%.

The hub motor also offers redundancy, where the electric propulsion can still operate if the manual propulsion is damaged or the manual propulsion can operate if the electric propulsion malfunctions. Furthermore, it may be possible to remove the electric propulsion by changing the rear wheel and disconnecting the battery pack, but this has not been investigated.

The battery pack comprises of Panasonic NCR18650PF lithium-ion cells with 10 sets of cells in series and 8 parallel cells in each set. These cells allow for the battery pack to have a capacity of 835.2W.hr, maintain a life of at least 80% after 500 cycles, and achieve an independent electrical propulsion range of 50km assuming a design factor of 1.2, but this may be highly dependent on the terrain and should be checked with experimentation. With a charging current greater than 3.48A, it will be possible to charge the battery pack in less than 8hr, assuming an efficiency loss of 20% - it is recommended for a charging current of at least 4A for a charging time of 6.96hr.

The battery pack will be electrically insulated with the controller components in an enclosure located between the structural members of the frame. The enclosure has an area of 0.03147m², is constructed from an ABS thermoplastic, and will be completely sealed to prevent tampering and for dirt, dust, and splash resistance. The controller was not fully developed, but it is proposed for various performance modes and the maximum speed to be limited to 25km/hr using the controller.

The manual propulsion features a roller chain with a pitch of 12.7mm and length of 102 links which was analysed based on a design factor of 1.33. Using the limits of the user inputs with a maximum continuous power of 240W, maximum input force of 200N, and cadence between 50rev/min and 110rev/min, the manual propulsion can achieve 25km/hr on a level grade and 20km/hr on slopes up to gradients of 3% with varying wind speeds up to 15km/hr, which satisfies the requirements for a speed of 25km/hr on a level grade and 15km/hr on a slope with a gradient up to 3%. With combined propulsion, the design is able to easily reach speeds of at least 30km/hr on slopes up to 3% gradient and speeds of at least 20km/hr on slopes up to 6% gradient with wind speeds over 10km/hr.

For the wheels, the rims with a crotchet-type profile classified as 19C were subjected to a standard test comparing aluminium 6061-T6 and steel AISI 1030 for various thicknesses. It was found that aluminium 6061-T6 with a thickness of 2.3mm was the most satisfactory to fulfil the criteria of the test and because it is compatible with the greatest range of tyre widths from 28mm to 62mm. Furthermore, if rim brakes are to be used, aluminium will provide more consistent performance under dry and wet conditions. There are also 36 holes on each rim for mounting the brass nipples of 4.6mm diameter to tension the spokes and a 6.3mm hole for the Presta valve of the tyres.

Hybrid tyres were specifically chosen for consistent performance on asphalt, pavement, cement, gravel, or flat soil. The spokes on each wheel were seen to be safe from fatigue failure with safety factor of 1.08 which is acceptable given that it indicates infinite life. The axle, bearings, and shell of the front hub were also analysed, where the axle was safe from failure with a diameter of 9mm to produce a static safety factor of 1.21 and fatigue safety factor of 1.20, 609-2RSH bearings with a contact seal were found to be the most suitable with a life of 6115hr or 2202 days when operating at an average of 18km/hr for 50km each day, and the hub shell had a static safety factor of 1.77 under extreme loading as simulated using a finite element analysis.

The frame was also satisfactory with support for the maximum user up to 100kg and sizing aimed towards users with heights between 1590mm to 1840mm but accommodating the extreme 5th percentile and 95th percentile users with heights of 1540mm and 1905mm respectively. It was tested through finite element analyses and found to have safety factors of 10.1 and 11.0 with a maximum deformation of 0.759mm for the two static tests mimicking normal operation, while the fork had a safety factor of 1.98 and deformation of 2.566mm under a test mimicking extreme operation.

The steering mechanism is able to successfully operated with an input force of 10N to achieve a steering torque of 6.4N.m. The steering mechanism is also able to achieve a steering angle of over 90° on either side of the inline plane before the front wheel contacts the frame, which satisfies the requirements of a turning radius of at least 3m and steering angle of at least 60°.

Overall, the components are compatible with the relevant standards such that the parts are repairable or replaceable with little modification. The masses of the designed components are listed in Table 25 for a total mass of 17.02kg. The design is planned to have a mass less than 19kg, which is possible as

long as the combined mass of the controller components, braking system, and other accessories is less than the allowance of 1.98kg. Thus, in their current states, the sub-systems fully satisfy the respective requirements and constraints of the product requirement specification. However, it is acknowledged that, if further development is carried out for the remaining sub-systems, these specifications may change slightly but not enough to invalidate the designs. This indicates that the design is fairly successful and can be seen as a transitional form of personal transport between traditional bicycles and private cars, with more mobility and flexibility than public services.

Table 25: Masses of the components for the designed sub-systems.

	Battery Pack	Front Wheel	Rear Wheel	Manual Propulsion	Frame	Fork, Headset	Enclosure	Total
Mass [kg]	3.840	2.036	6.295	0.955	2.365	1.161	0.368	17.02

5.3 MANUFACTURING

For the manufacturing, it is recommended to partner with a local production facility with machinery for welding, casting, forming, shaping, and machining. The simplest process will be for the enclosure which can be injection moulded with a base and lid, while more complicated and involved processes are necessary for the wheel, crankset, and frame components which will be explained in more detail - only the main considerations will be presented otherwise the detail would be needlessly exhaustive. The required materials include aluminium 6061-T6, steel AISI 4140, stainless steel, and ABS plastic which are common and can be sourced from local suppliers. The parts list is shown in Table 26 and the primary engineering drawings are included on the pages following this section while less pertinent engineering drawings are included in Appendix B.

The rim can be manufactured by creating the profile through drawing a tube through a die with a shaped mandrel to form a straight extrusion. This rod can then be bent through rolling into a helix with a diameter of 622mm and cut perpendicularly with a table saw to form multiple hoops starting and ending with each turn. Because the offset at helix ends is negligible since the radius of the wheels is large, the ends of the hoop can be welded together and the residual material of the weld can be removed through machining for a smooth surface finish to avoid punctures from sharp abrasions and allow compatibility with rim brakes. It should be noted that, if the offset is found to be a problem, any distortion can easily be removed when tensioning the spokes and truing the wheel. Finally, the holes for the nipples and 6.3mm hole for the Presta valve can be drilled perpendicularly into the rims.

The spokes are made from an initially continuous coil of wire with a diameter of 2.6mm. Firstly, this wire is straightened and then cut to rough lengths. The head can be formed on one end by holding the wire and stamping the end to create a bulge. The wire can then be cut on the other end to the precise spoke length of 295.6mm for the front wheel spokes or 197.1mm and 195.5mm for the rear wheel

spokes. The thread is subsequently created on each spoke through rolling the spoke between two flat threaded dies with the desired pitch of 0.454mm or 56tpi - this will produce a stronger thread than a cut thread. Lastly, the head end is bent to form the elbow to form a radius of 2.1mm and angle of 100° for compatibility with being mounted on the inside or outside of the hub flanges - although it will actually be required to over bend the spoke to account for springback which occurs due to the elastic recovery of the material after plastic deformation and tends to increase the bend radius and decrease the bend angle which leads to distortion. Since the entire spoke is cold formed, it actually becomes tougher through work hardening but this can also cause residue stresses that can accelerate fatigue. However, the cold forming effects will mostly affect the straight sections of the spoke but failure due to fatigue is expected to occur at either the elbow or thread and, so, this should not be an issue [55].

For the front hub, the threaded axle can be manufactured by cutting a 9mm steel AISI 4140 rod to the required length of 132.8mm and then cutting the threads on the outer surface with a 1mm pitch and length of at least 40mm on either end. The aluminium 6061-T6 hub shell can be easily machined on a lathe with turning to shape the outer surface, boring to form the inner hole of 24mm at the bearings and 15mm between the bearings, and drilling to create the 3mm holes to mount the spokes.

Since the nipples are standard components, it will most likely be more inexpensive to purchase manufactured nipples. This will also decrease the manufacturing complexity and risk of issues or delays. The nipples must be brass but they may be coated with cadmium or nickel for an improved appearance and to prevent tarnishing. The wheel can finally be built with the desired three-cross lacing for the front wheel and one-cross lacing for the rear wheel, where the spokes are tensioned and aligned by tightening the nipples such that the rim is true, which can be tested on standard apparatus.

The aluminium cranks may be cast, hot forged, or cold forged, where cold forging will have the highest strength and casting will be the most convenient. So, in favour of a simpler process, it is recommended for casting to be used since the cranks were found to be sufficiently safe. This will involve a solidification process where a molten aluminium 6061-T6 is poured through a passage into a mould of the hollowed shape of the cranks and allowed to solidify. For a high accuracy and without using an expendable mould, die casting will be the most appropriate where a permanent die is used as the hollowed shape. After the cranks have been cast, the threads for the pedals at 1.27mm or 0.5625tpi pitch and threads for the sprocket bolts at 0.8mm can be cut through tapping.

The frame is constructed from aluminium 6061-T6 members with various cross-sections, where the top tube and down tube can be purchased in the standard sizes of 20mm by 30mm and 30mm by 30mm respectively with thicknesses of 2mm. The head tube and seat tube have unique outer diameters of 35.8mm and 32.8mm respectively with thicknesses of 2.8mm and, so, a tube of 34mm for the head tube and 32mm for the seat tube can be purchased and drawn over a shaped mandrel to slightly increase the sizes. If the user desires to fit a larger sized seat post, the seat tube can be slightly reamed out and this should not affect the strength significantly as long as less than 1mm of material is removed. The seat stay uses a standard circular cross-section of 15mm in diameter, while the chain

stay has an elliptical cross-section which can be created by cold forging a circular cross-section of 20mm in diameter. The seat stay and chain stay will also need to be bent to avoid the rear wheel.

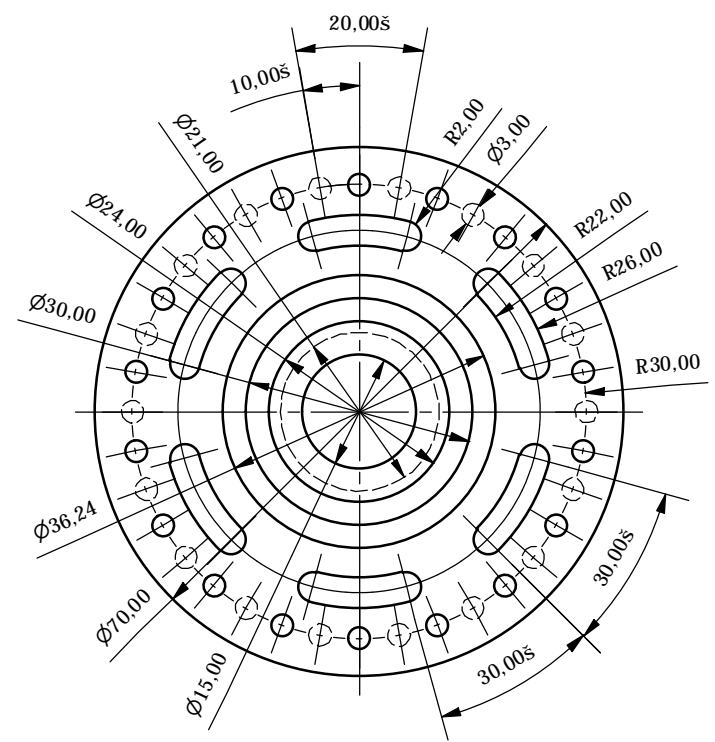
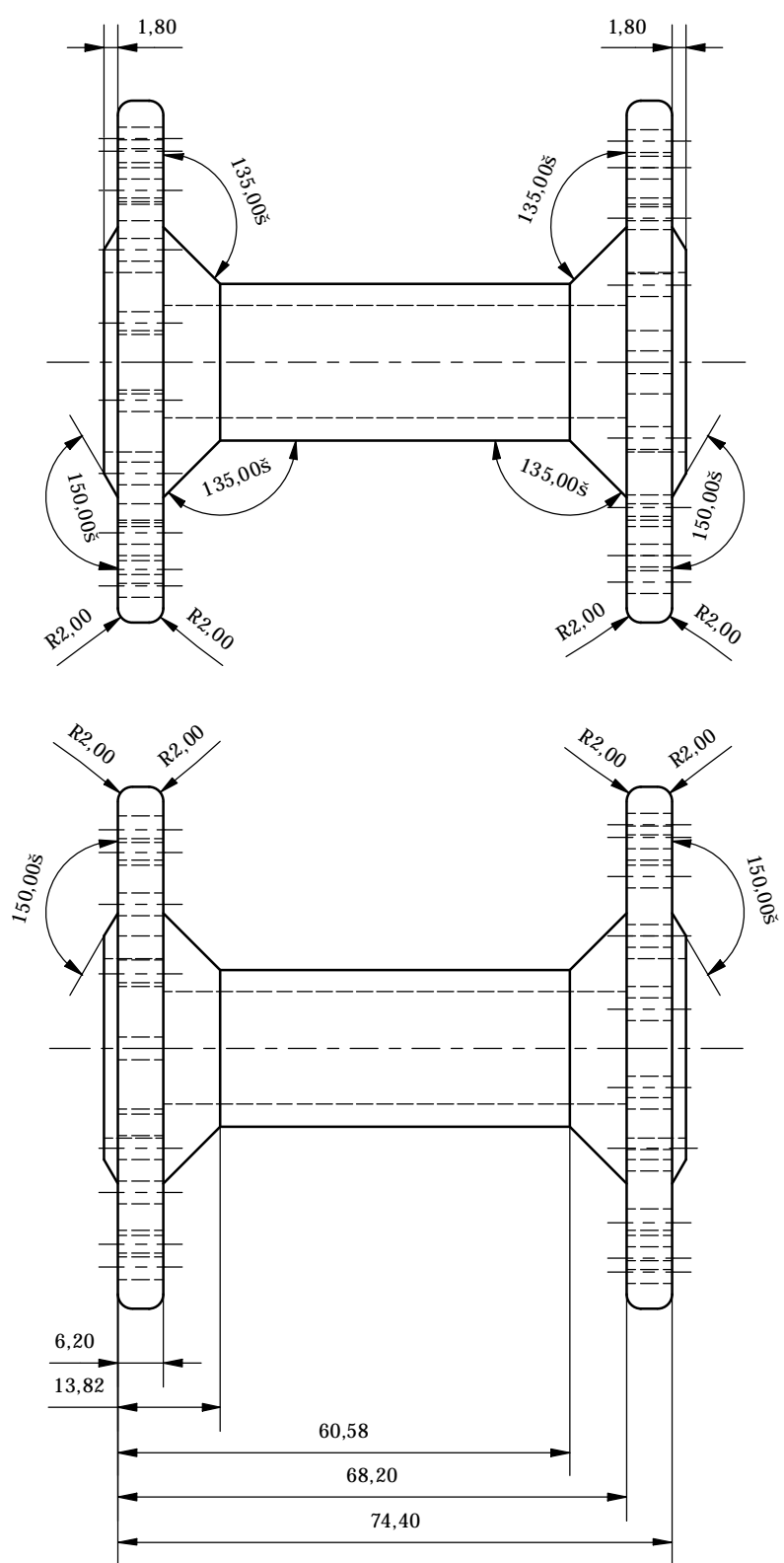
Once each of the frame members has been cut to the required length, TIG welding can be used to strongly join them. However, the heat-affected zones must be heat treated to relieve the created residual thermal stresses and restore most of the original properties of aluminium 6061-T6. Alternatively, as found on parts of aircraft wings and fuselages, a high-strength adhesive could be used with no degradation of properties, no residual thermal stresses, and considerable savings in time, cost, and energy, but this will require further investigation and is not recommended presently [12].

Since components of the wheels, crankset, and frame are constructed from aluminium, the possible protection coatings should be considered. Aluminium naturally and rapidly forms a self-sealing oxide that protects the outer surface, but this characteristic does not protect against more aggressive chemicals such as the salts and acids which may be found on wet roads [55]. To protect against these harsher conditions, a coating can be applied or an artificial oxide layer can be applied to the outer surface through anodising, which uses an electrolytic process to oxidise the aluminium in an acid bath after which a dye can be applied to colour the surface [55]. However, anodised aluminium rims are actually weaker because the oxide layer is brittle and it is more prone to forming surface cracks; and, furthermore, a coating can decrease braking performance due to the finish being smoother. Thus, it is decided for the rims not to be anodised or coated. The frame, fork, stem, and handlebar could be anodised but this is expected to have a high cost and a more inexpensive and available option is to powder coat the frame - aesthetic colours can also be used for unique styles. The cranks can benefit from anodising as they are relatively compact to warrant an inexpensive process and, so, a layer of approximately 0.03mm thick can be applied to protect them.

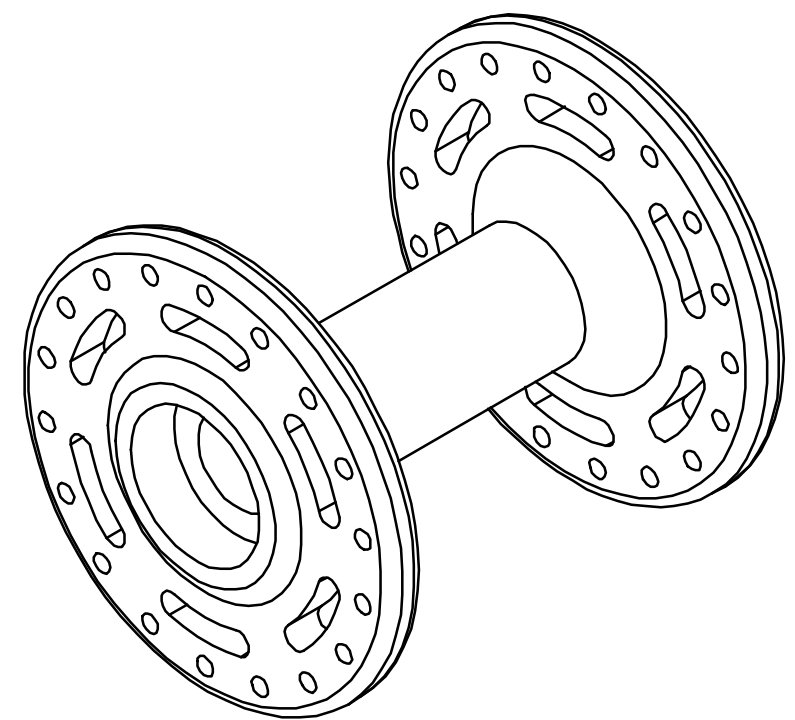
Table 26: Parts list including the item number, part name, and required quantity.

Item	Part Name	Qty.	Item	Part Name	Qty.	Item	Part Name	Qty.
1	Front Hub Shell	1	13	Enclosure Lid	1	25	Stem Bolt	1
2	Front Axle	1	14	Front Fork	1	26	Pinch Bolt	1
3	Front Spacer	2	15	Frame	1	27	Headset Lock Nut	1
4	Rim	2	16	Deep Groove Bearing	2	28	Top Cup-Cone	1
5	Stem Quill	1	17	Front Lock Nut	1	29	Bottom Cup-Cone	1
6	Stem Wedge	1	18	Front Axle Nut	1	30	Roller Chain Link	102
7	Handlebar	1	19	Front Spoke	36	31	Shimano Octalink	1
8	Right Crank	1	20	Rear Spoke - Long	18	32	Crank Bolt	2
9	Left Crank	1	21	Rear Spoke - Short	18	33	Sprocket Bolt	4
10	Driving Sprocket	1	22	Nipple	72	34	Cassette Rear Spacer	1
11	Driven Sprocket	1	23	Heinzmann Motor	1	35	Cassette Front Spacer	1
12	Enclosure Body	1	24	Challenge Tyre	2	36	Cassette Lock Nut	1

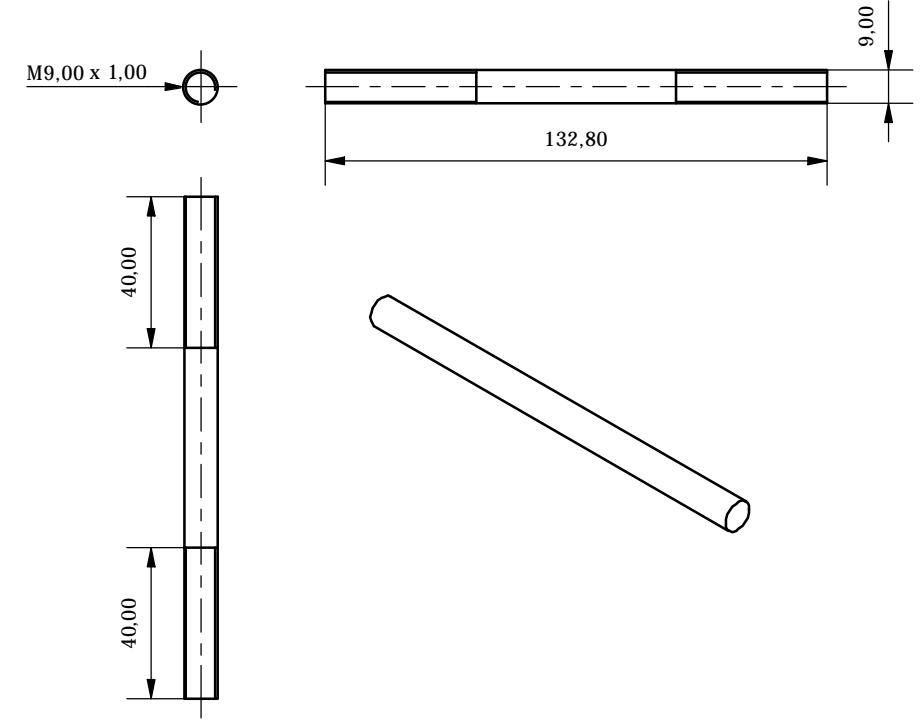
[1] FRONT HUB SHELL (1:1)



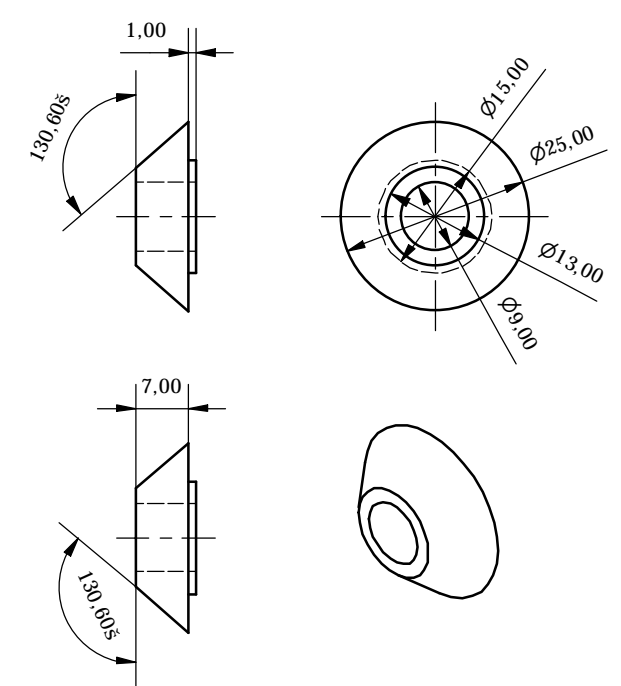
SPOKE HOLES \approx 3.00 SPACED AT 20.00s ON EACH FLANGE FACE.
SLOTS R2.00 30.00s SPACED AT 30.00s ON BOTH FLANGE FACES.



[2] FRONT AXLE (1:2)



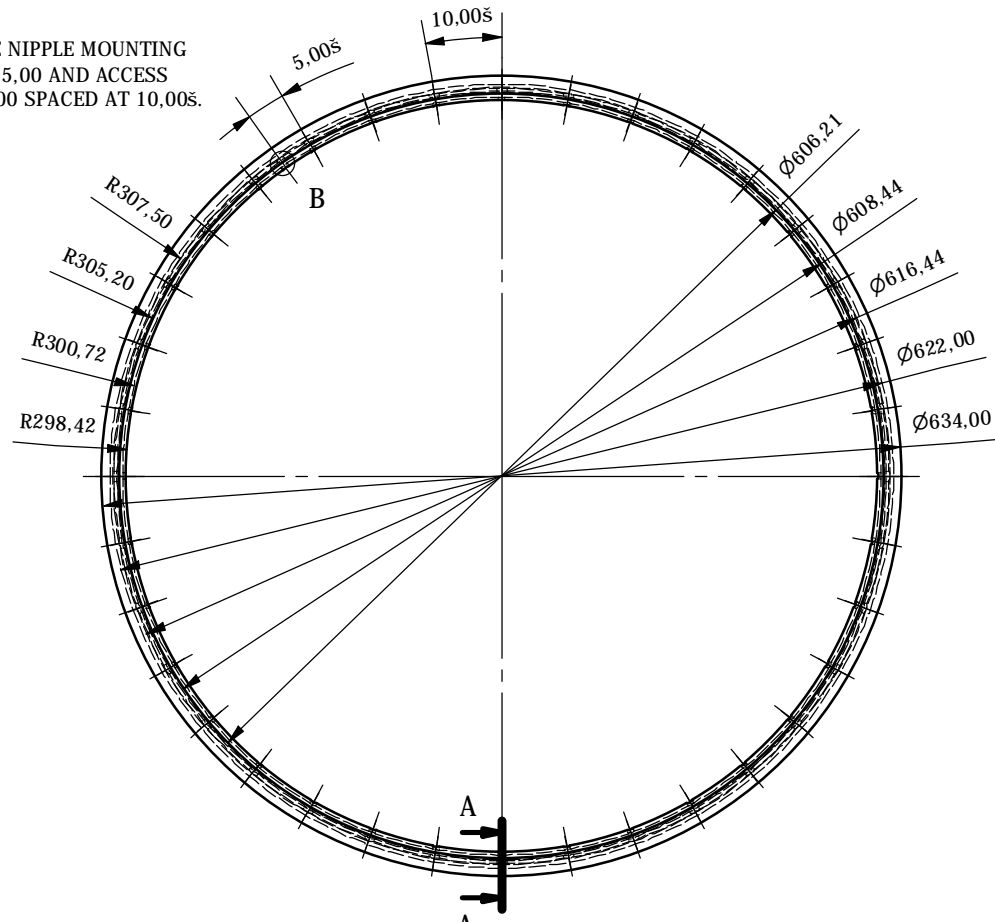
[3] FRONT SPACER (1:1)



NOTE: ALL DIMENSIONS ARE IN MILLIMETRES UNLESS OTHERWISE STATED.

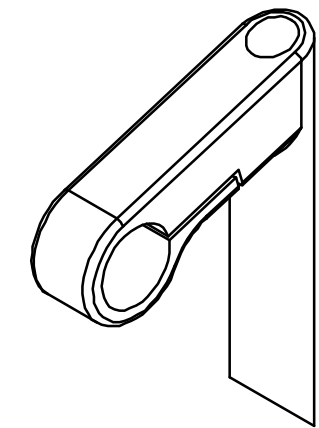
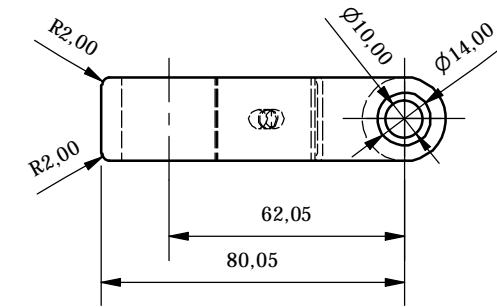
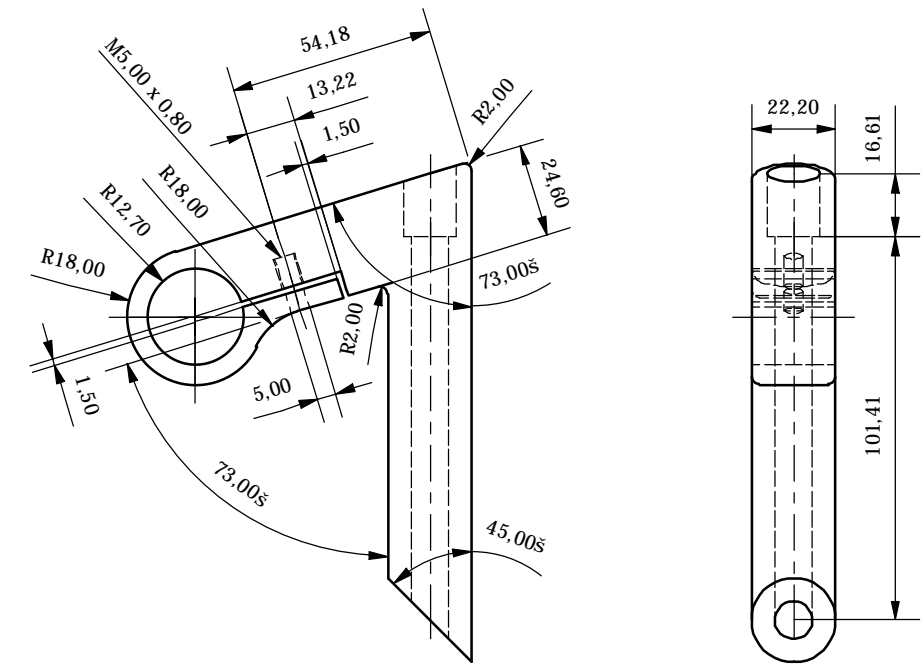
ELECTRICALLY ENHANCED PERSONAL TRANSPORTATION COMPONENTS		
SHEET NUMBER: 1	SCALE: VARIOUS	
DRAWN: EDWARD RYCROFT		SCHOOL OF MECHANICAL, INDUSTRIAL, AND AERONAUTICAL ENGINEERING, UNIVERSITY OF THE WITWATERSRAND
DATE: 2019/08/24		
COURSE: MECN4005		

36 SPOKE NIPPLE MOUNTING
HOLE \approx 5,00 AND ACCESS
HOLES \approx 8,00 SPACED AT 10,00 \bar{s} .

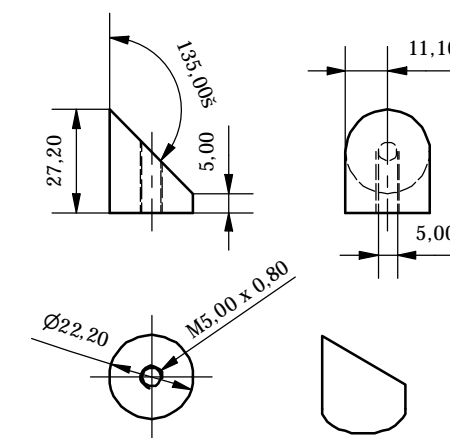


[4] RIM (1:6)

[5] STEM QUILL (1:2)



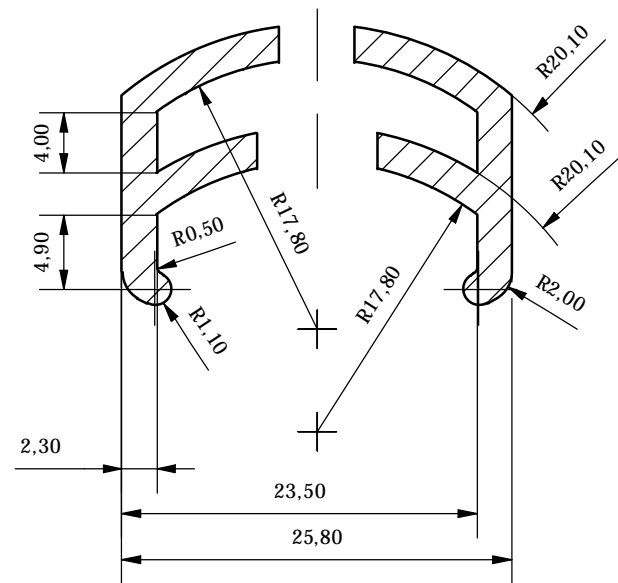
[6] STEM WEDGE (1:2)



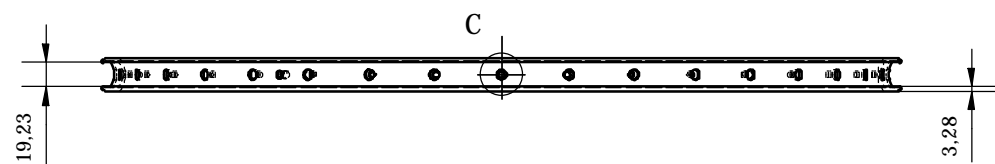
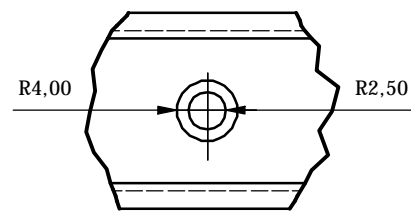
B (1:1)



A-A (2:1)

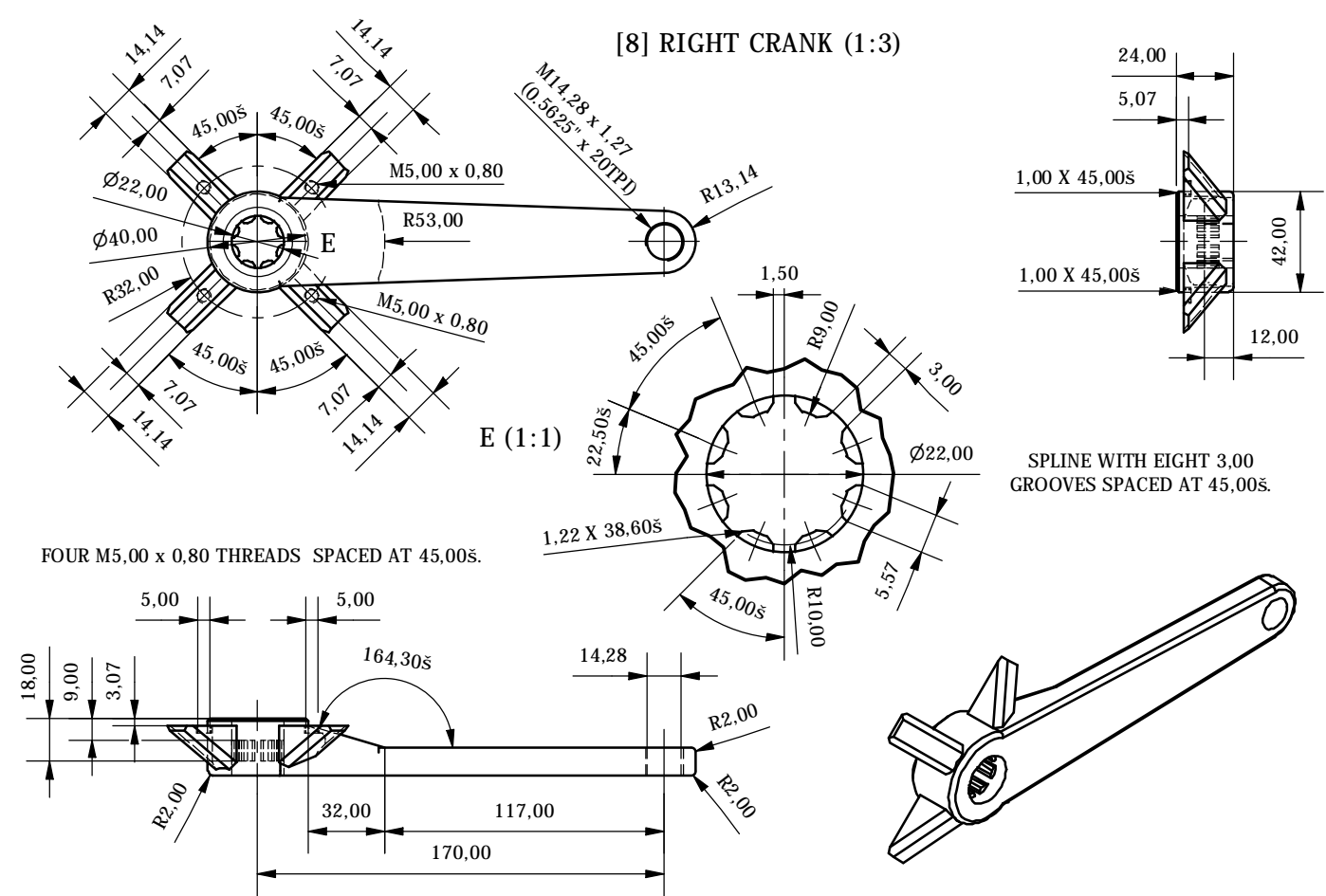


C (1:1)

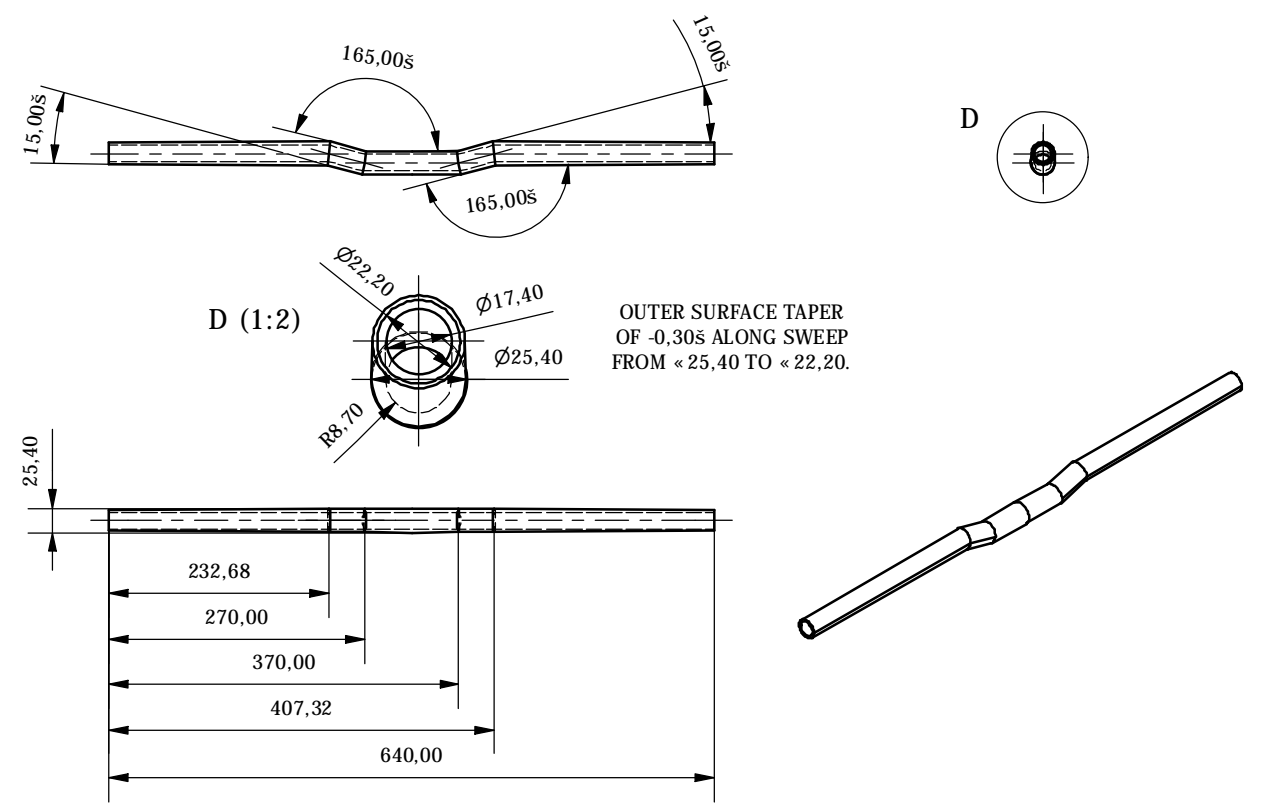


ELECTRICALLY ENHANCED PERSONAL TRANSPORTATION COMPONENTS		
SHEET NUMBER: 2	SCALE: VARIOUS	
DRAWN: EDWARD RYCROFT		SCHOOL OF MECHANICAL, INDUSTRIAL, AND AERONAUTICAL ENGINEERING, UNIVERSITY OF THE WITWATERSRAND JOHANNESBURG
DATE: 2019/08/24		
COURSE: MECN4005		

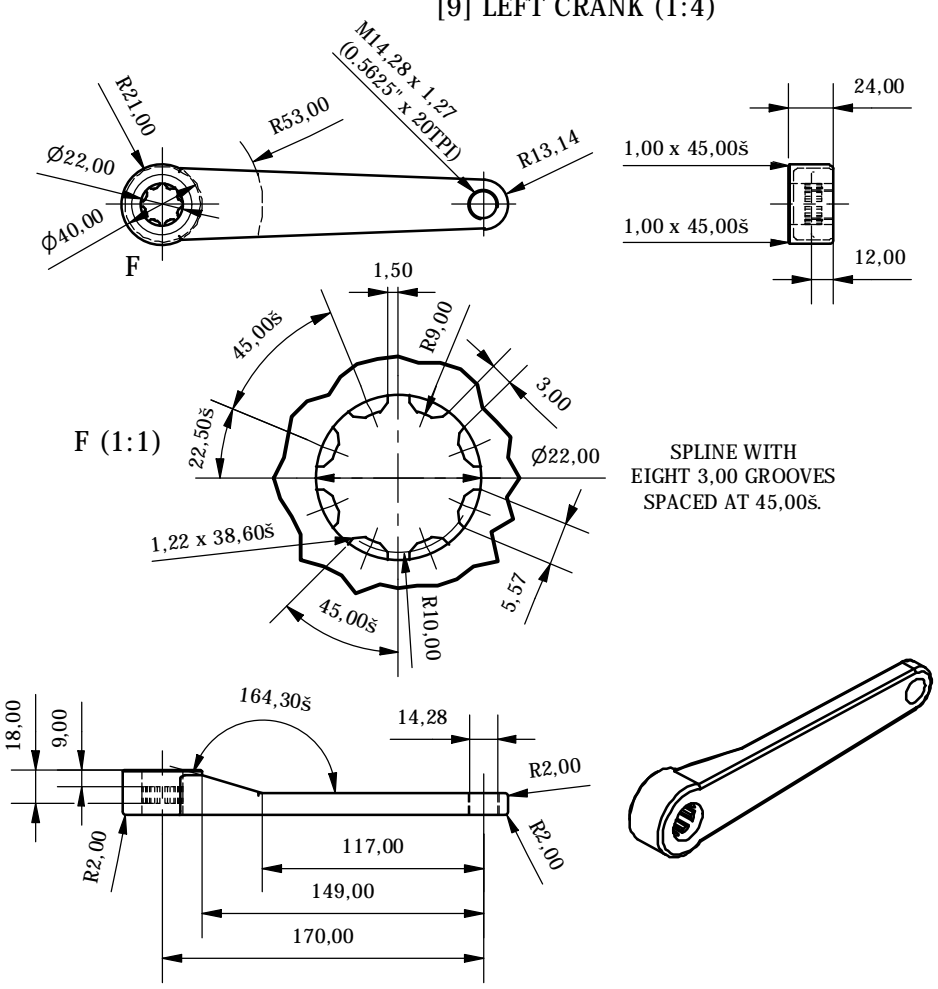
[8] RIGHT CRANK (1:3)



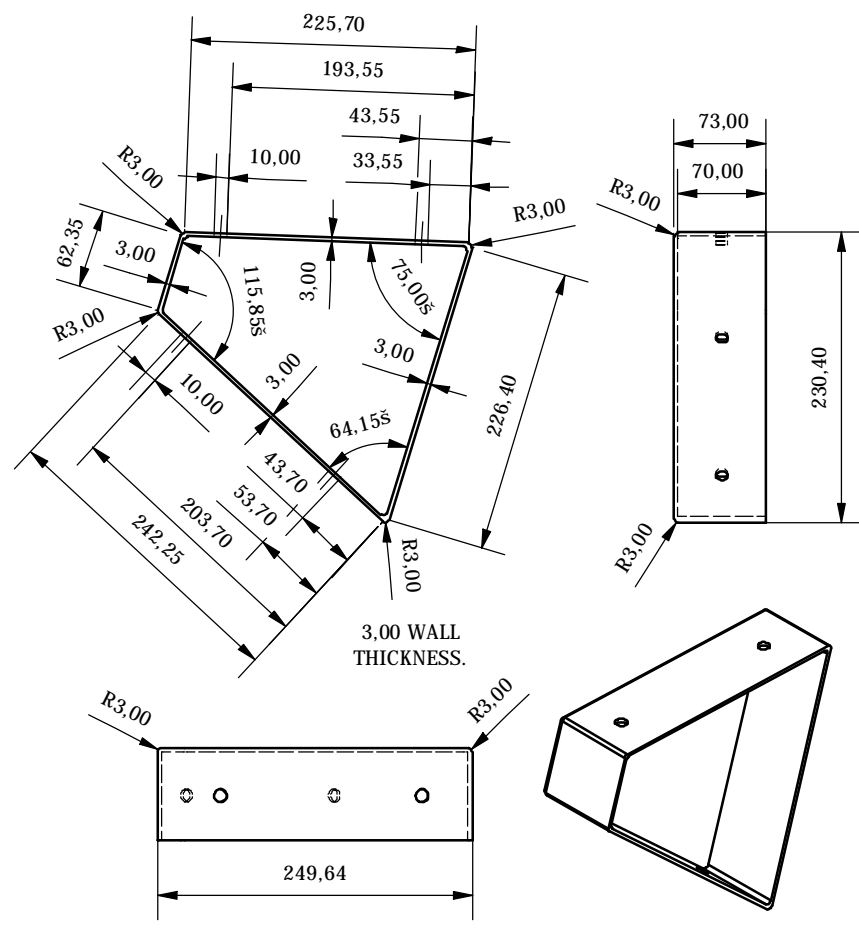
[7] HANDLEBAR (1:8)



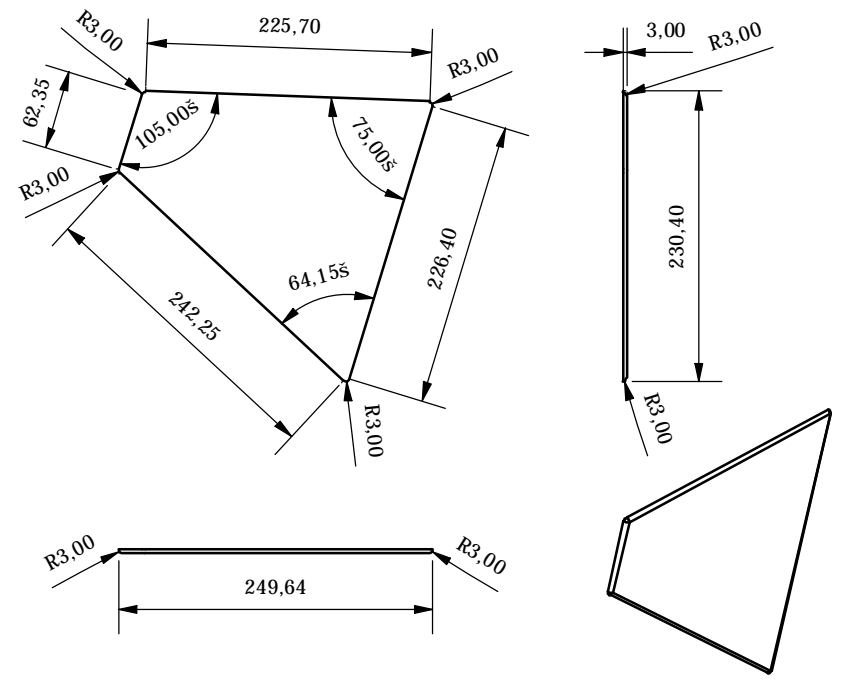
[9] LEFT CRANK (1:4)



[12] ENCLOSURE BODY (1:6)

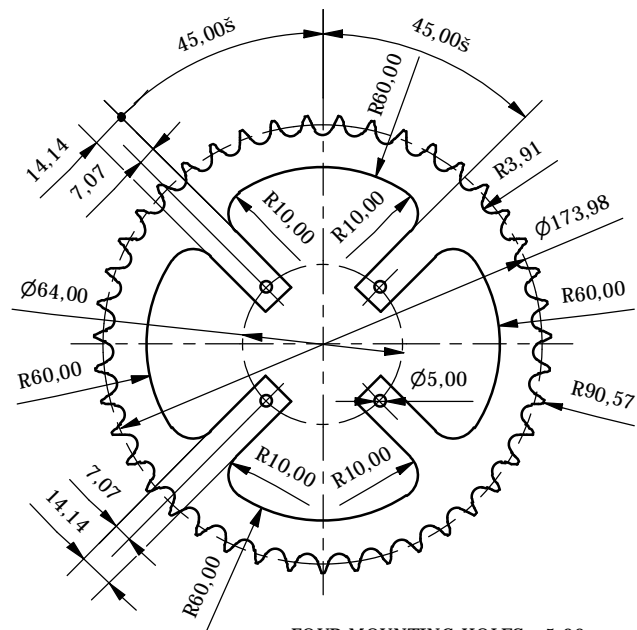


[13] ENCLOSURE LID (1:6)

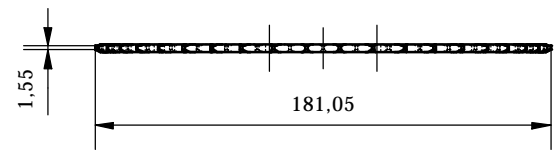


ELECTRICALLY ENHANCED PERSONAL TRANSPORTATION COMPONENTS		
SHEET NUMBER: 3	SCALE: VARIOUS	
DRAWN: EDWARD RYCROFT		SCHOOL OF MECHANICAL, INDUSTRIAL, AND AERONAUTICAL ENGINEERING, UNIVERSITY OF THE WITWATERSRAND
DATE: 2019/08/24		
COURSE: MECN4005		

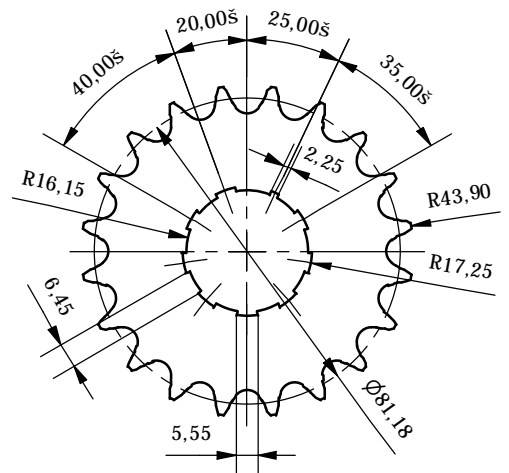
[10] DRIVING SPROCKET (1:3)



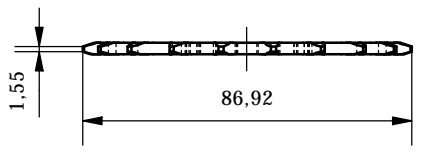
FOUR MOUNTING HOLES $\phi 5.00$
SPACED AT 45.00° . 45 TEETH ON
PITCH CIRCLE DIAMETER 173.98
SPACED EVENLY AND SYMMETRICALLY.



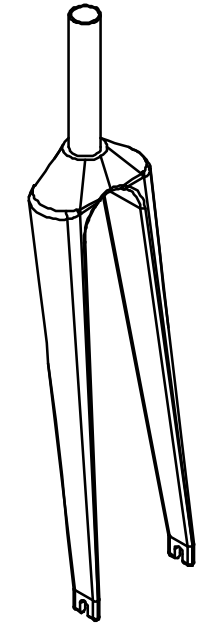
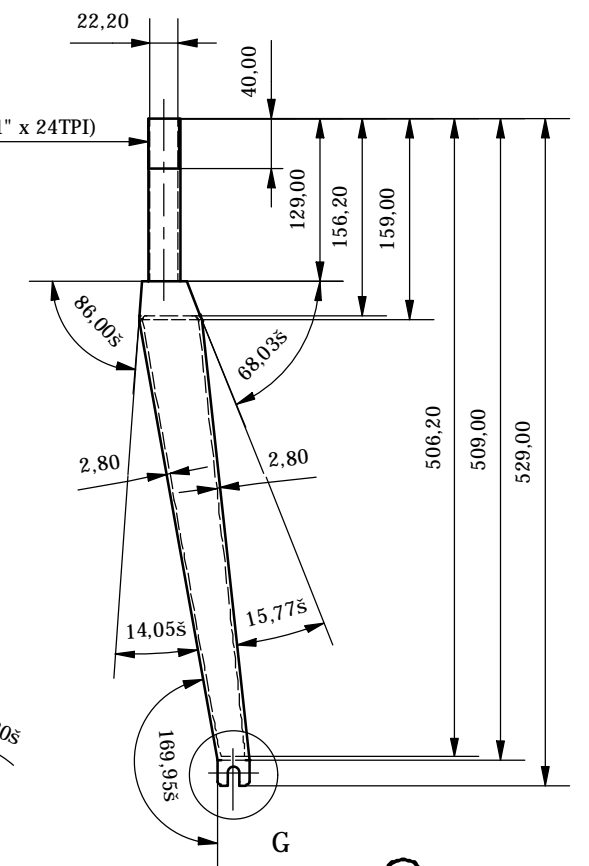
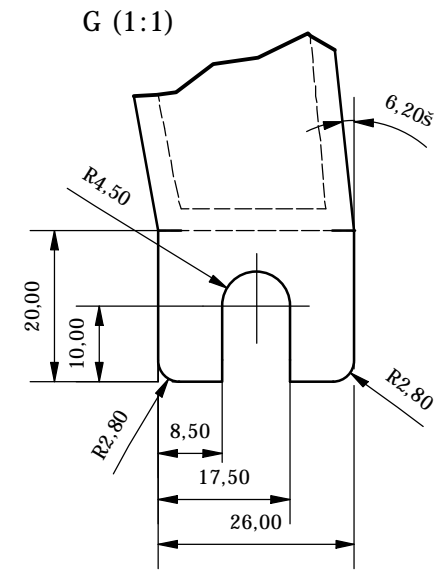
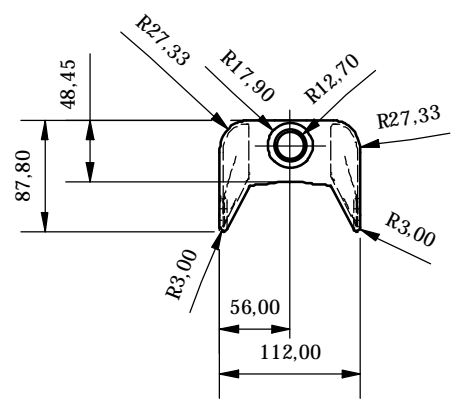
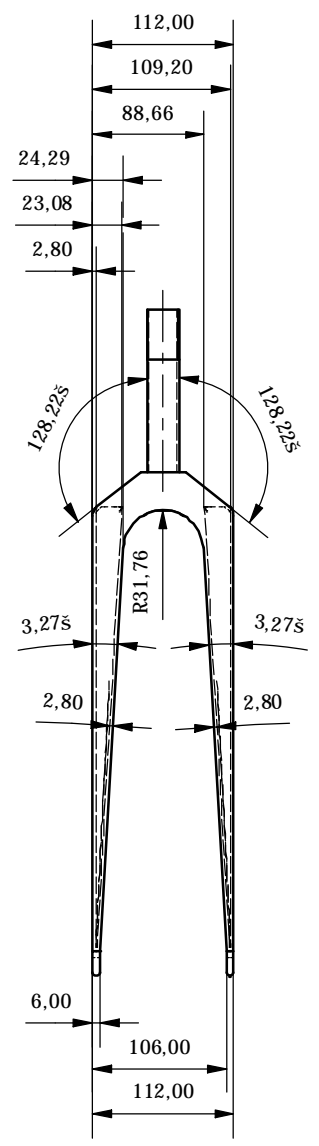
[11] DRIVEN SPROCKET (1:2)



20 TEETH ON PITCH CIRCLE DIAMETER 81.18
SPACED EVENLY AND SYMMETRICALLY.
STANDARD SHIMANO HYPERGLIDE
FREEHUB CASSETTE MOUNTING SPLINE.

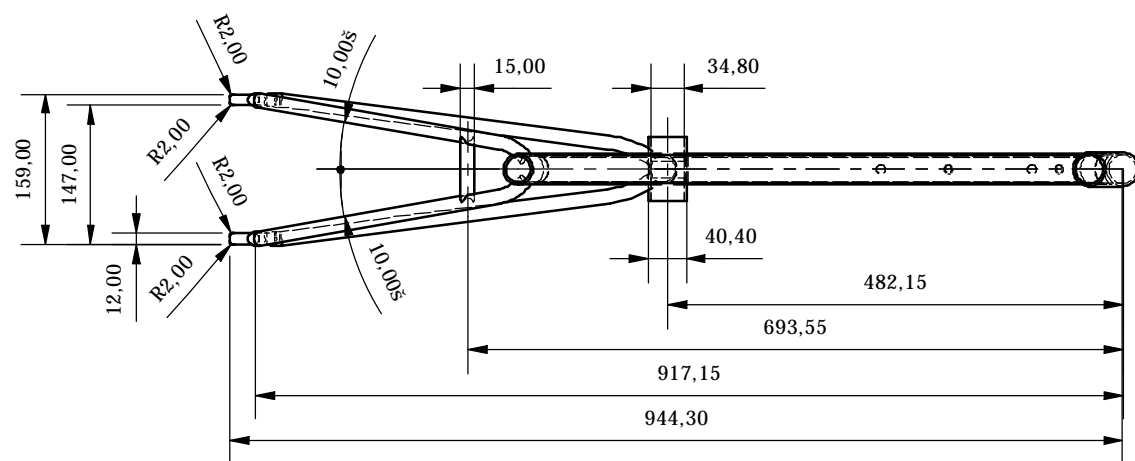
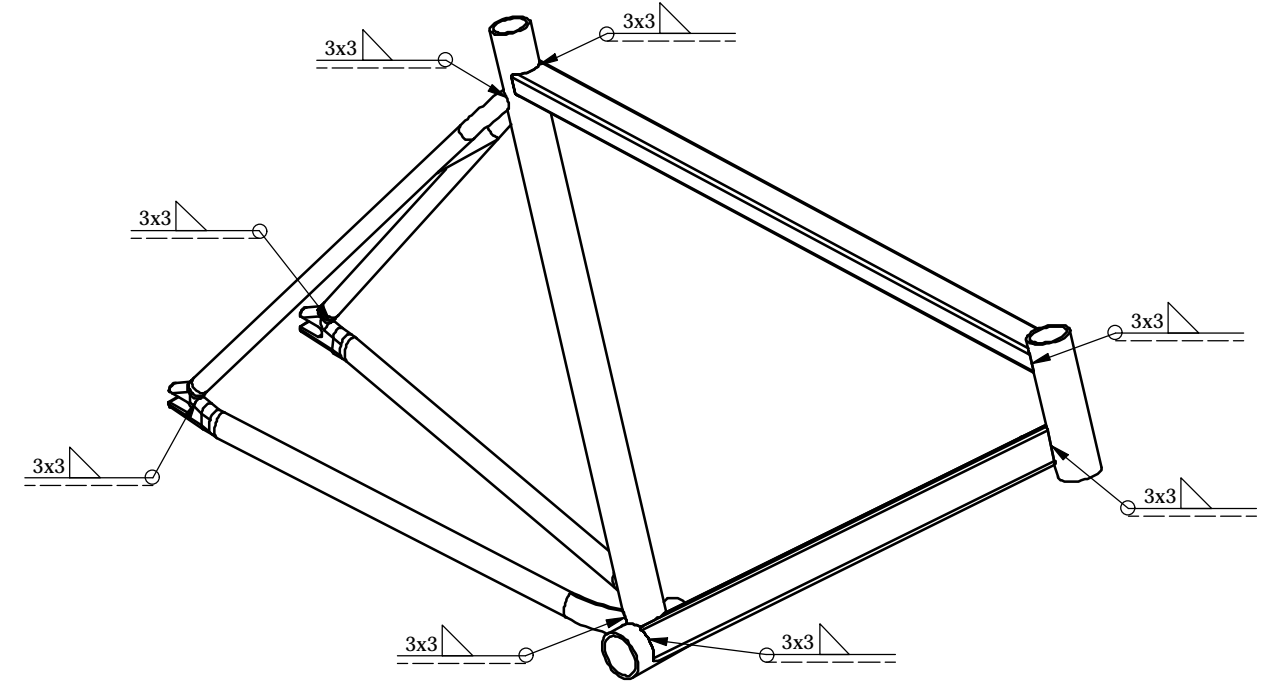
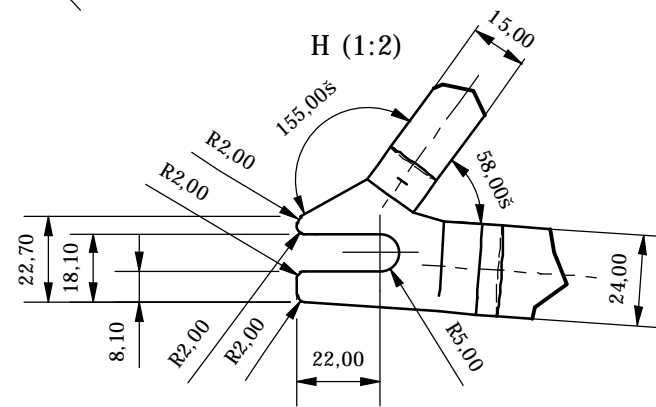
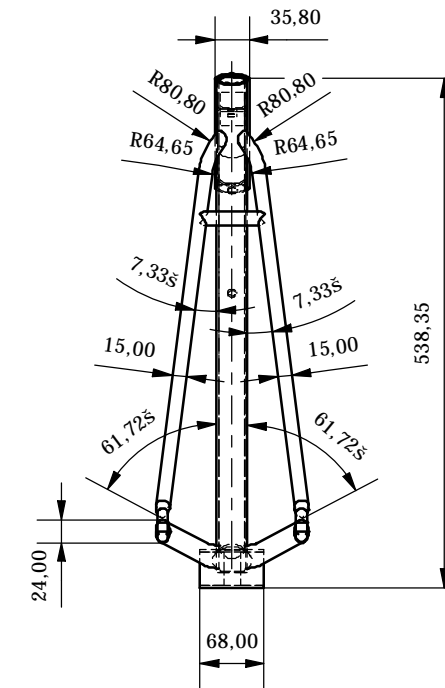
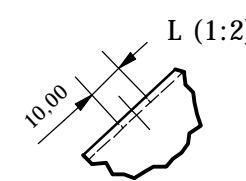
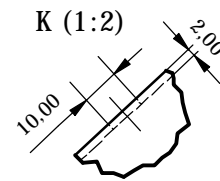
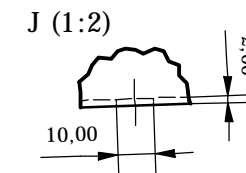
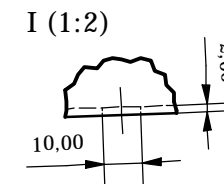
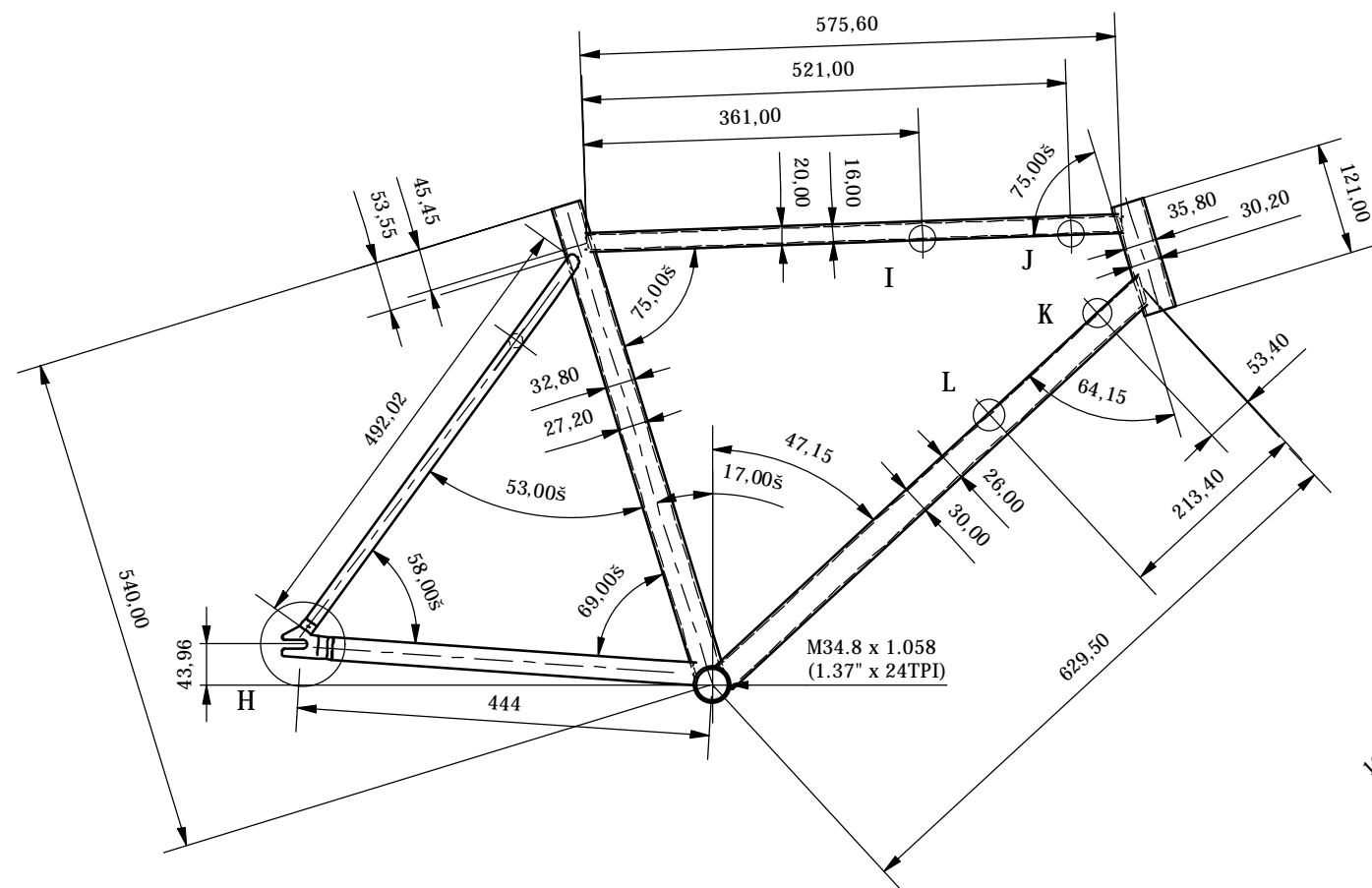




[14] FRONT FORK (1:6)



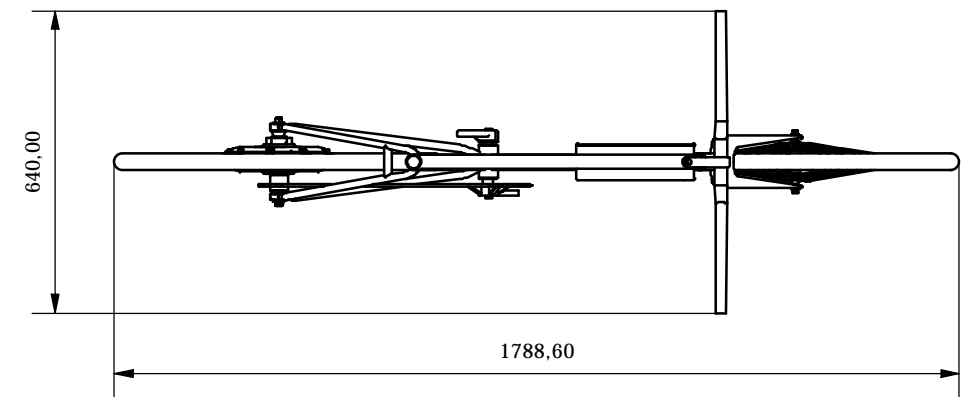
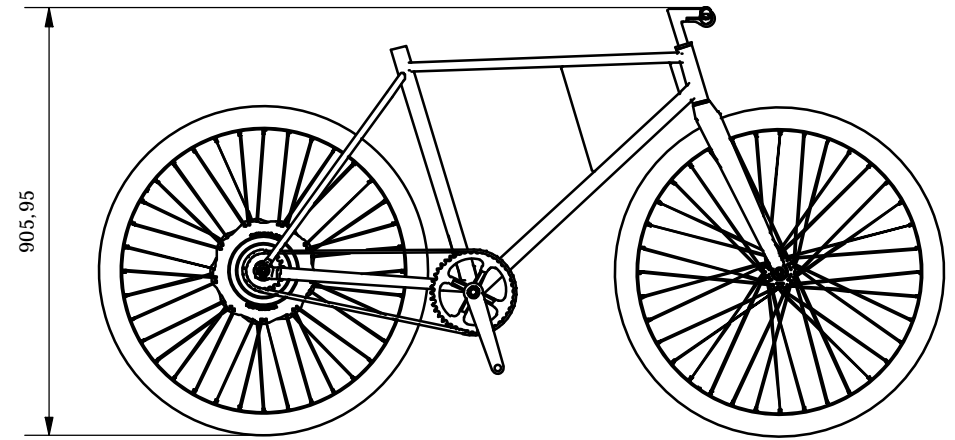
ELECTRICALLY ENHANCED PERSONAL TRANSPORTATION COMPONENTS		
SHEET NUMBER: 4	SCALE: VARIOUS	
DRAWN: EDWARD RYCROFT		SCHOOL OF MECHANICAL, INDUSTRIAL, AND AERONAUTICAL ENGINEERING, UNIVERSITY OF THE WITWATERSRAND
DATE: 2019/08/24		
COURSE: MECN4005		

[15] FRAME (1:8)

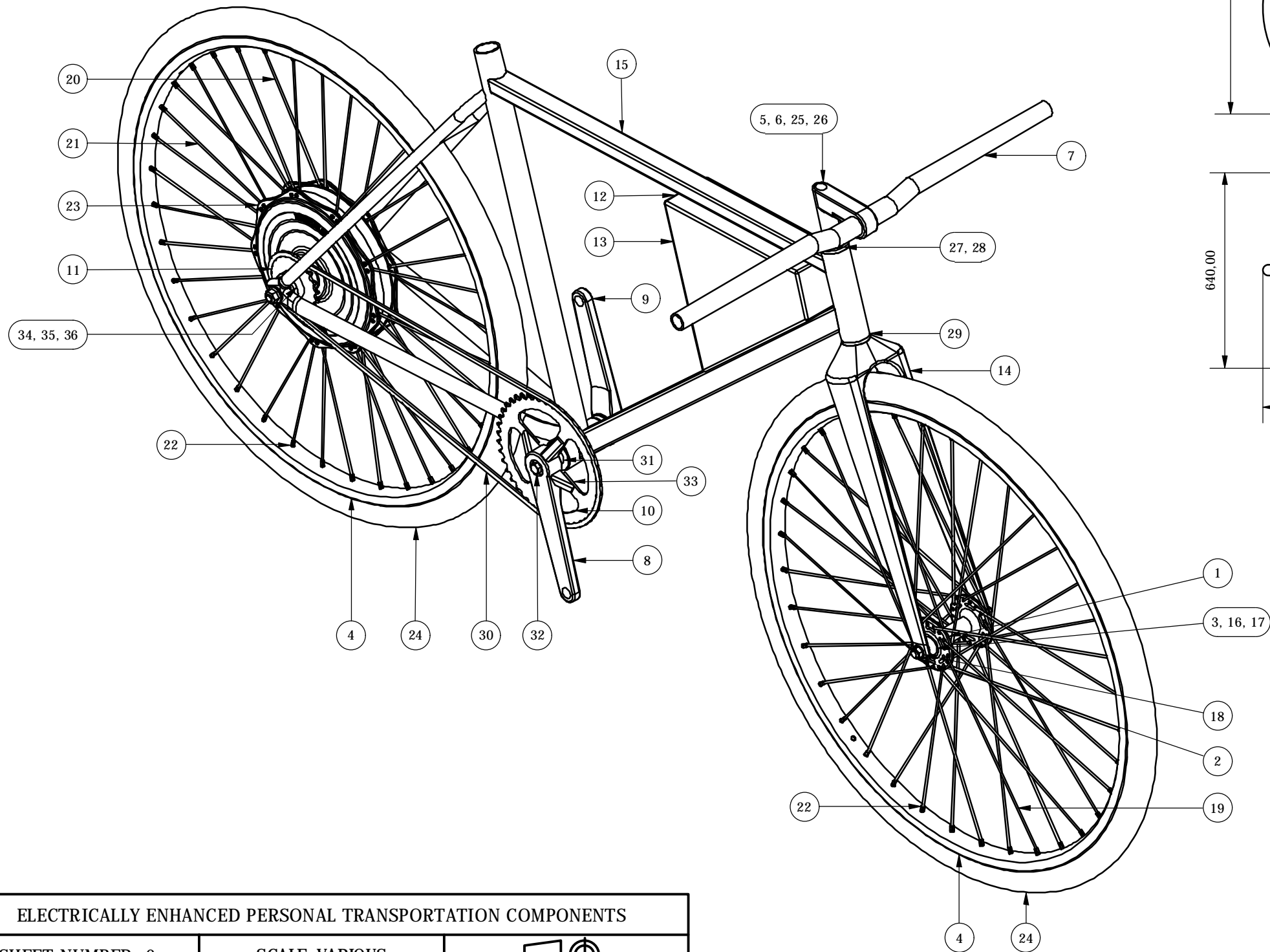


ELECTRICALLY ENHANCED PERSONAL TRANSPORTATION COMPONENTS		
SHEET NUMBER: 5	SCALE: VARIOUS	
DRAWN: EDWARD RYCROFT		SCHOOL OF MECHANICAL, INDUSTRIAL, AND AERONAUTICAL ENGINEERING, UNIVERSITY OF THE WITWATERSRAND
DATE: 2019/08/24		
COURSE: MECN4005		

ASSEMBLY (1:16)



ASSEMBLY (1:6)



ELECTRICALLY ENHANCED PERSONAL TRANSPORTATION COMPONENTS

SHEET NUMBER: 6

SCALE: VARIOUS



DRAWN: EDWARD RYCROFT

DATE: 2019/08/24

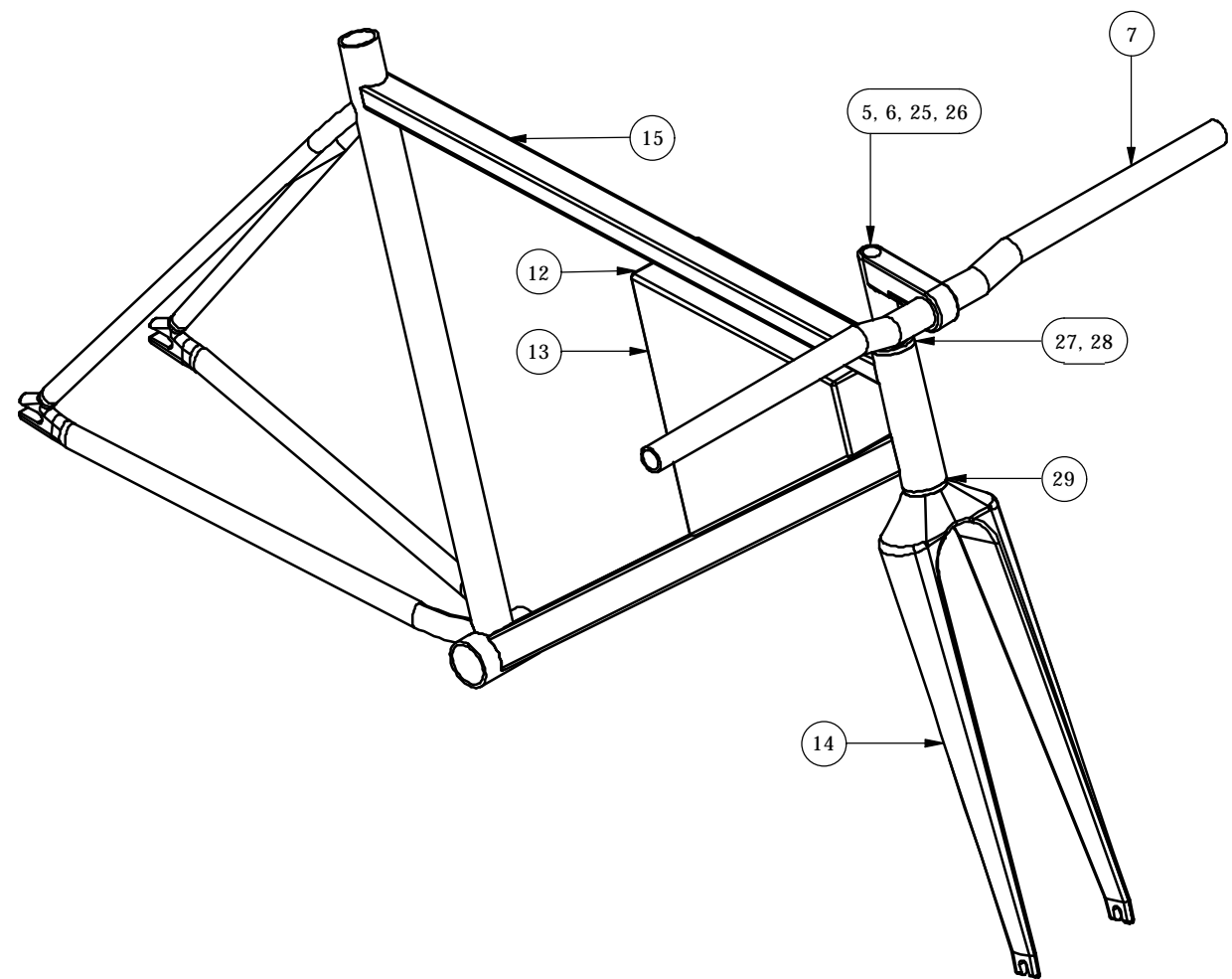
COURSE: MECN4005



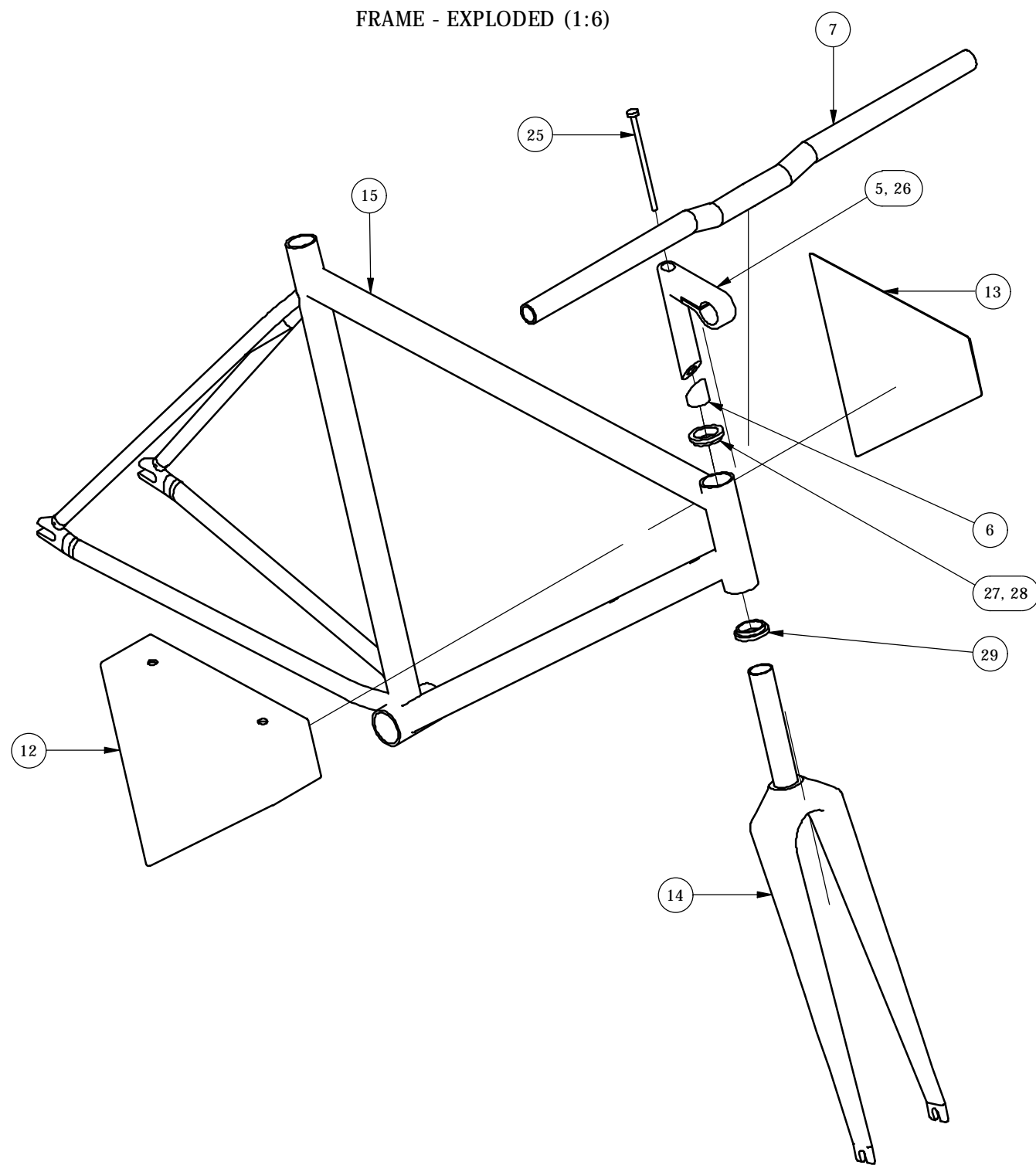
SCHOOL OF MECHANICAL, INDUSTRIAL,
AND AERONAUTICAL ENGINEERING,
UNIVERSITY OF THE WITWATERSRAND



FRAME - ASSEMBLED (1:6)



FRAME - EXPLODED (1:6)



ELECTRICALLY ENHANCED PERSONAL TRANSPORTATION COMPONENTS

SHEET NUMBER: 7

SCALE: VARIOUS



DRAWN: EDWARD RYCROFT

DATE: 2019/08/24

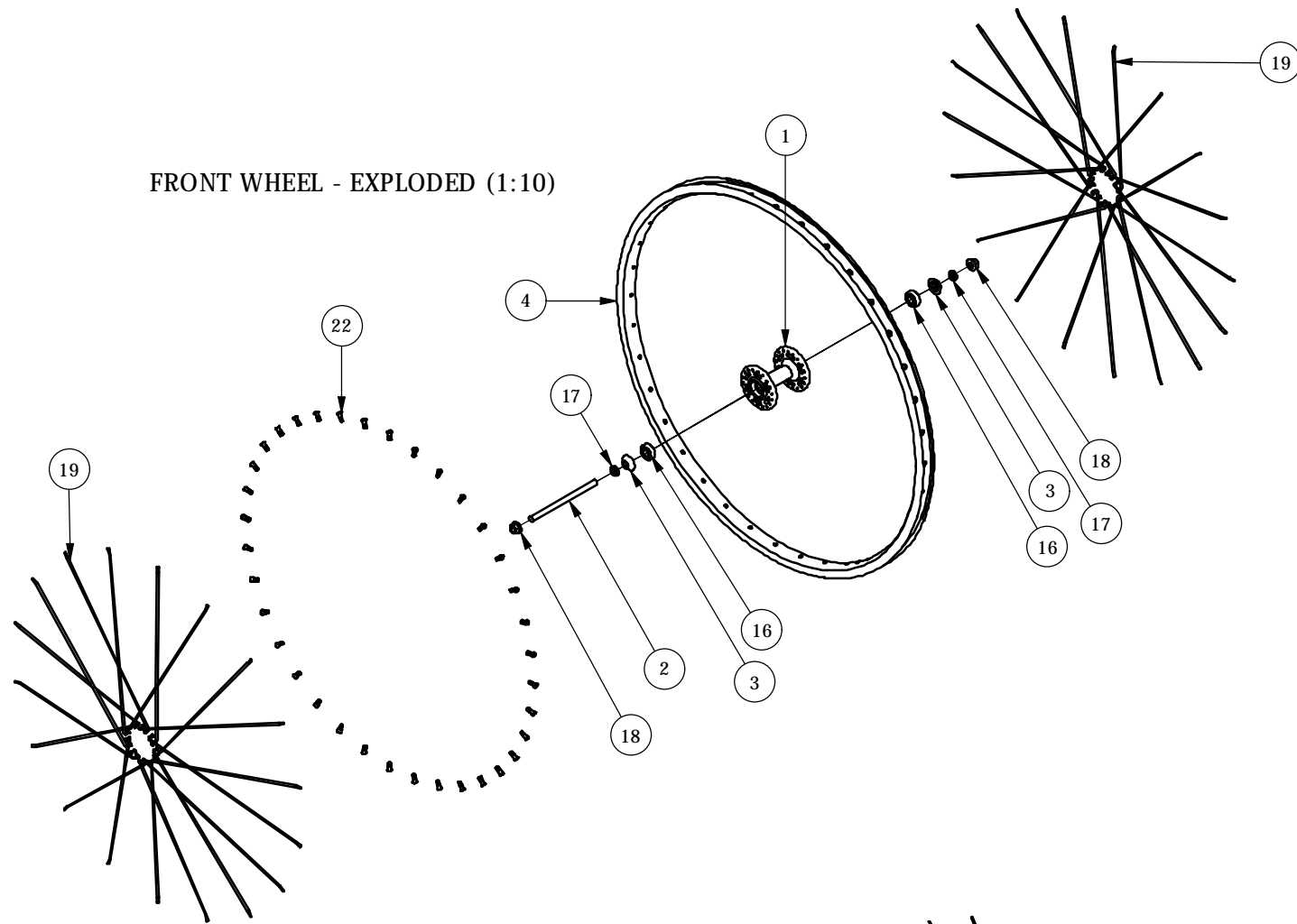
COURSE: MECN4005



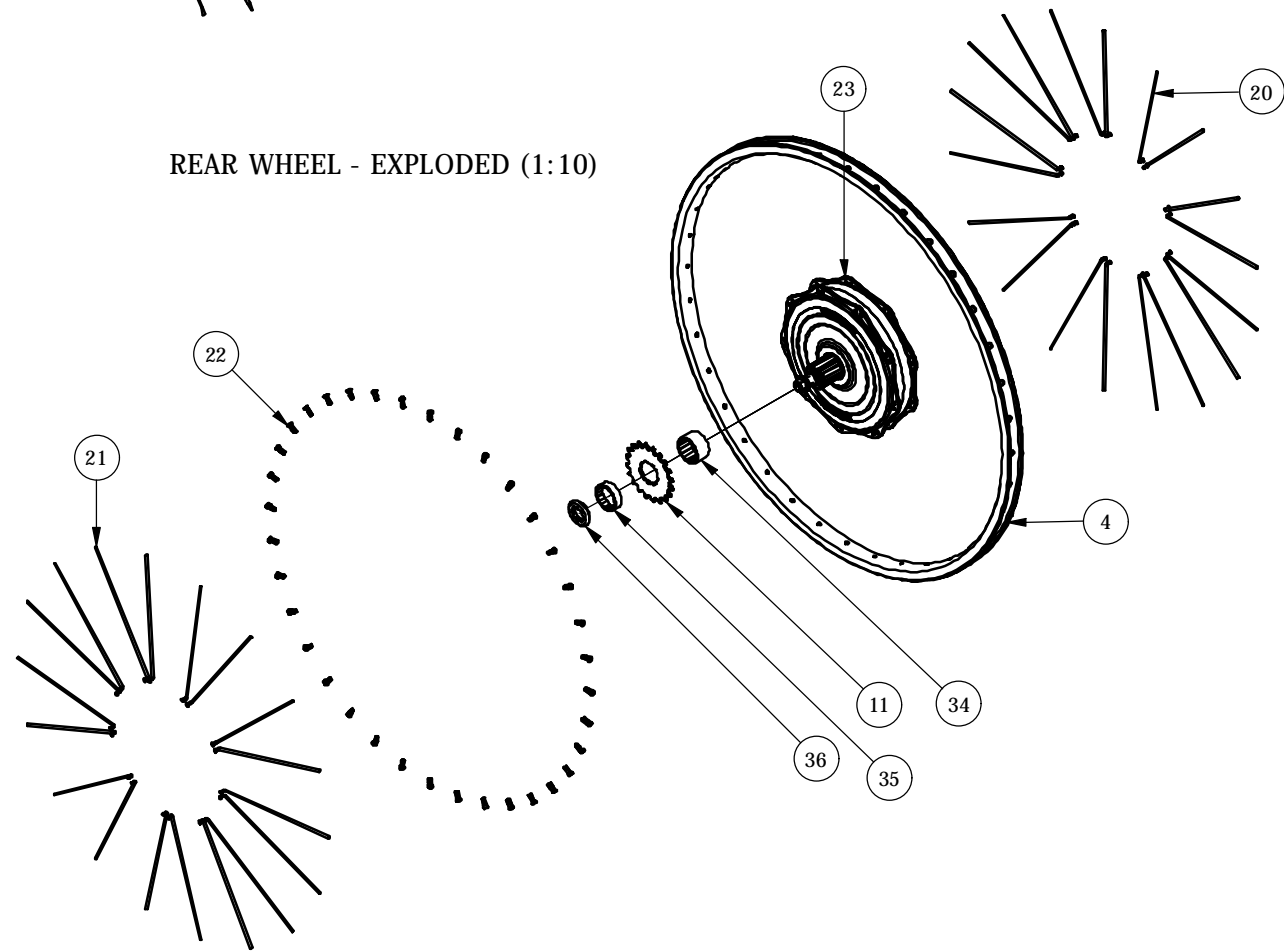
SCHOOL OF MECHANICAL, INDUSTRIAL,
AND AERONAUTICAL ENGINEERING,
UNIVERSITY OF THE WITWATERSRAND



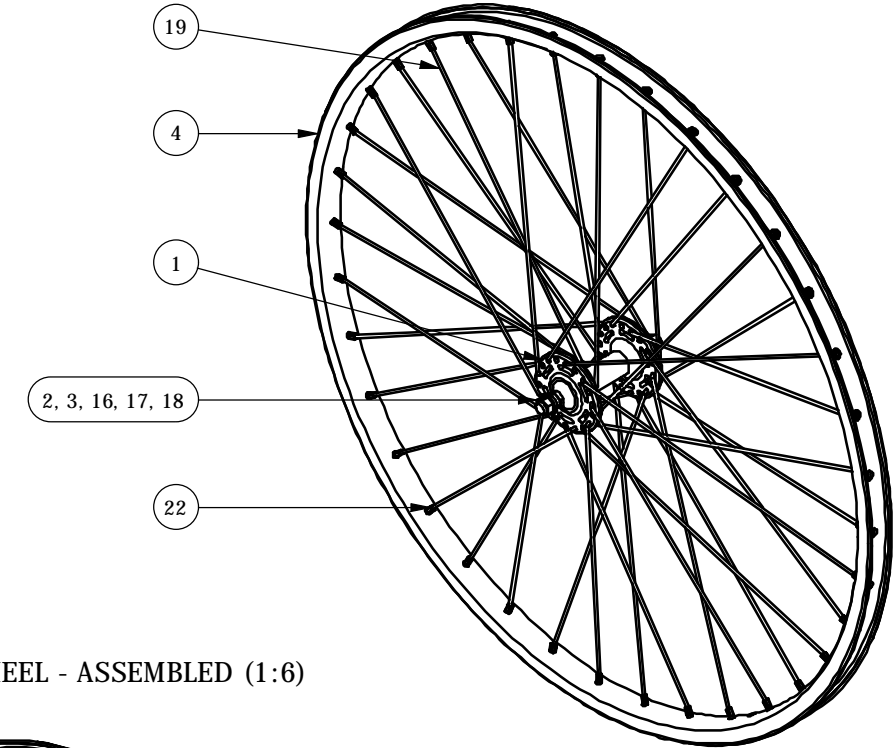
FRONT WHEEL - EXPLODED (1:10)



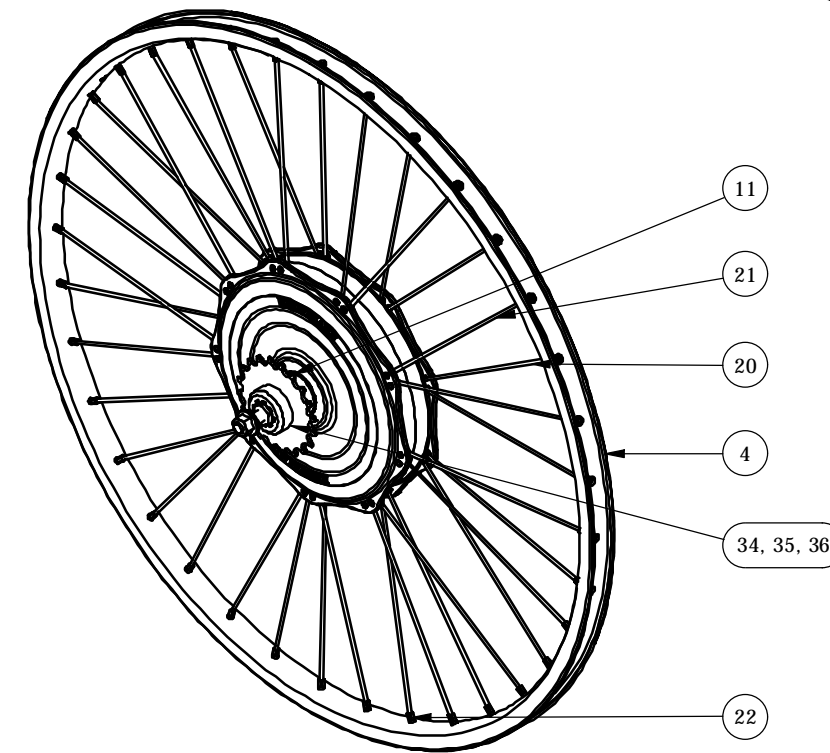
REAR WHEEL - EXPLODED (1:10)



FRONT WHEEL - ASSEMBLED (1:6)



REAR WHEEL - ASSEMBLED (1:6)



ELECTRICALLY ENHANCED PERSONAL TRANSPORTATION COMPONENTS

SHEET NUMBER: 8

SCALE: VARIOUS



DRAWN: EDWARD RYCROFT



SCHOOL OF MECHANICAL, INDUSTRIAL,
AND AERONAUTICAL ENGINEERING,
UNIVERSITY OF THE WITWATERSRAND



DATE: 2019/08/24

COURSE: MECN4005

5.4 COST ANALYSIS

For the capital costs analysis, it is expected for the bulk of the costs to come from purchasing the materials in the most convenient form and from the third-party components including the Heinzmann DirectPower PRA 180-25 brushless DC hub motor, Panasonic NCR18650PF lithium-ion battery cells, SKF 609 single row deep groove ball bearings, and various standard components for the front axle, manual propulsion, and headset. The predictions for this analysis are shown in Table 27 for a total capital cost of R27820, where the budget should be viewed as an order of magnitude or ratio estimate based on similar existing data, where the accuracy is expected to broadly vary and be within 30%. Based on the estimated cost of R0.10/km from Section 1.4.3, it is expected for the operating costs to be around only R5.00 per day while commuting 50km with only electric propulsion, which results in a monthly cost of approximately R150.00, which is cheaper than the modes discussed in Section 1.1.

Table 27: Costs analysis as an order of magnitude or ratio estimate with an accuracy within 30%.

	Cost [R]
Heinzmann DirectPower PRA 180-25	8580
Panasonic NCR18650PF Battery Pack	8540
Manual Propulsion Components	2200
Wheel Material And Components	3000
Frame Material And Components	4500
Labour And Production	5000
Total	27820

6 CONCLUSIONS

The following conclusions can be made relative to the task statements, requirements, constraints, and sub-systems for the manual propulsion, electric propulsion, wheel arrangement, and frame structure:

- The electric propulsion uses a Heinzmann DirectPower PRA 180-25 brushless DC hub motor producing 250W of continuous rated power, as limited by legal regulations, and 835.2W.hr battery pack using 80 Panasonic NCR18650PF cells each rated at 2.90A.hr for a range of 50km.
- A chain drive with an ISO 606 081-100 roller chain offers versatile manual propulsion, where a gear ratio of 1:2.15 is used between the 43-teeth driving sprocket and 20-teeth driven sprocket while receiving a pedalling input using 170mm cranks constructed from aluminum 6061-T6.
- For the wheel arrangement, a two-wheel layout provides a compromise between operating skill and performance with decreased drag, weight, and rolling resistances. Challenge Gravel Grinder TLR pneumatic tyres are chosen for the rims with a diameter of 622mm and profile classification of 19C, while 36 stainless steel spokes of 2.6mm diameter connect the rims to the hubs, where the front hub was designed with a 9mm steel AISI 4140 axle and SKF 609-2RSH bearings.

- To accommodate male and female users between the 5th and 95th percentiles and up to 100kg, the aluminium 6061-T6 frame and front fork are sized with a diamond structure for a seat tube angle of 73° , top tube length of 585mm, and wheelbase of 1095mm. The headset, stem, and handlebars are proposed with a width of 640mm for a steering torque up to 6.4N.m. An ABS enclosure with a volume of 22.0L is fitted within the frame for the controller and battery pack.
- The electric propulsion can sustain speeds of at least 25km/hr on a level grade within 4.809s when accelerating from rest and 15km/hr on a slope with a gradient up to 3% within 1.631s when accelerating from rest, while experiencing an incoming wind at 10km/hr.
- The manual propulsion is also able to obtain sustained speeds of at least 25km/hr on a level grade and 15km/hr on a slope with a gradient up to 3%, while experiencing incoming wind at 10km/hr.
- The combined propulsion is able to achieve sustained speeds of at least 30km/hr on slopes up to 3% gradient and 20km/hr on slopes up to 6% gradient with wind speeds over 10km/hr.
- The total mass of the designed components is 17.02kg, which allows for the controller, braking system, and other accessories to have a mass up to 1.98kg - this is slightly constraining but can be managed through optimisations to minimise mass.
- Overall, the design can be seen as fairly successful.

7 RECOMMENDATIONS

The following points are recommended for further research and design development:

- Perform a cost analysis based on a definite or project control estimate for accuracy within 10%.
- Verification of the electronic characteristics of the Heinzmann DirectPower PRA 180-25 brushless DC hub motor and Panasonic NCR18650PF lithium-ion battery cells, such as reliability, no-load current, and efficiency of the motor and actual current and voltages of each battery cells.
- Dynamic testing with models of the rims and frame to evaluate safety in the presence of dynamic amplifications and fatigue using resistance strain gauges and testing until failure.
- Assemble a prototype for experimentation to verify the analytical and simulation predictions with practical tests on asphalt, pavement, cement, gravel, or flat soil. Additionally, it would be possible to investigate aspects that could not be accurately predicted, such as regenerative braking, operating noise levels, and handling resulting from the mass distribution.
- If experimenting with multiple prototypes, perform a statistical analysis with the experimental data to predict the reliability and life expectancy of the critical components.
- Development of a multiple gear power transmission which can be installed if the user desires better versatility with more options for manual propulsion. This is possible since the hub motor supports cassette mounting, but it would be necessary for minimal modifications to the frame to support a rear derailleur. Alternatively, the hub motor could be moved to the front wheel and an internal gear hub gear could be used at the rear wheel with the single-speed power transmission.

- Development of a suspension front fork which can be installed if the user desires use on harsh off-road conditions. This should be compatible without any modifications required.
- If improved performance is desired, investigate using more expensive materials with lower densities and high strengths to relieve mass, such as carbon fibre or titanium for the frame.
- Because it presents a large obstacle to adoption, safety when operating on a road should be emphasised and improved, where an approved helmet should always be worn by the user as a minimum form of protection. Further forms of protection that are advisable to employ include protective clothing with high visibility stripes, such as gloves, eye protection, and padded jackets.
- Consider the possibility of a vehicle sharing framework for distributed costs, increased availability, and autonomy. For example, this has been relatively successful in European countries and the United States, where electric bicycles or scooters can easily be rented at sharing stations.

REFERENCES

- [1] South African Department of Transport and Statistics South Africa. *2013 National Household Travel Survey*. Pretoria, July 2014. As of 26th June 2019: <http://www.statssa.gov.za/publications/P0320/P03202013.pdf>.
- [2] South African Department of Transport. *Key Results Of The 2003 National Household Travel Survey: The First South African National Household Travel Survey*. Pretoria, Aug. 2005. As of 26th June 2019: <https://www.datafirst.uct.ac.za/dataportal/index.php/catalog/569>.
- [3] K. Crane et al. 'Chapter 4 - Personal Transportation: Sharing, Rather Than Owning, Vehicles'. In: *Energy Services Analysis: An Alternative Approach for Identifying Opportunities to Reduce Emissions of Greenhouse Gases*. RAND Corporation, 2012, pp. 19–20. As of 26th June 2019: <http://www.jstor.org/stable/10.7249/j.ctt3fh16f.11>.
- [4] N. McGuckin and A. Fucci. *Summary of Travel Trends: 2017 National Household Travel Survey*. Washington DC: U.S. Department of Transport and Federal Highway Administration, July 2018, pp. 12–81. As of 26th June 2019: https://nhts.ornl.gov/assets/2017_nhts_summary_travel_trends.pdf.
- [5] N. McGuckin and A. Fucci. *Summary of Travel Trends: Findings from the 2017 NHTS - Presentation*. Washington DC: U.S. Department of Transport and Federal Highway Administration, Aug. 2018. As of 26th June 2019: <http://onlinepubs.trb.org/onlinepubs/Conferences/2018/NHTS/McGuckinTravelTrends.pdf>.
- [6] OECD. 'Chapter 5 - Personal Transport Choices'. In: *Greening Household Behaviour: The Role of Public Policy*. Paris: OECD Publishing, 2011, pp. 97–118. ISBN: 978-92-64-063624. As of 27th June 2019: https://www.oecd-ilibrary.org/environment/greening-household-behaviour/personal-transport-choices_9789264096875-8-en.
- [7] T. Xia et al. 'Cobenefits of Replacing Car Trips with Alternative Transportation: A Review of Evidence and Methodological Issues'. In: *Journal of Environmental and Public Health* (0) (July 2013). ISSN: 1687-9805. DOI: 10.1155/2013/797312. As of 28th June 2019: <https://www.ncbi.nlm.nih.gov/pmc/articles/PMC3730154/>.
- [8] E. Salmeron-Manzano and F. Manzano-Agugliaro. 'The Electric Bicycle: Worldwide Research Trends'. In: *Energies* Vol. 11. (7) (July 2018). DOI: 10.3390/en11071894. As of 30th June 2019: <https://www.mdpi.com/1996-1073/11/7/1894>.
- [9] G. Smith, H. K. Stromberg and P. Wallgren. 'Chapter 16 - Electric Bicycle Adoption: Opportunities and Requirements'. In: *System Perspectives on Electromobility*. Ed. by B. Sanden and P. Wallgren. Gothenburg: Chalmers University of Technology, 2017, pp. 181–190. ISBN: 978-91-88041-07-4. As of 28th June 2019: <https://www.chalmers.se/en/areas-of->

advance/energy/publications-media/systems-perspectives/Documents/Download%20Systems%20Perspectives%20on%20Electromobility.pdf.

- [10] P. Plazier, G. Weitkamp and A. V. D. Berg. 'Exploring the Adoption of E-Bikes by Different User Groups'. In: *Frontiers in Built Environment* Vol. 4. (47) (Aug. 2018). ISSN: 2297-3362. DOI: 10.3389/fbuil.2018.00047. As of 28th June 2019: <https://www.frontiersin.org/article/10.3389/fbuil.2018.00047/full>.
- [11] P. Paige-Green, A. Maharaj and J. Komba. *Potholes: A technical guide to their causes, identification, and repair*. Pretoria: CSIR Built Environment, Dec. 2010. ISBN: 978-0-7988-5594-5. As of 10th July 2019: https://www.csir.co.za/sites/default/files/Documents/Pothole_CSIR_tech_guide.pdf.
- [12] D. G. Wilson and J. Papadopoulos. *Bicycling Science*. 3rd ed. Cambridge: Massachusetts Institute of Technology (MIT) Press, 2004. ISBN: 978-0-262-23237-1.
- [13] W. C. Morchin and H. Oman. *Electric Bicycles - A Guide To Design And Use*. 1st ed. New Jersey: Institute of Electrical, Electronics Engineers (IEEE) Press and Wiley-Interscience, Nov. 2005. ISBN: 978-0-471-67419-1.
- [14] A. R. Tilley and the Henry Dreyfuss Associates. *The Measure of Man and Woman: Human Factors in Design*. New York: Wiley, Dec. 2001. ISBN: 978-0-471-09955-0. Excerpt of *Chapter 1 - Anthropometry*, as of 6th July 2019: https://media.wiley.com/product_data/excerpt/54/04710995/0471099554-97.pdf.
- [15] V. F. Cassola et al. 'Standing adult human phantoms based on 10th, 50th and 90th mass and height percentiles of male and female populations'. In: *IOPscience, Physics in Medicine and Biology* Vol. 56. (13) (May 2011), pp. 3749–3772. ISSN: 0031-9155. DOI: 10.1088/0031-9155/56/13/002. As of 11th July 2019: <https://iopscience.iop.org/article/10.1088/0031-9155/56/13/002>.
- [16] Gary Hutter. *MEM30008A - Apply basic economic and ergonomic concepts to evaluate engineering applications - Chapter 5: Ergonomics*. LearnEASY. Online, Oct. 2004. Available: <http://www.learneasy.info/MDME/MEMmods/MEM30008A-EcoErgo/Ergonomics/Ergonomics.html> (visited 6th July 2019).
- [17] L. N. Mathesona et al. 'Age and gender normative data for lift capacity'. In: *Work, IOS Press* Vol. 49. (2) (Mar. 2014), pp. 257–269. ISSN: 1051-9815. DOI: 10.3233/WOR-131671. As of 10th July 2019: <https://content.iospress.com/download/work/wor01671?id=work%2Fwor01671>.
- [18] M. Jette, K. Sidney and G. Blumchen. 'Metabolic equivalents (METs) in Exercise Testing, Exercise Prescription, and Evaluation of Functional Capacity.' In: *Clinical Cardiology: International Journal for Cardiovascular Diseases* Vol. 13. (8) (Aug. 1990), pp. 555–565. DOI: 10.1002/clc.4960130809. As of 16th July 2019: <https://onlineibrary.wiley.com/doi/10.1002/clc.4960130809>.

- [19] W. J. Board and R. C. Browning. ‘Self-selected speeds and metabolic cost of longboard skateboarding’. In: *European Journal of Applied Physiology* Vol. 114. (11) (Aug. 2014), pp. 2381–2386. ISSN: 1439-6327. DOI: 10.1007/s00421-014-2959-x. As of 16th July 2019: <https://link.springer.com/article/10.1007%2Fs00421-014-2959-x>.
- [20] D. Johnstone. *How does your cycling power output compare?* Cycling Analytics. Online, 7th June 2018. Available: <https://www.cyclinganalytics.com/blog/2018/06/how-does-your-cycling-power-output-compare> (visited 8th Aug. 2019).
- [21] S. Brown and J. Allen. *Tire Sizing Systems*. Online, 2007. Available: <https://www.sheldonbrown.com/tire-sizing.html> (visited 10th July 2019).
- [22] International Organization for Standardization (ISO). *International Standard (ISO) 5775-1:2014, Bicycle Tyres And Rims - Part 1: Tyre Designations And Dimensions*. Sept. 2014.
- [23] S. Brown and J. Allen. *Bicycle Frame/Hub Spacing*. Online, 2008. Available: <https://www.sheldonbrown.com/frame-spacing.html> (visited 10th July 2019).
- [24] T. Hadland and H.-E. Lessing. *Bicycle Design - An Illustrated History*. 1st ed. Cambridge: Massachusetts Institute of Technology (MIT) Press, 2014. ISBN: 978-0-262-02675-8.
- [25] S. S. Wilson. ‘Bicycle Technology’. In: *Scientific American* Vol. 228. (3) (Mar. 1973), pp. 81–91. ISSN: 0036-8733. DOI: 10.2307/24923004. As of 14th July 2019: <https://www.jstor.org/stable/24923004>.
- [26] S. Brown and J. Allen. *Shimano Cassettes and Freehubs*. Online, 2007. Available: <https://www.sheldonbrown.com/k7.html> (visited 10th July 2019).
- [27] S. Brown and J. Allen. *Traditional Thread-on Freewheels*. Online, 2007. Available: <https://www.sheldonbrown.com/freewheels.html> (visited 10th July 2019).
- [28] Cube Bikes. *Cube Stereo 140 HPC Race 27.5*. Online, 2019. Available: <https://www.cube.eu/en/2019/bikes/mountainbike/fullsuspension/stereo/cube-stereo-140-hpc-race-275-greynwhite-2019/> (visited 1st July 2019).
- [29] C. Rye. *Cube Cross Hybrid Pro 400 Review*. Electric Bike Review. Online, 2019. Available: <https://www.cube.eu/en/2019/e-bikes/trekking/tour/cross/cube-cross-hybrid-pro-400-iridiumgreen-2019/> (visited 2nd July 2019).
- [30] Cube Bikes. *Cube Cross Hybrid Pro 400*. Online, 2019. Available: <https://www.cube.eu/en/2019/e-bikes/trekking/tour/cross/cube-cross-hybrid-pro-400-iridiumgreen-2019/> (visited 2nd July 2019).
- [31] A. Muetze and Y. C. Tan. ‘Electric Bicycles - A Performance Evaluation’. In: *IEEE Industry Applications Magazine* Vol. 13. (4) (Aug. 2007), pp. 12–21. ISSN: 1077-2618. DOI: 10.1109/MIA.2007.4283505. As of 18th July 2019: <https://ieeexplore.ieee.org/document/4283505>.

- [32] Tern Folding Bikes. *Vektron d8 - The Accelerator*. Online, 2019. Available: <https://www.ternbicycles.com/us/bikes/471/vektron-d8> (visited 1st July 2019).
- [33] N. Fajardo, P. Konyeaso and Z. Weissman. *Modular Electric Skateboard*. Worcester Polytechnic Institute (WPI), Apr. 2019. As of 4th July 2019: <https://web.wpi.edu/Pubs/E-project/Available/E-project-042519-020628/>.
- [34] Warehouse Skateboards. *Skateboard Decks Guide*. Online, 2019. Available: <https://www.warehouse skateboards.com/help/Skateboard-Decks-Buying-Guide> (visited 4th July 2019).
- [35] T. Walker. *Skateboarding as Transportation: Findings from an Exploratory Study. Dissertations and Theses*, Portland State University, Nov. 2013. DOI: 10.15760/etd.1515. As of 16th July 2019: https://pdxscholar.library.pdx.edu/open_access_etds/1505/.
- [36] Yocaher Skateboards. *Graphic Skateboard Complete - Geometric Series - Green*. Online, 2019. Available: <https://shop.yocaher.com/graphic-skateboard-complete-geometric-series-green/> (visited 4th July 2019).
- [37] Boosted Boards. *Boosted Plus Electric Skateboard*. Online, 2019. Available: <https://boostedboards.com/vehicles/longboards/boosted-plus> (visited 3rd July 2019).
- [38] Boosted Boards. *We Don't Call It Super Flex For Nothing*. Online, 25th April 2019. Available: <https://blog.boostedboards.com/super-flex/> (visited 3rd July 2019).
- [39] Light Electric Vehicle Revolution. *Boosted Board: The Leader of Electric Skateboard Technology*. Online, 2019. Available: <https://levrevolution.com/2016/12/18/boosted-board-the-electric-skateboards/> (visited 3rd July 2019).
- [40] Vokul. *Trii S2 Pro Scooter*. Online, 2019. Available: <http://www.vokulscooter.com/product/trii-s2-pro-scooter-black/> (visited 7th July 2019).
- [41] The Vault Pro Scooters. *Sizing Chart*. Online, 2019. Available: <https://www.thevaultproscoters.com/sizing-chart> (visited 7th July 2019).
- [42] C. Williams. *What wheel size should I ride - 100mm, 110mm, 120mm, or 125mm?* Smokin Scooters. Online, 3rd Jan. 2016. Available: <https://smokinscooters.com/blog/what-wheel-size-should-i-ride-100mm-110mm-120mm-or-125mm/> (visited 7th July 2019).
- [43] Xiaomi. *Mi Electric Scooter*. Online, 2019. Available: <https://www.mi.com/us/mi-electric-scooter/> (visited 7th July 2019).
- [44] H. Stoboy, B. W. Rich and M. Lee. 'Workload and energy expenditure during wheelchair propelling'. In: *Spinal Cord* Vol. 8. (4) (Feb. 1971), pp. 223–230. ISSN: 1476-5624. DOI: 10.1038/sc.1970.41. As of 16th July 2019: <https://www.nature.com/articles/sc197041>.

- [45] Karman. *Manual Wheelchairs - Ultra Lightweight - LT-980*. Online, 2019. Available: <https://www.karmanhealthcare.com/product/lt-980/> (visited 8th July 2019).
- [46] Forcemech. *Current Model Specifications - Navigator*. Online, 2019. Available: <https://www.forcemech.com/specifications/> (visited 8th July 2019).
- [47] V. Sullivan and A. Chartier. *How to choose your skates*. OLS Roller Skating Magazine. Online, 19th Aug. 2018. Available: <http://www.online-skating.com/articles-545-how-to-choose-your-roller-skates.html> (visited 5th July 2019).
- [48] A. Chartier. *Choosing your long distance skates*. OLS Roller Skating Magazine. Online, 17th Aug. 2018. Available: <http://www.online-skating.com/articles-1466-choosing-your-long-distance-skates.html> (visited 5th July 2019).
- [49] B. Lapichu. *Comparative: choosing your street frames*. OLS Roller Skating Magazine. Online, 3rd Jan. 2012. Available: <http://www.online-skating.com/articles-2759-comparative-choosing-your-street-frames-wisely.html> (visited 5th July 2019).
- [50] OLS Roller Skating Magazine, Press Release. *Physics of the inline skate wheel*. Online, 15th Sept. 2018. Available: <http://www.online-skating.com/articles-2661-physics-of-the-inline-skate-wheel.html> (visited 5th July 2019).
- [51] Epic Skates. *Quad Skates - Nitro Series - Super Nitro*. Online, 2019. Available: <http://www.epicskates.com/products/super-nitro-red/> (visited 5th July 2019).
- [52] K2. *F.I.T. 84 BOA*. Online, 2019. Available: <https://www.k2skates.com/en/inline-skates/fitness/fit-84-boa-2019.html> (visited 5th July 2019).
- [53] Daniel Souza. *Thundrblade - Ride the world's first electric inline skate on-road or off-road*. Indiegogo. Online, 2019. Available: <https://www.indiegogo.com/projects/thundrblade> (visited 4th July 2019).
- [54] T. Jones. *Ultimate Guide to Road Bike Tyres*. Bike Exchange. Online, 14th Mar. 2019. Available: <https://www.bikeexchange.com.au/blog/road-bike-tyres-what-to-know> (visited 28th July 2019).
- [55] J. Brandt. *The Bicycle Wheel*. 3rd ed. Palo Alto: Avocet Press Inc, June 1993. ISBN: 978-0-9607236-6-9.
- [56] H. P. Gavin. 'Bicycle Wheel Spoke Patterns And Spoke Fatigue'. In: *ASCE Journal of Engineering Mechanics* Vol. 122. (8) (Aug. 1996), pp. 736–742. DOI: 10.1061/(ASCE)0733-9399(1996)122:8(736). As of 10th Aug. 2019: <https://ascelibrary.org/doi/abs/10.1061/%28ASCE%290733-9399%281996%29122%3A8%28736%29> or <http://people.duke.edu/~hpgavin/papers/HPGavin-Wheel-Paper.pdf>.
- [57] Warehouse Skateboards. *Skateboard Wheel Guide*. Online, 2019. Available: <https://www.warehouse skateboards.com/help/Skateboard-Wheels-Buying-Guide> (visited 28th July 2019).

- [58] J. Brandt. *Relative Rolling Resistance Of Tires*. Usenet Archives, collected by Norman Yarvin. Online, 14th Mar. 2019. Available: https://www.yarchive.net/bike/rolling_resistance.html (visited 29th July 2019).
- [59] Micro Mobility. *Micro Suspension*. Online, 2019. Available: <https://www.micro-mobility.com/en/products/micro-suspension> (visited 3rd Aug. 2019).
- [60] BajaBoard. *BajaBoard G4X - 4WD, Extreme Off-Road E-Board*. Online, 29th July 2019. Available: <https://www.bajaboard.com.au/bajaboard-g4x> (visited 3rd Aug. 2019).
- [61] Heinzmann GmbH & Co. KG. *Electric Drives Product Catalogue*. Feb. 2019. As of 25th July 2019: <https://www.heinzmann-electric-motors.com/en/component/jdownloads/send/33-allgemein/137-product-catalogue-electric-drives>.
- [62] Bosch. *Products Catalogue 2019 - Bosch eBike Systems*. Sept. 2018. As of 25th July 2019: https://www.bosch-ebike.com/fileadmin/EBC/Service/Downloads/Broschuere_n/MY2019/Bosch-eBike-Product-Catalogue-MY2019-AU.pdf?_=1539094947.
- [63] L. Wagner. *Overview Of Energy Storage Methods*. Mora Associates Ltd, Dec. 2007. As of 19th July 2019: <http://www.moraassociates.com/reports/0712%20Energy%20storage.pdf>.
- [64] Cambridge University Engineering Department. *Materials Data Book*. 3rd ed. Cambridge, 2003. As of 1st Aug. 2019: <http://www-mdp.eng.cam.ac.uk/web/library/enginfo/cueddatabooks/materials.pdf>.
- [65] South African Bureau of Standards. *South African National Standards (SANS) 311:2007 - Part L: Category L Motor Vehicles*. 2nd ed. Dec. 2007. ISBN: 978-0-626-35831-0.
- [66] EU Publications Office. 'Regulation (EU) No 168/2013 on the approval and market surveillance of two- or three-wheel vehicles and quadricycles'. In: *Official Journal of the European Union* L 60 (2nd Mar. 2013), p. 94. As of 30th June 2019: <https://eur-lex.europa.eu/LexUriServ/LexUriServ.do?uri=OJ:L:2013:060:0052:0128:EN:PDF>.
- [67] G. Rose and P. Cock. *Encouraging E-Bike Use: The Need For Regulatory Reform in Australia*. Dec. 2003, pp. 13–16. As of 2nd July 2019: eng.monash.edu.au/civil/assets/document/research/centres/its/confs-workshops/archive/rose-tram.pdf.
- [68] NZ Transport Agency. *Vehicle Classes And Standards*. Online, 2019. Available: <https://www.nzta.govt.nz/vehicles/vehicle-types/vehicle-classes-and-standards/vehicle-classes/> (visited 2nd July 2019).
- [69] US Publications Office. *Code Title 15 - Commerce and Trade: 2085. Low-Speed Electric Bicycles*. P. 1554. As of 2nd July 2019: <https://www.govinfo.gov/content/pkg/USCODE-2011-title15/pdf/USCODE-2011-title15-chap47-sec2085.pdf>.

- [70] RSA Government Publications Office. *National Road Traffic Act 93 of 1996*. Nov. 1996. As of 2nd July 2019: <http://thornton.co.za/resources/National%20Road%20Traffic%20Act%20&%20Regulations.pdf>.
- [71] Bicycle South. *South African Rules of the Road and Cycling Legislation*. Aug. 2017. As of 2nd July 2019: <https://bicyclesouth.co.za/wp-content/uploads/2017/05/SOUTH-AFRICAN-RULES-OF-THE-ROAD.pdf>.
- [72] J. Prince. 'An Investigation Into Bicycle Performance And Design'. PhD thesis. Auckland University of Technology, July 2014. As of 10th Aug. 2019: <https://openrepository.auckland.ac.nz/handle/10292/8014>.
- [73] Heinzmann GmbH & Co. KG. *E-Bike Direct Drive - DirectPower PRA 150-25*. July 2019. As of 27th July 2019: <https://www.heinzmann-electric-motors.com/en/downloads/directpower-system/send/22-directpower/102-pra-180-25-directpower-motor-e>.
- [74] R. Cong et al. *Electric Bicycle System*. California Polytechnic State University, June 2010. As of 21st Aug. 2019: <https://digitalcommons.calpoly.edu/eesp/34/>.
- [75] Heinzmann GmbH & Co. KG. *Direct Drive Downtube Battery Data Sheet*. June 2019. As of 27th July 2019: <https://www.heinzmann-electric-motors.com/en/downloads/directpower-system/send/22-directpower/111-directpower-downtube-battery>.
- [76] Panasonic. *Lithium Ion - NCR18650PF*. Apr. 2018. As of 27th July 2019: <https://industrial.panasonic.com/cdbs/ww-data/pdf2/ACA4000/ACA4000C50.pdf>.
- [77] Panasonic. *Lithium Ion - UR18650RX*. Apr. 2018. As of 27th July 2019: <https://industrial.panasonic.com/cdbs/ww-data/pdf2/ACA4000/ACA4000CE421.pdf>.
- [78] Panasonic. *Lithium Ion - UR18650AA*. Apr. 2018. As of 27th July 2019: <https://industrial.panasonic.com/cdbs/ww-data/pdf2/ACA4000/ACA4000C59.pdf>.
- [79] Samsung SDI. *Specifications of Product for Lithium-ion Rechargeable Cell - Model: ICR18650-22F*. May 2009. As of 27th July 2019: <http://gamma.spb.ru/media/pdf/liion-lipolymer-lifepo4-akkumulyatory/ICR18650-22F.pdf>.
- [80] Samsung SDI. *Specifications of Product for Lithium-ion Rechargeable Cell - Model: ICR18650-25R*. Mar. 2014. As of 27th July 2019: <http://dalincom.ru/datasheet/SAMSUNG%20INR18650-25R.pdf>.
- [81] Samsung SDI. *Specifications of Product for Lithium-ion Rechargeable Cell - Model: ICR18650-26J*. Sept. 2014. As of 27th July 2019: <http://www.vanco.sg/wp-content/uploads/2017/01/Samsung-ICR18650-26J-2600mAh-01.pdf>.
- [82] Samsung SDI. *Specifications of Product for Lithium-ion Rechargeable Cell - Model: INR18650-29E*. Sept. 2012. As of 27th July 2019: <http://gamma.spb.ru/media/pdf/liion-lipolymer-lifepo4-akkumulyatory/INR18650-29E.pdf>.

- [83] B. Topf. *What's the best gravel tire? - 10 models in comparison*. Gran Fondo Cycling Magazine, Issue 010. Online, 23rd Nov. 2018. Available: <https://granfondo-cycling.com/the-best-gravel-tire/> (visited 30th July 2019).
- [84] Challenge. *Gravel Grinder TLR*. Online, 2019. Available: <https://www.challengetires.com/product/clincher/gravel-grinder-tlr/tlr/1716> (visited 30th July 2019).
- [85] Bike Components. *Challenge Gravel Grinder Race Open Folding Tyre*. Online, 2019. Available: <https://www.bike-components.de/en/Challenge/Gravel-Grinder-Race-Open-Folding-Tyre-p44488/> (visited 30th July 2019).
- [86] International Organization for Standardization (ISO). *International Standard (ISO) 5775-2:2015, Bicycle Tyres And Rims - Part 2: Rims*. Dec. 2015.
- [87] R. G. Budynas and J. K. Nisbett. *Shigley's Mechanical Engineering Design*. 10th ed. New York: McGraw-Hall Education, 2015. ISBN: 978-981-4595-28-5.
- [88] W. D. Pilkey and D. F. Pilkey. *Peterson's Stress Concentration Factors*. 3rd ed. New Jersey: John Wiley & Sons, Inc, 2008. ISBN: 978-0-470-04824-5.
- [89] T. Mangera and T. Frangakis. *MECN2014 Mechanical Engineering Design I Lecture Series*. University Of The Witwatersrand, Johannesburg, 2017.
- [90] International Organization for Standardization (ISO). *International Standard (ISO) 6701:1991, Cycles - External Dimensions Of Spoke Nipples*. Jan. 1991.
- [91] Japanese Standards Association. *Japanese Industrial Standard (JIS) D 9420:2010, Spokes For Bicycles (English)*. Jan. 2010.
- [92] Japanese Standards Association. *Japanese Industrial Standard (JIS) D 9421:2009, Bicycles - Rims (English)*. Dec. 2015.
- [93] MatWeb. *Aluminum 6061-T6; 6061-T651*. Material Property Data. Online, 2019. Available: <http://www.matweb.com/search/DataSheet.aspx?MatGUID=b8d536e0b9b54bd7b69e4124d8f1d20a&ckck=1> (visited 5th Aug. 2019).
- [94] J. P. Nobre, C. Polese and S. Schekman. *MECN3019 Mechanical Engineering Design And Production Lecture Series*. University Of The Witwatersrand, Johannesburg, 2018.
- [95] MatWeb. *AISI 1035 Steel, Rolled, 19-32mm Round*. Material Property Data. Online, 2019. Available: <http://www.matweb.com/search/DataSheet.aspx?MatGUID=cea798a6f9f64a20b8813f3c35f70df3> (visited 5th Aug. 2019).
- [96] D. S. D. Lorenzo and M. L. Hull. 'A Hub Dynamometer for Measurement of Wheel Forces in Off-Road Bicycling'. In: *Journal of Biomechanical Engineering* Vol. 121. (1) (Feb. 1999), pp. 132–137. ISSN: 0148-0731. DOI: 10.1115/1.2798034. As of 6th Aug. 2019: <http://biomechanical.asmedigitalcollection.asme.org/article.aspx?articleid=1401834>.

- [97] C. Jones. *Torque Specifications And Concepts*. Park Tool. Online, 24th Aug. 2015. Available: <https://www.parktool.com/blog/repair-help/torque-specifications-and-concepts> (visited 20th Aug. 2019).
- [98] MatWeb. *AISI 4140 Steel, Oil Quenched, 13mm Round [845°C Quench, 540°C Temper]*. Material Property Data. Online, 2019. Available: <http://www.matweb.com/search/DataSheet.aspx?MatGUID=423b97220479413cbecf2143727e8b3b&ckck=1> (visited 5th Aug. 2019).
- [99] C. Jones. *Basic Thread Concepts*. Park Tool. Online, 24th Aug. 2015. Available: <https://www.parktool.com/blog/repair-help/basic-thread-concepts> (visited 20th Aug. 2019).
- [100] SKF Group. *SKF General Catalogue - Rolling Bearings*. Oct. 2018. As of 6th Aug. 2019: https://www.skf.com/binary/21-121486/Rolling-bearings---17000_1-EN.pdf.
- [101] S. Brown et al. *Bicycle Glossary*. Online, 2007. Available: <https://sheldonbrown.com/glossary.html> (visited 11th Aug. 2019).
- [102] Iwis. *Handbook For Chain Engineering - Design And Construction / Examples Of Calculation*. 2010. As of 12th Aug. 2019: <https://www.iwis.com/as-handbook/iwis-handbook-for-chain-engineering-design-and-construction.pdf>.
- [103] Renold. *Transmission Chain - Installation, Maintenance, And Designer Guide*. Sept. 2010. As of 12th Aug. 2019: <https://www.renold.com/media/165418/transmission-i-and-m-ren12-eng-10-10.pdf>.
- [104] S. Brown. *Bicycle Crank/Chainring Bolt Circle Diameter*. Online, 2005. Available: <https://sheldonbrown.com/cribsheet-bcd.html> (visited 12th Aug. 2019).
- [105] Shimano. *Octalink Bottom Bracket - Alivio T4000 - BB-ES300*. Online, 2019. Available: <https://bike.shimano.com/en-EU/product/component/alivio-t4000/BB-ES300.html> (visited 12th Aug. 2019).
- [106] S. Brown. *Bottom Bracket Size Database*. Online, 2008. Available: <https://sheldonbrown.com/bbsize.html> (visited 12th Aug. 2019).
- [107] S. Brown. *Threaded Bicycle Bottom Bracket*. Online, 2008. Available: <https://sheldonbrown.com/cribsheet-bottombrackets.html> (visited 12th Aug. 2019).
- [108] S. Brown and J. Allen. *Bicycle Pedals*. Online, 2011. Available: <https://sheldonbrown.com/pedals.html> (visited 12th Aug. 2019).
- [109] International Organization for Standardization (ISO). *International Standard (ISO) 4210-8:2014, Cycles - Safety Requirements For Bicycles, Part 8: Pedal And Drive System Test Methods*. Nov. 2014.
- [110] S. Brown, J. Allen and H. Fell. *Seatpost Size Database*. Online, 2008. Available: <https://sheldonbrown.com/seatpost-sizes.html> (visited 16th Aug. 2019).

- [111] S. Brown and J. Allen. *Servicing Bicycle Headsets*. Online, 2016. Available: <https://sheldonbrown.com/headsets.html> (visited 16th Aug. 2019).
- [112] S. Brown. *Frame Materials For The Touring Cyclist*. Online, 2008. Available: <https://www.sheldonbrown.com/frame-materials.html> (visited 16th Aug. 2019).
- [113] Trek Bikes. *Trek FX Sport 5*. Online, 2019. Available: https://www.trekbikes.com/us/en_US/bikes/hybrid-bikes/fitness-bikes/fx/fx-sport-5/p/21561/?colorCode=black_grey (visited 18th Aug. 2019).
- [114] Trek Bikes. *Trek Verve+ 2*. Online, 2019. Available: https://www.trekbikes.com/us/en_US/bikes/hybrid-bikes/electric-hybrid-bikes/verve/verve-2-mens/p/28299/?colorCode=grey (visited 18th Aug. 2019).
- [115] Cube Bikes. *Cube Editor*. Online, 2019. Available: <https://www.cube.eu/en/2020/bikes/urban/editor/cube-editor-blackpurple-2020/> (visited 18th Aug. 2019).
- [116] BMC Switzerland. *BMC Alpenchallenge AMP City One*. Online, 2019. Available: <https://www.bmc-switzerland.com/alpenchallenge-amp-city-one-302008.html> (visited 18th Aug. 2019).
- [117] Momsen Bikes. *Momsen 700 GP300*. Online, 2019. Available: <https://momsenbikes.com/shop/gravel-bikes/mtb-momsen-700-gp300-2019/> (visited 18th Aug. 2019).
- [118] K. Y. Cheng, D. Bothman and K. J. Astrom. ‘Bicycle Torque Sensor Experiment’. In: (Aug. 2003). As of 18th Aug. 2019: https://www.researchgate.net/profile/David_Bothman/publication/228486690_Bicycle_Torque_Sensor_Experiment/links/54ea379d0cf27a6de113b876/Bicycle-Torque-Sensor-Experiment.pdf.
- [119] G. Dialynas, R. Happee and A. L. Schwab. ‘Design And Hardware Selection For A Bicycle Simulator’. In: *Mechanical Sciences* Vol. 10. (1) (Jan. 2019), pp. 1–10. DOI: 10.5194/ms-10-1-2019. As of 18th Aug. 2019: <https://www.mech-sci.net/10/1/2019/>.
- [120] International Organization for Standardization (ISO). *International Standard (ISO) 4210-6:2014, Cycles - Safety Requirements For Bicycles, Part 6: Frame And Fork Test Methods*. Nov. 2014.
- [121] Heinzmann GmbH & Co. KG. *DirectPower PRA 150-25 Dimensions*. Feb. 2019. As of 27th Aug. 2019: <https://www.heinzmann-electric-motors.com/en/downloads/directpower/send/18-directpower-e-bike-motor/86-pra-180-25-hinterrad-zeichnung> and <https://www.heinzmann-electric-motors.com/en/downloads/directpower/send/18-directpower-e-bike-motor/85-pra-180-25-hinterrad-step>.

A ETHICS CLEARANCE

The following pages are the received comments from the reviewers of the School Ethics Committee for this project with the protocol number MIAEC 067/19w. These reviews serve as proof of the qualification for an ethics waiver and clearance certificate.

B ADDITIONAL ENGINEERING DRAWINGS

Following the ethics reviews, additional engineering drawing are included for the motor [121] while the drawings for the minor components (such as the spokes, nipples, bolts, and nuts) were not included as they are either standard parts or their dimensions are highly dependent on the manufacturing.

C COMPONENT DATA SHEETS

Following the engineering drawings, excerpts of the data sheets are included for the Heinzmann DirectPower PRA 180-25 brushless DC hub motor, Panasonic NCR18650PF lithium-ion battery cells, SKF 609 single row deep groove ball bearings, and typical bicycle frame size chart [73, 76, 100].

D MISCELLANEOUS COMMENTS

In order to achieve the fixed upload limit of 10mb for the maximum file size, some images throughout the report have been compressed to lower resolutions - particularly for the finite element analyses which makes the meshes difficult to distinguish. The full quality version of the report can be found at <http://drive.google.com/file/d/1aWDQhhtyfnXfPCXMPpU6iKTHfRjRHKfI/view?usp=sharing> with a size of 36.498mb (access limited to accounts linked to the University of the Witwatersrand unless permission is requested).

REVIEWER'S COMMENTS: HUMAN RESEARCH ETHICS COMMITTEE (NON MEDICAL)

DATE:

SECTION A

Applicant's name: Rycroft Edward	Reviewer's name: Dillon Rossouw
Protocol number: MIAEC 067/19	
Degree: BSc Eng Hons.	
Title of the research project: Electrically Enhanced Personal Transportation.	

SECTION B

Comments for the applicant to address on the Ethics Application Form:
NA

Comments for the applicant to address on the Participant Information Sheet:
NA

Comments for the applicant to address on the Consent Form:
NA

Methodological comments for the applicant to consider:
NA

Reviewer's overall comments:
Waiver.

SECTION C

Summary of overall risk category of this study. Refer to risk category definitions for what these risks specifically refer to. Please TICK the appropriate boxes.

Risk category	Category identified by applicant	Category identified by reviewer
No risk	<input checked="" type="checkbox"/>	<input type="checkbox"/>
Minimal risk	<input type="checkbox"/>	<input checked="" type="checkbox"/>
Low risk	<input type="checkbox"/>	<input type="checkbox"/>
Medium risk	<input type="checkbox"/>	<input type="checkbox"/>
High risk	<input type="checkbox"/>	<input type="checkbox"/>

Does the reviewer believe that the applicant has adequately dealt with all the potential risks of this project?
 YES / NO

If NO, describe which specific risks need to be addressed and how
NA

SECTION D

Recommendation (please indicate):

Accept as is	<input checked="" type="checkbox"/>
Minor revisions	<input type="checkbox"/>
Moderate revisions	<input type="checkbox"/>
Major revisions	<input type="checkbox"/>
Resubmit	<input type="checkbox"/>

If revisions are required, please note that reviewers must see the revised version and approve the changes before an application can be approved.

REVIEWER'S COMMENTS: HUMAN RESEARCH ETHICS COMMITTEE (NON MEDICAL)

DATE:

SECTION A

Applicant's name: Rycroft Edward	Reviewer's name: Reviewer 2
Protocol number: MIAEC 067/19W	
Degree: BSc Eng Hons	
Title of the research project: Electrically Enhanced Personal Transportation	

SECTION B

Comments for the applicant to address on the Ethics Application Form:
Okay

Comments for the applicant to address on the Participant Information Sheet:
Okay

Comments for the applicant to address on the Consent Form:
Okay

Methodological comments for the applicant to consider:
Okay

Reviewer's overall comments:
Qualifies for waiver

SECTION C

Summary of overall risk category of this study. Refer to risk category definitions for what these risks specifically refer to. Please TICK the appropriate boxes.

Risk category	Category identified by applicant	Category identified by reviewer
No risk	<input checked="" type="checkbox"/>	<input type="checkbox"/>
Minimal risk	<input type="checkbox"/>	<input checked="" type="checkbox"/>
Low risk	<input type="checkbox"/>	<input type="checkbox"/>
Medium risk	<input type="checkbox"/>	<input type="checkbox"/>
High risk	<input type="checkbox"/>	<input type="checkbox"/>

Does the reviewer believe that the applicant has adequately dealt with all the potential risks of this project?
 YES / NO

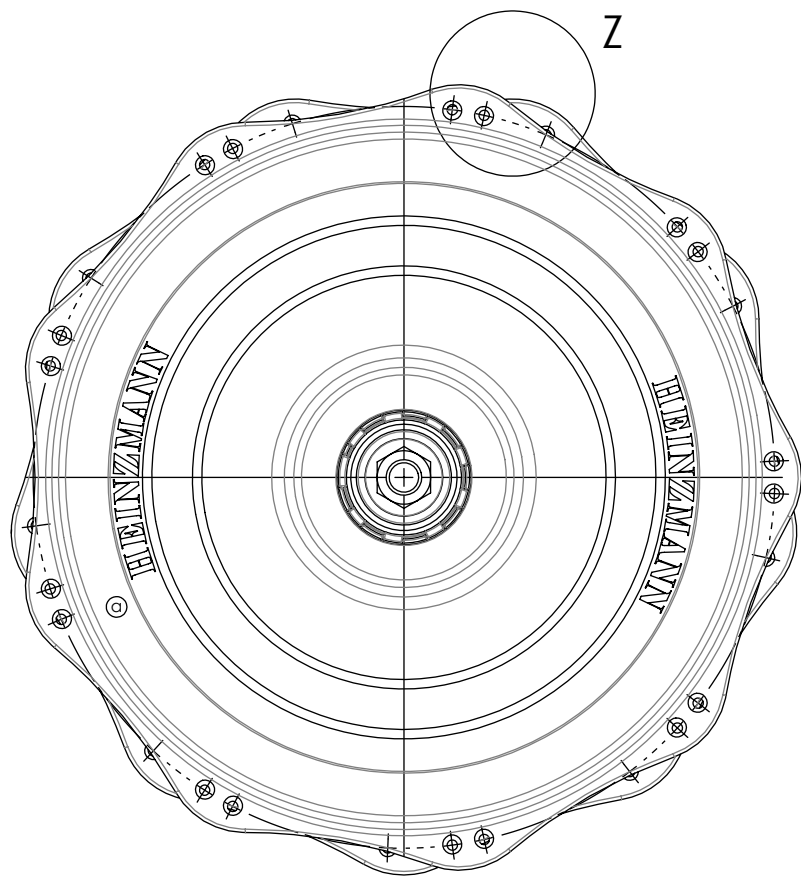
If NO, describe which specific risks need to be addressed and how

SECTION D

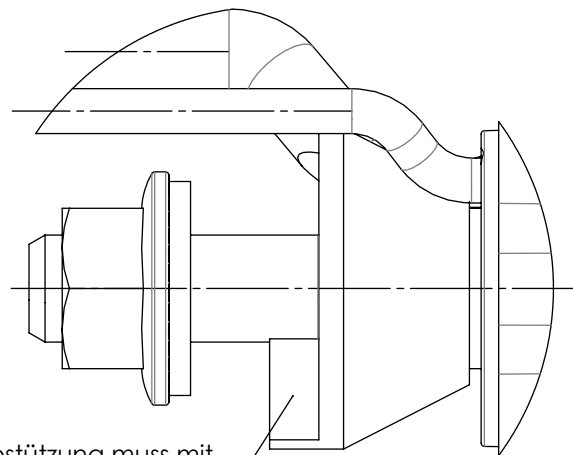
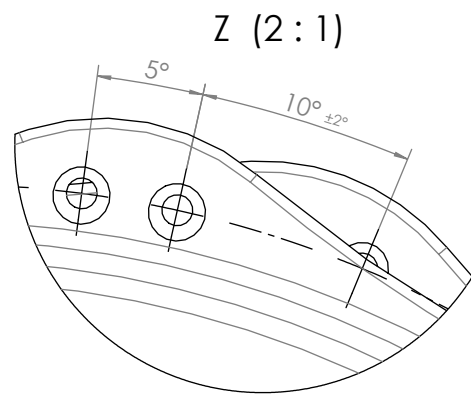
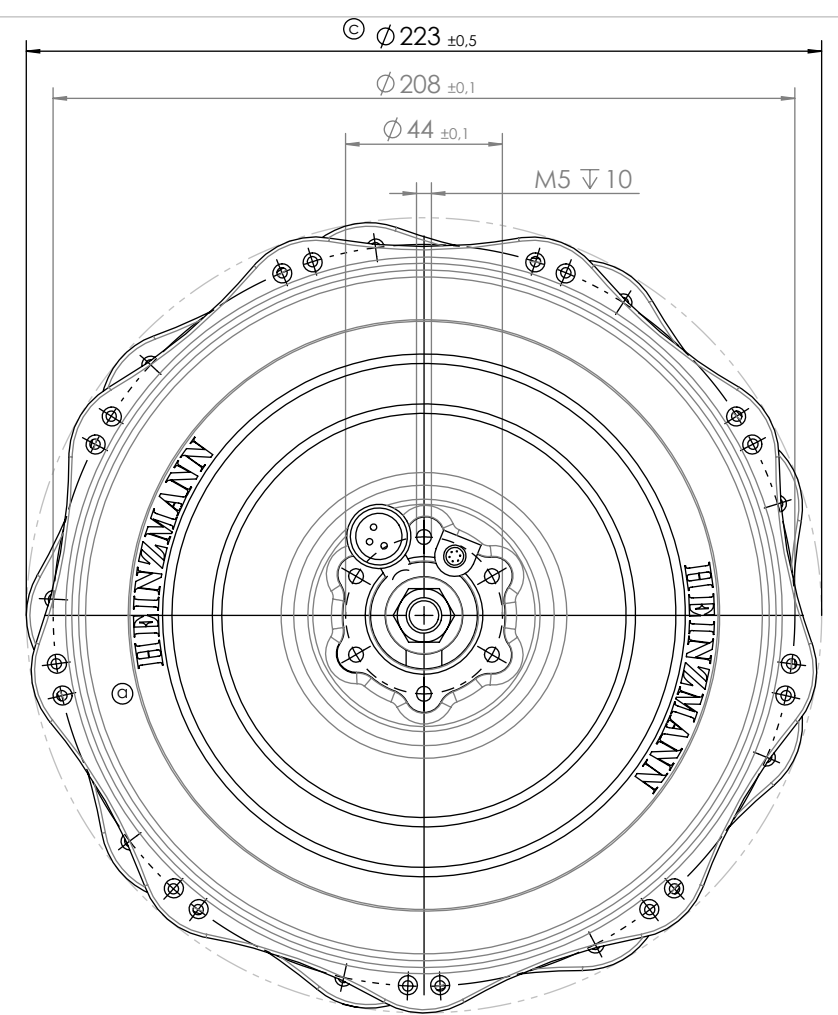
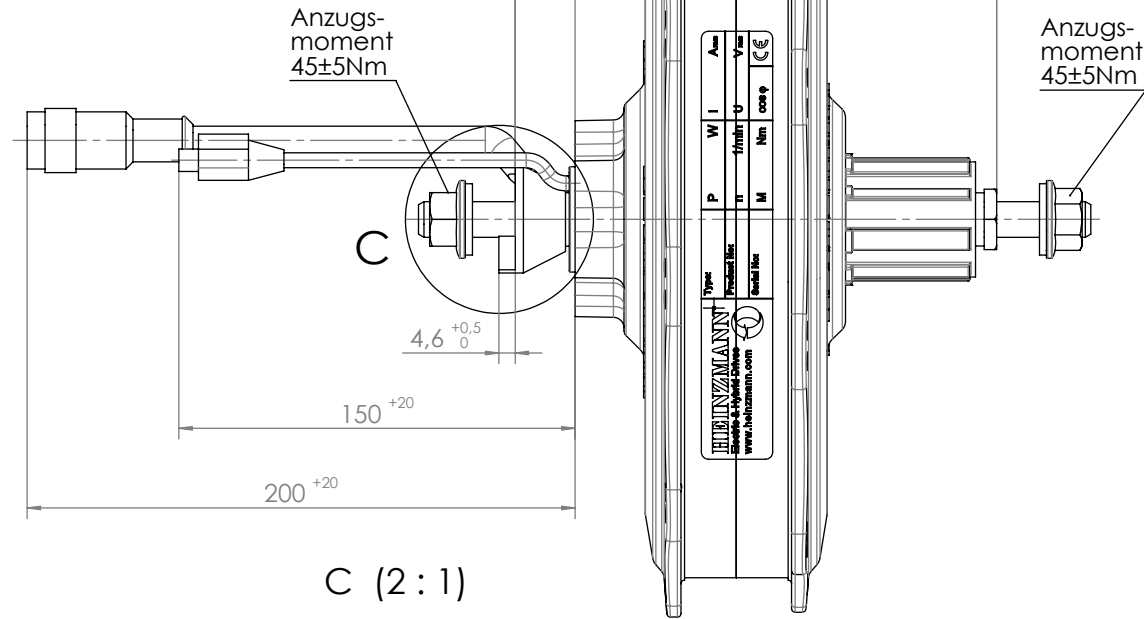
Recommendation (please indicate):

Accept as is	<input checked="" type="checkbox"/>
Minor revisions	<input type="checkbox"/>
Moderate revisions	<input type="checkbox"/>
Major revisions	<input type="checkbox"/>
Resubmit	<input type="checkbox"/>

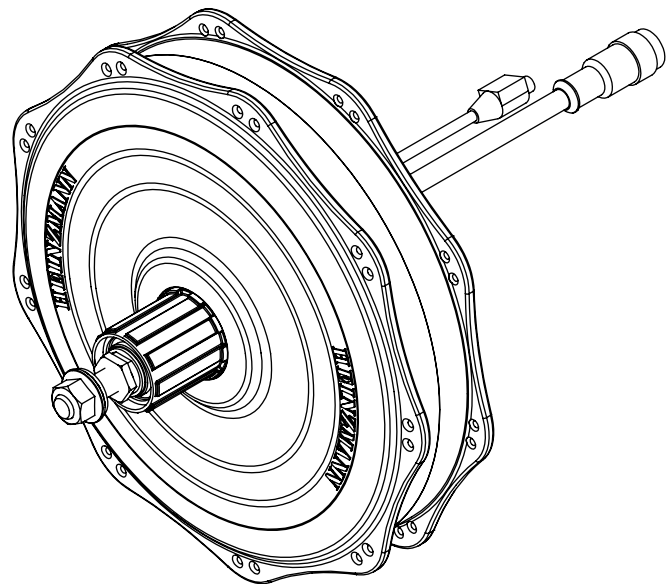
If revisions are required, please note that reviewers must see the revised version and approve the changes before an application can be approved.



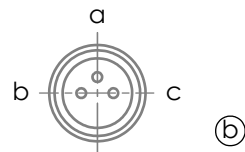
Alle Kabellängen sind in gestreckter Länge angegeben. Die maximal zulässige Zugbelastung an den Motorleitungen beträgt 80N.



Die Drehmomentabstützung muss mit ihrer vollen Länge im Rahmen oder in der Gabel abgestützt sein.

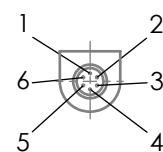


Ansicht Powerstecker



Pin	Farbe	Belegung
a	schwarz	U
b	blau	V
c	rot	W

Ansicht Signalstecker



Pin	Farbe	Belegung
1	weiß	Versorgungssp. V _{DD} (5V)
2	schwarz	Masse (GND)/Temp.-sensor (KTY-)
3	rot	Temperatursensor (KTY+)
4	grün	Signal Hallsensor 2 (S2)
5	gelb	Signal Hallsensor 1 (S1)
6	blau	Signal Hallsensor 3 (S3)

Diese Zeichnung ist für folgende Artikelnummern gültig:

Art.-Nr.	Art.-Bezeichnung	RAL-Nr.	RAL-Farbe
880-00-144-00	PRA180-25 Pedelec	9005	Schwarz matt
880-00-144-10	PRA180-25 Pedelec	9006	Weißaluminium
880-00-144-11	PRA180-25 Pedelec 20"	9005	Schwarz matt
880-00-144-12	PRA180-25 Pedelec 20"	9006	Weißaluminium
880-00-144-50	PRA180-25 Speed Pedelec	9005	Schwarz matt
880-00-144-51	PRA180-25 Speed Pedelec	9006	Weißaluminium
880-00-149-00	PRA180-25 High Torque	9005	Schwarz matt
880-00-151-00	PRA180-25 High Torque	9006	Weißaluminium

Bitte unbedingt die Montageanleitung beachten!

Maß	Abmaß	Maß	Abmaß	ISO-Passung	Ausgabe	Änderungst.	Änderung	Tag	Name
	d	11378					Neue Drehmomentstütze verbaut, 2x Scheibe (2mm Dicke) eingefügt	11.03.2015	Farbacher
	c	11470					Ø223 war Ø220,5; RAL9005 war RAL9017	26.06.2014	Doering
	b						Lochkreistoleranz 0,1 war 0,02	03.02.2014	Roller
	a						Position HEINZMANN Schriftzug geändert	22.04.2013	Roller
Status	Tag	Name	Werkstoff	Maßstab		Maße ohne Toleranzangabe nach DIN ISO 2768-mK		HEINZMANN GmbH & Co. KG Electric & Hybrid Drives Am Haselbach 1 D-79477 Schönau Telefon: +49 (0) 7673 8208-0 Telefax: +49 (0) 7673 8208-199	
Bearbeitet	07.02.2013	Körting	Mat-Nr.:	1:1.5				Zeichnungs-Nr. 880-00-144-..	
Geprüft								Ersatz für:	Blatt 01
Normgepr.								Ersetzt durch:	von Bl.
Benennung PRA180-25 HR+BF+SK Druckguß			Ausgangsteil/Halbzeug:						

DirectPower PRA 180-25

DATA SHEET



Description

DirectPower E-Bike Drives by HEINZMANN impress with their innovative technology and extreme flexibility.

Thanks to their independent control which is integrated in the battery box they can be used for a variety of systems. The power electronics is not built into the motor. The motor power rating is not affected by the heating of the electronics. Backwards travel is possible for special applications.

Optimised geometry of flanges allows to spoke rims from 20" up to 28" without crossing.

As front wheel or rear wheel drive – HEINZMANN e-bike drives adapt to your requirements. Customised design or colour of choice on request.

Features

Maintenance-free, noiseless

Brushless and gearless

Front or rear wheel option

Regeneration in front and rear wheel

Brake disc support

Built in cassette

Separate power electronics not affected by motor temperature ensuring maximum performance

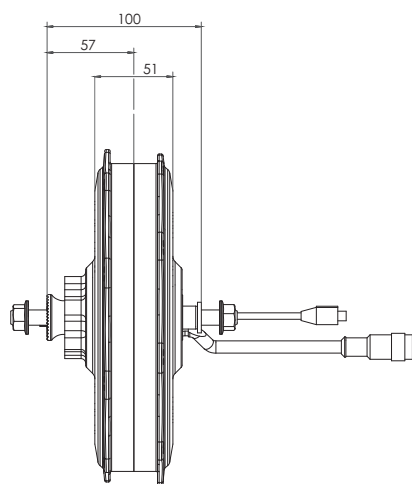
Optimised geometry of flanges, no crossed spoking, rim range 20" up to 28"

Technical data

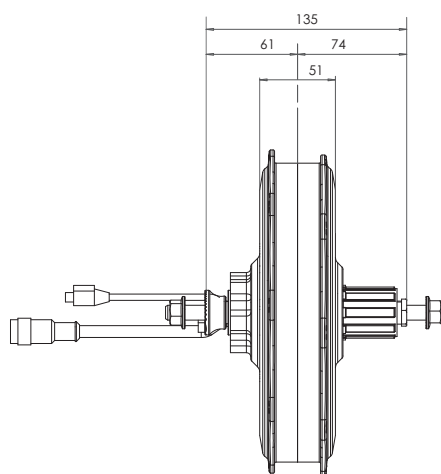
Motor									
Type	Pedelec			Pedelec 20"			Speed Pedelec ^{*)}		
DC supply voltage	36 VDC								
Rated power	250 W			250 W			500 W		
Nominal speed	210 1/min			275 1/min			380 1/min		
Typical speed limit according to rim size *) Comply with the relevant legal requirements when using	20"	25 km/h		38 km/h		38 km/h			
	24"	32 km/h		42 km/h		42 km/h			
	26"	34 km/h		46 km/h		46 km/h			
	28"	37 km/h		50 km/h		50 km/h			
Weight	4.5 kg front wheel; 4.7 kg rear wheel								
Cooling	Ext. ventilation > 5 m/s								
Operating points									
Operational mode	S1	S2 10 min	S2 4 min	S1	S2 10 min	S2 4 min	S1	S2 10 min	S2 4 min
Rated torque	11.4 Nm	30 Nm	40 Nm	8.7 Nm	30 Nm	40 Nm	12.6 Nm	30 Nm	40 Nm
Related AC current	9.3 A	25 A	33 A	11.6 A	40 A	55 A	17.5 A	40 A	55 A
Impulse torque	60 Nm								

Electrical data			
Type	Pedelec	Pedelec 20"	Speed Pedelec
DC supply voltage	36 VDC		
Motor voltage	22.8 VAC	17.44 VAC	24.25 VAC
EMF constant	84.5 $\frac{V}{1000 \text{ min}^{-1}}$	51.7 $\frac{V}{1000 \text{ min}^{-1}}$	51.7 $\frac{V}{1000 \text{ min}^{-1}}$
Torque constant	1.22 $\frac{\text{Nm}}{\text{A}}$	0.75 $\frac{\text{Nm}}{\text{A}}$	0.75 $\frac{\text{Nm}}{\text{A}}$
Resistance phase-phase	244 m Ω	88 m Ω	88 m Ω
Winding inductance phase-phase	1.4 mH	0.36 mH	0.36 mH
Moment of inertia	102 kg·cm ²		
Degree of protection	IP54		
Sensor system			
Motor feedback	Hall sensors		
Temperature sensor	KTY84-130		

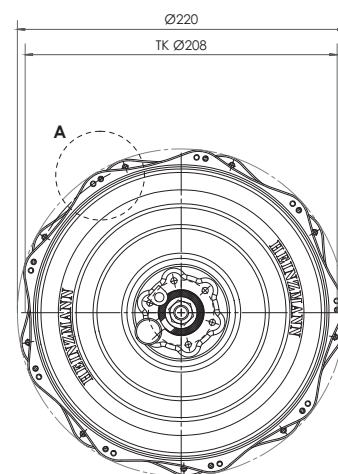
Dimensions



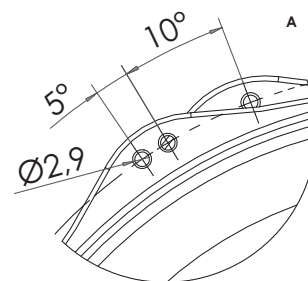
Front wheel



Rear wheel



With this drawing the regulations for copy right protection are effective.



Subject to alterations. ©HEINZMANN GmbH & Co. KG, 2019

Features & Benefits

- High energy and power density
- Long, stable, high power
- High safety performance
- Ideal for power assisted bicycles, 2-way radios, medical devices and robotics.

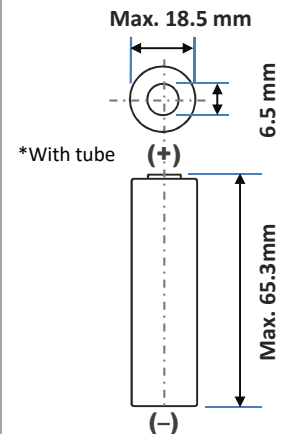
* At temperatures below 10°C, charge at a 0.25C rate.

Specifications

Rated capacity ⁽¹⁾	Min. 2700mAh
Capacity ⁽²⁾	Min. 2750mAh Typ. 2900mAh
Nominal voltage	3.6V
Charging	CC-CV, Std. 1375mA, 4.20V, 4.0 hrs
Weight (max.)	48.0 g
Temperature	Charge*: 0 to +45°C Discharge: -20 to +60°C Storage: -20 to +50°C
Energy density ⁽³⁾	Volumetric: 577 Wh/l Gravimetric: 207 Wh/kg

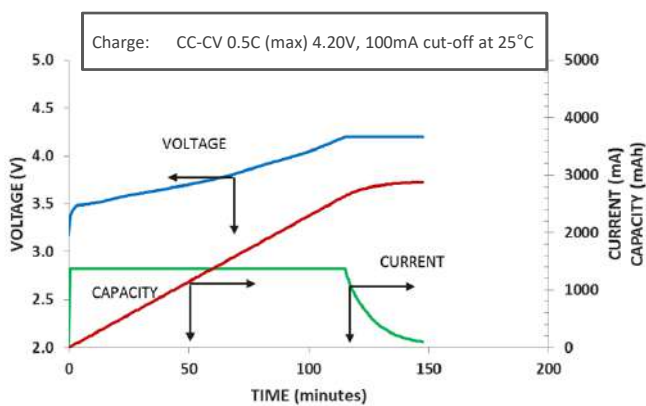
⁽¹⁾ At 20°C ⁽²⁾ At 25°C ⁽³⁾ Energy density based on bare cell dimensions

Dimensions

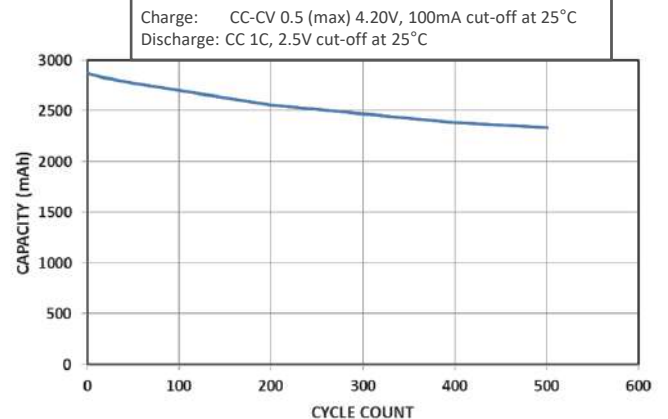


For Reference Only

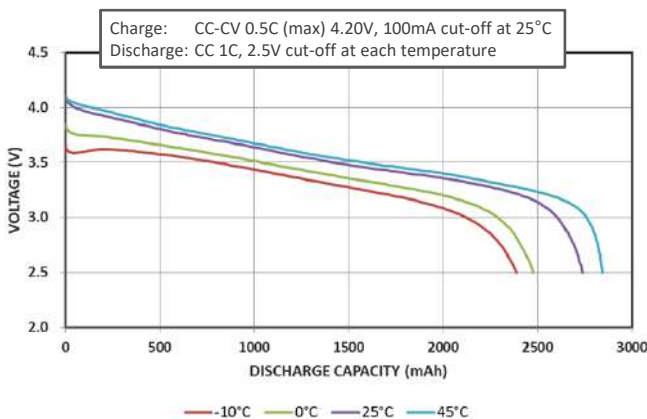
Charge Characteristics



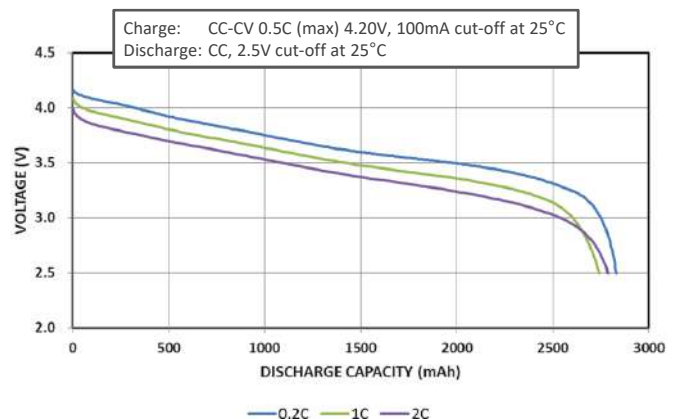
Cycle Life Characteristics



Discharge Characteristics (by temperature)



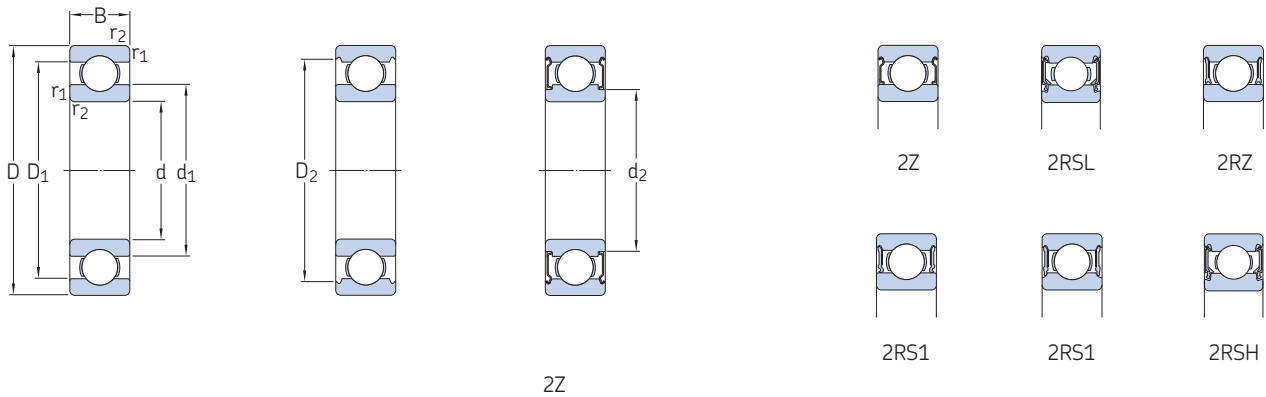
Discharge Characteristics (by rate of discharge)



The data in this document is for descriptive purposes only and is not intended to make or imply any guarantee or warranty.

1.1 Single row deep groove ball bearings

d 7–9 mm

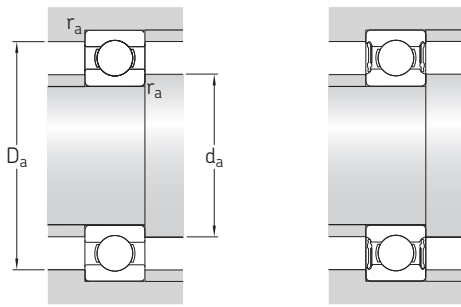


Principal dimensions			Basic load ratings		Fatigue load limit	Speed ratings		Mass	Designations		
d	D	B	dynamic	static		Reference speed	Limiting speed ¹⁾		Bearing open or capped on both sides	capped on one side ¹⁾	
mm			kN		kN	r/min	kg	–			
7	14	3,5	0,78	0,26	0,011	100 000	63 000	0,0022	618/7	–	
	14	5	0,956	0,4	0,017	100 000	50 000	0,0031	628/7-2Z	–	
	17	5	1,06	0,375	0,016	90 000	45 000	0,0049	619/7-2Z	–	
	17	5	1,06	0,375	0,016	90 000	56 000	0,0049	619/7	–	
	19	6	2,34	0,95	0,04	85 000	53 000	0,0076	▶ 607	–	
	19	6	2,34	0,95	0,04	–	24 000	0,0078	▶ 607-2RSH	607-RSH	
	19	6	2,34	0,95	0,04	85 000	43 000	0,0078	▶ 607-2RSL	607-RSL	
	19	6	2,34	0,95	0,04	85 000	43 000	0,0084	▶ 607-2Z	607-Z	
	22	7	3,45	1,37	0,057	70 000	45 000	0,012	▶ 627	–	
	22	7	3,45	1,37	0,057	–	22 000	0,013	▶ 627-2RSH	627-RSH	
	22	7	3,45	1,37	0,057	70 000	36 000	0,013	▶ 627-2RSL	627-RSL	
	22	7	3,45	1,37	0,057	70 000	36 000	0,013	▶ 627-2Z	627-Z	
	8	16	4	0,819	0,3	0,012	90 000	56 000	0,003	618/8	–
		16	5	1,33	0,57	0,024	–	26 000	0,0036	▶ 628/8-2RS1	–
		16	5	1,33	0,57	0,024	90 000	45 000	0,0036	▶ 628/8-2Z	–
16		6	1,33	0,57	0,024	90 000	45 000	0,0043	638/8-2Z	–	
19		6	1,46	0,465	0,02	–	24 000	0,0071	619/8-2RS1	–	
19		6	1,46	0,465	0,02	85 000	43 000	0,0071	619/8-2Z	–	
19		6	1,46	0,465	0,02	85 000	53 000	0,0071	619/8	–	
19		6	2,34	0,95	0,04	85 000	43 000	0,0072	607/8-2Z	607/8-Z	
22		7	3,45	1,37	0,057	75 000	48 000	0,012	▶ 608	–	
22		7	3,45	1,37	0,057	–	22 000	0,012	▶ 608-2RSH	▶ 608-RSH	
22		7	3,45	1,37	0,057	75 000	38 000	0,012	▶ 608-2RSL	608-RSL	
22		7	3,45	1,37	0,057	75 000	38 000	0,013	▶ 608-2Z	608-Z	
22		11	3,45	1,37	0,057	–	22 000	0,016	▶ 630/8-2RS1	–	
24		8	3,9	1,66	0,071	63 000	40 000	0,018	628	–	
24		8	3,9	1,66	0,071	–	19 000	0,017	628-2RS1	628-RS1	
24	8	3,9	1,66	0,071	63 000	32 000	0,017	628-2RZ	628-RZ		
24	8	3,9	1,66	0,071	63 000	32 000	0,018	▶ 628-2Z	628-Z		
28	9	1,33	0,57	0,024	60 000	30 000	0,03	638-2RZ	638-RZ		
9	17	4	0,871	0,34	0,014	85 000	53 000	0,0034	618/9	–	
	17	5	1,43	0,64	0,027	–	24 000	0,0043	628/9-2RS1	–	
	17	5	1,43	0,64	0,027	85 000	43 000	0,0043	628/9-2Z	628/9-Z	
	20	6	2,34	0,98	0,043	80 000	40 000	0,0076	619/9-2Z	–	
	20	6	2,34	0,98	0,043	80 000	50 000	0,0076	619/9	–	
	24	7	3,9	1,66	0,071	70 000	43 000	0,014	▶ 609	–	

SKF Explorer bearing

▶ Popular item

¹⁾ For bearings with only one shield or one non-contact seal (Z, RZ) the limiting speeds of the open bearings are valid.

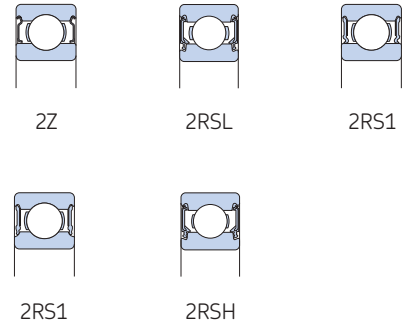
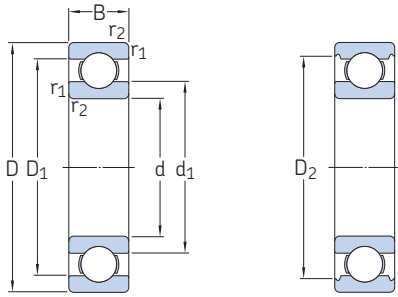


Dimensions						Abutment and fillet dimensions				Calculation factors		
d	d ₁ ≈	d ₂ ≈	D ₁ ≈	D ₂ ≈	r _{1,2} min.	d _a min.	d _a max.	D _a max.	r _a max.	k _r	f ₀	
mm						mm				-		
7	9	-	12	-	0,15	7,8	-	13,2	0,1	0,015	7,2	
	-	8,5	-	12,7	0,15	7,8	8	13,2	0,1	0,015	11	
	10,4	-	-	14,3	0,3	9	9,7	15	0,3	0,02	7,3	
	10,4	-	-	14,3	0,3	9	-	15	0,3	0,02	7,3	
	11,1	-	-	16,5	0,3	9	-	17	0,3	0,025	13	
	-	9,5	-	16,5	0,3	9	9,4	17	0,3	0,025	13	
	-	9,5	-	16,5	0,3	9	9,4	17	0,3	0,025	13	
	11,1	-	-	16,5	0,3	9	11	17	0,3	0,025	13	
	12,1	-	-	19,2	0,3	9,4	-	19,6	0,3	0,025	12	
	-	10,5	-	19,2	0,3	9,4	10,5	19,6	0,3	0,025	12	
	-	10,5	-	19,2	0,3	9,4	10,5	19,6	0,3	0,025	12	
	12,1	-	-	19,2	0,3	9,4	12,1	19,6	0,3	0,025	12	
8	10,5	-	13,5	-	0,2	9,4	-	14,6	0,2	0,015	7,5	
	10,1	-	-	14,2	0,2	9,4	9,4	14,6	0,2	0,015	11	
	10,1	-	-	14,2	0,2	9,4	10	14,6	0,2	0,015	11	
	-	9,6	-	14,2	0,2	9,4	9,5	14,6	0,2	0,015	11	
	-	9,8	-	16,7	0,3	9,5	9,8	17	0,3	0,02	6,6	
	-	9,8	-	16,7	0,3	9,5	9,8	17	0,3	0,02	6,6	
	10,5	-	-	16,7	0,3	10	-	17	0,3	0,02	6,6	
	11,1	-	-	16,5	0,3	10	11	17	0,3	0,025	13	
	12,1	-	-	19,2	0,3	10	-	20	0,3	0,025	12	
	-	10,5	-	19,2	0,3	10	10,5	20	0,3	0,025	12	
	-	10,5	-	19,2	0,3	10	10,5	20	0,3	0,025	12	
	12,1	-	-	19,2	0,3	10	12	20	0,3	0,025	12	
	11,8	-	-	19	0,3	10	11,7	20	0,3	0,025	12	
	14,4	-	-	21,2	0,3	10,4	-	21,6	0,3	0,025	13	
	14,4	-	-	21,2	0,3	10,4	14,4	21,6	0,3	0,025	13	
	14,4	-	-	21,2	0,3	10,4	14,4	21,6	0,3	0,025	13	
	14,4	-	-	21,2	0,3	10,4	14,4	21,6	0,3	0,025	13	
	14,8	-	-	22,6	0,3	10,4	14,7	25,6	0,3	0,03	12	
	9	11,5	-	14,5	-	0,2	10,4	-	15,6	0,2	0,015	7,7
		-	10,7	-	15,2	0,2	10,4	10,5	15,6	0,2	0,015	11
		-	10,7	-	15,2	0,2	10,4	10,5	15,6	0,2	0,015	11
11,6		-	-	17,5	0,3	11	11,5	18	0,3	0,02	12	
11,6		-	-	17,5	0,3	11	-	18	0,3	0,02	12	
14,4		-	-	21,2	0,3	11	-	22	0,3	0,025	13	

1.1 Single row deep groove ball bearings

d 9 – 10 mm

1.1

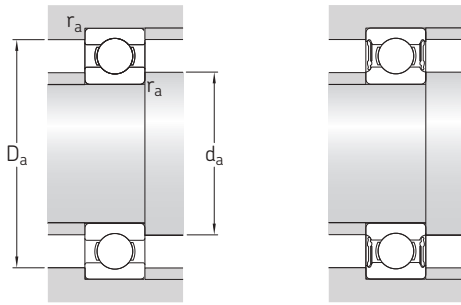


Principal dimensions			Basic load ratings		Fatigue load limit	Speed ratings		Mass	Designations		
d	D	B	dynamic	static		Reference speed	Limiting speed ¹⁾		Bearing open or capped on both sides	capped on one side ¹⁾	
mm			kN		kN	r/min	kg	–			
9	24	7	3,9	1,66	0,071	–	19 000	0,015	▶ 609-2RSH	609-RSH	
	cont.	24	7	3,9	1,66	0,071	70 000	0,014	▶ 609-2RSL	609-RSL	
		24	7	3,9	1,66	0,071	70 000	0,015	▶ 609-2Z	609-Z	
		26	8	4,75	1,96	0,083	60 000	0,02	▶ 629	–	
		26	8	4,75	1,96	0,083	–	19 000	▶ 629-2RSH	629-RSH	
		26	8	4,75	1,96	0,083	60 000	0,02	▶ 629-2RSL	629-RSL	
	26	8	4,75	1,96	0,083	60 000	30 000	0,021	▶ 629-2Z	629-Z	
10	19	5	1,72	0,83	0,036	–	22 000	0,0055	61800-2RS1	–	
		19	5	1,72	0,83	0,036	80 000	0,0055	61800-2Z	–	
		19	5	1,72	0,83	0,036	80 000	0,0053	61800	–	
		22	6	2,7	1,27	0,054	–	20 000	0,01	61900-2RS1	–
		22	6	2,7	1,27	0,054	70 000	0,01	61900-2Z	–	
		22	6	2,7	1,27	0,054	70 000	0,01	61900	–	
		26	8	4,75	1,96	0,083	67 000	40 000	0,019	▶ 6000	–
		26	8	4,75	1,96	0,083	–	19 000	0,019	▶ 6000-2RSH	6000-RSH
		26	8	4,75	1,96	0,083	67 000	34 000	0,019	▶ 6000-2RSL	6000-RSL
		26	8	4,75	1,96	0,083	67 000	34 000	0,02	▶ 6000-2Z	▶ 6000-Z
		26	12	4,62	1,96	0,083	–	19 000	0,025	63000-2RS1	–
		28	8	5,07	2,36	0,1	60 000	30 000	0,026	16100-2Z	–
		28	8	5,07	2,36	0,1	60 000	38 000	0,024	16100	–
		30	9	5,4	2,36	0,1	56 000	36 000	0,031	▶ 6200	–
		30	9	5,4	2,36	0,1	–	17 000	0,032	▶ 6200-2RSH	6200-RSH
		30	9	5,4	2,36	0,1	56 000	28 000	0,032	▶ 6200-2RSL	6200-RSL
		30	9	5,4	2,36	0,1	56 000	28 000	0,034	▶ 6200-2Z	6200-Z
		30	14	5,07	2,36	0,1	–	17 000	0,04	62200-2RS1	–
		35	11	8,52	3,4	0,143	50 000	32 000	0,053	▶ 6300	–
		35	11	8,52	3,4	0,143	–	15 000	0,054	▶ 6300-2RSH	6300-RSH
		35	11	8,52	3,4	0,143	50 000	26 000	0,053	6300-2RSL	6300-RSL
	35	11	8,52	3,4	0,143	50 000	26 000	0,055	▶ 6300-2Z	6300-Z	
	35	17	8,06	3,4	0,143	–	15 000	0,06	62300-2RS1	–	

SKF Explorer bearing

▶ Popular item


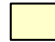
¹⁾ For bearings with only one shield or one non-contact seal (Z, RZ) the limiting speeds of the open bearings are valid.



Dimensions						Abutment and fillet dimensions				Calculation factors	
d	d ₁ ≈	d ₂ ≈	D ₁ ≈	D ₂ ≈	r _{1,2} min.	d _a min.	d _a max.	D _a max.	r _a max.	k _r	f ₀
mm						mm				–	
9 cont.	–	12,8	–	21,2	0,3	11	12,5	22	0,3	0,025	13
	–	12,8	–	21,2	0,3	11	12,5	22	0,3	0,025	13
	14,4	–	–	21,2	0,3	11	14,3	22	0,3	0,025	13
	14,8	–	–	22,6	0,3	11,4	–	23,6	0,3	0,025	12
	–	12,5	–	22,6	0,3	11,4	12,5	23,6	0,3	0,025	12
	–	12,5	–	22,6	0,3	11,4	12,5	23,6	0,3	0,025	12
	14,8	–	–	22,6	0,3	11,4	14,7	23,6	0,3	0,025	12
10	–	11,8	–	17,2	0,3	11,8	11,8	17	0,3	0,015	15
	12,7	–	–	17,2	0,3	12	12,5	17	0,3	0,015	15
	12,7	–	16,3	–	0,3	12	–	17	0,3	0,015	15
	–	13,2	–	19,4	0,3	12	12	20	0,3	0,02	14
	13,9	–	–	19,4	0,3	12	12,9	20	0,3	0,02	14
	13,9	–	18,2	–	0,3	12	–	20	0,3	0,02	14
	14,8	–	–	22,6	0,3	12	–	24	0,3	0,025	12
	–	12,5	–	22,6	0,3	12	12,5	24	0,3	0,025	12
	–	12,5	–	22,6	0,3	12	12,5	24	0,3	0,025	12
	14,8	–	–	22,6	0,3	12	14,7	24	0,3	0,025	12
	14,8	–	–	22,6	0,3	12	14,7	24	0,3	0,025	12
	17	–	–	24,8	0,3	14,2	16,6	23,8	0,3	0,025	13
	17	–	–	24,8	0,3	14,2	–	23,8	0,3	0,025	13
	17	–	–	24,8	0,6	14,2	–	25,8	0,6	0,025	13
	–	15	–	24,8	0,6	14,2	15	25,8	0,6	0,025	13
	–	15	–	24,8	0,6	14,2	15	25,8	0,6	0,025	13
	17	–	–	24,8	0,6	14,2	16,9	25,8	0,6	0,025	13
	17	–	–	24,8	0,6	14,2	16,9	25,8	0,6	0,025	13
	17,5	–	–	28,7	0,6	14,2	–	30,8	0,6	0,03	11
	–	15,5	–	28,7	0,6	14,2	15,5	30,8	0,6	0,03	11
	–	15,5	–	28,7	0,6	14,2	15,5	30,8	0,6	0,03	11
17,5	–	–	28,7	0,6	14,2	17,4	30,8	0,6	0,03	11	
17,5	–	–	28,7	0,6	14,2	17,4	30,8	0,6	0,03	11	

Bicycle Frame Size Chart: 700c Road Bikes, Adult

NOTES: Frame sizes are in cm, center-to-top (C-T)
Subtract 1.5cm - 2 cm from frame size for center-to-center (C-C) measurement
Frame sizes and crank lengths are starting points only. No guarantees here.
CONSULT YOUR LOCAL BICYCLE SHOP FOR A PROFESSIONAL FITTING.

 Common frame size for your height/inseam
 Possible frame size for your height/inseam

Height		Inseam (inches or cm)																																	
		25.0	25.5	26.0	26.5	27.0	27.5	28.0	28.5	29.0	29.5	30.0	30.5	31.0	31.5	32.0	32.5	33.0	33.5	34.0	34.5	35.0	35.5	36.0	36.5	37.0	37.5	38.0	in						
overall	in	cm	64	65	66	67	69	70	71	72	74	75	76	77	79	80	81	83	84	85	86	88	89	90	91	93	94	95	97	cm					
4'8"	56.0	142	43	44	45	46	47	47																											
4'8.5"	56.5	144	43	44	45	46	47	47	48																										
4'9"	57.0	145		44	45	46	47	47	48																										
4'9.5"	57.5	146		44	45	46	47	47	48	49																									
4'10"	58.0	147			45	46	47	47	48	49																									
4'10.5"	58.5	149			45	46	47	47	48	49	50																								
4'11"	59.0	150			45	46	47	47	48	49	50																								
4'11.5"	59.5	151				46	47	47	48	49	50	51																							
5'	60.0	152				46	47	47	48	49	50	51																							
5'5"	60.5	154					47	47	48	49	50	51	52																						
5'1"	61.0	155					47	47	48	49	50	51	52																						
5'1.5"	61.5	156						47	48	49	50	51	52	53																					
5'2"	62.0	157						47	48	49	50	51	52	53																					
5'2.5"	62.5	159							48	49	50	51	52	53	54																				
5'3"	63.0	160							48	49	50	51	52	53	54																				
5'3.5"	63.5	161							48	49	50	51	52	53	54	54																			
5'4"	64.0	163								49	50	51	52	53	54	54																			
5'4.5"	64.5	164								49	50	51	52	53	54	54	55																		
5'5"	65.0	165									50	51	52	53	54	54	55																		
5'5.5"	65.5	166									50	51	52	53	54	54	55	56																	
5'6"	66.0	168										51	52	53	54	54	55	56																	
5'6.5"	66.5	169										51	52	53	54	54	55	56	57																
5'7"	67.0	170										51	52	53	54	54	55	56	57																
5'7.5"	67.5	171											52	53	54	54	55	56	57	58															
5'8"	68.0	173											52	53	54	54	55	56	57	58															
5'8.5"	68.5	174												53	54	54	55	56	57	58	59														
5'9"	69.0	175													53	54	54	55	56	57	58	59													
5'9.5"	69.5	177														54	54	55	56	57	58	59	60												
5'10"	70.0	178															54	54	55	56	57	58	59	60											
5'10.5"	70.5	179																54	55	56	57	58	59	60	60										
5'11"	71.0	180																	54	55	56	57	58	59	60	60									
5'11.5"	71.5	182																		54	55	56	57	58	59	60	60	61							
6'	72.0	183																			55	56	57	58	59	60	60	61							
6'5"	72.5	184																				55	56	57	58	59	60	60	61	62					
6'1"	73.0	185																					56	57	58	59	60	60	61	62					
6'1.5"	73.5	187																					56	57	58	59	60	60	61	62	63				
6'2"	74.0	188																						57	58	59	60	60	61	62	63				
6'2.5"	74.5	189																						57	58	59	60	60	61	62	63	64			
6'3"	75.0	191																							58	59	60	60	61	62	63	64			
6'3.5"	75.5	192																							58	59	60	60	61	62	63	64	65		
6'4"	76.0	193																							58	59	60	60	61	62	63	64	65		
6'4.5"	76.5	194																								59	60	60	61	62	63	64	65	66	
6'5"	77.0	196																								59	60	60	61	62	63	64	65	66	
6'5.5"	77.5	197																									60	60	61	62	63	64	65	66	
6'6"	78.0	198																									60	60	61	62	63	64	65	66	
6'6.5"	78.5	199																									60	61	62	63	64	65	66		
6'7"	79.0	201																									60	61	62	63	64	65	66		
Crank sizes	165mm																																		
													170mm																						
																			172.5mm																
													175mm																						